Title
Laser Inertial Fusion-based Energy: Neutronic Design Aspects of a Hybrid Fusion-Fission Nuclear Energy System

Author
Kramer, Kevin James

Publication Date
2010

Peer reviewed|Thesis/dissertation

Laser Inertial Fusion-based Energy: Neutronic Design Aspects of a Hybrid Fusion-Fission Nuclear Energy System

by

Kevin James Kramer

A dissertation submitted in partial satisfaction of the

requirements for the degree of

Doctor of Philosophy

in

Engineering - Nuclear Engineering

in the

Graduate Division

of the

University of California, Berkeley

Committee in charge:

Professor Per Peterson, Chair
Professor Ehud Greenspan
Professor Todd LaPorte
Dr. Jeffery Latkowski

Spring 2010

Laser Inertial Fusion-based Energy: Neutronic Design Aspects of a Hybrid Fusion-Fission Nuclear Energy System

by Kevin James Kramer

Abstract

Laser Inertial Fusion-based Energy: Neutronic Design Aspects of
a Hybrid Fusion-Fission Nuclear Energy System

by

Kevin James Kramer

Doctor of Philosophy in Engineering - Nuclear Engineering

University of California, Berkeley

Professor Per Peterson, Chair

This study investigates the neutronics design aspects of a hybrid fusion-fission energy system called the Laser Fusion-Fission Hybrid (LFFH). A LFFH combines current Laser Inertial Confinement fusion technology with that of advanced fission reactor technology to produce a system that eliminates many of the negative aspects of pure fusion or pure fission systems. When examining the LFFH energy mission, a significant portion of the United States and world energy production could be supplied by LFFH plants.

The LFFH engine described utilizes a central fusion chamber surrounded by multiple layers of multiplying and moderating media. These layers, or blankets, include coolant plenums, a beryllium (Be) multiplier layer, a fertile fission blanket and a graphite-pebble reflector. Each layer is separated by perforated oxide dispersion strengthened (ODS) ferritic steel walls. The central fusion chamber is surrounded by an ODS ferritic steel first wall. The first wall is coated with 250-500 μm of tungsten to mitigate x-ray damage. The first wall is cooled by $Li_{17}Pb_{83}$ eutectic, chosen for its neutron multiplication and good heat transfer properties. The $Li_{17}Pb_{83}$ flows in a jacket around the first wall to an extraction plenum. The main coolant injection plenum is immediately behind the $Li_{17}Pb_{83}$, separated from the $Li_{17}Pb_{83}$ by a solid ODS wall. This main system coolant is the molten salt flibe (2LiF-BeF_2), chosen for beneficial neutronics and heat transfer properties. The use of flibe enables both fusion fuel production (tritium) and neutron moderation and multiplication for the fission blanket. A Be pebble (1 cm diameter) multiplier layer surrounds the coolant injection plenum and the coolant flows radially through perforated walls across the bed. Outside the Be layer, a fission fuel layer comprised of depleted uranium contained in Tristructural-isotropic (TRISO) fuel particles having a packing fraction of 20% in 2 cm diameter fuel pebbles. The fission blanket is cooled by the same radial flibe flow that travels through perforated ODS walls to the reflector blanket. This reflector blanket is 75 cm

thick comprised of 2 cm diameter graphite pebbles cooled by flibe. The flibe extraction plenum surrounds the reflector bed. Detailed neutronics designs studies are performed to arrive at the described design.

The LFFH engine thermal power is controlled using a technique of adjusting the $^{6}Li/^{7}Li$ enrichment in the primary and secondary coolants. The enrichment adjusts system thermal power in the design by increasing tritium production while reducing fission. To perform the simulations and design of the LFFH engine, a new software program named LFFH Nuclear Control (LNC) was developed in C++ to extend the functionality of existing neutron transport and depletion software programs. Neutron transport calculations are performed with MCNP5. Depletion calculations are performed using Monteburns 2.0, which utilizes ORIGEN 2.0 and MCNP5 to perform a burnup calculation. LNC supports many design parameters and is capable of performing a full 3D system simulation from initial startup to full burnup. It is able to iteratively search for coolant ^{6}Li enrichments and resulting material compositions that meet user defined performance criteria. LNC is utilized throughout this study for time dependent simulation of the LFFH engine.

Two additional methods were developed to improve the computation efficiency of LNC calculations. These methods, termed adaptive time stepping and adaptive mesh refinement were incorporated into a separate stand alone C++ library name the Adaptive Burnup Library (ABL). The ABL allows for other client codes to call and utilize its functionality. Adaptive time stepping is useful for automatically maximizing the size of the depletion time step while maintaining a desired level of accuracy. Adaptive meshing allows for analysis of fixed fuel configurations that would normally require a computationally burdensome number of depletion zones. Alternatively, Adaptive Mesh Refinement (AMR) adjusts the depletion zone size according to the variation in flux across the zone or fractional contribution to total absorption or fission.

A parametric analysis on a fully mixed fuel core was performed using the LNC and ABL code suites. The resulting system parameters are found to optimize performance metrics using a 20 MT DU fuel load with a 20% TRISO packing and a 300 μm kernel diameter operated with a fusion input power of 500 MW and a fission blanket gain of 4.0.

LFFH potentially offers a proliferation resistant technology relative to other nuclear energy systems primarily because of no need for fuel enrichment or reprocessing. A figure of merit of the material attractiveness is examined and it is found that the fuel is effectively contaminated to an unattractive level shortly after the system is started due to fission product and minor actinide build up.

Contents

List of Figures

List of Tables

Nomenclature

α	Alpha Particle or Helium Nucleus
$v\Sigma$	Interaction Frequency
σ	Cross Section
AMR	Adaptive Mesh Refinement
BOL	Beginning of Life
BOP	Balance of Plant Utilization
C/HM	Carbon-to-Heavy Metal
DOE	Department of Energy
DPA	Displacements Per Atom
DT	Deuterium-Tritium
DU	Depleted Uranium
FIMA	Fission of Initial Metal Atoms
flibe	The molten salt coolant 2LiF+BeF2
FOM	Figure of Merit
G	Target Gain
GNEP	Global Nuclear Energy Partnership
HEU	Highly Enriched Uranium
HSI	Hot Spot Ignition
IAEA	International Atomic Energy Agency

ICF	Inertial Confinement Fusion
IFE	Inertial Fusion Energy
IPCC	Intergovernmental Panel on Climate Change
MCNP	Monte Carlo N-Particle Transport Code
MFE	Magnetic Fusion Energy
MOX	Mixed Oxide
NES	Nuclear Energy System
NIF	National Ignition Facility
ODS	Oxide Dispersion Strengthened
PBR	Pebble Bed Reactor
PDF	Probability Distribution Function
PyC	Pyrolytic Carbon
SiC	Silicon Carbide
SNF	Spent Nuclear Fuel
SNM	Special Nuclear Material
SQ	Significant Quantity
T	Triton is an Isotope of Hydrogen
TBR	Tritium Breeding Ratio
wgPu	Weapons Grade Plutonium

Acknowledgments

The total number of people that influenced me during the course of this dissertation is too long to list, but I would like to thank them. I would like to begin by thanking them for their support, help in developing and running computer codes, and help in learning and understanding the physics necessary to complete this work.

I'd also like to thank those individuals that encouraged me to pursue a doctorate while at LLNL. They included Zig Jandrisevits, Mohammad Dehghani and Peter Raboin of LLNL. Their encouragement was instrumental in my decision to return to school and pursue this work. I also thank Richard Procassini for bringing me into his transport group at LLNL and encouraging me early in my studies. He first got me interested in neutron transport and saw me through the process of completing my coarse work and written examinations. I also thank my management at LLNL, Robert Ferencz, Sue Taylor, P. Derek Wapman, Ed Moses and Tomas Diaz De La Rubia, for their encouragement and support during this process.

Two individuals that were instrumental during my studies are the Nuclear Engineering Graduate Student Affairs Officer, Lisa Zemelman, and Lesa Christman of LLNL. They helped me navigate the every day hurdles of graduate school and ensured that I didn't get sidetracked. I sincerely appreciate their help with everything. I also thank everyone in the LLNL education office that helped me navigate the many hurdles of being an employee and student at the same time. Kathy Zobel, in particular, deserves my thanks.

I sincerely thank my dissertation committee for all their comments and continual support. My committee chair, Per Peterson, was instrumental in seeing me through the entire process. He provided excellent feedback on many areas of this work. Ehud Greenspan also provided useful and detailed suggestions on how to improve and complete my work. His insights into neutronics and fusion-fission hybrids were extremely valuable. Likewise, Todd LaPorte provided many insightful and stimulating ideas on how to better improve future efforts.

Many thanks to all of the LIFE team members for their support and comments. From the materials team including Joe Farmer and Magdalena Serrano de Caro, to the neutronics team including Massimiliano Fratoni, Jeff Seifried and Jeff Powers, to the engineering team, there are many people that influenced my work and I thank them. In particular, I'd like to thank Ryan Abbott for his effort on the mechanical design and willingness to help me when asked. The engine and plant mechanical designs are largely of his making. Likewise, Massimiliano Fratoni provided valuable advice on various areas of this dissertation. I found

discussions with him to be very enlightening and useful. Their input was invaluable in my research.

If there is one single person that I must thank, it is Jeffery Latkowski of LLNL. Jeff brought me onto the LIFE project. He mentored me through the process and supported me while doing my research. He served as an invaluable committee member and can be credited with many of the design innovations related to the LLNL effort as a whole. I can not thank him enough. I would not be where I am today without his help and support.

I also thank my family for their love, support and patience over the years. I thank my mother, Mary, for providing the moral support that saw me through to the finish. Likewise, I thank my brother and sister for all their encouragement. My wife, Lisa, and I met while I was working on my Ph.D. and she has seen me through this effort to the end. She supported me through many conversations when things were tough. Her excitement for me upon the successes throughout this work helped keep me going. I am truly blessed by my family and love them dearly.

Last, but not least, I thank my late father, Jim Kramer, for his love and support over the years. He always encouraged me to strive to be the best I could and to produce the best work I could. My dad passed away while I was pursuing this work and never got to see me finish. I miss him and dedicate this work to him.

Chapter 1

Introduction

"We simply must balance our demand for energy with our rapidly shrinking resources. By acting now we can control our future instead of letting the future control us." - Jimmy Carter -

1.1 Energy Resources

Energy in its various forms has been and continues to be the single most important resource available to humankind. Energy from the sun is used to grow food. Energy from a fire can be used to cook that food and forge the tools we take for granted every day. Energy is the single resource that allows us to grow, mine, extract and utilize every other resource used in society today. Our society depends on it so much that changes in the price of energy commodities, like fossil fuels, have huge ramifications on the world economy and many people's livelihoods. Since the Industrial Revolution, world energy supply and demand have grown virtually in lock step. As more countries advance and require more energy per capita, new sources of energy are produced. These new sources typically take the form of fossil fuel burning power plants, but nuclear, solar and wind power plants are beginning to play an increasing role. However, the future is uncertain because by some estimates our fossil fuels, like petroleum, are running out [1, 2, 3, 4, 5, 6, 7]. At some point, humanity will exhaust the world's fossil fuel supply and be forced to take one of two paths: significantly reduce energy consumption or produce energy (preferably renewable) from different means.

1.1.1 Future Energy Demand

World energy demand is continuously increasing and expected to grow by 44 percent from 2006 to 2030 [8]. In fact, even in current times, when a global recession dominates the news headlines, energy consumption is continuously growing. Energy demand is primarily

driven by population growth and an increasing consumption per person as countries like China, India and others further develop. Projections by the Energy Information Agency and current Intergovernmental Panel on Climate Change (IPCC) scenarios show that worldwide electric power demand is expected to double from its current level of about 2 TWe to 4 TWe by 2030 and could reach 8-10 TWe by 2100 [8, 9]. The principal question is whether supply will be able to keep pace.

1.1.2 Current and Future Energy Supply

It is expected that for the next 30 to 50 years, the bulk of electricity production demand will continue to be provided by fossil fuels such as coal and natural gas. Today, coal supplies 41% of the world's electric energy and is expected to supply 45% by 2030 [8]. At the same time, the most recent report from the IPCC has placed the likelihood at 90% that man-made sources of CO_2 emissions into the atmosphere are having a significant effect on the climate of planet earth [9]. The "business as usual" baseline scenarios show that CO_2 emissions could be almost two and a half times the current level by 2050. Clearly, new technologies and alternative sources of energy will be required as early as possible to meet the increasing energy demand in both the developed and the developing nations, while attempting to stabilize the concentration of CO_2 in the atmosphere and mitigate CO_2 induced climate change.

Current world and U.S. energy use is embodied in Figures 1.1 and 1.2[1]. Each major source of energy is identified in the left-most column. As can be seen from Figure 1.2, approximately 29 petajoules (PJ), or 73%, of U.S. energy production are derived from CO_2 producing, non-renewable petroleum, natural gas and coal resources. Likewise, worldwide energy use from non-renewable resources is slightly better at 148 PJ, or 65% of total use.

1.1.2.1 Coal and Natural Gas

The two largest contributors to worldwide CO_2 production are also the two largest sources of energy production, coal and natural gas. Worldwide use of gas and coal alone accounts for over 60% of net electricity production and is increasing. Contrary to that of petroleum reserves, a large supply of coal and natural gas is still available [8, 10, 11]. Worldwide, compared to all other fossil fuels, coal is considered the most abundant and is widely distributed across each of the continents. As of January 1, 2006, it is estimated that 930 billion short tons of reserves exist, which would last approximately 138 years given consumption rates at that time. However, there is some evidence to suggest that reserve estimates are overstated and must be re-evaluated [12].

[1] Courtesy A.J. Simon, Science and Technology Directorate, Lawrence Livermore National Laboratory, Livermore, CA

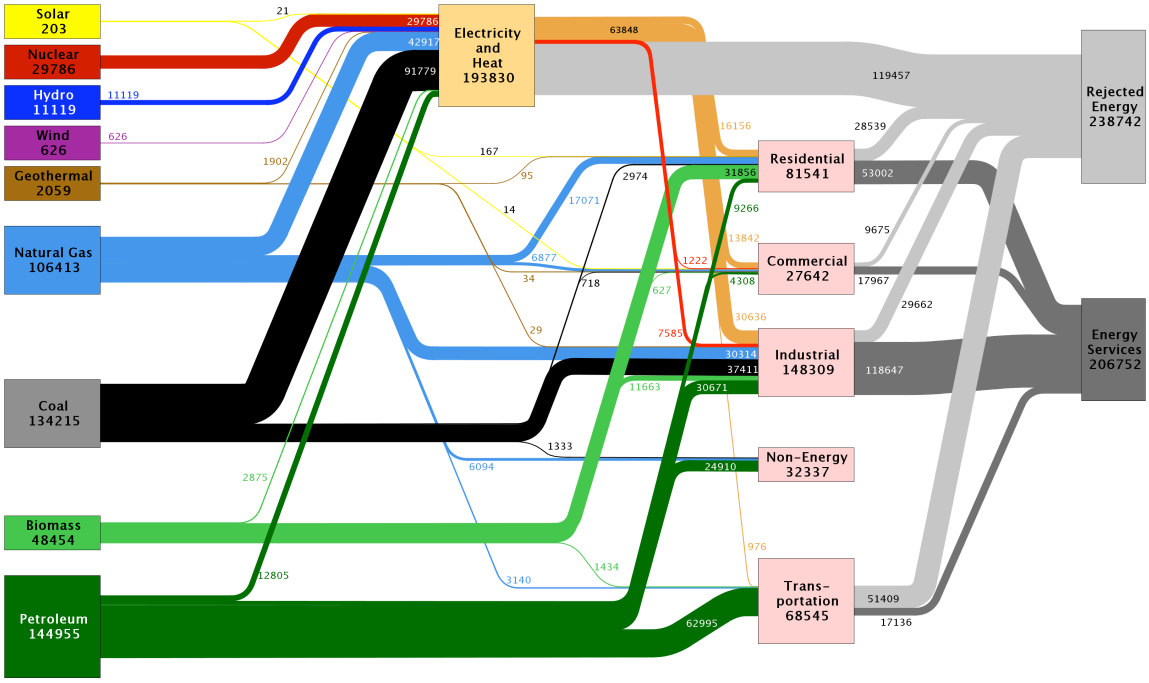

Figure 1.1: Current World Energy Production Broken Down by Type

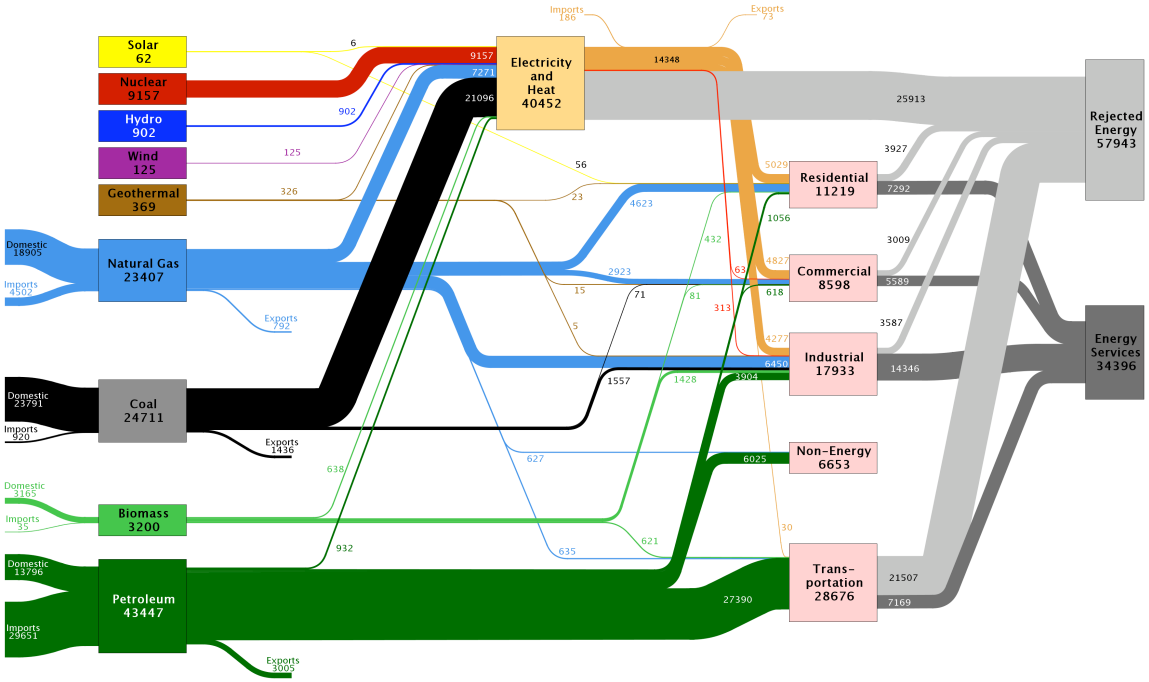

Figure 1.2: Current US Energy Production Broken Down by Type

1.1.2.2 Wind, Solar and Hydroelectric

Renewable energy sources like wind, solar and hydroelectric only account for < 3% and ~19% of net energy use in the U.S. and worldwide, respectively. Efforts to increase the use of these renewable technologies have often been stymied by a variety of issues surrounding each technology. For instance, the inconsistent and sometimes sporadic production times of wind and solar hamper their widespread adoption by utility companies. Likewise, limited availability of rivers to place hydroelectric dams at limit it's use to a small fraction of potential energy use. For these reasons, true renewable energy sources like these continue to be only a small fraction of energy production capability worldwide [7].

1.1.3 Nuclear Energy

Nuclear energy, a non-carbon emitting energy source and has been a key component of both the United States' and world's energy production since the 1960's. It currently accounts for about 13% of the world's electricity production, a fraction that could be increased [13]. Currently, the only nuclear energy systems that are used worldwide to produce power are based on fission, but the future holds promise of a cleaner and more effective solution, nuclear fusion.

1.1.3.1 Fission Energy

The mechanism by which typical fission can occur is illustrated in equation 1.1. Namely, a free neutron is captured by a fissile atom (uranium-235, plutonium-239, etc.). The resulting "neutron rich" atom is unstable and it splits apart into fission products and additional free neutrons (on average about 2.5 or more). When those neutrons reach new fissile atoms, the fission chain reaction continues. This chain reaction can continue until it is no longer sustainable due to either fission product poisoning, or some other mechanism that alters the criticality of the system.

$$n + {}^{235}_{92}U \rightarrow \left({}^{236}_{92}U^{*}\right) \rightarrow\sim 2.5n + fission\,reaction\,products. \tag{1.1}$$

Several factors make fission energy's long-term sustainability difficult. There are concerns associated with the risk of proliferation of nuclear materials and technologies, the generation of radioactive waste that requires burial in deep geological repositories, and the availability of low-cost uranium ore resource for the long term because of the current U.S. reliance on the once-through, open nuclear fuel cycle.

In the United States alone, the past and current fleet of nuclear reactors has generated approximately 55,000 metric tons (MT) of Spent Nuclear Fuel (SNF), and we will soon have enough SNF to fill the Yucca Mountain geological waste repository to its legislated limit of 70,000 MT. In general, uranium resource utilization is fairly poor for light water reactors. Current U.S. light water reactors are only able to burn the nuclear fuel to a

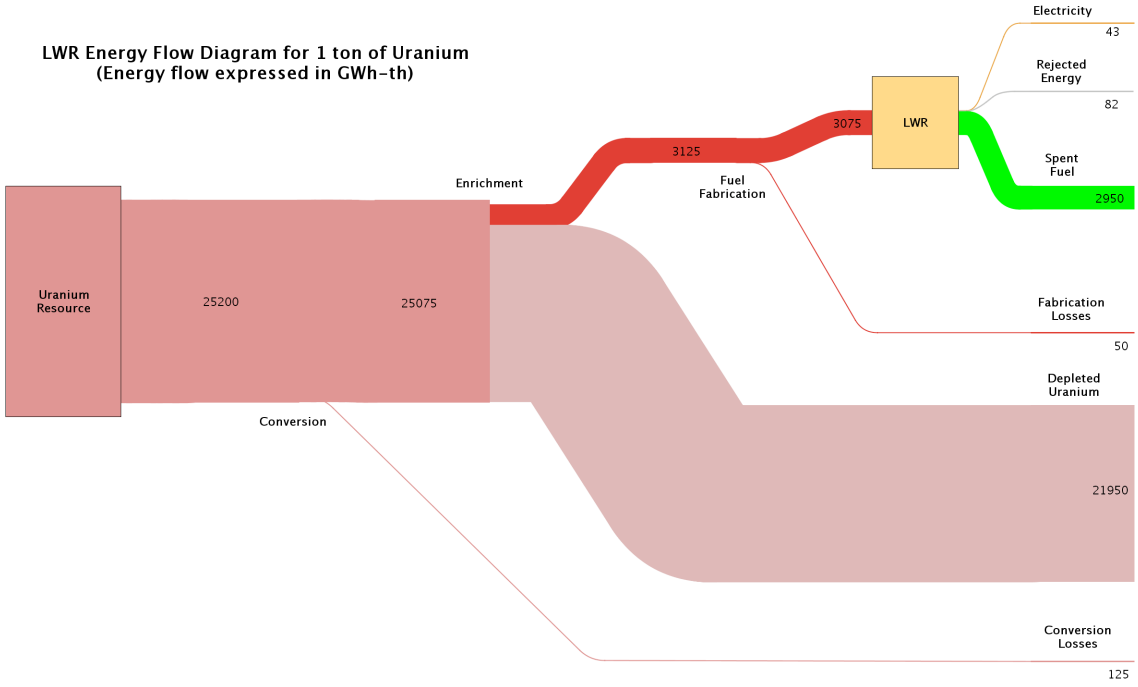

Figure 1.3: Uranium Resource Utilization by U.S. Light Water Reactor Fleet

maximum of approximately 3.5-10% Fission of Initial Metal Atoms (FIMA), but the overall utilization of the energy in the fuel is approximately 0.17%. For example, Figure 1.3 shows the energy use of 1 MT of Uranium as it is mined from the earth[2]. That initial 1 MT of uranium contains approximately 25,200 GWh-th of potential fission energy. 21,950 GWh-th of that available energy is discarded in the form of depleted uranium (DU). The remaining ~3,075 GWh-th is utilized by the LWR as enriched fuel. Of that, only 43 GWe is made available in the form of electricity. The vast majority of the available energy is stored in the form of DU and Spent Nuclear Fuel (SNF), or fuel that cannot be consumed by the reactor without further enrichment or reprocessing.

Various proposed advanced reactors [e.g., various candidates for the Global Nuclear Energy Partnership (GNEP)] might be employed to stretch existing uranium ore supplies, albeit with fuel reprocessing to remove fission product poisons. Also, it is likely that the systems will employ significantly higher fuel burnup over several fuel reprocessing cycles. The technology for some types of fuel reprocessing are well developed and used in other countries like France, but fuel reprocessing has not been used in the US because of cost, safety, and proliferation concerns. Reprocessing nuclear fuel after burn in a reactor is far

[2]Courtesy A.J. Simon, Science and Technology Directorate, Lawrence Livermore National Laboratory, Livermore, CA

more hazardous compared to initial fuel enrichment and compared to underwater transfer of spent-fuel rod bundles into nearby cooling ponds (current U.S. practice) [14, 15]. In addition, fuel cycles with frequent reprocessing might require large numbers of hot (recent from reactor burn) fuel shipments by truck and rail back and forth between reactors and reprocessing centers, and state permits for such transport are not in hand nor guaranteed in the United States. Nuclear energy options with various levels of required fuel reprocessing need to be considered, but the licensing of dispersed reprocessing and transport of hot fuel with adequate safeguards against fission product release and diversion (proliferation) are uncertain. Finally, uncertainties in future nuclear power cost, including both uranium ore cost and fuel reprocessing costs, remain a significant concern for nuclear power. This is true for new advanced reactor designs, or for large increases in LWRs as a possible 50-year bridge to a sustainable energy future. For these reasons, it is unlikely that nuclear fission power plants will overtake coal and gas as the energy production method of choice without significant external funding influences or policy changes.

1.1.3.2 Fusion Energy

Since the development of nuclear fusion weapons, humankind has searched for a way to control this seemingly limitless source of energy. Nuclear Fusion has long held the promise of clean, safe energy production with zero greenhouse gas emissions. Fusion power plants could be fueled by deuterium from sea water and open the world to a virtually limitless source of energy.

Fusion occurs when light nuclei, are joined. The process can only occur under extreme temperatures and pressures that allow such nuclei to overcome Coulomb repulsive forces [16]. In practice, the easiest fusion reaction to produce in the laboratory is deuterium and tritium as

$$D + T \rightarrow \alpha(3.5MeV) + n(14.1MeV). \tag{1.2}$$

For each DT fusion reaction, 17.6 MeV or 2.819×10^{-12} J is produced primarily in the form of kinetic energy of a fusion neutron and alpha particle. This may seem like a small amount, but fusion of 1 mole of fusion fuel every 10 minutes would release enough energy for a 1000 MWe power plant [17]. So much energy is released in a single fusion reaction that the fusion of a single mole of deuterium with a mole of tritium releases as much energy as combustion of almost 70 tons of coal [17]. In addition, fusion by-products can be better contained as opposed to the tons of CO_2 produced by a coal-fired power plant generating the same amount of energy. Although, in practice, it will be impossible to completely prevent any tritium release, fusion plants will have much lower release source terms for severe accidents than a fission plant.

Currently, three different methods of fusion plasma confinement are known: gravitational, magnetic and inertial. Gravitational confinement is the method that drives the sun and other stars. When a mass becomes large enough, gravitational forces become strong

enough to confine high temperature ions long enough to induce fusion. Obviously, gravitational confinement is not practical for terrestrial applications.

Magnetic fusion energy (MFE) has seen over five decades of research and development with good progress. MFE uses powerful magnetic fields to confine a low-density DT plasma and to generate the conditions required to sustain the burning plasma for a sufficiently long time to generate energy gain. However, the most likely facility to achieve break-even fusion (point where energy output exceeds energy input) is at least a decade away from fruition. This International Tokamak Experimental Reactor (ITER) machine, sited in France, has undergone numerous budget and schedule setbacks and the future of the project is unclear [18]. Even when ITER is built, it will require significant research and development to reach the point of technological and economic feasibility as a power plant.

Inertial Fusion Energy (IFE) has arguably not progressed as far as magnetic fusion. Reasons for the lack of progress on IFE include lack of funding and classification issues that, until the last two decades, have prevented most international collaboration on the subject. Even so, experiments carried out on the NOVA and OMEGA laser systems show promise and better understanding of the implosion physics occurring in an IFE target [19]. The successful completion of the National Ignition Facility (NIF) and experiments over the next 2-3 years should lay to rest any questions of the basic physics feasibility of Inertial Confinement Fusion (ICF) for IFE applications.

ICF and MFE fusion both continue to be explored as attractive energy options for the future [20, 21]. The current vision of ICF would use lasers, heavy ion beams, or pulsed power to rapidly compress a capsule containing a mixture of DT gas. As the capsule radius decreases and the DT gas density and temperature increase, DT fusion reactions are initiated in a small spot in the center of the compressed capsule. These DT fusion reactions generate both helium nuclei, or alpha particles, and 14.1-MeV neutrons. As the fusion burn front propagates, it generates significant energy gain [22].

The capability of lasers to create the conditions required for ignition and propagate thermonuclear burn in the laboratory with ICF is expected to be demonstrated on the the NIF, possibly a decade ahead of MFE experiments planned for the ITER facility under construction in Cadarache, France [23, 18]. The National Ignition Campaign (NIC) began in mid-2009 seeking ignition and modest target gain ~10 (G= fusion yield/laser energy) for laser energies of 1-1.3 MJ in FY 2010/2011. Ultimately fusion yields of 100 MJ are expected on the NIF. Successful demonstration of ignition and net energy gain will be a transforming event for inertial fusion and is likely to focus the world's attention on the possibility of IFE as a potential energy option.

The first experiments to demonstrate ignition and gain will use 350-nm laser light with a central hot spot ignition (HSI) target in an indirect drive configuration for which the scientific basis exists [24, 25]. The NIF ignition and burn experiments with HSI targets are expected to be successful. The target gains of the order of 100 that would be required for efficient, cost competitive power generation, with which HSI targets should ultimately be possible. However, the relatively large laser energies (> 4-5 MJ) and corresponding

fusion yields (> 400-500 MJ) are not likely to be compelling for pure inertial fusion energy systems.

1.1.3.3 Fission-Fusion Hybrids

Although the technological progress of fission systems is superior to that of fusion systems, the requirements for long term underground disposal of long-lived fission products, Pu and minor actinides continues to hamper widespread adoption across the United States. The current waste repository, Yucca Mountain, has been indefinitely postponed by politicians illustrating the challenges in dealing with nuclear waste, without reprocessing. [26].

IFE has made major advancements with the recent completion of the NIF and beginning of the NIC. Even so, IFE embodied as a pure fusion power plant is still decades away because of challenges associated with materials, fusion gain and target production. Difficulties in developing the large lasers and high gain fusion targets still require much development. As stated earlier, pure fusion is a panacea for energy production. However, technological challenges could hamper full adoption of fusion as an energy source alone.

To mitigate the challenges of nuclear energy and advance the time scale of the usefulness of fusion sources, Lawrence Livermore National Laboratory (LLNL), along with many University and national laboratory collaborators, is developing a concept for a fusion-fission engine that combines attractive aspects of nuclear fusion and fission. This approach, termed a Laser Fusion-Fission Hybrid, or simply LFFH, surrounds a relatively modest ICF neutron source with a spherical sub-critical fuel blanket. In a LFFH engine, the point source of fusion neutrons acts as a catalyst to drive the fission blanket, which obviates the need for a critical assembly to sustain the fission chain reaction. It is possible to show that starting from as little as 300 to 500 MW of fusion power, a single LFFH engine can generate 2,000 to 3,000 MWth in steady state for periods of years to decades, depending on the nuclear fuel and engine configuration. The source of 'external neutrons' drives the subcritical fission blanket and makes the various LFFH engines capable of burning any fertile or fissile nuclear material, including natural or depleted uranium (DU) and SNF. A LFFH engine can theoretically extract nearly 100% of the fission energy content of its fission fuel resulting in greatly enhanced energy generation per metric ton of nuclear fuel. The external source of neutrons also allows the LFFH engine to burn the initial fertile or fissile fuel to extremely high FIMA burnup without refueling or reprocessing, allowing for nuclear waste forms with significantly reduced concentrations of long-lived actinides per GWe-yr of electric energy produced.

LFFH engines thus could provide the ability to generate base-load electricity while greatly reducing the actinide content of any existing or future nuclear waste and extending the availability of low-cost nuclear fuels for thousands of years. LFFH also provides an attractive pathway for burning excess weapons Pu or HEU without the need for fabricating or reprocessing mixed oxide (MOX) fuels, as will be discussed later in Chapter 2. Because of all of these advantages, LFFH engines offer a pathway toward sustainable and safe nu-

clear power that potentially mitigates nuclear proliferation concerns and minimizes nuclear waste.

This is not to say this technology does not have its challenges to make a this concept work. LFFH engines will share many of the challenges associated with pure fusion systems like first wall survival, cooling and materials damage. Likewise, further advances in fuel and structural materials will be required as part of the LFFH development. Currently, no fuel form exists that can withstand the high burnups that are proposed in this work. Nevertheless, the LFFH concept could offer an alternative pathway sustainable nuclear energy.

Andrei Sakharov first discussed the idea of fusion-fission engines in the 1950s [27]. Hans Bethe and Nikolai Basov expanded on his ideas in the 1970s and 1980s, as did many other groups around the world [27, 28]. The focus of many of these studies was on the use of fusion neutrons to generate fuel for fast nuclear reactors, although Basov and others discussed the possibility of using laser-driven fusion targets to drive a fission blanket for generating commercial power. In addition, Greenspan and his colleagues suggested the idea of combining the benefits of fusion and fission to generate nuclear energy without enrichment and without solid fission products separation [29, 30, 31, 32]. Unfortunately, fusion-fission engines never advanced beyond the discussion stage mainly because powerful high-average-power lasers and other required technologies did not exist.

Alternatively, many proposals have also been made to use particle accelerators to generate neutrons that can then be used to transmute nuclear waste and generate electricity [33, 34]. Unfortunately, accelerator-based schemes never advanced past the conceptual study phase, in part because a complete nuclear fuel cycle including U enrichment and nuclear waste reprocessing was still required to generate economical electricity. As a result, the efficiency and cost of those systems proved to be prohibitive relative to the benefit of transmuting nuclear waste.

Today, however, advances at the NIF and other ICF facilities around the world are putting scientists and engineers close to demonstrating the physics and key technologies required to make LFFH a reality. In fact, with the appropriate research and development, LFFH engines could start providing electricity to U.S. consumers relatively soon and could provide a very significant fraction of U.S. and international electricity demand by 2100.

1.2 Scope and Purpose of current study

This study investigates the neutronics design and modeling aspects of the LFFH energy system. It explores the novel use of developed technologies in both the fusion and fission areas to produce nuclear energy using a closed fuel cycle as an alternative to existing nuclear, hydrocarbon-based or alternative energy power plants. The concept requires no reprocessing or enrichment of the fission fuel as the fusion driver breeds the necessary fissile material, while incinerating the fuel to the maximum burnup possible. The goals of this

study were specifically to model this hybrid fusion-fission system based on laser ICF for an energy production mission using a depleted uranium fuel. Although developing a fusion-fission hybrid system will require significant research and development in many areas like materials, target physics, lasers and engineering, the scope of this work focuses only on the neutronics aspects.

To accomplish this, multiple simulations of neutron transport and nuclear burnup as a function of time were performed. Since the goal is to develop a system that requires no enrichment or reprocessing of the fuel, power and burnup transients will exist as fissile fuel is produced and burned down in the fission blanket. At the same time, it is desired that the design be tritium self-sufficient, meaning it produces its own fusion fuel. To model this concept, existing Monte Carlo transport and depletion numerical methods can be used, but additional software and methods were required to control the system according to power, burnup or tritium inventory constraints.

This work is divided into three main aspects. The first is dedicated to the modeling methodologies that were developed to simulate various aspects of this system. Since this system is a new design, significant effort was put forth in developing new software codes and methods to simulate it. These methods rely on the the Monte Carlo and Matrix Exponential methods to guarantee high fidelity in modeling the geometry and accurately representing the multiple levels of heterogeneity in the fuel. This methodology work involved two parts where the required fidelity for the transport calculations and the fidelity for the depletion calculations are addressed in the first. Since this is a hybrid fusion-fission system, assumptions as to the required fidelity of the simulation models needed to be explored in an effort to balance computational speed with simulation accuracy. In addition, a new method to control the tritium production and engine power via burnable tritium producing isotopes in the system coolants is developed. Next, methods to dynamically adjust both time step and spatial zoning requirements for depletion calculations are discussed. These efforts culminated with the design and development of a new software program named the LFFH Nuclear Control (LNC) code and an Adaptive Burnup Library (ABL) together comprised of ~20,000 lines of C/C++ code, which integrates multiple separate physics packages to simulate and control the LFFH engine from initial startup to final shutdown.

The second major aspect of this work is focused directly on the LFFH neutronic design for a depleted uranium fuel by applying the developed tools and analyzing the results. Besides attainable burnup, many system parameters are studied, including thermal power and other performance metrics. The LNC code enabled a detailed time depended parametric study of the LFFH engine. Parameters explored included the multiple variables associated with the fission and multiplier blankets, as well as operational parameters.

The last part of this study focuses on the nonproliferation aspects of the LFFH engine design. The elimination of fuel enrichment and reprocessing somewhat alters the perceived notions of proliferation concerns related to this form of nuclear power. A material attractiveness figure of merit is used to form a basis for quantifying how proliferation resistant the LFFH system is relative to reprocessing alternatives.

This manuscript is organized in six chapters. Chapter 1 motivates the need for nuclear energy and as an introduction and background on fusion, fission and hybrids. Chapter 2 details the LFFH concept from a engineering perspective by giving a detailed overview of the design. Chapter 3 describes the physics models and methodologies utilized to study the LFFH system. New software developed to implement the control and simulation methods is also discussed here. Results for the simulation models are discussed in detail in Chapter 4. The full details of the neutronics design are also given with results and discussion. Following the detailed results, Chapter 5 focuses on the nonproliferation aspects of the LFFH concept and evaluates its proliferation resistance. Chapter 6 summarizes the achievements of this study and recommends future work for the effort.

Chapter 2

Laser Inertial Fusion-based Energy

"The science of today is the technology of tomorrow."

Dr. Edward Teller

2.1 Potential Missions

The LFFH concept began based on the fact that it is challenging to envision an efficient and economical pure fusion power plant. Many different types of fusion power plants have been envisioned in the past, but none of the designs ever developed beyond a paper study [17]. The LFFH could fulfill a suite of potential missions ranging from pure energy production, to destruction of spent nuclear fuel (SNF) or weapons grade fissile material via stockpile systems draw down. Ideally, a single point design could achieve each of these missions while only requiring the fuel to be changed. As will be discussed later, this is what partially motivates the LFFH neutronics engine design.

2.1.1 Energy Production

Pure fusion is the ultimate goal as an energy production mission. However, earlier discussed issues hamper its development. A LFFH can fulfill the energy production mission by placing lower requirements on the fusion yield with the lower yield being balanced by a multiplying fission blanket. In other words, energy gain in the fusion target yield can be traded for fission blanket gain. For example, a gain 200 fusion system could be replaced by a hybrid that achieves gain 20 from fusion and gain 10 from the fission blanket. Each would produce similar system thermal power. As discussed earlier in Figure 1.3, current LWR power plants only extract 43 GWh of energy in the form of electricity for every metric ton (MT) of uranium used (containing 25,200 GWh_{th} of energy). The energy production

mission embodied in Figure 2.1[1] illustrates how much additional energy could be extracted from existing uranium resources. In fact, if a LFFH engine were to utilize the depleted uranium discarded from an LWR, an additional 9,513 GWh_{th} of energy could theoretically be generated, a factor of ~220 improvement, assuming 99% burnup of the LFFH fuel. Alternatively, also shown in Figure2.1, if that original 1 MT of natural uranium were used in parallel with a LWR, and employing LFFH SNF burners, a full 10,835 GWh_{th} of energy could theoretically be extracted from the ore. The advantages of this approach are apparent.

2.1.2 Spent Nuclear Fuel Destruction

The current U.S. light water nuclear reactor fleet generates ~0.12 MT of spent nuclear fuel (SNF) for every 1 MT of Uranium, or ~94% of the original enriched fuel is discarded as high-level radioactive waste. This waste is currently stored on site in cooling ponds awaiting long-term storage in a deep burial waste repository. However, with the current administration's decision to stop all work on the Yucca Mountain project, long term disposition of spent nuclear fuel is again in question. Reprocessing the fuel into new fuel normally enriched to ∼4.5% for LWRs is also currently not supported by the administration or the public. As an alternative, SNF could serve as a potentially limitless source of fuel for a LFFH fleet to burn beyond the current 5% FIMA discharge burnup. In other words, one technology's waste could become a fuel for another. A LFFH has the ability to burn SNF because it is an externally-sourced subcritical system.

2.1.3 Weapons Material Destruction

Methods of weapons material disposition have historically included immobilization or recycling of the fissile weapons grade Pu (wgPu) or highly enriched uranium (HEU) [35]. Immobilization options include typically include vitrification in glass, ceramics or metals as a means of rendering the fissile material chemically inert. In the past, the National Academy of Sciences (NAS) argued that the immobilization options must meet three key objectives [36]:

- Minimize the risk of unauthorized parties obtaining the weapons material.
- Prevent the weapons materials from being reintroduced into the arsenals from which they came.
- Strengthen the international control mechanisms and incentives to ensure continued reduction and spread of nuclear weapons.

[1] Courtesy A.J. Simon, Science and Technology Directorate, Lawrence Livermore National Laboratory, Livermore, CA

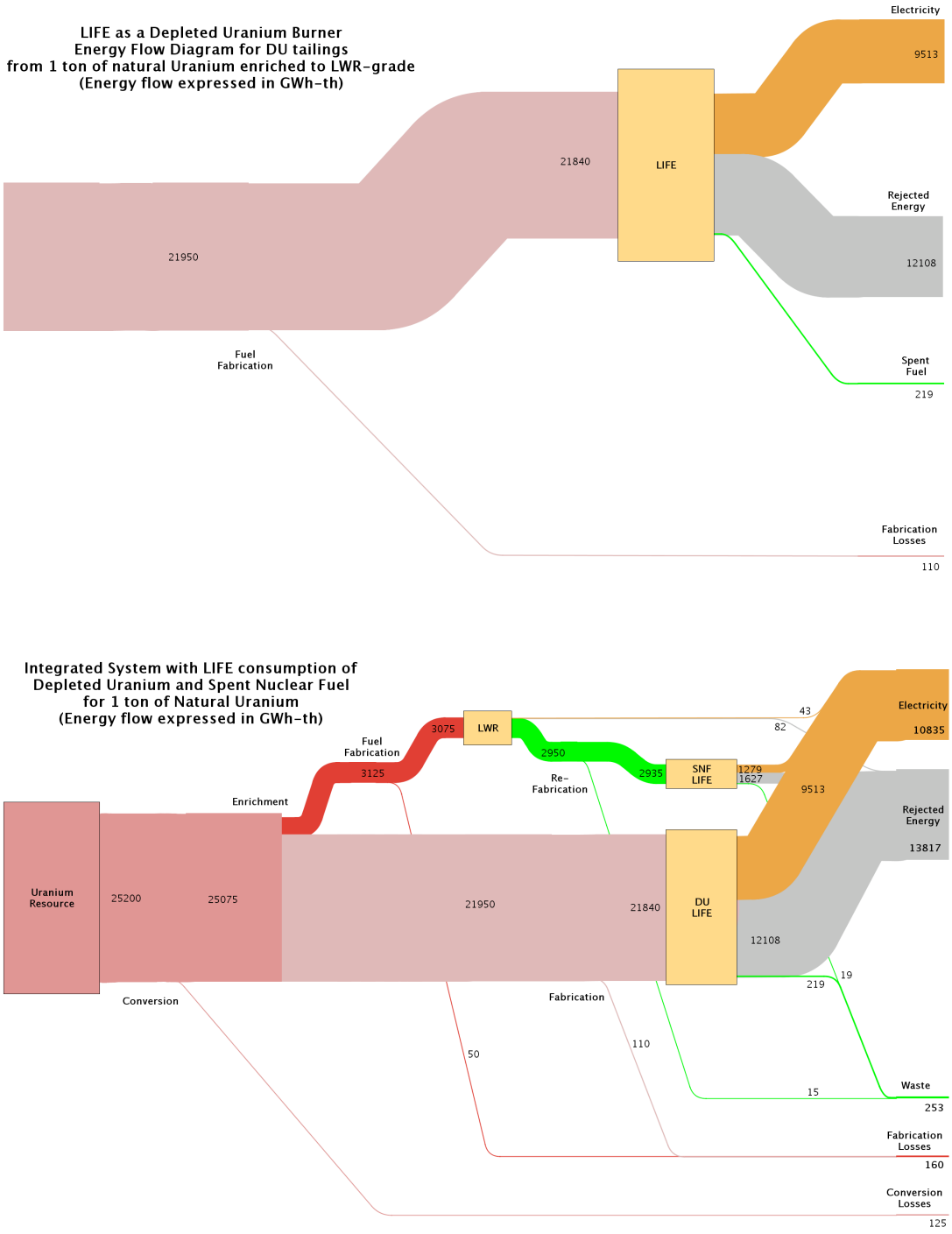

Figure 2.1: US Energy Utilization of 1 MT of Uranium in an LWR showing the majority of the available energy is wasted and how that energy could be recovered with LFFH plants.

The United Kingdom, France, Russia, India, Japan and China have begun using Mixed oxide or MOX fuel as a means of both disposing of weapons grade material and reprocessing fissile Pu and U from SNF. European countries have been fabricating MOX fuel for many years to supply commercial MOX-fueled light water reactors in France, the United Kingdom, Germany, Switzerland, and Belgium. Likewise, in the U.S., MOX fuel was fabricated and used in several commercial reactors in the 1970's as part of an early development program.

Two key facts remain. Immobilization requires long-term storage of weapons material with the more common SNF and adds to the waste problem. MOX fuel fabrication requires reprocessing technologies for SNF. The LFFH concept requires neither. LFFH would require re-fabrication of the fuel into a suitable mechanical package for use in the engine, but the isotopic quality would not be an issue. Likewise, the long-lived heavy metal waste produced by the LFFH plant would be reduced significantly as compared to a MOX fuel assembly because of the reactor requirement on fuel enrichment. For these reasons, LFFH could be an attractive option to burn wgPu or HEU in the future.

2.2 Design Goals

The vision of LFFH includes the deployment of LFFH plants around the world as a viable, clean source of energy for the 21st century and beyond [37]. With that in mind, A LFFH could fulfill multiple missions including nuclear waste incineration and energy production. As primary design criteria, six goals were initially set to govern the concept's nuclear design:

- Do not require fuel enrichment to operate.
- Do not require fuel reprocessing to completely dispose of the heavy metal, assuming a structural fuel material able to withstand the high irradiation levels can be developed.
- Remain subcritical at all times.
- Employ tritium self-sufficiency at each individual plant if physically and economically possible.
- Maximize the balance of plant utilization.
- Minimize proliferation concerns after the fuel has been delivered to the plant.

Each of these goals are applied to produce the system described in this work, but it should be noted that although these are the primary design goals, alternatives are also explored because different missions either raise or lower requirements for each goal. For instance,

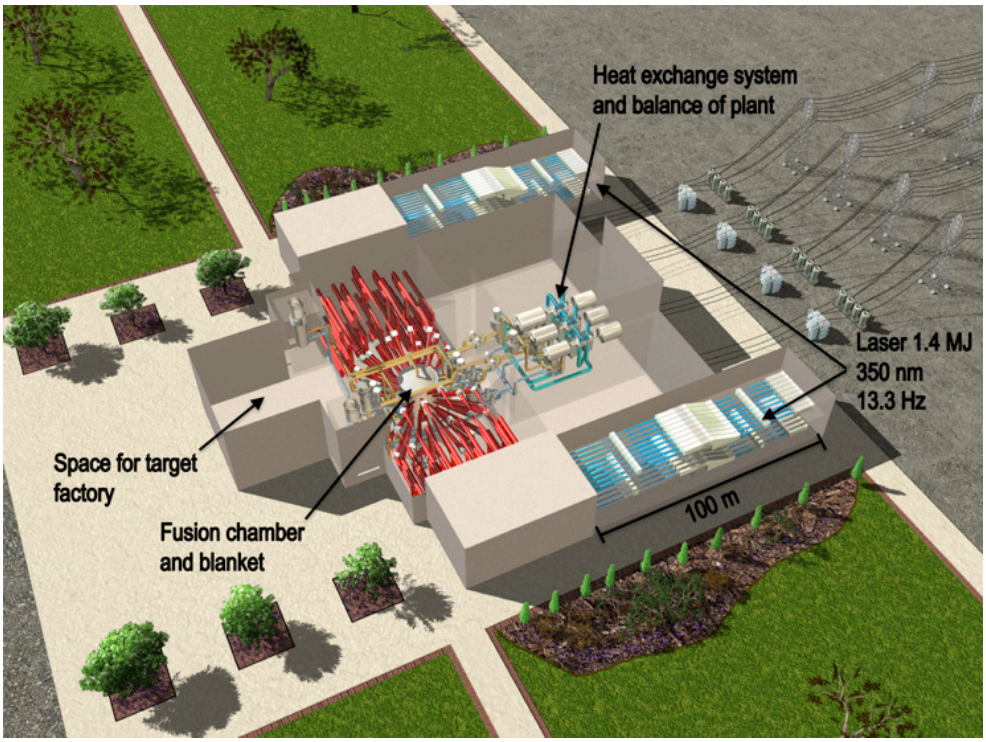

Figure 2.2: Artist's rendition of a LFFH power plant based on 35 MJ yield targets expected from hot-spot ignition targets similar to those used on NIF.

maximizing the balance of plant utilization for weapons material destruction is not as important as for commercial power production. It is quite possible that a state actor interested in destroying weapons material would be more interested in proliferation aspects instead of extracting electricity from the process. Likewise, tritium self-sufficiency may be relaxed if multiple plants are sited at the same location, which allows for tritium sharing amongst plants.

Given the early design goals focused on analyzing the physics of the LFFH concept, the resulting design tends towards a spherical design utilizing unproven materials and manufacturing techniques to satisfy those designs [37, 38]. The layout for a possible LFFH power plant is shown in Figure 2.2 [39]. An example of a baseline design is shown in Figure 2.3 where the chamber encompasses NIF-like hot spot illumination. A NIF-like illumination geometry is chosen to reduce the risk associated with successful ignition of two-sided illumination targets like fast ignition targets. The multipoint illumination concept will be demonstrated on NIF in 2010 and it is natural to attempt a LFFH design using the same illumination geometry. This reduces target design demands, additional structural design issues, etc. and is the basis of the design for which this manuscript describes.

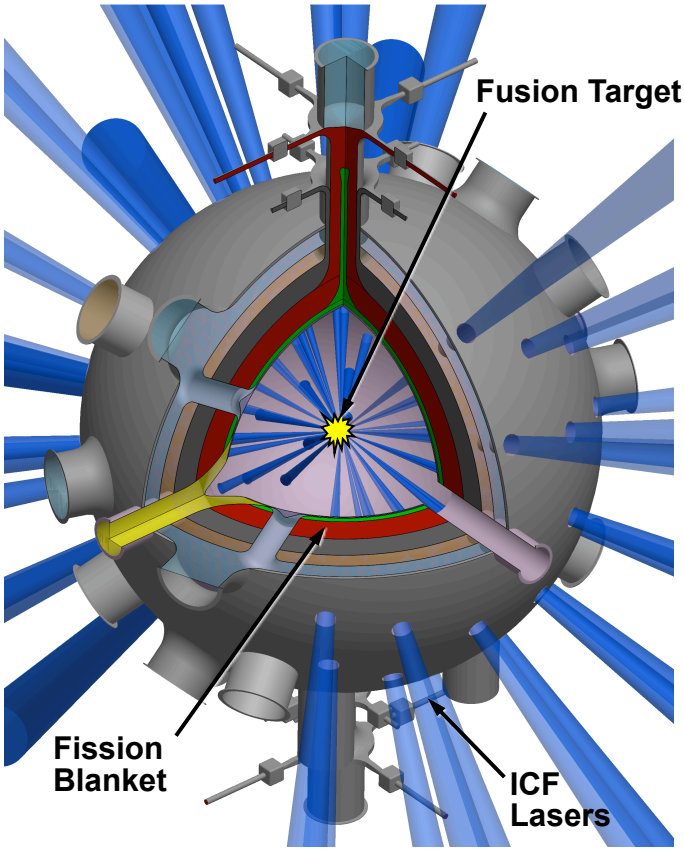

Figure 2.3: Overview of LFFH Engine

2.3 Nuclear Design Aspects

This manuscript focuses on the nuclear design aspects and simulation methods of the LFFH engine. The model described in this work utilizes a spherical design. In reality, any LFFH engine that would ultimately be built will employ a modular design to ensure easy replacement of damaged components in a minimal amount of time. However, since the nuclear engineering and physics will not change significantly, the spherical system is discussed.

2.3.1 System Overview and Introduction

Each primary component of the design is outlined in the following sections. A general overview of what the LFFH engine would look like is given in Figure 2.3. A central chamber encompasses the fusion targets as they burn. This chamber consists of multiple layers of structural, multiplying, moderating and fissionable materials. The chamber has holes throughout it located to allow for the lasers to enter and travel to target chamber center. The chamber is filled with low pressure inert gas that acts to stop most fusion born recoil ions and x-rays from reaching the first wall. Figure 2.4 shows a section view of the LFFH chamber and associated blankets. Beginning with the fusion target, neutrons, ions and x-rays stream outward towards the first wall. Most of the x-rays and ions are completely stopped in the background gas. Those that aren't deposit their energy on the first wall. Neutrons are not stopped by either the chamber gas or the first wall. They stream outward to the first wall coolant region consisting of a $Li_{17}Pb_{83}$ eutectic. It serves to multiply the neutrons via (n,xn) reactions and produce tritium via ^{6}Li(n,α)T reactions. Next, the neutrons travel through the beryllium pebble region, cooled by the molten salt $2LiF + BeF_2$ (flibe), where multiple scattering and (n,2n) reactions occur. The neutrons are effectively multiplied and moderated, or slowed down, in this region. Following the Be blanket, the neutrons encounter the actual fission blanket. It too is cooled by flibe. The remaining layers consist of a graphite pebble reflector bed, cooled by flibe, and a flibe extraction plenum. Each of the blanket layers is separated by a structural wall perforated to allow coolant to flow through it, with the exception of the $Li_{17}Pb_{83}$ plenum.

2.3.2 Fusion Target Design

The fusion target assumed for this study consists of a NIF-like hohlraum utilizing hot spot ignition (HSI) shown in Figure 2.5[2]. The expected target output is 37.5 MJ per target with a 13.33 Hz repetition rate to produce 500 MW of fusion. HSI targets in the indirect-drive configuration are currently being used for the first ignition demonstration on NIF. HSI relies on simultaneous compression and ignition of the spherical fuel capsule during implosion. In the indirect-drive configuration, the spherical DT-filled capsule is placed

[2]Courtesy LLNL

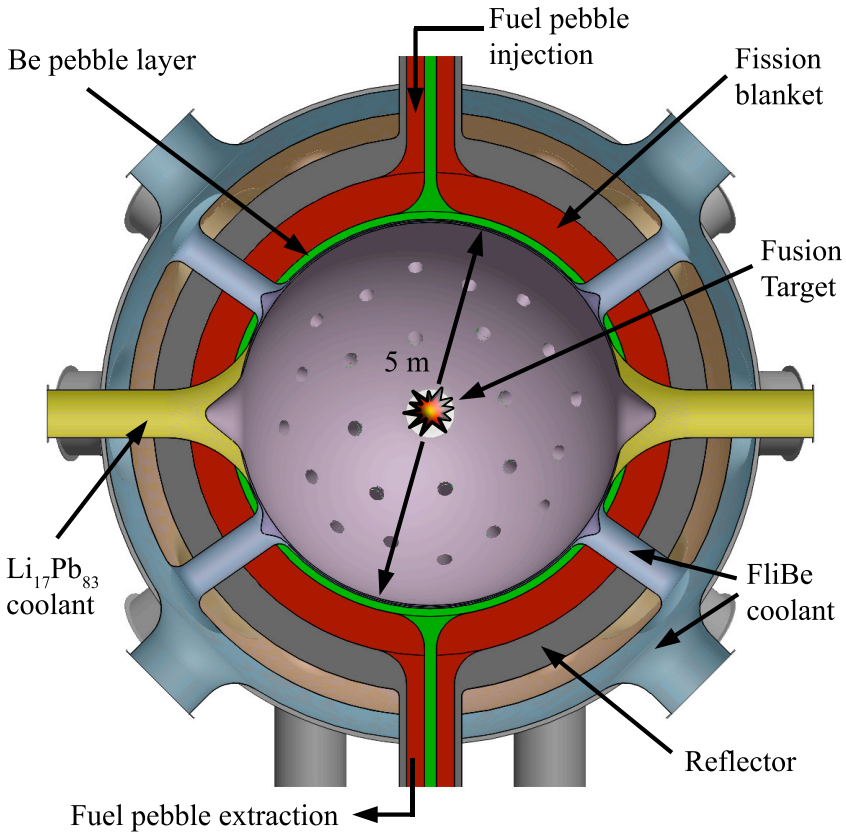

Figure 2.4: Early Design of LFFH Engine

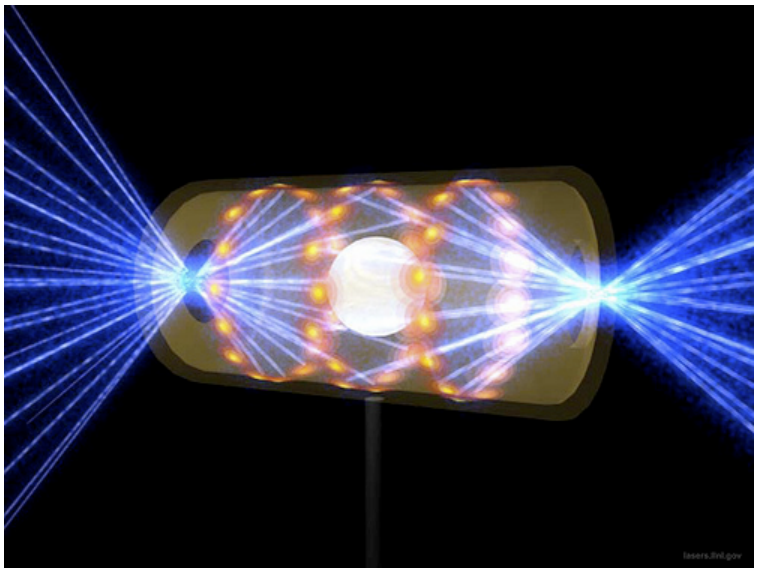

Figure 2.5: Example of NIF fusion target hohlraum with multiple beam illumination

inside a cylindrical cavity of a high-Z metal (a hohlraum), and the implosion pressure is provided by focusing the 350-nm NIF laser energy onto the interior walls of the hohlraum and converting it to x-rays as illustrated in Figure 2.5. The small (<1% of the total DT fuel mass), high-temperature central part of the imploded fuel ignites the cold, high-density portion of the fuel. This approach has a high probability of success, but requires a highly symmetric implosion configuration to maintain spherical symmetry in the imploding fuel to avoid mixing of the cold main fuel into the hot spot. Such a mix would quench the ignition process and places limits on the mass of DT fuel (and hence the fusion yield) per MJ of compression laser energy that can be assembled to the required conditions. Further details on the physics of ICF can be found in the literature [24, 25].

2.3.3 Buffer Gas

Inertial fusion chamber designs over the past 30 years have primarily focused on three first wall protection schemes. These options include thick and thin liquid protection and a low pressure gas [40, 41, 42]. The LFFH utilizes a low pressure inert gas at 5 μg/cc density. The target chamber and beam path will be filled with a mixture of argon, krypton and xenon gas. These gases will absorb the majority of the x-ray energy and stop essentially all ions emitted from the indirect-drive target within a few centimeters. The hot gas will then cool via radiation on a timescale sufficiently long (a few hundred µsec) to prevent damage to the tungsten first wall. Ideally, the gas density would simply be at atmospheric pressure. However, a low enough gas pressure is required prevent ionization of gas and development of a plasma as the laser beams converge on the fusion target. Too high of a gas density will

result in various plasma processes that scatter and reduce the laser energy arriving at the target [37, 43].

2.3.4 First Wall

The first wall is one of the most challenging components to successfully design in a fusion system. This is because the first wall is subjected to the highest neutron and x-ray fluence in the system. This presents many challenges to cooling and maintaining structural integrity in a high radiation environment. In fact, first wall survivability has been identified as one of the few major hurdles to pure fusion systems operating as power plants. The LFFH first wall is currently designed to withstand the high neutron and x-ray fluence by utilizing a thermal buffering material (tungsten) to mitigate x-ray temperature pulses and a high strength oxide dispersion strengthened (ODS) ferritic steel alloy that is potentially able to survive much higher damage rates than conventional structural materials. The ODS first wall is coated with a 250-500 μm tungsten layer that serves to absorb and smooth out the x-ray temperature pulse. Even so, estimates on material damage rates suggest the first wall will require frequent replacement approximately every 5-7 years [44].

2.3.5 $Li_{17}Pb_{83}$ First Wall Coolant

The first wall of the LFFH chamber is cooled by a $Li_{17}Pb_{83}$ coolant. This coolant was chosen based on experience in the fusion community suggesting it had excellent cooling and tritium breeding properties. First wall survival is a key issue with any fusion or fusion-fission hybrid because it is the first component subjected to the high x-ray, ion and neutron fluxes resulting from the fusion reactions. Consequently, care must be taken to adequately cool it.

2.3.6 Molten Salt Main Coolant

The main system coolant is flibe. This molten salt is chosen for its good cooling, tritium breeding and neutron multiplication properties relative to other coolants. Numerous fusion studies have identified flibe as a primary coolant because of its high heat capacity and ability to produce tritium. The use of two different coolants requires different flow paths throughout the system shown in Figure 2.6 [44]. The $Li_{17}Pb_{83}$ flows in a jacket around the first wall from the top injection point to the bottom removal point with a mass flow rate of 4.6 MT/s at 260°C. The flibe, identified in green, flows radially throughout the whole system from blanket to blanket and requires a high mass flow rate of 24 MT/s via 24 internal tubes having a 50 cm diameter.

For the LFFH system, multiple potential coolants are listed in table 2.1. The ideal coolant would be a low density liquid that would have a high heat capacity so it could carry heat away more effectively, able to maintain a high tritium breeding ratio (TBR) so that

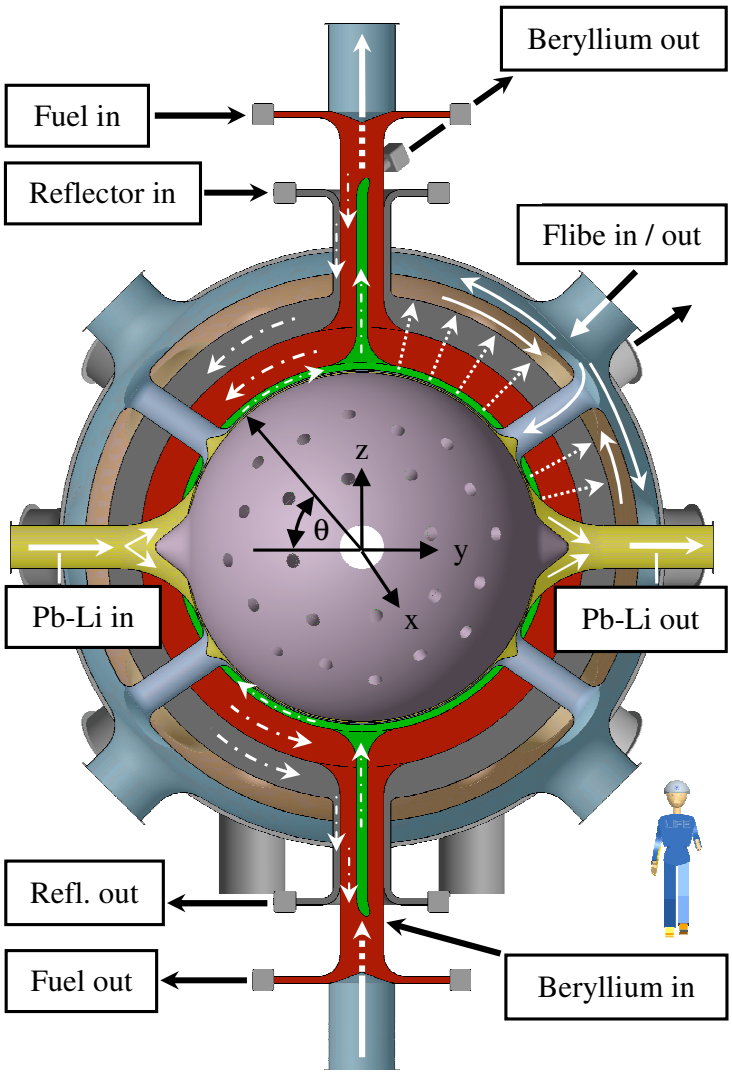

Figure 2.6: Coolant flow paths through LFFH engine.

the fusion fuel could be replenished and have a high moderating ratio to effectively slow neutrons down without absorbing them. The moderating ratio is a good measure of how well a material is able to moderate high energy neutrons down to lower energies (improves fission probability) without absorbing them and is defined as

$$Moderating\ ratio = \frac{\xi \Sigma_s}{\Sigma_a}, \tag{2.1}$$

where Σ_s and Σ_a are the macroscopic scattering and absorption cross sections and ξ is the average lethargy gain per collision. This average lethargy gain is a useful parameter that can quickly be used to calculate the number of collisions required to slow a neutron from an initial energy down to a lower energy. It can be calculated from

$$< \# >= \frac{\ln\left(\frac{E_i}{E_f}\right)}{\xi} \tag{2.2}$$

where E_i and E_f are the initial and final energies and ξ is defined as

$$\xi = 1 - \frac{(A-1)^2}{2A} \ln\left(\frac{A+1}{A-1}\right). \tag{2.3}$$

It can be seen from equation 2.3 that an isotope with a lower atomic mass is desired because this will result in higher lethargy gain per collision. Likewise, an isotope with a high scattering cross section and low absorption cross section is desirable to increase the moderating ratio. For the coolants examined in table 2.1, flibe is a chosen for its heat transfer, tritium production and moderating properties. It has a moderating power of 83 as compared to 6.8 for LiF+NaF+KF or 71 for H_20 [45]. Although other coolants like $Li_{17}Pb_{83}$ are desirable as well, the factor of $4\times$ increase in density and corresponding weight for a given volume makes it impractical to cool the entire system. Given the variety of coolant choices available, table 2.2 shows that even though other coolants like H_20 are superior moderators, they are simply too restricting by limiting the coolant operating temperature. For these reasons, flibe is chosen as the main coolant for the LFFH engine.

2.3.7 Beryllium Multiplier Layer

An equilibrium neutron balance in the system suggests that for each sourced neutron, one neutron must be absorbed by ^{6}Li to produce one triton. Likewise, one neutron must be absorbed by ^{238}U capture to produce a fissile ^{239}Pu atom and one neutron to induce fission. Although the average number of neutrons produced per fission event can exceed 3.0, the system is designed to remain subcritical. Since the total number of neutrons produced from fission will not be enough to sustain a chain reaction, the system is operated in a subcritical regime. Hence, a total number of three neutrons per sourced neutron are, on average,

Coolant	Density 700°C (g/cm^3)	Heat Capacity C_p (J/gK)	Vol. Heat Capacity 700°C (J/cm^3K)	Thermal Conductivity 700°C (W/mK)
LiF + NaF + KF	2.02	1.89	3.82	0.6-1.0
2LiF + BeF_2	1.94	2.8	4.54	1.0
$Li_{17}Pb_{83}$	8.8	0.19	1.64	21
Liquid Pb	10.16	0.16	1.7	16
Liquid Na	0/7	1.25	0.88	55
H_2O	1.0 @ 20 °C	4.18	4.18	0.58

Table 2.1: Main Coolant options for LFFH Engine

Coolant	Advantages	Disadvantages
LiF + NaF + KF	No Be, cheaper than flibe, similar properties to flibe	High melt temp, lower heat transfer than liquid metals
2LiF + BeF_2	Good moderator, chemically stable, high volumetric heat capacity, good neutron multiplier, good tritium producer	High melt temp, lower heat transfer than liquid metals
$Li_{17}Pb_{83}$	No Be (human safety issues and cost), good neutron multiplier	Weight exceeds allowable limits
Liquid Pb	Low melt temp, high thermal conductivity	Weight, no tritium breeding
Liquid Na	Very high thermal conductivity, low density, high heat capacity	Fire hazard, no tritium breeding, no neutron multiplication
H_2O	liquid at room temp, very good moderator, cheap and easy to work with	criticality issues, low operating temp, no tritium breeding, no neutron multiplication

Table 2.2: Advantages and Disadvantages of each coolant

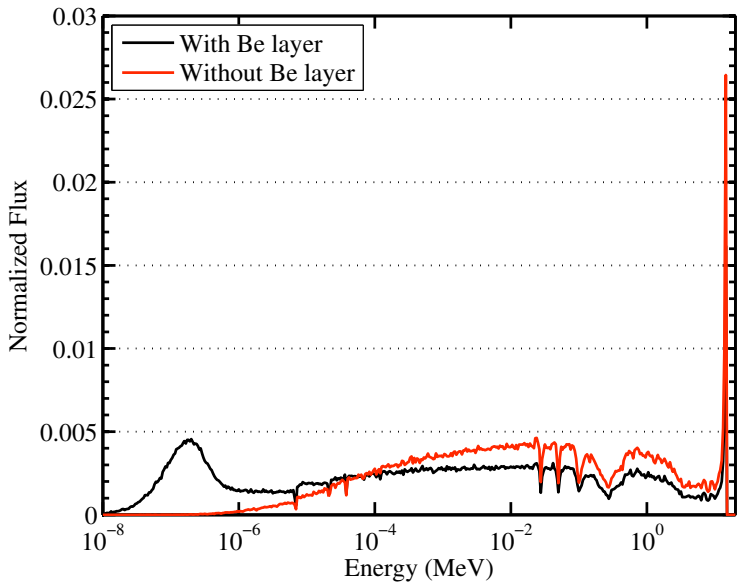

Figure 2.7: Neutron spectrum in fuel blanket region with and without Be pebble layer.

required to run the system in an equilibrium manner. This is difficult to achieve without a neutron multiplying media. Beryllium and lead are two very good neutron multipliers via (n,2n) and (n,3n) reactions. Lead has a high energy threshold of ∼8.5 MeV, whereas Be has a threshold of 1.8 MeV. The lower threshold energy allows for multiple (n,2n) reactions to occur from a single 14.1 MeV fusion neutron or even a high energy fission neutron. Beryllium also acts as an excellent neutron moderator. This can be seen in Figure 2.7 at the beginning of life (BOL). Significant thermalization of the neutron flux is achieved with the inclusion of Be pebbles and is advantageous for both producing and fissioning the fissile fuel. These are the primary reasons Be is chosen as the multiplying layer located radially directly inside of the fission fuel region. The Be is in the form of 1 cm diameter pebbles flowing through the system to allow for easy inspection and replacement.

Solid Be structures were studied, but discarded because of swelling and replacement issues. Be undergoes exothermic (n,2n) and (n,α) threshold reactions (approximately 2.7 and 1.4 MeV, respectively), which gives rise to significant amounts of He production. This He gas remains in the metal matrix and causes the material to swell. To combat this effect, the Be pebbles flow through the system over the course of less than 1 year and are periodically removed, heat treated and compressed to remove the He gas. To help prevent corrosion, the Be is encapsulated in an ODS ferritic steel layer that it is approximately 0.54% by volume of each pebble. The Be pebbles are cooled by flibe flowing radially throughout the system.

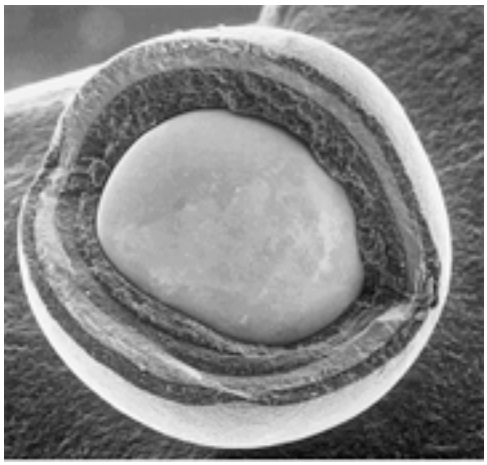

Figure 2.8: An Electron microscope image of a cracked TRISO particle to show each coating layer.

2.3.8 Fission Blanket

After moving radially outward passed the Be blanket, the flibe encounters the fission blanket where its primary cooling function resides. The use of a fission blanket with an external source of neutrons allows for, among other things, energy multiplication from the original neutron source. Fission is typically referred to as an *energy rich* process because $\sim$208 MeV is released per reaction as compared to 14.1 MeV for (D,T) fusion. Fusion is *neutron rich* because the majority of the energy from the reaction ($\sim$80%) is carried away in the form of kinetic energy of the neutron. The addition of a fission blanket to the LFFH engine helps multiply the fusion power by a factor of 4-10, depending on the design. The fission blanket can contain any type of fissionable fuel, albeit with different operating performance. For the purposes of this work, we only discuss a solid fuel form containing depleted uranium.

2.3.8.1 TRISO Fuel for Pebble Bed System

The baseline fuel examined in the LFFH engine consists of a modified Tristructural-isotropic (TRISO) fuel originally developed in Germany for high-temperature gas-cooled reactors. The fuel consists of a microsphere, or kernel, made of uranium-oxycarbide (UCO) and is encapsulated by four layers of isotropic materials. The layers are typically chemical vapor deposited coatings consisting of a porous carbon buffer, followed by a layer of dense pyrolytic carbon (PyC), followed by a ceramic layer of silicon carbide (SiC), followed by a final layer of PyC. An electron microscope image of a TRISO particle is shown in Figure 2.8. TRISO fuel particles are designed not to crack from differential thermal or fission gas pressure stresses at temperatures beyond 1600°C and can be expected not to fail under most extreme accident scenarios.

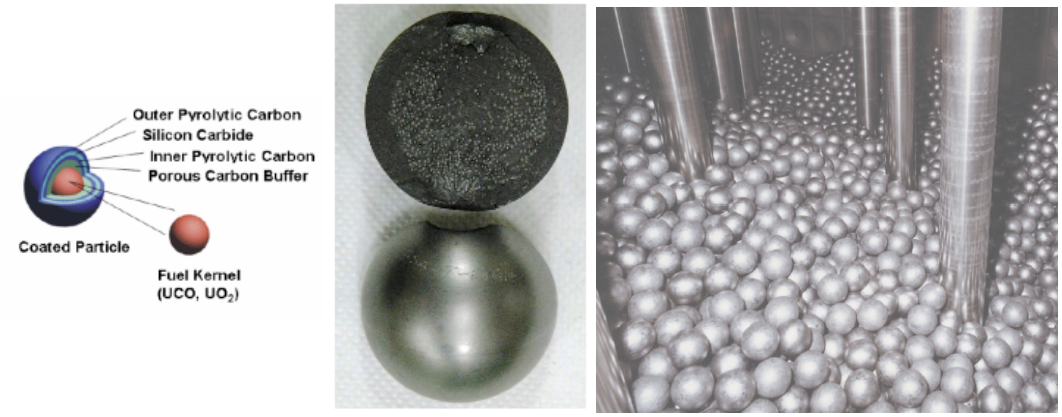

(a) TRISO particles packed in a fuel pebble (b) Fuel pebbles packed in a bed

Figure 2.9: Arrangement of the nuclear fuel in a reactor.

Each of the four surrounding layers provides a specific function in the design. The porous carbon buffer serves three main functions. First, it provides a recoil attenuation buffer from fission fragments to prevent direct kinetic energy transfer to the higher density layers. Second, it provides adequate void volume to contain fission gasses produced during the course of the burnup. Third, it accommodates dimensional changes due to kernel swelling and contraction of the outer coatings. The inner PyC layer surrounds the porous buffer to provide structural support against building fission gas pressure and creates a smooth bonding surface on which to deposit the SiC layer. It also protects the SiC layer from fission product chemical attack (palladium and lanthanides), as well as preventing other fission products from depositing on the SiC layer. The main function of the SiC layer is to serve as a pressure vessel. SiC has an extremely high yield strength and maintains it at high temperatures. Likewise, the SiC acts as a diffusion barrier to metallic fission products as they migrate out the kernel. The outer layer of PyC serves to structurally support the SiC, reduce tensile stress in the SiC after irradiation via layer shrinkage and acts as a final barrier to fission gas products should the SiC fail [46]. Additional details as to TRISO failure mechanisms are not discussed in detail in this manuscript, but can be found in the literature [47, 48, 46, 49, 50, 51, 52, 53, 54].

Multiple TRISO particles are packed into a pebble consisting of a graphite matrix surrounded by an outer ODS encapsulation. The number of TRISO particles contained in each pebble is a function of the packing fraction and pebble diameter. Figure 2.9a shows how the particles are packed into a fuel pebble. The particles are randomly dispersed in a graphite matrix with a typical packing fraction of 10% to 30% by volume. This design allows for neutrons to slow down in the graphite matrix as they escape from the fuel kernel. Likewise, Figure 2.9b shows those pebbles packed into a bed. Again, pebbles are randomly packed in the LFFH engine so the packing fraction within the coolant is not easily controllable.

Layer	Density [g/cm^3]	Outer radius [μm]
fuel kernel (UCO)	10.5	300
buffer layer (C)	1.10	402
high-density IPyC	1.95	407
SiC	3.20	497
high-density OPyc	1.95	500
Pebble matrix (C)	1.70	9,990
Pebble ODS layer	3.20	10,000

Table 2.3: Table of TRISO and fuel pebble properties

The theoretical packing fraction that the pebbles will flow through the system is 60% by volume.

The TRISO design utilized for the LFFH concept is considered altered because the layer dimensions were sized to accommodate higher burnup of the fuel kernels relevant to that system. In other words, the relative volume of kernel to surrounding layers can be adjusted to accommodate higher burnup and larger fission product gas production instead. Table 2.3 shows the TRISO design parameters utilized for this study. Details as to how these parameters were determined are discussed by Caro, et al. [55]. Comparisons between the LFFH modified TRISO design and that commonly discussed in the literature illustrates that our SiC layer is significantly thicker than typically used for high temperature reactors. This modification was made to accommodate larger gas pressure expected from higher fuel burnup.

2.3.9 Structural Materials

The LFFH engine contains multiple blanket and coolant layers weighing many MT. In addition, a high coolant outlet temperature of $\sim$650 $^{\circ}C$ is desired for high energy conversion efficiency. This implies that fuel pebbles directly in contact with the structural wall materials could be in excess of 900 $^{\circ}C$ and the structural material must maintain high strength at these temperatures [44]. Likewise, the high radiation environment severely limits the lifetime of many high temperature materials. For these reasons, ODS steel is chosen as the structural material for the engine. Its combination of high temperature strength and high resistance to radiation damage make it preferable to other structural materials [56, 57, 58, 59, 60, 61].

2.3.10 Reflector Design

In an effort to minimize neutron leakage from the engine, a flibe-cooled graphite pebble reflector is used. Graphite pebbles are chosen because they can flow through the system similar to the fuel and beryllium pebbles and be periodically inspected and replaced. Like-

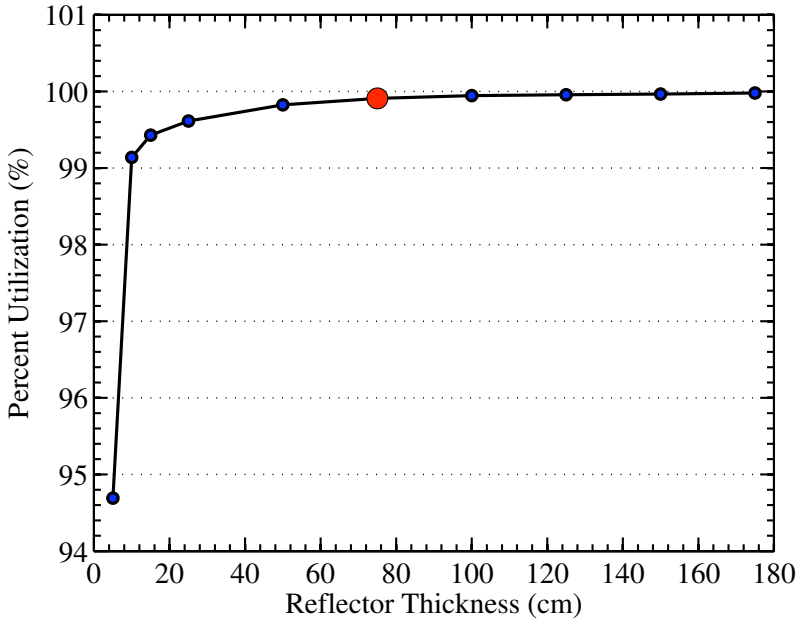

Figure 2.10: Neutron utilization (100.0 - % leakage) as a function of reflector thickness with chosen reflector thickness highlighted in red for system operated at startup.

wise, graphite offers a better medium through which neutrons could slow down and be scattered back into the fissile blanket region, as opposed to flibe alone. Using flibe alone results in direct absorption by ^{6}Li and yields fewer neutrons reflected back into the fission fuel blanket. Hence, the maximum random packing fraction of 60% is used for the graphite pebbles, cooled by the main flibe coolant.

The optimum reflector thickness was found to be 75 cm, based on parametric studies of different thicknesses ranging from 5 cm to 175 cm as shown in Figure 2.10. Namely, we seek to minimize the reflector thickness (to reduce overall material mass) while maintaining the minimum neutron leakage. Beyond 75 cm thickness, the reflector acts as an infinite reflector and the addition material does not improve the albedo.

2.4 LFFH Engine Operating Characteristics

The neutronics and burnup analyses encompass a variety of physics calculations, along with LFFH-specific control mechanisms discussed in further detail in Chapter 3. In the remaining sections, a brief overview of the system operation is provided to allow the reader a better understanding of the LFFH engine design aspects prior to detailed discussion of the methods and models. In doing so, a summary of the LFFH engine design and operating parameters is given in table 2.4. Key factors relating to blanket gain, fusion power and blanket dimensions for a baseline system are provided.

Design Parameter	Value
Thermal Power (MWth)	2,000
Fusion Yield (MWth)	500
Corresponding Fission Blanket Gain	4
Fission Blanket Heavy Metal Mass (MT)	20
First Wall Coolant	$Li_{17}Pb_{83}$
Primary Coolant	$2LiF + BeF_2$
First Wall Inner Radius (m)	2.5
TRISO packing fraction (%)	20
Fuel Pebble packing fraction (%)	60
Be multiplier thickness (cm)	16
Be pebble packing fraction (%)	60
Fission blanket thickness (cm)	74
Graphite reflector thickness (cm)	75
Graphite pebble packing (%)	60

Table 2.4: Baseline design parameters for LFFH engine design

2.4.1 Power flattening via ^{6}Li/^{7}Li Control

The LFFH engine relies on the fact that neutrons, provided by the fusion source, can be used to produce fissile ^{239}Pu from fertile ^{238}U, as well as to produce tritium, and fission that fuel. A representative engine initially loaded with 40 MT of DU fuel, contains very little fissile material (0.26% ^{235}U by mass). Without control, the thermal power would continue to rise until the Pu production and absorption rates equilibrate after about 12 years (solid curve Fig.2.11). Following peak Pu inventory, the system continues to produce and fission Pu over 4-5 decades. The Pu inventory falls with corresponding reduction in fission and total thermal power. This is unattractive primarily because of poor balance of plant (BOP) utilization defined later as the ratio of the average to the peak thermal powers. To improve this, we can reduce the fusion pulse repetition rate (rep-rate) to flatten the power curve over much of the system life (dashed curve in Fig. 2.11), but this results in laser under utilization. As an alternative, we can employ a control scheme using a time varying ^{6}Li/^{7}Li concentration in the flibe and $Li_{17}Pb_{83}$ coolants resulting in the dotted curve in Fig. 2.11. By increasing the ^{6}Li concentration early in time, excess tritium is produced and the thermal power is suppressed. This tritium is stored for later use, thereby allowing for increased thermal power late in time at the expense of tritium production. By adjusting the ^{6}Li enrichment over time, we can maintain a nearly constant thermal power of 2,000 MWth for almost 12 years longer than simply via laser rep-rate reduction. This technique allows the LFFH engine to reach 80-90% FIMA while at full power before the power falls due to either the exhaustion of stored tritium or depletion of the fertile and fissile materials. Once this occurs, a ramp-down and incineration period begins. At this time, the system can

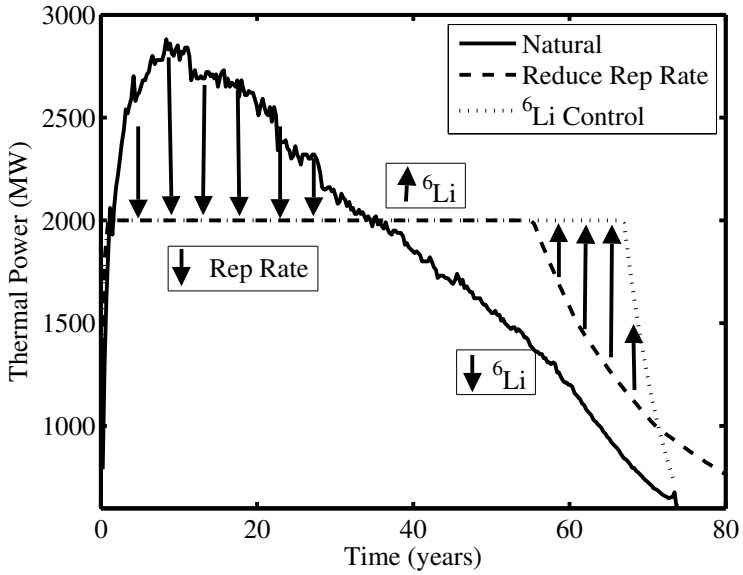

Figure 2.11: LFFH engine operation with TBR > 1.0, laser rep-rate control and ^{6}Li control

either be shut down, refueled, or allowed to incinerate the remaining actinides, albeit with a continuously decreasing thermal power output.

Although the economic implications of utilizing ^{6}Li depleted or enriched flibe has not been assessed for this system, multiple groups have explored various enrichment schemes including laser isotope separation [62, 63]. In practice, it has been suggested that this could be accomplished using multiple separate streams of depleted and natural flibe [64]. As the required enrichment in the LFFH engine changes, the mixture of these separate coolant streams would be adjusted. A detailed design and analysis of this system remains as future work.

2.4.2 Tritium Breeding Ratio

An example system generates the thermal power history shown in Fig. 2.12. The power ramp-up phase takes less than six months. Fissile production continues past this point, but the thermal power is controlled, via coolant ^{6}Li enrichment, to remain at 2,000 MWth for over 50 years with no fuel enrichment or reloading. During the fuel production phase, the TBR begins at 1.0, but rises up to a peak of $\sim$1.2, shown in Figure 2.13. During the years that the TBR exceeds 1.0, tritium storage is required. The TBR is allowed to fall over time so as to maintain the thermal power as the fissile production slows due to fertile depletion. This constant power is effectively maintained until the stored tritium inventory is exhausted. At that point, the tritium breeding ratio (TBR) is brought back to $\sim$1.0 (from $\sim$ 0.7) by increasing the ^{6}Li enrichment to approximately 52% in the $Li_{17}Pb_{83}$ and 1.1% in

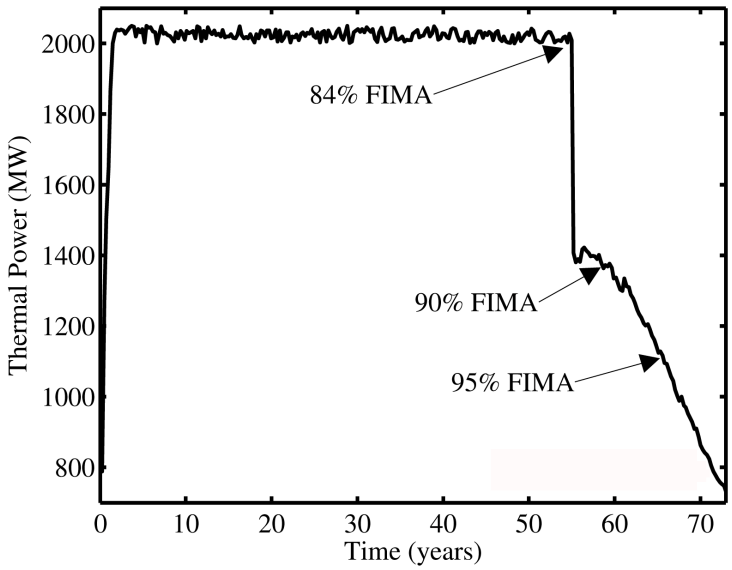

Figure 2.12: LFFH 2,000 MWth DU engine power vs. time

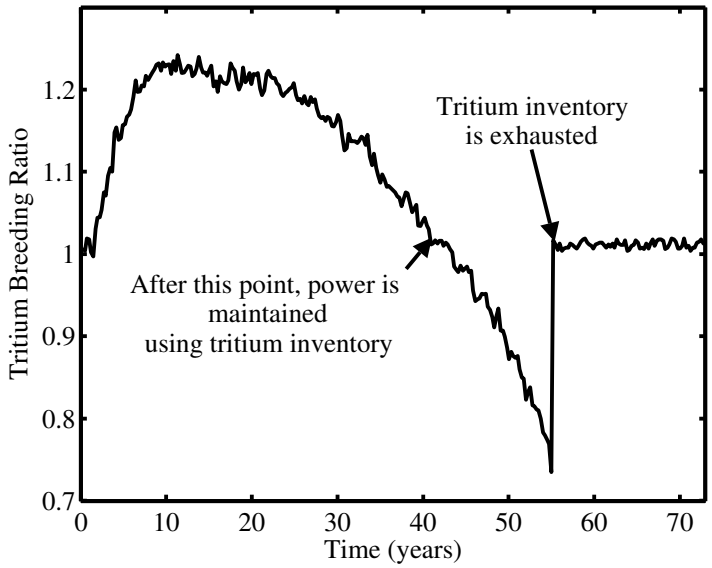

Figure 2.13: LFFH 2,000 MW_{th} DU LFFH engine TBR over time

the flibe. This ratio of coolant enrichments was found to offer the best performance. Doing so causes an immediate drop in system power from 2,000 MWth to approximately 1,400 MWth. The remaining time is used to incinerate the residual actinides to reach the desired burnup.

2.5 Summary

This hybrid concept and resulting power plant and engine designs are envisioned to fulfill multiple possible missions. The initial design presented keeps in mind the different missions by requiring little change to the design to fulfill a waste burning mission vs an energy production mission. To accommodate the various mission types, a TRISO-based fuel is chosen and the operational and design characteristics are altered to suit the mission of interest. An introduction to the engine design parameters and performance has been given to introduce the reader to the concept and motivate the work in the following chapters.

Chapter 3

Methodologies

The fundamental point in fabricating a chain reacting machine is of course to see to it that each fission produces a certain number of neutrons and some of these neutrons will again produce fission.

- Enrico Fermi -

3.1 Neutron Transport

Simulation of the LFFH engine include modeling fusion, fission, activation and depletion processes. To accurately model all of these physical processes, a number of different simulation methods and models are required. Simulation of the fusion neutrons as they traverse through the chamber materials and fission blanket requires multiple different models. Ideally, one would model the neutron, photon and charged particle transport throughout the engine and the reactions associated with collisions of various particles with atoms and molecules composing the materials inside the engine.

Particle transport, in general, is the simulation of how particles, charged or neutral, interact with surrounding materials. For the purposes of simulating the LFFH engine, focus is placed only on neutron and photon transport. This is justified by the fact that, charged particles generated from fusion and debris from the target hohlraum are stopped by the background gas quite readily and need not be tracked. Instead, their kinetic energy can be treated as a heating term in the background gas. However, neutrons and high energy photons travel through the gas and interact with the surrounding materials and must be modeled.

3.1.1 Fundamentals

When determining what happens inside of any nuclear system, the ultimate variable of interest is a particular reaction rate. In other words, how often does a reaction occur? This

can mean many things: the number of fissions occurring in a reactor, the number of capture reactions that produce fissile material, the number of scattering reactions resulting in material damage, and so on. The reaction rate is a function of the probability that a reaction will occur (reaction cross section) when an incident particle travels through a material. In the case of nuclear fission reactions, the fundamental particle of interest is the neutron and the distribution of those neutrons within a reactor. To determine the distribution of neutrons in a reactor, one must study the motion of the neutrons as they move throughout a region of fissile material via neutron transport.

At any point in a volume of fissile material, the *neutron density* $n(\mathbf{r},t)$ is defined by

$$n(\mathbf{r},t)d^3r \equiv expected\ number\ of\ neutrons\ in\ d^3r\ about\ r. \tag{3.1}$$

We wish to know the neutron density at any point in time and space because it allows us to calculate the rate of any nuclear reaction of interest. Likewise, we need the *interaction frequency* given by

$$\nu\Sigma = interaction\ frequency, \tag{3.2}$$

where ν is the speed of the particle and Σ is the macroscopic cross section of the reaction. This implies we can define the *reaction rate density RR*(**r**,t) at any point as

$$RR(\mathbf{r},t)d^3r \equiv \nu\Sigma n(\mathbf{r},t)d^3r. \tag{3.3}$$

The *reaction rate* is effectively the expected rate at which nuclear interactions occur in d^3r about r at any given time t. We can also extend the concept of *neutron density* to include the energy and angular dependence. In that case, we have

$$angular\ neutron\ density \equiv N(\mathbf{r},E,\hat{\Omega},t)d^3rdEd\hat{\Omega} \tag{3.4}$$

This is the expected number of neutrons in a given volume d^3r about r, at energy dE about E, moving in direction $d\hat{\Omega}$ about $\hat{\Omega}$ at time t. If we multiply the angular neutron density by the neutron speed v, we get the *angular neutron flux*, given by

$$\psi(\mathbf{r},E,\hat{\Omega},t) \equiv \nu N(\mathbf{r},E,\hat{\Omega},t). \tag{3.5}$$

The angular neutron flux is the fundamental quantity we seek to find throughout the LFFH engine core. Once the neutron flux is accurately determined, virtually any reaction rate of interest can be found. Of course, defining the neutron flux is insufficient. We must define an equation to describe the angular neutron flux as it evolves in space and time. To do so, we formulate the neutron transport equation.

3.1.2 The Neutron Transport Equation

This equation is a simplified form of the Boltzmann Transport Equation and its derivation can be found in any nuclear reactor physics textbook [45]. It is derived here in a shortened form to motivate the need for the tools described later in this chapter.

To derive it, we simply balance the various source and loss mechanisms by which neutrons are either produced or lost from the system. Given an arbitrary volume, the number of neutrons at a given energy dE about E, traveling in a direction $d\hat{\Omega}$ about $\hat{\Omega}$ within that volume is given by

$$\left[\int_V n(\mathbf{r},E,\hat{\Omega},t)d^3r\right] dEd\hat{\Omega}. \tag{3.6}$$

The time rate of change of this quantity is

$$\frac{\partial}{\partial t}\left[\int_V n(\mathbf{r},E,\hat{\Omega},t)d^3r\right] dEd\hat{\Omega}. \tag{3.7}$$

If the volume does not depend on time, then the integral can be reduced to

$$\left[\int_V \frac{\partial n}{\partial t}d^3r\right] dEd\hat{\Omega}. \tag{3.8}$$

The neutron flux can be determined by simply summing up the neutron sources and losses in a given volume. These sources and loses include:

1. External neutron sources (important for LFFH)
2. Neutrons streaming into the volume through a surface S
3. Neutrons scattered from energy E' and angle $\hat{\Omega}'$ via collisions into the E and $\hat{\Omega}$
4. Neutrons leaking out of the volume through surface S
5. Neutrons lost due to a collision with nuclei in the in the volume

Starting with the sources, the rate of neutrons appearing in a given volume is given by

$$(1)\int_V s(\mathbf{r},E,\hat{\Omega},t)d^3rdEd\hat{\Omega} \tag{3.9}$$

and is a function of position, energy angle and time. Likewise, the rate at which neutrons leak into or out of a volume through a surface S (items 2 and 4 above) can be written as

$$\mathbf{J}(\mathbf{r},E,\hat{\Omega},t)\cdot d\mathbf{S} = v\Omega n(\mathbf{r},E,\hat{\Omega},t)\cdot d\mathbf{S}, \tag{3.10}$$

where $\mathbf{J}(\mathbf{r},E,\Omega,t)$ is the neutron current through a differential surface $d\boldsymbol{S}$. Thus, leakage over the entire surface is

$$(2-4)\ \textit{Leakage into } S - \textit{Leakage out of } S = \int_S d\mathbf{S}\cdot v\hat{\Omega}n(\mathbf{r},E,\hat{\Omega},t). \tag{3.11}$$

Rewriting in terms of a volume integral and using Gauss's theorem, the leakage into or out of the volume becomes

$$\left[\int_S d\mathbf{S}\cdot v\hat{\Omega}n(\mathbf{r},E,\hat{\Omega},t)\right]dEd\Omega=\left[\int_V d^3r\bigtriangledown\cdot v\hat{\Omega}n(\mathbf{r},E,\hat{\Omega},t)\right]dEd\hat{\Omega}, \tag{3.12}$$

which can be rewritten via $\nabla\cdot v\hat{\Omega}=v\hat{\Omega}\cdot\nabla$ to

$$\left[\int_S d\mathbf{S}\cdot v\hat{\Omega}n(\mathbf{r},E,\hat{\Omega},t)\right]dEd\hat{\Omega}=\left[\int_V d^3rv\hat{\Omega}\cdot\nabla n(\mathbf{r},E,\hat{\Omega},t)\right]dEd\hat{\Omega}. \tag{3.13}$$

Neutrons scattered into the energy E and angle $\hat{\Omega}$ of interest, or *in-scattered* neutrons, are defined in terms of the *double-differential scattering* cross section and must be integrated over all E' and Ω' yielding

$$(3)\left[\int_V d^3r\int_{4\pi}d\hat{\Omega}'\int_0^\infty dE'v'\Sigma_s(E'\rightarrow E,\hat{\Omega}'\rightarrow\hat{\Omega})n(\mathbf{r},E',\hat{\Omega}',t)\right]dEd\hat{\Omega}. \tag{3.14}$$

Finally, the neutron loss rate due to collisions in a volume V is $v\Sigma_t(\mathbf{r},E)n(\mathbf{r},E,\hat{\Omega},t)$, where Σ_t is the *macroscopic total* cross section. The total collision rate over the whole volume can be integrated over V giving

$$(5)\left[\int_V v\Sigma_t(\mathbf{r},E)n(\mathbf{r},E,\hat{\Omega},t)d^3r\right]dEd\hat{\Omega}. \tag{3.15}$$

Summing each of the terms yields $(1+2-3-4-5)$

$$\begin{aligned}\left[\int_V d^3r\int_{4\pi}d\hat{\Omega}'\int_0^\infty dE'v'\Sigma_s(E'\rightarrow E,\hat{\Omega}'\rightarrow\hat{\Omega})n(\mathbf{r},E',\hat{\Omega}',t)\right]dEd\hat{\Omega}&\\ +\int_V s(\mathbf{r},E,\hat{\Omega},t)d^3rdEd\hat{\Omega}&\\ -\left[\int_V d^3r\bigtriangledown\cdot v\hat{\Omega}n(\mathbf{r},E,\hat{\Omega},t)\right]dEd\hat{\Omega}&\\ -\left[\int_V v\Sigma_t(\mathbf{r},E)n(\mathbf{r},E,\hat{\Omega},t)d^3r\right]dEd\hat{\Omega}=0.&\end{aligned} \tag{3.16}$$

However, this balance equation can be simplified by the fact that for any integral over a volume V, the integrand must be equal to zero for the integral to disappear as in,

$$\int_{anyV}d^3rf(\mathbf{r})=0\Rightarrow f(\mathbf{r})=0. \tag{3.17}$$

This implies equation 3.16 can be simplified to

$$\int_V d^3r \left[\int_{4\pi} d\hat{\Omega}' \int_0^\infty dE' \nu' \Sigma_s(E' \to E, \hat{\Omega}' \to \hat{\Omega}) n(\mathbf{r}, E', \hat{\Omega}', t) \right] dE d\hat{\Omega} \tag{3.18}$$
$$+ s(\mathbf{r}, E, \hat{\Omega}, t) dE d\hat{\Omega}$$
$$- \left[\bigtriangledown \cdot \nu \hat{\Omega} n(\mathbf{r}, E, \hat{\Omega}, t) \right] dE d\hat{\Omega}$$
$$- \left[\nu \Sigma_t(\mathbf{r}, E) n(\mathbf{r}, E, \hat{\Omega}, t) \right] dE d\hat{\Omega} = 0.$$

This is known as the *neutron transport equation*. This equation is so fundamental that the primary goal of any transport calculation is to solve this equation for the neutron flux (the equation is actually either angular or scalar). Once the neutron flux is determined, all quantities of interest can be determined. Unfortunately, it is a challenging equation to solve and generally for anything more than simple 1 dimensional problems requires a numerical method.

3.1.3 Monte Carlo Methods

Numerous methods have been developed over the years to solve the fundamental neutron transport equation. These methods have foundations in two families of numerical methods, deterministic and stochastic. Deterministic methods seek to solve the neutron transport equation in a closed form solution. Perhaps the most common, discrete ordinates, solves the transport equation for average particle behavior. Stochastic methods, however, seek to solve the transport equation via statistical approximations to the true solution. Monte Carlo method, for instance, simulates the behavior of each individual particle in the system and then the average behavior is inferred using the central limit theorem.

The discrete ordinates (Sn) method utilizes the concept of a phase space (position, energy, angle, etc.) divided into many small boxes, and the particles move from one box to another. As the boxes get progressively smaller, particles moving from box to box take a differential amount of time to move a differential distance in space. In the limit, this approaches the integro-differential transport equation, which has derivatives in space and time. Monte Carlo, however, transports particles between events that are separated in space and time. The distance a particle must travel before the next event is randomly sampled from a variety of probability distribution functions (PDFs), unlike deterministic methods.

Monte Carlo can be used to solve complicated three-dimensional, time-dependent problems. Sn must use fine enough resolution of the phase space boxes to accurately approximate the transport equation and becomes extremely memory intensive due to large arrays that must be stored. In contrast, Monte Carlo method there are no averaging approximations required in space, energy, and time because there are no phase space boxes. This is especially important in allowing detailed representation of all aspects of physical data. Both families of methods are in common use today in the form of a variety of codes [65, 66, 67, 68, 69].

Monte Carlo method was first invented by John von Neumann while at Los Alamos National Laboratory in the early 1940's [70]. This method is highly accurate with essentially no approximations, but very computationally expensive. In the past, it was often considered the method of last resort. However, recent advances in computing capabilities have brought Monte Carlo codes to even the desktop PC and it is quickly becoming the solution method of choice for many particle transport problems. Monte Carlo can be used to theoretically predict a statistical process and is most useful for complex problems that cannot be modeled by deterministic methods. The probabilistic events that comprise a process are simulated sequentially and are considered *Markovian* [71]. The statistical sampling is based on the selection of random numbers, analogous to throwing dice, hence giving the name Monte Carlo. In particle transport, the Monte Carlo technique is a realistic numerical experiment. Each of many particles from a source are followed, or tracked, throughout its life to its death in some terminal category like absorption, escape, etc. To determine when and where an event occurs, probability distributions are randomly sampled to determine the outcome at each step of its life.

3.1.3.1 The Monte Carlo N-Particle Transport (MCNP) Code

The Monte Carlo N-Particle Transport (MCNP) code is a general-purpose, continuous-energy, time-dependent coupled neutron and charged particle transport code. It supports a a variety of physics calculations and geometric capabilities not found in other software packages [72]. Von Neuman's work directly led to the development of MCNP at Los Alamos. That national laboratory has, in the 60 years since, continued to actively develop MCNP such that it is considered a gold standard of transport codes. MCNP is utilized for all transport calculations throughout this work.

3.1.3.2 Basic Assumptions

When implementing Monte Carlo method in a numerical code, a few assumptions and simplifications are made to the solution. The simplifications need not be made to solve the transport equation, but generally result in highly accurate results regardless.

The first assumption made is that the medium through which the particles are transported though is static. This is typically the case for virtually all transport problems. If a material changes over a cell, the cell is usually broken up into smaller and smaller cells to ensure a uniform and homogeneous medium. Otherwise, cross sections would become a function of position $\boldsymbol{r}$ instead of just the isotope(s) that the material consists of. Likewise, it is assumed that material properties are not affected by particle reactions. For instance, the material's scattering cross section is not changed by a scattering event with a neutron. In reality, a material composition does change over time as reactions occur. However, this is accounted for in the depletion calculation (section 3.2) and is typically not occurring at a high enough rate to warrant material composition changes during the solution of the trans-

port equation. Third, particles (neutrons) do not interact with each other. This assumption is based on the fact that the neutron-neutron interaction rate is very small compared to the other neutron interactions with the background material. This assumption is pervasive in all numerical methods applied to solve the neutron transport equation because equation 3.18 in its current form contains no information about interactions between neutrons. Likewise, Monte Carlo method assumes *Markovian* statistics meaning that the probabilities of a reaction event occurring are due only to the neutron's current position, velocity and energy. It does not depend on previous events. This assumption is valid until one begins to resolve reactions on a quantum level because information about previous events is not "remembered" by the neutron. Quantum mechanics tells us that all particles exist as waves and exhibit particle-like properties under most conditions. Although some advanced cross section generation codes account for quantum mechanical effects, these effects generally are ignored when utilizing Monte Carlo method to solve the transport equation. The justification is that the Debroglie wavelength of the neutron is so small due to its high energy that it can be treated as a particle.

Beyond the above assumptions, three simplifications are generally made. First, the transport is most often treated as time independent. Temporal effects are usually not needed because the flux is not changing rapidly enough to warrant it. Likewise, relativistic effects are neglected. Now if one where simulating protons in a collider, these effects could not be ignored. Yet, most neutron transport problems consist of a stationary geometry with neutrons moving throughout that geometry, non-relativistically. After all, a 14 MeV neutron born from fusion is moving at an average speed of 5.17×10^7 m/s, which is 17% of the speed of light. Typically, a Lorentz transformation is not needed until the particle is traveling closer to the speed of light. Lastly, long-range forces are ignored like gravity, etc. This means that the particles travel in straight lines and are not deflected by forces outside the media through which the particles are transporting moving.

3.1.3.3 Solution Method

Monte Carlo method relies the notion of random sampling. It is important to note that software codes like MCNP do not directly solve equation 3.18. Instead, as particles are simulated and tracked from the source to their final absorption or leakage point, each event is modeled by sampling a from a PDF. The full sequence of events for a particle including the source location, particle energy and direction, scattering angles, track length distances between collisions, absorption probabilities, etc. is considered a history.

MCNP, as with all Monte Carlo codes, can be broken down into multiple code subroutines that define and calculate the source parameters, distance to the next collision, type of collision and termination event [73]. Source parameters are used to define the source distribution using either correlated or uncorrelated PDF's. PDF's are sampled for the particle type, the source location in 3 dimensional space, the energy of the particle, the angular distribution (used to determine velocity vector) and, for time dependent problems, the time of

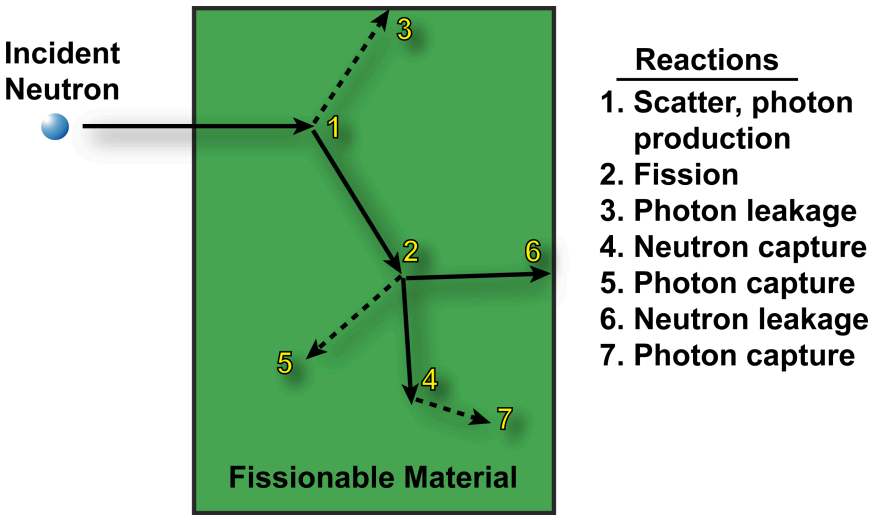

Figure 3.1: An example neutron history showing multiple photon and neutron production paths

particle creation. After each PDF is sampled, the source particle is completely defined and tracking can begin. The tracking of particles consists of evaluating the distance to the next collision and the distance to the next geometric zone. The shorter of the two determines the next event with the distance to the next collision allowing for multiple collision types (scatter, absorption, fission). The determination of which type of collision is a function of the particle type, energy and background material's cross section. The reaction cross section of a material is effectively a probability of the event. After a collision occurs, the outgoing particle(s) properties must be found. This is done by calculation reaction physics parameters and sampling scattering angle distributions [73]. Ultimately, after a particle has undergone multiple collisions and perhaps traversed through many cells, the particle history will terminate. In analog Monte Carlo method, termination means either escape or absorption by the surrounding material. Absorption can be followed by the generation of an addition photon to track, but either way, the neutron is no longer tracked. After all particles, both primary and secondary neutrons and photons, for the current history are terminated, the next history is started and the process continues. Figure 3.1 shows an example neutron history as it is tracked through a fissionable material. Each history is carried out independent of the others by sampling from PDF for each event. Multiple histories are combined and averaged via superposition to produce an expected result. More detailed mechanics of MCNP are not discussed in this work, but can be found in multiple references on the subject [65, 74, 75, 76].

3.2 Nuclide Depletion and Activation

Nuclide inventories are determined by depletion and activation calculations throughout the system. Depletion is the term used to refer to transmutation reactions resulting in a fission product of lower Z number. Activation is the process of altering the stable isotopes, structural materials for example, into unstable and stable isotopes that will radioactively decay. Both processes entail similar physical nuclear reactions and are correspondingly found using similar software codes. When we are interested in depleting the fission fuel, it is considered a burnup calculation because we are reducing the available fuel through the fission process. Burnup calculations typically involve the determination of the neutron flux in a fissile or fissionable material. Then that flux is used to calculate reaction rates of fission and absorption. Those reaction rates are used to solve for the new material compositions and the process repeated.

3.2.1 Monteburns

As computational power has increased over the years, the use of Monte Carlo methods to perform burnup calculations has gained popularity. Advantages include the ability to represent the fuel and structural geometry exactly and the ability to perform continuous energy transport, while performing simplified burnup calculations.

The software programs, or codes, used for the radioactive decay and burnup analyses in this manuscript are ORIGEN2 and Monteburns [77, 78]. Monteburns 2.0 is a software code developed by Poston and Trellue at Los Alamos National Laboratory to serve as a controller and linker code for MCNP and ORIGEN2. It is specifically designed to transfer one-group effective cross-sections and fluxes from MCNP to ORIGEN2 and transfer back the resulting material compositions from ORIGEN2 to MCNP. Monteburns simplifies the otherwise tedious process of parsing MCNP output for use in ORIGEN2 because the cyclic data transfer process is completely automatic.

Monteburns typically performs multiple MCNP and ORIGEN calculations for each time step. The number of each is dependent on user input. Time steps in Monteburns are referred to as outer burn steps to signify the outermost time step in the cycle and sub-cycling scheme.

3.2.2 ORIGEN2 and Matrix Exponential

As previously mentioned, ORIGEN2 performs the radioactive decay and the generation or depletion of all isotopes tracked in the simulation. It was originally developed by Croff in the early 1980's at Oak Ridge National Laboratory (ORNL). A sustained effort by ORNL to update the earlier version and its associated databases, simply called ORIGEN, resulted in a robust and useful package that is still used today [79, 80].

Nuclide inventories are found by solution of a stiff system of first order ordinary differential equations know as the Bateman equations [81]. Solution of the transmutation solutions for radioactive decay schemes involving a particle flux adds complexity, but a number of methods have been developed to solve this system of differential equations including linear chain, transmutation trajectory analysis, and the matrix exponential methods [82, 83, 84, 85]. The Matrix Exponential method begins with the solution of an equation defining the rate at which nuclides are transmuted.

The rate at which a nuclide is created or destroyed can be written as

$$\frac{dN_i}{dt} = F_i + \phi \sum_{k=1}^{n} f_{ik}\sigma_k N_k + \sum_{j=1}^{n} l_{ji}\lambda_j N_j - (\lambda_i + \sigma_i\phi + R_i)N_i,\ i = 1,2,3....n \tag{3.19}$$

where:
N_i = atom density of nuclide i,
N_k = atom density of a parent nuclide k that can produce nuclide i via transmutation,
N_j = atom density of a parent nuclide j that produces nuclide i via radioactive decay,
l_{ji} = fraction of radioactive decay of nuclide j that leads to nuclide i,
f_{ik} = fraction of neutron absorption by nuclide k that leads to nuclide i,
F_i = continuous feed rate of nuclide i,
R_i = continuous fractional removal rate of nuclide i,
σ_k = spectrum-averaged neutron absorption cross section of nuclide k,
σ_i = spectrum-averaged neutron absorption cross section of nuclide i,
λ_j = radioactive decay constant of nuclide j,
λ_i = radioactive decay constant of nuclide i,
ϕ = spatially and energy averaged neutron flux.

This system of equations can be solved for the quantities of each nuclide in the system at the end of each time step. For the analysis used in this dissertation, we assume no continuous addition or removal of material by ORIGEN2. Also, the time step size is chosen so the neutron flux throughout the depletion region varies slowly with time. The resulting system can be considered linear, first-order ordinary differential equations with constant coefficients [79]. It can be written in the form of

$$\dot{\mathbf{N}} = \mathbf{A}\mathbf{N} \tag{3.20}$$

with:
$\dot{\mathbf{N}}$ = time derivative of the nuclide concentrations;
$\mathbf{A}$ = transition matrix of rate coefficients for decay and neutron capture;
$\mathbf{N}$ = nuclide concentrations at the current time t.
The solution to equation 3.20 is

$$\mathbf{N}(t) = e^{\mathbf{A}t}\mathbf{N}(0) \tag{3.21}$$

where:
$\mathbf{N}(t)$ = the nuclide concentrations at time t;
$\mathbf{N}(0)$ = the initial nuclide concentrations;
t = time at end of time step.

The exponential function $e^{\mathbf{A}t}$ is referred to as the matrix exponential function and can be approximated by a Taylor series expansion written as

$$e^{\mathbf{A}t} = \mathbf{I} + \mathbf{A}t + \frac{(\mathbf{A}t)^2}{2!} + ... = \sum_{m=0}^{\infty} \frac{(\mathbf{A}t)^m}{m!} \tag{3.22}$$

with $\mathbf{I}$ being the identity matrix [79]. Equation 3.19 illustrates that it is theoretically possible to generate each nuclide from all (n−1) of the other nuclides in the system. However, the average number of parents is normally less than 12. Thus, if a case is considering 1700 nuclides, then at least 1688 of the coefficients of the $\mathbf{N}$ on the right side of equation 3.19 would be zeros and similarly for all other nuclides. The net result would be a sparse 1700 × 1700 matrix of coefficients. The sparseness of the matrix (~98% zeros) is taken advantage of by employing indexing techniques to store only the nonzero elements of the matrix. This array is called the transition matrix. This transition matrix can be used, along with a recursion relation,

$$c_i^0 = N_i(0), \tag{3.23}$$

$$c_i^{n+1} = \frac{t}{n+1} \sum_{j=1} a_{ij} c_j^n \tag{3.24}$$

to derive

$$N_i(t) = \sum_{n=0}^{\infty} c_i^n \tag{3.25}$$

with a_{ij} being an element of the transition matrix containing the rate constant for formation of nuclide i from nuclide j. After the transition matrix and its associated arrays have been established, it is possible to begin irradiation and decay calculations.

The material composition at the end of the irradiation step is then calculated in three general steps:

1. The transition matrix parameters that are time-step dependent are set.

2. The neutron flux is calculated from the power (or vice versa) and the transition matrix is adjusted accordingly.

3. The nuclide composition at the end of the time step is then calculated.

In general, the transition matrix parameters (including fission product yields) are assumed to be constant for all time steps unless the entire transition matrix is regenerated. At this point, the next step is to calculate the power or flux. For the sake of clarity, we assume that the power to be generated from the fuel is specified and that the flux must be

calculated. This can be calculated as

$$\phi = \frac{P}{\sum_{i=1}^{m} \frac{N_i^f}{V} \sigma_i^f Q_i}, \tag{3.26}$$

where ϕ = neutron flux in the material, P is the power in the depletion volume, N_i^f is the amount of fissile nuclide i in the fuel, V is the volume, σ_i^f is the microscopic fission cross section for nuclide i, and Q_i is the recoverable energy per fission for nuclide i.

The average neutron flux is desired for this calculation, but the flux is only known at the beginning of the time step. Consequently, ORIGEN2 expands equation 3.21 into a 2nd order Taylor series with the fissile nuclide composition as the time-dependent variable. The average flux is then calculated by integrating this expansion over the length of the time step and dividing by the length of the time step. This average neutron flux for the current time step is then divided by the average neutron flux for the previous time step producing a ratio of the two fluxes. The ratio of fluxes is multiplied by all of the flux-dependent transformation rates in the transition matrix, implying no change in the cross sections via spectrum changes, and thus adjusting them to the correct flux for the current time step.

The final step is to solve the system of simultaneous differential equations represented by the coefficients in the transition matrix. The composite solution procedure utilizes a set of asymptotic solutions that is suitable for handling the buildup and decay of short-lived nuclides. These nuclides reach equilibrium within the time step and simple asymptotic solutions can be used calculate their concentrations at the end of the time step. The next phase involves generation of a reduced transition matrix, formed from only the long-lived members of the full transition matrix. The final phase of the composite solution method involves using yet another set of asymptotic solutions to the differential equations to calculate the concentrations of the short-lived nuclides which have long-lived parents. A Gauss-Seidel successive substitution algorithm is employed to solve the asymptotic solutions for this limited category of nuclides. Now the concentrations of all nuclides at the end of the time step have been calculated and stored.

3.3 Radiation Damage Model

Irradiation of a material by neutrons will change the physical properties of that material. The changes can include neutron induced embrittlement, swelling and creep. This is of particular interest to those focused on structural materials or fuels. For the purposes of this study, the radiation damage calculations are focused primarily on the fuel in the form of displacements-per-atom (DPA) from within the material's lattice. Namely, collisions of neutrons with primary knockon atoms (PKA) causes those atoms to move within the material's lattice structure, potentially causing secondary atom displacements also. DPA calculations have long been a popular method to characterize the damage caused by neutron irradiation [86].

The DPA in a material is determined from the probability of displacing an atom in the lattice and is a function of the neutron energy, the neutron interaction cross sections, the energy of the recoil atom, and the probability of secondary recoils. This probability is typically expressed as:

$$\sigma_{dis}(E) = \sum_i \sigma_i(E) \int_{T_0}^{T_1} k(E,T)\nu(T)dT, \tag{3.27}$$

where E is the neutron energy, T is the energy of the recoil nucleus, $k(E,T)$ is the energy transfer kernel between the neutron and the atom, $v(T)$ is the secondary displacement function and σ_i is the ith reaction channel at the energy E [87]. Detailed DPA analyses typically require microscopic models like this, but they also require lengthy molecular dynamics simulations to generate the DPA cross-section data. As an alternative, the model utilized for the LFFH system analyses is that detailed for use as an MCNP tally by Hogenbirk [88]. As he explains, in a simple macroscopic model, the DPA in a material can be expressed as

$$DPA = \kappa \frac{E_a}{2E_d} \cong \frac{\int dV \int dE \phi(\mathbf{r},E) \sum_{i=1}^{N} \rho_i \sigma_{R,DPA,i}(E)}{\sum_{i=1}^{N} \rho_i}, \tag{3.28}$$

where κ is the displacement efficiency, E_a is the available neutron energy, E_d is the energy required to displace an atom, N is the number of isotopes in the material, $\phi(\mathbf{r},E)$ is the spatial and energy dependent neutron flux, ρ_i is the ith isotope's atom density and $\sigma_{R,DPA,i}(E)$ is the DPA response cross section for isotope i at energy E. To perform this calculation, a cross section processing code named NJOY is used to generate the necessary DPA cross sections [89]. However, since the displacement energy is material specific, the DPA response cross section is formulated as

$$\sigma_{R,DPA,i}(E) = \frac{1}{E_{d,i}} \sigma_{DPA,i}(E), \tag{3.29}$$

where $E_{d,i}$ is the displacement energy for isotope *i*. Substituting the cross section, we can calculate the DPA as

$$DPA = \frac{\int dV \int dE \phi(\mathbf{r},E) \sum_{i=1}^{N} \left(1/E_{d,i}\right) \rho_i \sigma_{DPA,i}(E)}{\sum_{i=1}^{N} \rho_i}. \tag{3.30}$$

MCNP provides the damage cross sections for most materials of interest in this study and DPA rates can correspondingly be calculated using a tally multiplier. In addition, MCNP normalizes the isotope densities for each tally, so the densities are not needed to calculate the DPA. Since MCNP returns a damage tally via the reaction MT=444 in units of $\left(MeV \times barns/cm^2\right)$, we must normalize the tally by our fusion source power and rate. To do so, we calculate the fusion source power in units of $\left(neutrons \times cm^2/day\right)$ assuming a

37.5 MJ target yield as

$$P_{source} = \frac{1\ neutron}{17.589\ MeV} \times \frac{1\ MeV}{1.602176 \times 10^{-19}\ MJ} \times \frac{\#\ shots}{sec} \times \frac{37.5\ MJ}{shot} \times \frac{86,400\ sec}{day} \times 10^{-24}\ cm^2/barn. \tag{3.31}$$

Recalling a displacement efficiency of 0.8, we calculate the DPA as

$$DPA\ (\#/day) = 0.8 \left(\frac{1 \times 10^6\ eV/MeV}{2E_d(eV)} \right) P_{source} \times MCNP_{Tally444}. \tag{3.32}$$

The resulting DPA rate is utilized later in this work for system level analysis of the first wall, Be layer and fuel structural carbon layers.

3.4 Neutron and Gamma Dose Effects

The calculation of dose from the LFFH fuel involves three steps. First, the fuel must be depleted to generate fission products that produce gamma radiation. Next, the spectra of the gamma radiation must be determined. This is a non-trivial task because each fission product isotope emits radiation at a variety of frequencies and strengths. The sum of all these isotopes must be calculated and treated as a source term over which those photons and neutrons are subsequently transported. This transport problem can be performed using MCNP, but the development of the source term requires an additional code to generate the correct gamma spectra from each isotope in the system. This calculation is performed using a code named ACAB.

3.4.1 ACAB Activation Analysis Code

ACAB is an International Atomic Energy Agency (IAEA) standard activation code that has been thoroughly benchmarked and tested for a variety of fusion activation and dose calculations [90, 91, 92, 93]. ACAB can model decay transitions that proceed from the ground, first, or second isomeric states. Reactions occurring at energies ranging from the thermal region to 20 MeV can be included in the calculations. ACAB is also able to model sequential charged particle reactions as an additional mechanisms for the production of activity. Each neutron reaction can begin from a target atom in the ground, first or second isomeric state and result in a product that is in any of these states as well.

Using a Monteburns generated isotopic inventory from a burnup calculation, we can assemble those inventories into a spherical mass of interest. ACAB is then used to determine the photon emission spectra from that sphere assuming a uniform concentration of each isotope in the sphere. This photon emission spectra can then be used as a spherical source in a transport calculation using MCNP to determine dose. In other words, ACAB is used

to generate the photon source term for MCNP and MCNP is used to perform the photon transport to determine dose.

3.5 LFFH Nuclear Control Code

The *LFFH Nuclear Control* code (LNC) was developed by this author to deal with calculations and control mechanisms not readily available in existing depletion codes like Monteburns. More specifically, LNC leverages the Monteburns capabilities by adding features necessary to model LFFH. Two particular control aspects necessitated the development of LNC. First, we desire the ability to calculate and control the system tritium production and thermal power. Second, as additional design metrics were added, we required control over those metrics directly without altering the fundamental depletion or transport packages. With modularity in mind, LNC was developed to simulate a LFFH engine from beginning to end using a coupled code approach. The current implementation supports the transport package MCNP and the depletion package Monteburns, but future efforts will support MCNPX as well. The LNC code is general enough to allow for different transport and depletion packages to be used with minimal effort.

The general code flow of the LNC code suite is shown in Figure 3.2. The calculation begins with three input files or decks: a MCNP deck, a Monteburns input deck and a LNC input deck. The MCNP input is used to define all geometric and material composition details for the simulation. Additional tallies of interest like flux, DPA and reaction rate tallies can also be included. The Monteburns input deck is used to define parameters of the burn, including which zones to burn and for what duration. The use of a Monteburns input deck is historical in nature and future work will eliminate the need for this input deck as the information will be passed directly from LNC to Monteburns. The LNC input deck contains all the necessary control parameters, like TBR and power ranges, minimum inventories, removal isotopes, etc. to perform the full time-dependent simulation. Additional details can be found in Appendix B for each input file.

The LNC code is the client code that begins execution by verifying existence of all necessary input files and the requisite transport and depletion data. After parsing the input files, the first step is to run a baseline MCNP calculation using the provided input deck for two reasons. First, this serves as a test to assure the deck actually runs in MCNP. Second, volumes and masses of each cell are tallied and parsed by LNC for later use. The next operation is to calculate the total system power and TBR and to check if it inside of the user defined ranges. If not, LNC begins to iterate on the ^{6}Li/^{7}Li concentrations in the coolant materials until a suitable enrichment is found such that the TBR and power are acceptable, or the maximum number of user-defined iterations has been exceeded. The other mechanism that can force an iteration sequence is if the total tritium inventory in the system falls below a user defined level, described in section 3.5.1.

After iterating and finding suitable enrichment of the coolants, the calculated fission

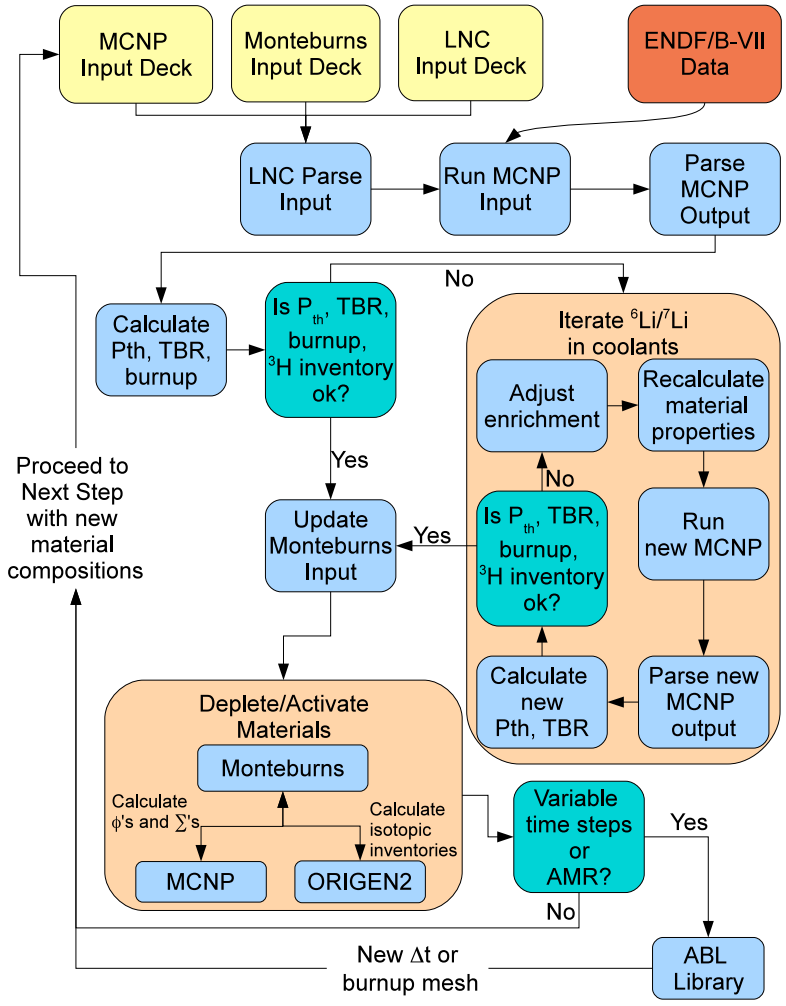

Figure 3.2: Overview of LFFH Nuclear Control code suite

neutron power is updated in the Monteburns input deck. Monteburns is then called by LNC to perform a depletion step. Monteburns begins executing by first calling MCNP to generate the necessary material cross section data. This data is stored and ORIGEN2 is called to calculate the new material compositions half way through a step. MCNP is then called again to perform a detailed transport calculation and provide updated cross sections and neutron fluxes at the half way point. These resulting fluxes and cross sections are then fed back to ORIGEN2 by Monteburns to calculate the complete material compositions at the end of the step. This process employs a predictor-corrector methodology and is described in detail in the Monteburns manual [78]. LNC then calls the ABL library if either variable time stepping or adaptive meshing is enabled by the user. Further details on the ABL library implementation are provided in section 3.6.1. It then outputs various tallied data for the step including the TBR, power, burnup, tritium inventory, DPA rates and other metrics pertaining to system performance. After outputting all tally information and completing a full depletion step, LNC updates the base MCNP input deck with the new material compositions, cell densities, surfaces and volumes (if a new mesh is calculated). If the ABL library calculated a new time step size, that value is stored and necessary calculations and input decks are updated with the new time step size, e.g. the tritium inventory and burnup calculations and the Monteburns input deck. After all updates are performed, the LNC code loops back to the start to perform the next step.

Overall, the LNC code serves to provide two primary functions. First, it controls the system based on the TBR or thermal power. This is accomplished by adjusting the ^{6}Li/^{7}Li ratio in all cells containing a coolant with these constitutive isotopes. It iterates these isotopic concentrations until a satisfactory TBR or thermal power is found. Second, it maintains a consistent set of tallies and tracks material compositions over the entire duration of the simulation. The system control, iteration routine and ABL library are further detailed in the following sections.

3.5.1 TBR, Tritium Inventory and Power Control

The TBR and power calculations are performed using a 616 group F4 and F6 flux and energy deposition tallies specified in MCNP. Each tallied cell in the problem contributes to the total sum of tritium production and thermal power.

Recalling that the fusion fuel consists of tritium and deuterium and understanding that deuterium is plentiful in natural water resources, it becomes obvious that tritium must be produced to fuel the fusion process. The TBR is defined as the ratio to tritium production over consumption given as

$$TBR \equiv \frac{^{3}H_{prod}}{^{3}H_{cons}}. \tag{3.33}$$

It is important for fusion systems to operate with a TBR > 1.0 to ensure the system does not run out of fuel, assuming 100% recovery. If we assume losses for recovery and decay, this value must be maintained higher (~1.1 to 1.2). The TBR and tritium inventory calculations

are given in Figures 3.3 and 3.4. The TBR is calculated over all cells in the problem, over 616 energy groups for both ^{6}Li and ^{7}Li tritium producing reactions. The reaction cross sections are provided in an external file named *Lixsec.dat* and can be extended to include other isotopic reactions by simply adding the group cross sections to the file.

As described previously, the net system tritium can cause the LNC code to begin iterating enrichment levels if it falls below a user specified value. The tritium inventory at each step is calculated via Figure 3.4. The net tritium burned is the product of the time step size, the fusion power produced and the burn fraction of the tritium in the capsule. This burn fraction is approximated as

$$B_{frac} = 86,400\,(sec/day) \times \frac{3.55\times10^{17}(tritons/MJ)}{6.0221415\times10^{23}\,(tritons/mole)} \times \frac{3.016\,(g/mole)}{1000\,(g/kg)}. \tag{3.34}$$

This is an approximate mass of tritium required to produce the desired fusion power. The amount tritium produced over the time step is the product of the TBR and the B_{frac}. This easily gives the net tritium inventory (in kg) over the time step as the difference between that produced and that consumed. The tritium, however, does decay over the time step so this must be accounted for as well. The decay is calculated as the product of the net tritium over the time step decayed over 1/2 the time step length. The final calculation of the remaining tritium is simply the net tritium produced during the time step minus the amount decayed. If the TBR is less than 1.0, the net tritium produced over the time step will be negative. To account for this, the net and decayed tritium are summed to produce the total tritium inventory remaining at the end of the time step. This allows one to run the system at a tritium deficit, while still accounting for the decay of that externally supplied tritium. The existing tritium inventory for the system, if one exists, is decayed as well prior to summing the net tritium produced in the current step to the total inventory.

Like the TBR and tritium inventory, thermal powers from photon and neutron energy deposits are calculated in each cell as a separate quantity. The thermal power in each cell is obtained via conversion of the tally results to MW from

$$P^{\gamma}_{th} = \frac{P_{fusion}(MW)}{17.6(MeV)} \times M_{cell}(grams) \times E^{\gamma}_{dep}(MeV/gram) \tag{3.35}$$

and

$$P^{n}_{th} = \frac{P_{fusion}(MW)}{17.6(MeV)} \times M_{cell}(grams) \times E^{n}_{dep}(MeV/gram), \tag{3.36}$$

where P_{fusion} is the input fusion power, M_{cell} is the total mass of the cell in grams and E_{dep} is the neutron or photon energy deposit using MCNP F6 and F7 tallies in $(MeV/gram)$. The E_{dep} tallies over each cell include power from fission, (n,xn) and other reactions.

After the TBR, tritium inventory and thermal power for the simulated system are calculated, the control algorithm can determine whether to adjust the necessary coolant ^{6}Li enrichment or simply continue to the next phase of the depletion calculation. This is accomplished via the logic illustrated in Figure 3.5. The LNC code enters a control logic routine

```
// Loop over all cells
for (int i = 0;
    i < num_cells;
    i++)
{
    // If the cell contains tritium producing material
    if (cell[i].is_tbr_cell)
    {
        // Loop over all isotopes in the cell
        for (int j = 0;
            j < cell[i].num_isos;
            j++)
        {
            // Compute the reaction rate over all groups, isotopes and cells
            for (int k = 0;
                k < num_energy_bins;
                k++)
            {
                // Total reaction rate per group for each cell
                cell[i].iso[j].reaction_rate_per_group[k] =
                    (cell[i].iso[j].group_cross_section[k] *
                    cell[i].group_flux[k] * cell[i].iso[j].num_atoms * 1.0e-24);

                // Total reaction rate for the cell
                cell[i].iso[j].total_reaction_rate = (cell[i].iso[j].
                    total_reaction_rate +
                    cell[i].iso[j].reaction_rate_per_group[k]);
            }

            // Calculate the total reaction rate
            total_react_rate = total_react_rate + cell[i].iso[j].total_reaction_rate;
        }
    }
}

// Compute tritium breading ratio
tritium_breeding_ratio = total_react_rate/(num_neutrons_per_MJ * fusion_yield *
    fusion_rep_rate);
```

Figure 3.3: Algorithm to calculate TBR in the LNC code

```
// Calculate the amount of tritium used for fusion
tritium_burned = time_step_size * burn_fac * fusion_power;

//  Now calculate the total tritium produced
tritium_produced = tritium_breeding_ratio * tritium_burned;

// Net tritium is the difference between produced and burned
tritium_net = tritium_produced - tritium_burned;

// Followed by the amount decayed this time step
tritium_decayed = tritium_net * (1.0 - exp(decay_fac*time_step_size));

if (tritium_net >= 0)
{
    // To give the total tritium remaining in this power step SUBTRACT decayed
    tritium_remaining = tritium_net - tritium_decayed;
}
else
{
    // To give the total tritium remaining in this power step ADD decayed
    tritium_remaining = tritium_net + tritium_decayed;
}
```

Figure 3.4: Algorithm illustrating calculation of tritium inventory in LNC code

illustrated in the top of the figure. After calculating the current TBR, thermal power and tritium inventory, the LNC code checks to see which run mode the system is operating in. There are two basic run modes for this system design, TBR mode and power mode. When in TBR mode the LNC code seeks to maintain the system TBR within user specified limits. When in this mode, the thermal power is ignored. This mode is useful during the ramp up and incineration phases of a thermal power curve, shown in Figure 3.6. During these phases, the desired system thermal power cannot be maintained, so in an effort to maintain tritium self-sufficiency, the LNC code operates in TBR mode instead of power mode. This feature can be overridden if desired by the user. When in power mode, the LNC code seeks to maintain the system thermal power within a user specified range. In this case, the system TBR is ignored, unless the tritium inventory falls below a user defined value. The flat power curve is maintained at the expense of TBR when enough fissile material exists in the fission blanket to produce the desired power.

If the system is operating in TBR mode, LNC first checks to see if the current TBR is within the desired range. If not, the iteration algorithm is immediately called. If it is within the desired range, the net tritium inventory is checked. If it is below the allowable limit, the iteration algorithm is called. If it is not, the control loop is exited and the LNC code continues on to call Monteburns and perform a depletion step.

If the system is currently operating in power mode, the LNC code first checks to see if this is the first time that the code has reached the operating power. If so, this signals the transition from the ramp up phase to the power phase and forces the code to check

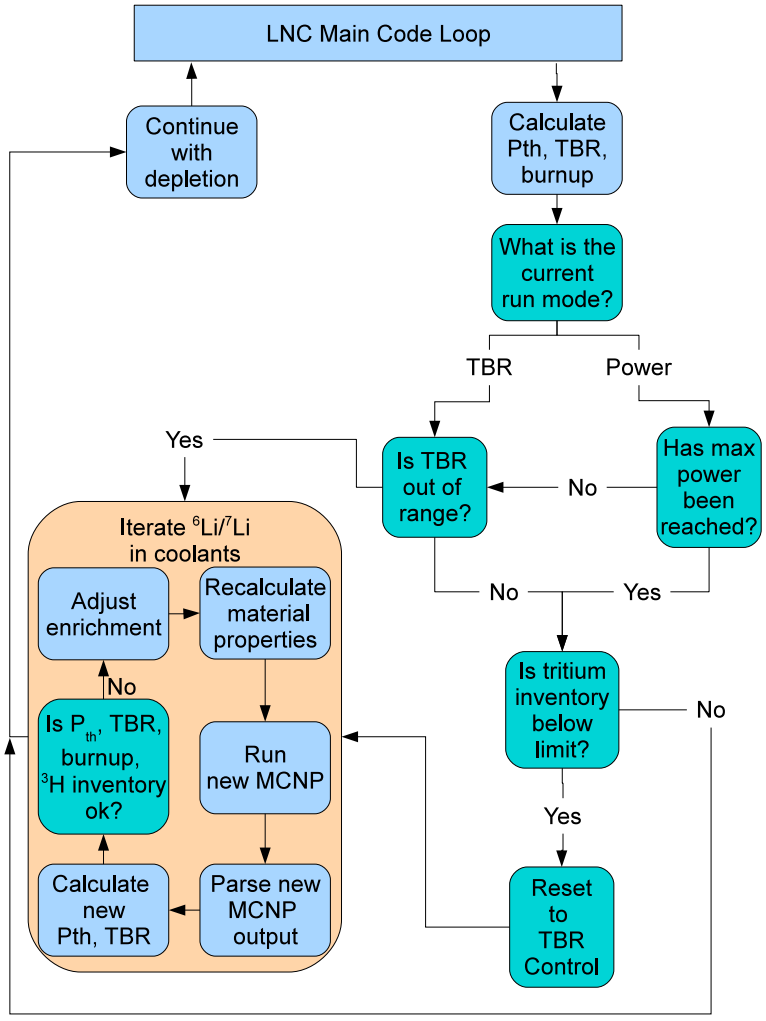

Figure 3.5: LNC system control logic

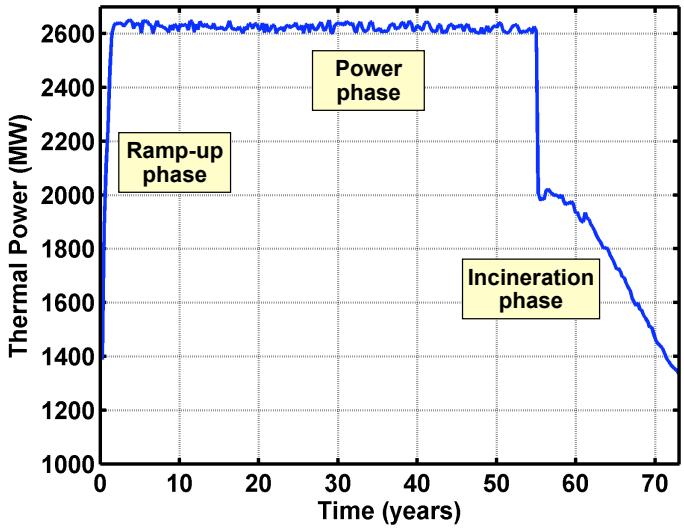

Figure 3.6: Example of tritium self-sufficient power curve

the TBR against the TBR range. If it is within range, the tritium inventory is checked. If either of these checks fail, the iteration algorithm is called. Similarly, if the power has been reached in previous steps, this implies that the system is operating in the power phase of the burn or transitioning to the incineration phase. Under these circumstances, the TBR range is ignored, unless the tritium inventory falls below allowed limits. If it does, the LNC code switches back to TBR mode and the iteration routine is called. As complicated as this logic may seem, it functions very well in generating a smooth thermal power curve under different operating conditions. After the iteration algorithm has found an acceptable ^{6}Li enrichment in the coolants, the routine returns to the control loop to continue with the remainder of the depletion step.

3.5.2 ^{6}Li Iteration Routine

The primary system control of the LFFH engine relies on the continuous adjustment of the ^{6}Li/^{7}Li ratio in the coolants. Hence, significant effort was put forth to develop the ^{6}Li iteration routine that could converge quickly and ensure atomic conservation and stoichiometric accuracy. The method developed utilizes a modified binary search. Gradient-based methods proved to be unstable because of statistical variations in thermal powers and the TBR associated with Monte Carlo methods. While a binary search method only satisfies the requirement that the solution exist within the search bounds, it tends to be more stable when using Monte Carlo transport to determine the associated system power.

The iteration routine is shown in Figure 3.7 and begins with a check of the current run mode. The system is either operating in a predefined TBR or power mode. If operating in

TBR mode and the TBR is below the desired range, a check on the previous state is made. If the previous TBR is also below the range, the ^{6}Li enrichment is increased relative to ^{7}Li in the coolants. This has the effect of increasing the system TBR, while reducing the system thermal power. Alternatively, if the current TBR is above the range, the ^{6}Li is decreased to achieve the opposite effect. If previous and current TBR are on opposite sides of the defined range, the binary search routine is applied where the ^{6}Li adjustment is continuously altered via smaller and smaller amounts to converge on an acceptable enrichment.

If operating in power mode, effectively the opposite sequence of events yields adjustments in the ^{6}Li enrichment. If the power is too low, the ^{6}Li enrichment is decreased instead of increased. If it is too high, the ^{6}Li enrichment is increased to reduce the system thermal power.

The actual adjustments to enrichment levels are performed on a molar basis such that one ^{6}Li atom is exchanged for one ^{7}Li atom to maintain stoichiometric balance and conserve molar quantities. After the adjustment, cell and material masses and densities are recalculated and renormalized for use in the MCNP input deck. This deck is updated and MCNP is run using the new material compositions. Following completion of the MCNP run, the power and TBR are recalculated and the process iterates again (typically 1-3 times) until either a satisfactory solution is found or the maximum number of iterations is performed as determined by the user.

3.6 Methods to Improve Computational Efficiency

Even with the advent of modern supercomputers, fully detailed Monte Carlo depletion calculations can require computing resources beyond most individual's access. In the LFFH system, as with other nuclear systems relying on fuel breeding and burning to occur in separate regions of the core, the flux varies dramatically across the core. An example of this effect can be seen in Figure 3.8. An external neutron source is on the left side with neutrons streaming to the right. Inset is a representation of a 1D problem zoned into 9 separate regions. The neutron flux magnitude is overlaid and shown as continuous, while the actual calculation of that same flux, shown in the main figure, is discontinuous. The flux used for the calculation in each zone is identified by the red star and is an average of the flux in that zone. As the burn wave propagates outward through the blanket, the flux variations in the zones of interest can become quite discontinuous. This is a numerical effect arising from the problem being too coarsely zoned. Results describing the nuclide inventories and neutron reaction rates will be erroneous for a fixed fuel loading because of these discontinuities. In other words, the assumption of constant flux over a depletion time step is not held. As a result, the simulation requires either re-running with shorter time steps or a more finely zoned region around where the neutron flux is changing most rapidly. This can become quite tedious and easily overlooked. To address these issues, two methods to automatically determine the necessary time step and spatial zone size were developed.

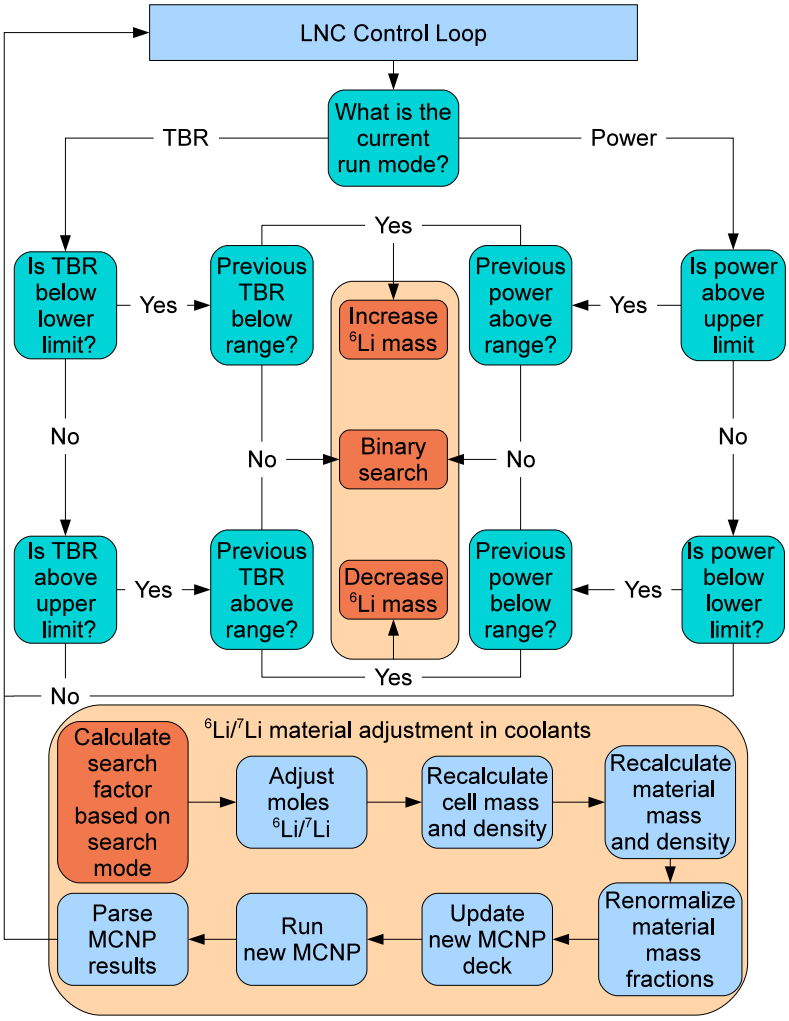

Figure 3.7: ^{6}Li iteration algorithm in LNC code

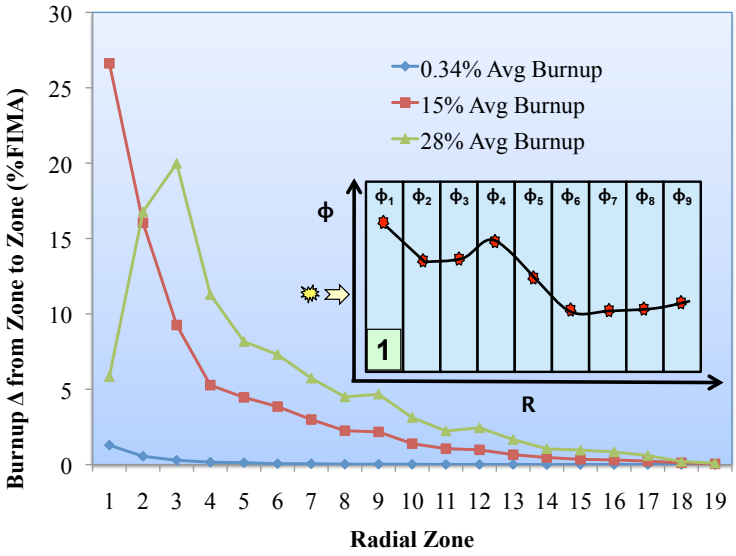

Figure 3.8: Neutron burnup variations as function of burnup show unacceptably large changes from zone to zone through fission blanket.

3.6.1 Adaptive Burnup Library

In an effort to incorporate two new methods, variable time step and adaptive mesh methods into the LNC code, implementation of the routines occurs in an external library. The goal of this implementation is to allow for code reuse outside of the LNC code by others seeking to dynamically adjust the depletion step size and mesh using MCNP based analyses. This library is termed the *Adaptive Burnup Library* and is tailored to work directly with MCNP or MCNPX and Monteburns, but can be extended to work with other transport codes and depletion packages.

3.6.2 Variable Time Step Depletion

Typical burnup calculations employ the assumption of either constant power or constant flux over the depletion step. In addition, most reactor burnup calculations assume the reactor operates at full power with startup and shutdown events not being a part of the burnup simulation. The LFFH system, alternatively, incorporates ramp up and incineration periods lasting a few to many years. During those periods, the engine power and flux are changing continuously and that motivates the need to adjust the depletion time step as the engine power changes. Low power years will have a lower average system neutron flux, but rapidly changing power. This warrants shorter time steps to capture the necessary nuclide inventory evolution accurately. High power years will result in much faster burnup from a higher average system flux, but possibly justifies longer depletion time steps to speed up the simulation, while capturing the necessary details. However, if we utilize the wrong size

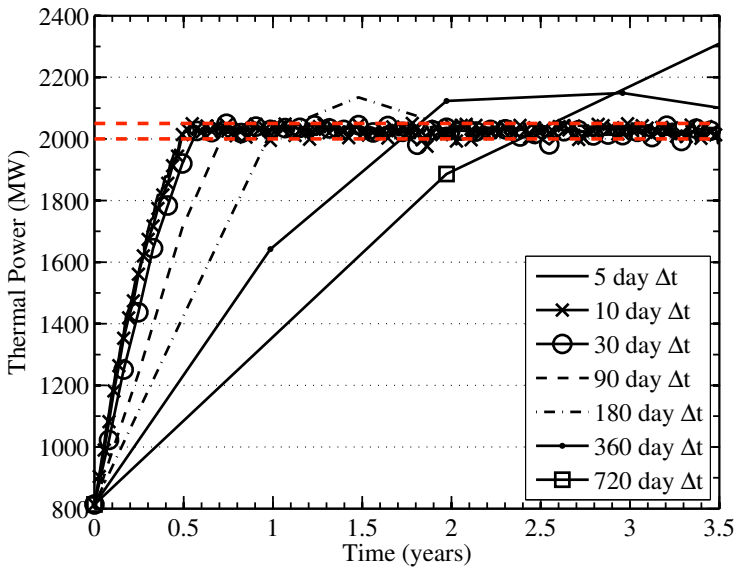

Figure 3.9: Effect of using time steps that are too large during the ramp up power phase

time steps during periods of changing power, errors will be introduced. One such example is shown in Figure 3.9. Time step sizes are varied from 5 days up to 720 days. The 720 day case clearly shows that the power as a function of time is erroneously used. This is due to the fact that the flux from a low power value (720 MW) is used to calculate the nuclide inventories at a much higher power. In other words, the wrong power is used to calculate the flux, which is used to compute the nuclide evolution. As one shortens the time step size, the errors are reduced until they become negligible, as in the case of a time step less than 10 days. This leads to the expectation that each system design will require a different sized time step during a power change period and the size of that time step is a function of how rapidly the power changes. The difficulty with this assertion is that it requires a convergence study to be performed for any design variations that alter the rate of power changes. Likewise, 10 day time steps may be required during periods when the power is changing, but not when the power is held constant. Given this, we seek a method for automatically computing the necessary time step size based on some apriori knowledge of the system and burnup requirements.

As a result, the concept of variable time step depletion is implemented into the LNC code. If we are interested in adjusting the time step size for a given depletion step, we are adjusting the reaction rate calculated using a given flux. Assuming the neutron flux is constant in time over the depletion step, any particular reaction rate RR_k in a volume V can be found as

$$RR_k = \int_V d^3r \int_0^\infty N_k \sigma_k(E) \phi(\mathbf{r}, E) dE. \tag{3.37}$$

where V is the volume, N_k is the atom density of nuclide i, $\sigma_k(E)$ is the energy dependent

reaction microscopic cross section, and $\phi(\mathbf{r},E)$ is the spatial and energy dependent neutron flux. Integrating over the whole volume, the total reaction rate becomes

$$RR_k = N_k V \int_0^\infty \sigma_k(E)\phi(E)dE, \tag{3.38}$$

where $\phi(E)$ and $\sigma_k(E)$ are the flux and cross section as a function of energy, respectively. Utilizing a multigroup approximation to the energy dependent flux and cross section, the reaction rate becomes

$$RR_k = N_k V \frac{\sum_{g=1}^{m} \int_{E_g}^{E_{g+1}} \sigma_k(E)\phi(E)dE}{\sum_{g=1}^{m} \int_{E_g}^{E_{g+1}} \phi(E)dE} \int_0^\infty \phi(E)dE. \tag{3.39}$$

where g represents each discrete energy group. This can be further reduced to

$$RR_k = N_k V \bar{\sigma}_k \int_0^\infty \phi(E)dE, \tag{3.40}$$

where $\bar{\sigma}_k$ is the microscopic 1-group effective cross section. Further, integration of the flux over all energies gives

$$RR_k = \Sigma_k V \phi, \tag{3.41}$$

where Σ_k is the effective macroscopic cross section equal to the product of the atom density and microscopic cross section for reaction k. The total number of reactions for a given depletion time step, holding Σ_k and ϕ constant over that step, will be

$$R_k = \int_{t_0}^{t_1} \Sigma_k V \phi dt \tag{3.42}$$

Hence, if we wish to ensure an accurate number of reactions over a depletion time step, we must ensure that not only the flux is relatively constant, but also the effective 1-group cross section as it is a weighted function of the spectrum. This is true of all absorption and fission reactions. However, it is difficult to quantify an acceptable change in the flux spectrum at any given point in time because it is the product of the cross section and flux that determines the change in reaction rate.

Alternatively, we can make a determination that any particular reaction rate should only be allowed to change by a small amount over a depletion step. For fissile systems, we can assume that the net fission rate in any volume is a good measure of changes in neutron flux because subsequent daughter isotopes causing increased capture reactions will result in flux depressions in the spectrum and change the fission rate. It is simply defined as

$$RR_{fis} = \Sigma_{fis} V \phi. \tag{3.43}$$

The number of fission reactions also reduces the total heavy metal inventory in the system such that the net energy produced per unit mass of fissile material, or burnup, can be defined as

$$Burnup\left(^{GWd}/_{MT_{HM}}\right) \equiv \int_{t_0}^{t_1} \frac{Q_{fis} RR_{fis}}{M_{HM}} dt = \int_{t_0}^{t_1} \frac{Q_{fis} \Sigma_{fis} V \phi}{M_{HM}} dt, \tag{3.44}$$

where Q_{fis} is the energy released by each fission reaction. Hence, given a starting heavy metal (typically Z=92 and higher) material inventory represented by M_{HM}, the burnup in a material or zone is an integral quantity and a function of a single group effective cross section and flux measured in units of GWd/MT_{HM}. Given that burnup is simply a measure of the power produced times the length of time it was produced per unit of heavy metal mass. We quickly realize that the burnup is also a measure of the change in fissile nuclide inventory as well as a measure of the number of fuel atoms that underwent fission. Thus by limiting the change in burnup over a series of depletion steps, we limit the overall change in fissile nuclide inventory as well. Extending this concept to multiple materials containing multiple fissile nuclides of interest, the burnup B_i of a material containing heavy metal mass M^i_{HM} can be approximated as

$$B_i = \int_{t_0}^{t_1} \sum_{j=1}^{m} \frac{Q^j_{fis} \Sigma^{ij}_{fis} V^i \phi^i}{M^i_{HM}} dt \tag{3.45}$$

where Q^{ij}_{fis} is the fission energy released in, Σ^{ij}_{fis} is the macroscopic fission cross section of, V^i is the volume occupied by, and ϕ^i the neutron flux in material M_i of n total materials for nuclide j of m total nuclides. Similarly, the power produced by a material i can be expressed as

$$P_i = \sum_{j=1}^{m} Q^j_{fis} \Sigma^{ij}_{fis} V^i \phi^i. \tag{3.46}$$

Likewise, the average burnup and total power in the system can be expressed as the superposition of all materials in the system as

$$B_{avg} = \int_{t_0}^{t_1} \frac{\sum_{i=0}^{n} \sum_{j=1}^{m} Q^j_{fis} \Sigma^{ij}_{fis} V^i \phi^i dt}{\sum_{i=0}^{n} M^i_{HM}} dt \tag{3.47}$$

and

$$P_{total} = \sum_{i=0}^{n} \sum_{j=1}^{m} Q^j_{fis} \Sigma^{ij}_{fis} V^i \phi^i \tag{3.48}$$

Since we seek to limit changes in the flux over a time step, it is natural to limit changes in the integral quantities of burnup and power. To solve for the P_{total} and B_{avg}, depletion codes make the approximation that the flux ϕ and corresponding macroscopic effective cross sections are constant over the depletion time step [84, 85].

Given this approximation, if we let B_0 and B_1 represent the burnups at the current time and the next point in time that the nuclide inventories are evolved, the change of the burnup from one time step to the next can be expressed as

$$\Delta B = B_1 - B_o. \tag{3.49}$$

Likewise, the change in power can similarly be expressed as

$$\Delta P = P_1 - P_o. \tag{3.50}$$

We can attempt to control the absolute change in the scalar neutron flux by controlling both the change in burnup and power. This arises from the fact that at certain times (power ramp up and ramp down), we have rapidly changing power and slowly changing burnup. At other times (power plateau), we have slowly changing or constant power and more rapidly changing burnup. Hence, we need to control via both quantities. If we assume that the deltas are constant over the depletion time step, regardless of step size, we can impose limits of

$$\begin{cases} \Delta B_{min} \leq \Delta B \leq \Delta B_{max} \\ \Delta P_{min} \leq \Delta P \leq \Delta P_{max} \end{cases}. \tag{3.51}$$

Applying these limits, we can calculate a new time step based on the expected change in burnup and power as

$$\begin{cases} \Delta t_{B_{min}} = \frac{\Delta B_{min}}{\Delta B} \Delta t_{current} & \Delta t_{B_{max}} = \frac{\Delta B_{max}}{\Delta B} \Delta t_{current} \\ \Delta t_{P_{min}} = \frac{\Delta P_{min}}{\Delta P} \Delta t_{current} & \Delta t_{P_{max}} = \frac{\Delta P_{max}}{\Delta P} \Delta t_{current} \end{cases} \tag{3.52}$$

depending on what regime the burnup calculation occupies. If we seek to maximize the time step given each of the constraints in equation 3.52 and impose a stability requirement that the time step not grow by more than twice the current step size, then the time step size for the next depletion period will be

$$Min(\Delta t_{B_{min}}, \Delta t_{P_{min}}, 2\Delta t_{current}) \tag{3.53}$$

if the current depletion period results in the ΔB and ΔP being below the allowed ranges and

$$Min(\Delta t_{B_{max}}, \Delta t_{P_{max}}, 2\Delta t_{current}) \tag{3.54}$$

if they are above the allowed ranges.

3.6.2.1 Implementation of Variable Time Steps

The use of fixed size time steps by Monteburns, ORIGEN2 and LNC complicates the implementation of variable sized time steps because each particular code utilizes a typically

different sized time step. The outermost loop of LNC was chosen to call the ABL library and adjust the time step size. This was done to ensure that all quantities relying on the depletion time step size were adjusted accordingly. This includes the calculations of various isotopic inventories including the tritium and calculations of burnup parameters like the GWday/MT$_{HM}$. Likewise, adding the variable time stepping functionality as a library callable by a client code allows for easy implementation and extension to other code systems in the future.

The adjustment of the time step size is shown in Figure 3.10. The LNC code begins by reading user inputs for the minimum and maximum allowed changes in burnup and power via an input deck. It then starts its main loop and calculates the current power and burnup of each material and cell in the system. The client code, LNC, then loops over all cells containing burnable material and calls the ABL library with the current step number, time step size, current time, thermal power and burnup in each cell. If no previous power or burnup history exists, the ABL library simply returns the current time step size as a result and the LNC code continues its main loop. Such is the case if the current step is the start of the problem, or a restart step.

This method can also be applied to a multizone problem where multiple depletion zones are simulated. In that case, the time step is chosen such that it is the minimum of each ith time step calculated for each of n zones given as

$$\Delta t = \min\left(\sum_{i=1}^{n} \Delta t_i\right). \tag{3.55}$$

For example, a two zone problem, shown in Figure 3.11, the computed time step of each zone yields a different sized time step for each zone. However, the problem time step is constrained by the minimum of the two. Ideally, the zones would be sized appropriately such that the time step required for each would be equal. In order to accomplish this, the zones must be dynamically sized, which is discussed in section 3.6.3.

This solution method allows us to optimize the depletion time step size for any given problem with constrains on the minimum and maximum changes in power and burnup over the step. One advantage of this method is that the time step will be self-correcting as shown in Figure 3.12 . If an initial time step size chosen is too large or too small for the relative changes in power and burnup, the method will adjust it appropriately. However, this feature can also be a disadvantage if one desires accurate depletion information at the exact point that the time step is being adjusted because it arguably will require more than one depletion time step for the method to converge to the correct size time step.

3.6.2.2 Fixed time steps vs variable time stepping

As discussed earlier, the LFFH engine is simulated by performing a fixed-power depletion calculation over a short period of time. The material is then updated and the power recalculated. The fact that there are power ramp up and ramp down periods at the beginning and

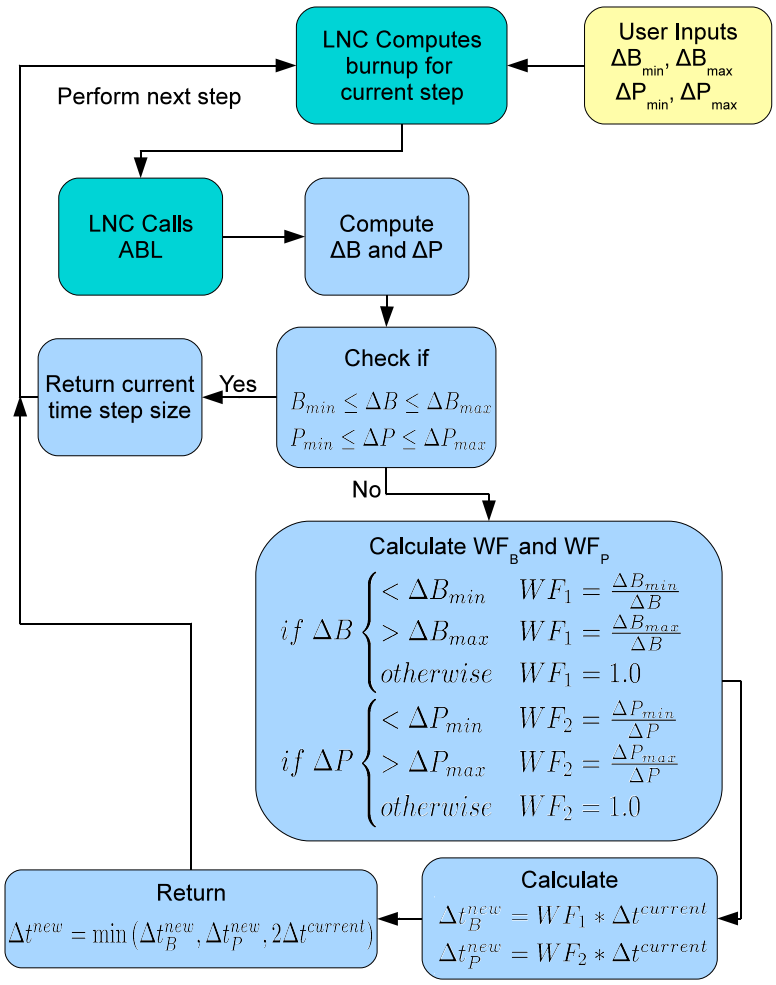

Figure 3.10: Variable time stepping implemented in the Adaptive Burnup Library

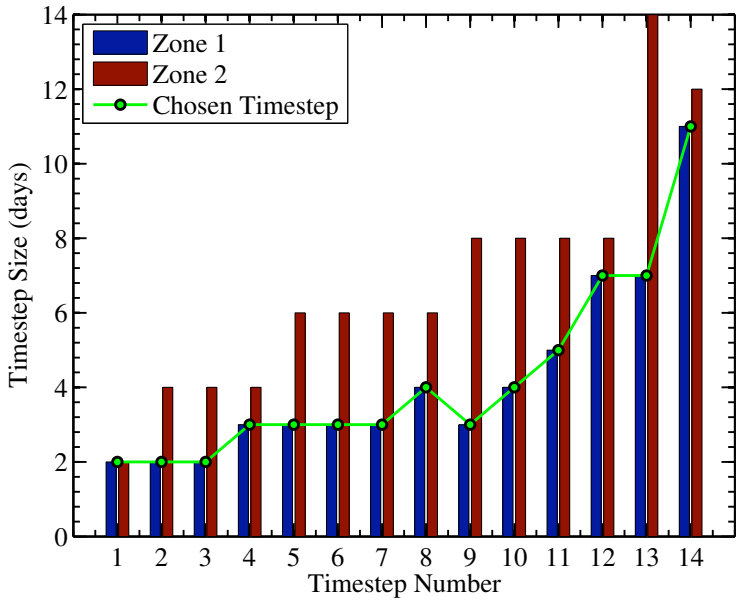

Figure 3.11: Chosen time step size for a multizone problem

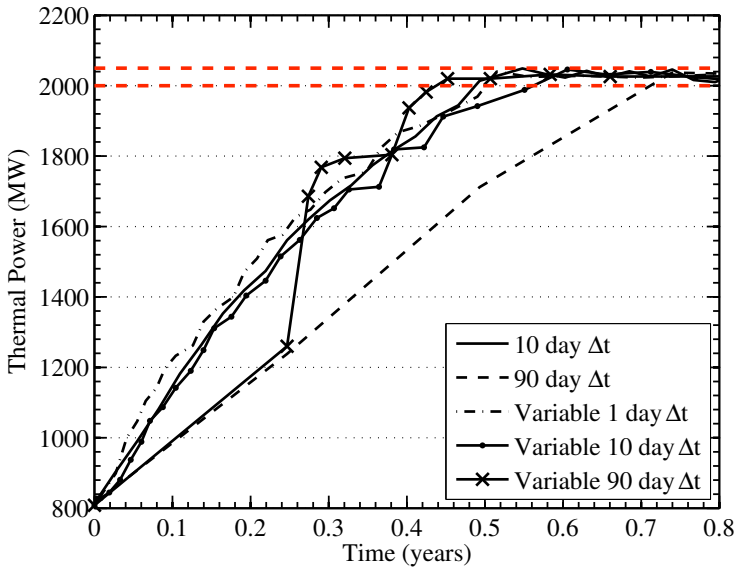

Figure 3.12: Variable time step algorithm corrects for too small or too large of an initial time step size

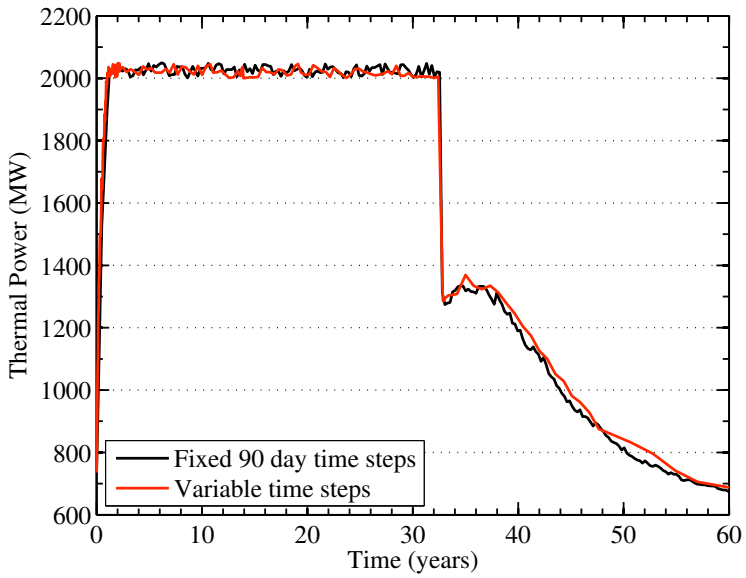

Figure 3.13: Thermal power curve using fixed and variable time step sizes shows little difference in power curve

end of the burnup calculation requires the use of small time step on the order of 1-2 days long because the power and corresponding flux are changing so rapidly. However, when power is held constant during the burn, the time steps can be longer. Fixed time steps do not allow for that change. Variable sized time steps do, but at what expense to accuracy? To determine this, we examine a particular simulation using fixed 90 day time steps and compare that same exact simulation using variable time steps. The variable problem imposes a maximum of 1 GWday/MT$_{HM}$ and maximum 50 MW change in power.

Starting with the thermal power curve, shown in Figure 3.13, we see that there is little difference between using variable time steps or fixed time steps. There are no discernible differences in the ramp up phase. Likewise, during the full power operation phase, statistical variations dominate. However, during the ramp down phase, the two curves vary slightly around 35 years into the burn. This can be attributed to an overshoot by the LNC code when trying to maintain the tritium inventory. In other words, the time steps at this point are 144 days for the variable sized problem and 90 days for the other. At the point of the power drop, the tritium inventory is at approximately 0 kg. It is being reduced by $\sim$3 kg over this period. The variable time step calculation appropriately reduces the time step to 12 days long, which is proportional to the drop in power. In the fixed 90 day case, the tritium inventory is depleted below zero before LNC can switch into TBR mode and build the inventory backup. This is purely an artifact of the control algorithm and not the use of variable sized time steps. This effect is shown quite clearly in Figure 3.14a. The fixed time step calculation happens to switch to TBR mode slightly below when the inventory falls to zero. The variable time step simulation does not. One simple way to prevent this is

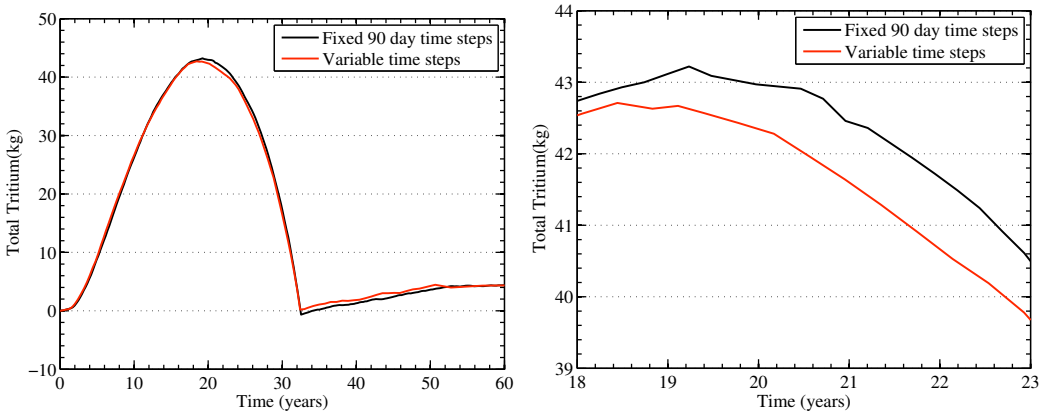

(a) Tritium inventory over time

(b) Zoomed view of tritium differences at peak

Figure 3.14: Tritium inventory using fixed and variable time step sizes.

achieved by raising the minimum tritium inventory threshold to 1-2 kg, which prevents the overshoot.

Careful examination of Figure 3.14a also shows a slight difference in the tritium inventory at the peak, around 20 years into the burn. Figure 3.14b shows a zoomed view of this region. In this case, the fixed time step problem shows $\sim$1 kg excess tritium as compared to the variable time step problem, or a 2.4% difference. Since the only difference between the two simulations is the size of the time steps, this difference can be attributed to the fact that using short fixed time steps more closely approximate the continuous production of tritium. This difference, however, is conservative in the fact that the variable stepped simulation produces less tritium than the fixed time step simulation.

The burnup as a function of time yields a similar result, shown in Figure 3.15. The differences are barely discernible for most of the burn. However, near the end of the burnup, around 40 years, the two curves begin to slightly diverge. The divergence can again be attributed to the difference in tritium inventory. The tritium inventory in the variable time step case is higher, which causes a slight difference in the rate at which burnup flattens at the end, a maximum <1.0% relative error at 99% FIMA burnup.

The more important issue is how accurately the method predicts isotopic inventories of interest. The masses of ^{239}Pu and other fissile isotopes are of particular interest because they determine the system operating characteristics. Figure 3.16 shows that the differences in ^{239}Pu mass are negligible. Throughout the entire burnup calculation, the inventories are virtually identical at every point in time. All of the important actinide and fission product masses, as well as all remaining actinides match quite well. In fact, if we examine the spectral differences at startup and at the time of peak plutonium between the two cases, Figure 3.17, the spectra are quite similar as well. Only statistical variations are visible.

Variable stepping improves the use of computational resources by reducing the simu-

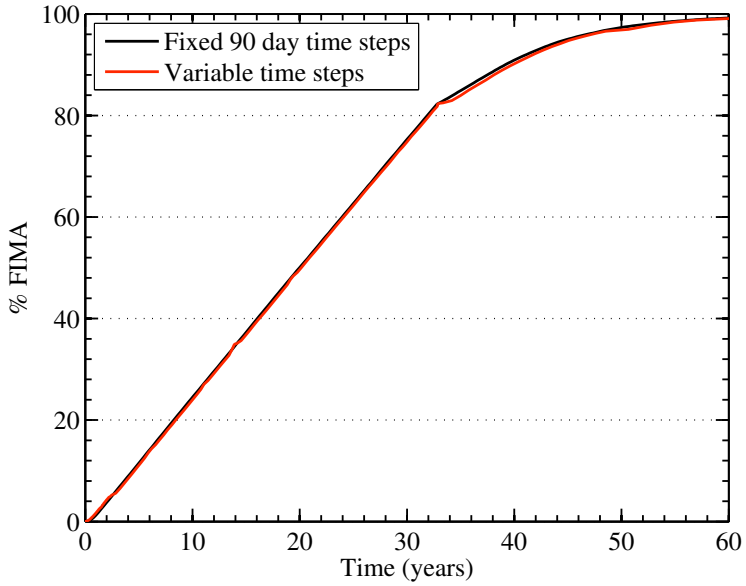

Figure 3.15: Fuel burnup using fixed and variable time step sizes shows little difference in power curve

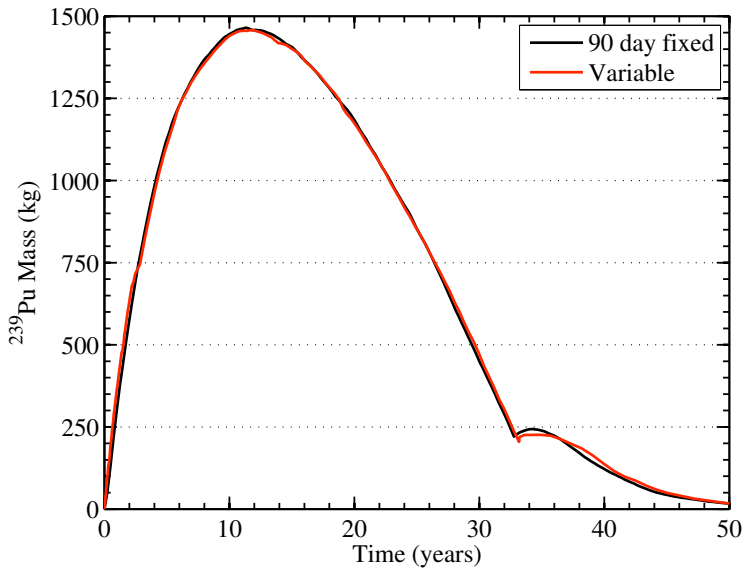

Figure 3.16: ^{239}Pu mass inventories for fixed and variable time steps

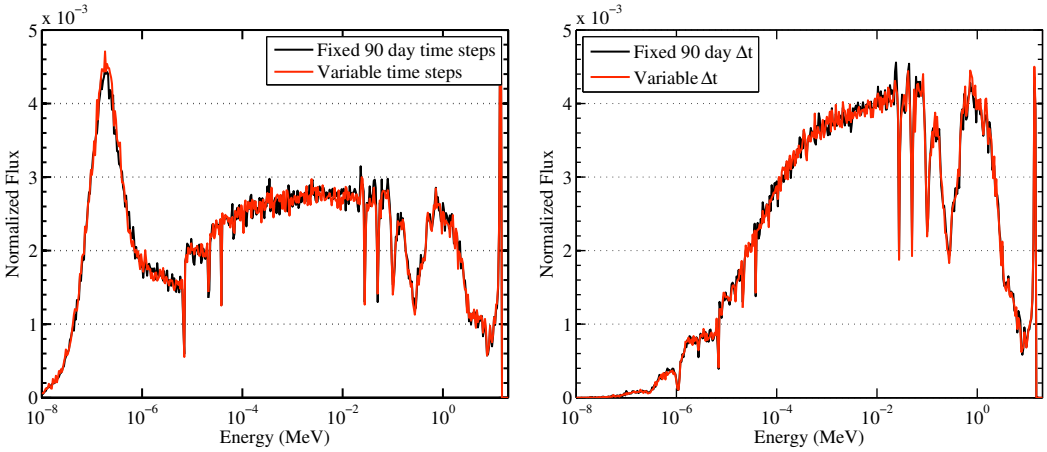

(a) Neutron flux at startup

(b) Neutron flux at Peak Pu inventory

Figure 3.17: Neutron flux in fission blanket at two points in the burnup show nearly identical spectra.

lation requirements. Table 3.1 shows how these two problems differed in wall clock time and CPU-hrs to reach full burnup. Use of fixed size time steps presents the problem that a single depletion calculation for a LFFH engine can take approximately 5-7 wall-clock days to complete utilizing, 40-64 cpus per calculation. This equates to an average of over 5,000 cpu-hrs. per simulation. To perform a detailed engineering design of a new system, not including safety and shielding calculations, hundreds to thousands of simulations are required. This presents an obvious issue of computational resource availability. When compared to a 30 day step size calculation, the 90 day step size offers about a 3× improvement in speed simply from the fact that there are 3 times fewer Monteburns and associated transport calculations required. However, accuracy early in time is sacrificed at the expense of this speedup as shown earlier. The variable step calculation results in a further 2.33× speedup for this particular problem. If we take 30 day steps as a baseline to ensure accuracy, we get a total 7× improvement. As an added benefit, the metrics of interest in performing a burnup calculation (power and burnup) are controlled to stay within a user-defined range. The same is not true in the case of fixed time steps and care must be taken to ensure changes in power and burnup do not grow too large.

	30 Day Fixed Steps	90 Day Fixed Steps	Variable Sized Steps
Wall Clock Time	210 (hr.)	70 (hr.)	30 (hr.)
CPU-hrs	8,400	2,800	1,200
Speedup	-	3×	7×

Table 3.1: Computational speedup from variable time steps

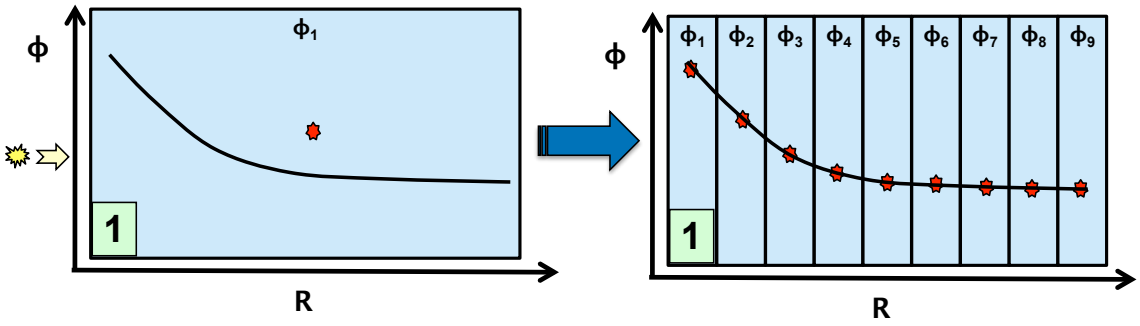

Figure 3.18: A stencil for a depletion problem to capture flux variations and resulting changes in nuclide inventory. A single depletion zone is shown with 1 average flux (left) and multiple zones with multiple average fluxes (right).

3.6.3 Adaptive Mesh Refinement

Adaptive time stepping is useful for determining the appropriate depletion step size for a problem on a global scale. In other words, the time step can be adjusted on a zonal basis because of the solution method utilized. However, this can lead to particular zones dominating the solution time step because of high flux variations, while other zones in slowly changing and low flux regions are carried along in the calculation with little or no change in flux or composition. For instance, it is possible to have a high burnup rate in a zone near the neutron source, but have a much lower burnup rate in zones far away. If the time step were set based on the minimum requirement, calculations become computationally intensive because the time step is set by a single zone requiring potentially much smaller steps relative to all other zones in the problem. This situation is directly akin to that of Monte Carlo transport work where a large number of the particles are concentrated in a particular region. One method to deal with this involves domain decomposition of the problem into multiple separate sub-domains [66]. In this method, a stencil is overlaid on the solution domain with zones in that stencil representing work done by the CPU's in that domain. As the amount of work per domain changes, the domain sizes and number of CPU's assigned to those domains are adjusted to balance out the amount of work per CPU.

In the depletion problem, the actual depletion calculation, as shown by equation 3.19, is a zero dimensional problem. However, variables that the nuclide evolution are a function of, like the neutron flux, do indeed vary in all three dimensions. With the spatial dependence of flux, the nuclide evolution implicitly evolves spatially as well. The spatial evolution of the nuclide inventory is typically captured by considering multiple separate depletion problems over regions where the flux can be considered constant in the seven dimensional phase space consisting of three spatial dimensions, energy, angle and time. In doing so, a stencil is overlaid on the depletion problem like that shown in Figure 3.18. To capture the spatial variations in flux, the depletion problem is *zoned* into separate regions and the nuclide

evolution is solved for in each region independently, given a previously group collapsed neutron flux for each region. If we start with equation 3.19 and represent the neutron flux, cross sections, feed and removal rates as true functions of spatial position in the problem, we have

$$\frac{dN_i(\mathbf{r})}{dt} = F_i(\mathbf{r}) + \phi(\mathbf{r}) \sum_{k=1}^{m} f_{ik}\sigma_k N_k(\mathbf{r}) + \sum_{j=1}^{m} l_{ji}\lambda_j N_j(\mathbf{r}) \\ -(\lambda_i + \sigma_i\phi(\mathbf{r}) + R_i(\mathbf{r}))N_i(\mathbf{r}), \qquad i = 1,2,3....m. \tag{3.56}$$

We can assume there is no feed or removal rate for a simplified problem reducing this to

$$\frac{dN_i(\mathbf{r})}{dt} = \phi(\mathbf{r}) \sum_{k=1}^{m} f_{ik}\sigma_k N_k(\mathbf{r}) + \sum_{j=1}^{m} l_{ji}\lambda_j N_j(\mathbf{r}) \\ -(\lambda_i + \sigma_i\phi(\mathbf{r}))N_i(\mathbf{r}), \qquad i = 1,2,3....m. \tag{3.57}$$

Given equation 3.57, we can represent the spatial variable in a Cartesian coordinate system by

$$\mathbf{r} = (\mathbf{x},\mathbf{y},\mathbf{z}), \tag{3.58}$$

thus transforming equation 3.56 into

$$\frac{dN_i(\mathbf{x},\mathbf{y},\mathbf{z})}{dt} = \phi(\mathbf{x},\mathbf{y},\mathbf{z}) \sum_{k=1}^{m} f_{ik}\sigma_k N_k(\mathbf{x},\mathbf{y},\mathbf{z}) + \sum_{j=1}^{m} l_{ji}\lambda_j N_j(\mathbf{x},\mathbf{y},\mathbf{z}) \\ -(\lambda_i + \sigma_i\phi(\mathbf{x},\mathbf{y},\mathbf{z}))N_i(\mathbf{x},\mathbf{y},\mathbf{z}), \qquad i = 1,2,3....m, \tag{3.59}$$

where the position variable vectors $(\mathbf{x},\mathbf{y},\mathbf{z})$ represent the n spatial positions in a Cartesian coordinate system. This new system of equations represents the change in position with time of each nuclide at all spatial positions in the problem. As the number of spatial positions approaches infinity, representing the continuum solution, the number of equations also goes to infinity and becomes too large to solve using modern supercomputers as shown in equation 3.60. Instead, if the position vectors represent discrete zones over which the nuclide field can be considered constant across each zone, the problem becomes more tenable. In doing so, the limit to reach the continuous solution can be expressed as

$$N_{equations} = \lim_{n\to\infty} \sum_{j=1}^{n} \sum_{i=1}^{m} \sum_{k=1}^{l} \frac{dN_{ijk}(x,y,z,t)}{dt} \to \infty \tag{3.60}$$

where $N_{ijk}(x,y,z,t)$ is the 3D continuous solution and represents the superposition of the discrete solutions and n, m, and l are the number of separately and equally spaced zonal regions over which the nuclide and flux fields are solved. As the number of zones increases and their corresponding size decreases, we approach the true solution. However, practical

Number of Depletion Zones	CPU-Hours to complete
1	2,800
20	∼8,640

Table 3.2: Computational timings for full depletion of a 3D spherically symmetric system to reach 99 %FIMA

limits typically restrict Monte Carlo depletion to 10's to 100's of depletion zones. Even these problems can be extremely taxing as shown in Table 3.2.

An alternative method is to employ variable sized zoning, or adaptive mesh refinement (AMR). A 1D example of this concept is shown in Figure 3.19. Instead of zoning the problem using uniform zones, we can use variable sized zones with smaller zones in more rapidly changing flux, e.g. higher burnup, regions and larger zones in regions where the flux is not changing as quickly.

If we begin with equation 3.56 and treat it as a 1D problem, we can replace the position vector **r** with the 1D radial dimension *r*. The 1D nuclide field can now be represented by

$$\frac{dN_i(r)}{dt} = \phi(r)\sum_{k=1}^{m} f_{ik}\sigma_k N_k(r) + \sum_{j=1}^{m} l_{ji}\lambda_j N_j(r) \\ -(\lambda_i + \sigma_i\phi(r))N_i(r), \qquad i = 1,2,3....m. \tag{3.61}$$

Each set of nuclides is only dependent on the spatial radius *r,* analogous to a symmetric set of spherical shells. Functions of the position variable *r* can be evaluated over discrete zones in space, instead of continuously. This is accomplished by assuming the function constant over some Δr over a time period Δt. The flux and nuclide field are treated this way to yield

$$\frac{\Delta N_i(r_z)}{\Delta t} = \phi(r_z)\sum_{k=1}^{m} f_{ik}\sigma_k N_k(r_z) + \sum_{j=1}^{m} l_{ji}\lambda_j N_j(r_z) \\ -(\lambda_i + \sigma_i\phi(r_z))N_i(r_z), \qquad i = 1,2,3....m \text{ and } z = 1,2,3...n. \tag{3.62}$$

Since the functions of the discrete variable r_z can be considered discrete as well, equation 3.62 can be expressed simply as

$$\frac{\Delta N_{iz}}{\Delta t} = \phi_z\sum_{k=1}^{m} f_{ik}\sigma_k N_{kz} + \sum_{j=1}^{m} l_{ji}\lambda_j N_{jz} \\ -(\lambda_i + \sigma_i\phi_z)N_{iz}, \qquad i = 1,2,3....m \text{ and } z = 1,2,3...n, \tag{3.63}$$

where ΔN_{iz}, ϕ_z, N_{jz}, and N_{iz} represent the discrete change in the nuclide density over a delta t, the zonal averaged flux and the zone averaged nuclide densities in each zone z, respectively. If we considered the typical application with a constant Δr setting the zone radius, the mesh that is developed consists of a regular spacing of node points across the

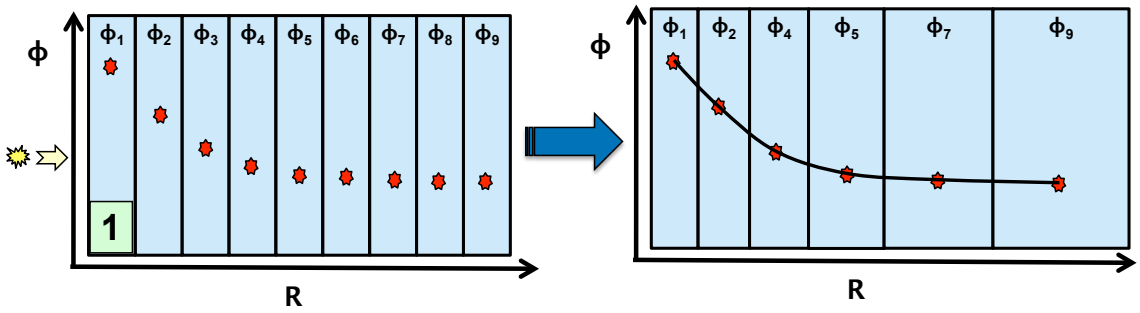

Figure 3.19: Schematic for 1D variable zoning concept

problem like that shown to the left in Figure 3.19. However, as shown previously, treating the problem with constant spatial resolution is computationally taxing. Alternatively, we can vary the Δr over the spatial domain to resolve the problem more finely in regions of interest and more coarsely in other regions, like that on the right of Figure 3.19.

Multiple metrics can be used to determine how large a zone can be. Some metrics could include the relative change in nuclide density over a zone, the relative difference in scalar flux over a set of zones, and even spectrally dependent reaction rates or cross sections. However, each of these metrics is a function of the neutron flux. It determines nuclide densities, macroscopic cross sections, reaction rates, burnups and powers. In the case of variable time step calculations, we utilized changes in burnup and power over a given time step as the metrics to control the time step size. This won't work here because we need to know by how much the flux is changing across a zone. Utilizing the full flux spectrum would be ideal, but is extremely challenging because of statistical variations. The shear number of histories required to ensure a smooth enough spectrum for the comparison would be prohibitive. For the purposes of this work, we use the single group flux as metric of interest. Changes in this flux reflect both real changes in composition of the material due to depletion and capture zone sizing effects as well. We can begin by using a simple 1-group flux in each zone as the metric of interest, but concept can be easily extended to many more groups. If we only allow the 1-group flux to change from zone to zone, similar to the variable time step treatment in section 3.6.2, we can set the constraint that

$$\Delta\phi_{min} < \phi_g^2 - \phi_g^1 \leq \Delta\phi_{max}, \tag{3.64}$$

where ϕ_g represents the group flux in two adjacent radial zones and $\Delta\phi_{max}$ and $\Delta\phi_{max}$ are the maximum and minimum allowable change in fluxes between those two zones. This comparison can be made for any number of energy groups that one would wish to compare. However, use of the group flux does present a problem of statistical noise if we are using many groups and requiring a small change in each group from zone to zone.

At every calculation point, we must evaluate the flux across each zone and calculate the relative change from one zone to the next. If the change is too large, zones are split.

Alternatively, if it is too small, the zones could be combined. Splitting implies altering a zone originally of thickness Δr to be $\Delta r/2$ and the number of zones in the problem to increase by one. Likewise, combining implies taking two adjacent zones of thickness Δr_1 and Δr_2 are summed to create a single zone of a new thickness Δr_3 such that

$$\Delta r_3 = \Delta r_1 + \Delta r_2. \tag{3.65}$$

Mass and volume of materials in problem must be conserved, such that combining or splitting zones maintains a constant material composition after each refinement. Mass is conserved when splitting one zone into two by distributing the material according to the ratio of their volumes. Likewise, when combining two zones into one, we must assume that the entire zone can represent an average composition instead of variable composition across the zone. This is done because of the constant nuclide density and flux requirements across a depletion zone in solving equation 3.61. Utilizing the above information, we can formulate a system of equations for at each mesh point representing the quantities particular to a zone z as

$$\left[\begin{array}{l} \frac{\Delta N_{i,1}}{\Delta t} = \phi_1 \sum_{k=1}^{m} f_{ik}\sigma_k N_{k,1} + \sum_{j=1}^{m} l_{ji}\lambda_j N_{j,1} - (\lambda_i + \sigma_i\phi_1)N_{i,1} \\ \frac{\Delta N_{i,2}}{\Delta t} = \phi_2 \sum_{k=1}^{m} f_{ik}\sigma_k N_{k,2} + \sum_{j=1}^{m} l_{ji}\lambda_j N_{j,2} - (\lambda_i + \sigma_i\phi_2)N_{i,2} \\ \qquad\qquad \vdots \\ \frac{\Delta N_{i,z}}{\Delta t} = \phi_z \sum_{k=1}^{m} f_{ik}\sigma_k N_{k,z} + \sum_{j=1}^{m} l_{ji}\lambda_j N_{j,z} - (\lambda_i + \sigma_i\phi_z)N_{i,z} \end{array}\right], \tag{3.66}$$

where i=1,2,3....m. Extending equation 3.66 to three dimensions in Cartesian geometry can be performed using equation 3.59 to produce the set of equations

$$\left[\frac{\Delta N_{i,x,y,z}}{\Delta t} = \phi_{x,y,z}\sum_{k=1}^{m} f_{ik}\sigma_k N_{k,x,y,z} + \sum_{j=1}^{m} l_{ji}\lambda_j N_{j,x,y,z} - (\lambda_i + \sigma_i\phi_{x,y,z})N_{i,x,y,z}\right], \tag{3.67}$$
$$i = 1,2,3....m,\ x = 1,2,3...q,\ y = 1,2,3...p,\ z = 1,2,3...n.$$

In this case, a similar nomenclature for the fluxes and nuclide densities is used such that $\phi_{x,y,z}$ represents the flux in a particular zone at independent x,y, and z coordinates. This is useful for a general 3D analysis, but for our purposes, we are interested in a simplified 1D approach for a radial system.

Given the average fluxes from zone to zone, we can determine if two zones can be combined. However, to determine if a zone should be split, we require the fluxes at the boundaries of the zone. This, in effect, is the flux at the boundary surfaces, rather than the zone averaged flux. If we apply equation 3.64 at the boundaries to a 1D radial zone and examine the relative change from one boundary to another, we have

$$\frac{\phi^{R_2} - \phi^{R_1}}{\phi^{R_2}} \leq \%\Delta\phi_{max}, \tag{3.68}$$

where ϕ^{R_1} and ϕ^{R_2} are the fluxes at each radial surface. This change in flux across a zone can be used to identify which zones require splitting. However, we are presented with a problem of the relative change in flux may exceed a defined limit of say 10%, but the product of the flux and the cross sections of interest in that zone are very low. This could be the case for a zone that is far away from the external source and most fissile material or is completely burned up. Recalling that we are interested in accurately predicting the burnup details in each zone, we can borrow the concept of importance from Monteburns for a zone. Namely, if the fractional absorption or fission contribution from the zone in question is small compared to that of the rest of the system, splitting is not required. We can define the fractional absorption rate as

$$f_{abs} = \frac{\phi_i \Sigma_a^i V_i}{\sum_{j=1}^{n} \phi_j \Sigma_a^j V_j}, \tag{3.69}$$

where ϕ_j is the flux and Σ_a^j is the total macroscopic 1 group absorption cross section in each respective zone. Similarly, the fractional fission contribution can be expressed as

$$f_{fis} = \frac{\phi_i \Sigma_f^i V_i}{\sum_{j=1}^{n} \phi_j \Sigma_f^j V_j}, \tag{3.70}$$

where Σ_f is the macroscopic 1 group fission cross section of the material in the zone. This can be extended to multigroup approximations as well, but is left as future work. Given the fractional contribution to total absorption and fission in the problem, we can first determine if the neutron flux varies by more than an allowed amount across a zone. Then, if so, we check how important that zone is to the total absorption and fission rates in the problem. If the zone is not contributing much, there is no reason to split the zone up into smaller zones. Likewise, if two adjacent zones either do not have a large variation in neutron flux across them, or are not contributing much to the overall fission and absorption rates, we can combine them.

3.6.3.1 AMR Implementation

The primary goal of AMR is to reduce the overall computational requirements while accurately simulating the LFFH system with a fixed fuel configuration. When the fuel is not flowing through the system, the assumption of constant mixing cannot be used and requires finely zoning the depletion problem to capture changes in the nuclide field and neutron flux. By applying AMR, we can capture these details in areas that require it, but in areas that don't we can leave these areas coarsely zoned. Specifically these are zones where the flux is not changing much across the zone, or the fractional contribution to reaction rates of interest (primarily fuel absorption and fission) in this zone are negligible relative to the rest of the system.

Unlike adaptive time stepping, AMR presents the additional challenge of requiring detailed knowledge of geometric cell and surface definitions and their connectivity through out the problem. Namely, in order to adjust the depletion geometry, details of the transport geometry are required. This proves quite detailed in practice utilizing even 2D geometries. Hence, for the purposes of this work, only 1D spherically symmetric geometry is implemented. This geometry was chosen for its simplicity and applicability to the current LFFH engine design. This amounts to depletion zones consisting of concentric spherically symmetric shells representing the depletion zones.

The AMR implementation into LNC is modular and extensible. It is implemented so that the first operation performed at the top of a depletion step is the AMR operation as showing in Figure 3.20. The calculation begins with LNC reading the user input files and initializing necessary data structures. After this initialization, the Adaptive Burnup Library AMR routine is called. The AMR routines iterate on the depletion mesh for the current depletion step until satisfactory zoning is found. Next, the control is returned to the LNC code to perform a TBR and power update. The iteration routines are called within LNC to find an acceptable ^{6}Li enrichment in the coolants and the corresponding material compositions. At this point, the Adaptive Burnup Library is called again to perform adaptive time stepping. Once the appropriate time step size is determined, LNC executes Monteburns to deplete the materials. After Monteburns finishes, the LNC code returns to the top of the execution loop and performs the same series of calls for the next depletion step.

The AMR algorithm is shown in Figure 3.21. The ABL Library is called by the client code, LNC, via a method named *AdjustBurnupMesh*. This method immediately initializes data structures and calls various class constructors. Next, the MCNP input is parsed to determine all the cell, surface and material information for the problem. This data could also be passed directly to the library via public setter methods to avoid disk file reads. After the input file is read, burnup cell and surface connectivity is determined, as well as identification of cell that require calculation of their volume.

In order to correctly split and combine cells, the volumes of these cells must be calculated. If the cell to be used as a burnup zone utilizes the universe fill and lattice capabilities of MCNP, the universe tree must be traversed until the ultimate filling universe is found. Each cell containing this universe or making up a cell with this universe filling it must have an accurate volume assigned to it for flux tally normalization. For example in the LFFH simulations, the fuel material is located inside kernel of the TRISO particle, which makes up a universe. The carbon layers surrounding that kernel are also located in that same universe and shown in Figure 3.22a. This universe fills a pebble shown in Figure 3.22b. Likewise, this pebble is part of another universe that fills the fuel blanket and comprises a burnup zone. To split this burnup zone, the volumes of each cell contained in every universe that fills the burnup zone must be calculated. This process had to be automated to ensure the library could deal with any arbitrary number of cells and universes. The same is true of surfaces making up the burnup zone. The surface areas are required for flux calculations across those surfaces. It should be noted that the limit of 50 burnup zones applies

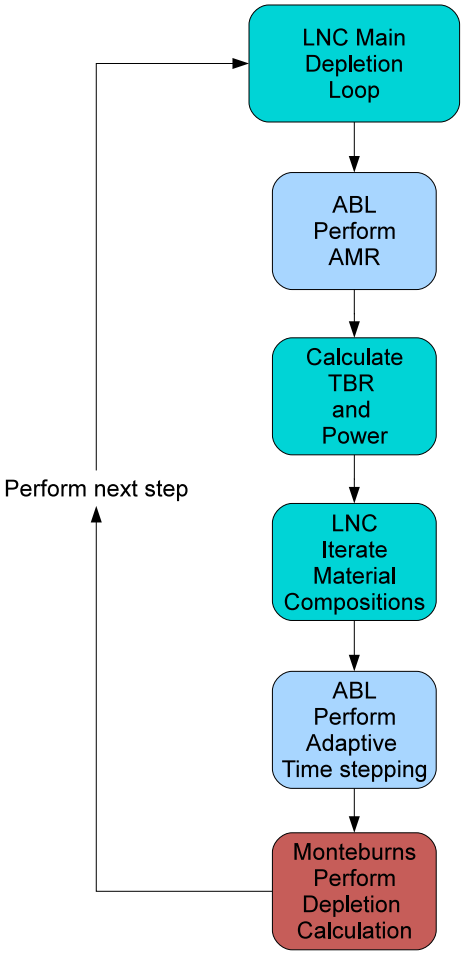

Figure 3.20: Adaptive Burnup Library calls within the LNC main execution loop

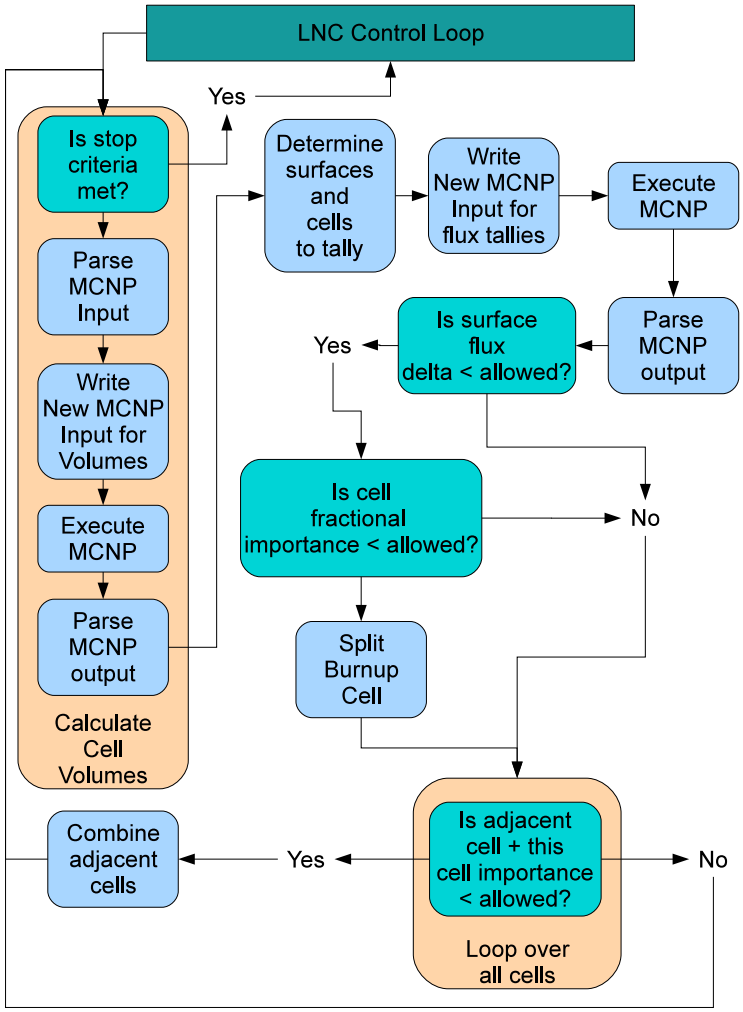

Figure 3.21: Adaptive Burnup Library algorithm

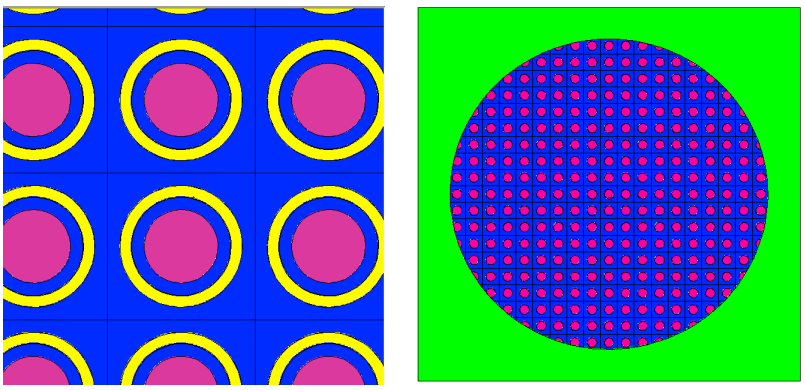

(a) TRISO particles in lattice

(b) Pebble filled with universe of TRISO particles

Figure 3.22: TRISO particles modeled in a lattice consisting of the kernel and carbon layers

when using AMR because that limitation is imposed by Monteburns due to tally numbering limitations in MCNP5.

Once the list of cells requiring a calculated volume is formulated, a MCNP input deck to is generated utilizing the stochastic volume capability of MCNP. This effectively turns off all physics in the calculation and floods the geometry with particles in an effort to utilize ray tracing to stochastically calculate the volumes and surface areas of required cells and surfaces. Upon completion, the ABL Library parses the MCNP output to read in the calculated cells and surface areas and stores those values for later use.

Now that the volumes have been determined, the *AdjustBurnupMesh* routine writes and executes MCNP with a modified input deck containing the new volumes and additional cell and surface flux tallies with associated multiplier cards. The ABL library utilizes two types of information to split or combine cells. First, it utilizes the 1 group neutron flux across the cell. Rather than tallying the average flux in the cell, the flux across the two radial surfaces comprising the burnup zone are tallied. For example, Figure 3.23 shows a single fuel zone filled with a lattice of fuel pebbles (pebbles are not shown). The entire burnup zone is contained within surfaces 9 and 10. Thus, if we want to know the change in flux across the zone, we can measure the flux across these bounding surfaces. The ABL library inserts one such tally for each burnup zone of interest. Similarly, F4 type neutron flux tallies are written for each cell containing a burnable material. This tally utilizes tally multiplier cards to measure the total absorption and fission in each cell. An example of these tallies can be seen in Appendix B.3.

Once the cell reaction rates and surface fluxes are tallied, the ABL parses the MCNP results and stores this information for use in the *SplitCells* and *CombineCells* methods. *SplitCells* is called first and begins by examining the surface fluxes across each burnup zone. If the the relative change in flux is greater than the user specified value (e.g. 10%),

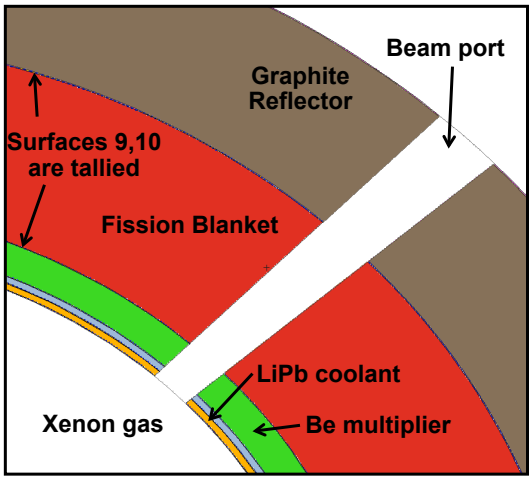

Figure 3.23: Fuel lattice contained within radial surfaces 9 and 10

the zone is split into two equal thickness zones. All cells that fill the original zone are duplicated and renumbered and a new material is created for the new burnup zone. Prior to performing the split, however, the fractional absorption and fission rates are compared to the maximum allowable defined by the user. This is to prevent splitting of a burnup zone in a low flux region that meets the surface flux criteria to split it, but the actual contribution of that zone to the fission or absorption rates are so low that it need not be split. Thus is the case for zones on the outer edge of the LFFH fission blanket. They are far away from the source and where all the fission is happening. The neutron flux is $\sim$1 order of magnitude lower in these zones and we are not interested in splitting them.

The *CombineCells* method operates slightly differently than the splitting routine. First, the fractional absorption and fission rates for every adjacent zone are checked. If the sum of the contributions of the two zones falls below the user defined limit (e.g. 10%), the cells are combined. The old surfaces, materials and filling cells are removed and the *AdjustBurnupMesh* routine continues to the beginning of the loop to calculate the new volumes. The process continues until either no more burnup zones are split or combined, or the maximum number of burnup zones is reached (currently 50).

After converging on a solution for the current burnup step, a new monteburns input file is written to instruct it to burn the correct materials and the new mcnp input deck is handed back to LNC to continue its main loop. This overall approach is utilized in the Adaptive Burnup Library to generate the depletion mesh shown in Figure 3.24. The external neutron source in this image is located in the center of this cutaway from the spherical chamber. As expected, the problem is more finely zoned in regions of high neutron flux changes and more coarsely zoned in regions of lower flux changes or fission/absorption importance. This figure illustrates how the adaptive meshing can reduce the overall number of depletion zones by tailoring the zone size to maintain a finely zoned mesh only where needed.

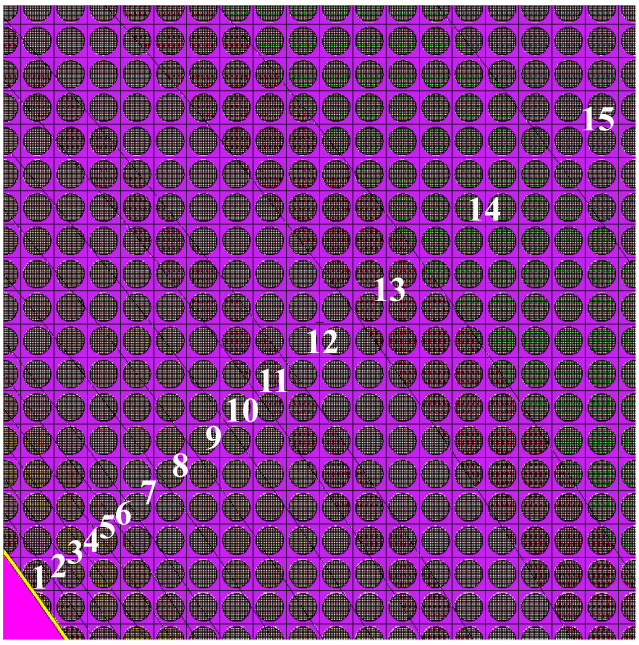

Figure 3.24: Example AMR mesh generated for LFFH engine showing increasing zone thickness moving outward.

3.6.4 Operator Splitting of the Two Methods

Both the variable time step and adaptive mesh refinement methods adjust parameters that affect how quickly reaction rates and the neutron flux change. Since the two methods operate on separate independent variables, they can be treated separately via an operator splitting concept. Namely, over the coarse of any given depletion time step we can employ one operation first, followed by the second. Normally, the choice of splitting is determined by the physics being solved. For these methods, however, we are simply adjusting the resolution of the calculation to ensure accuracy while performing the minimum amount of computational work. We could choose to adjust the mesh size and then the time step or vice versa. The advantage in choosing to adjust the mesh size first lies with the fact splitting or combining of zones requires recalculation of the fluxes, burnups and powers in all zones to compute the new time step size. If the time step size were already adjusted, this work would have to be performed twice. The new time step would be calculated, the zone sizes and quantities adjusted, and then the time step would have to be recalculated. Instead, if we first adjust the zone sizes such that the changes in flux from zone to zone is within acceptable limits, the time step could then be adjusted accordingly after the mesh has been adjusted.

3.7 Summary

In order to simulate the LFFH engine design, multiple physics calculations must be performed including neutron and photon transport, nuclide depletion and radiation dose calculations. Depletion and radiation dose calculations are performed using Monte Carlo transport methods coupled to matrix exponential solution method of the Bateman equations.

The LNC code was written to enable the fully-time dependent simulation of the LFFH engine. It serves as a control code for Monteburns 2.0 and MCNP5 and was written in C++ for fast efficient operation. It allows for any arbitrary hybrid fusion-fission system design and can fully deplete and control the system thermal power and TBR in a time dependent manner. Control is achieved via iteration on the ^{6}Li enrichment in the flibe and $Li_{17}Pb_{83}$ coolants, but any material could be used. The iteration algorithm is robust and virtually always converges to a successful solution at every time step in the problem.

Approximations like full blanket mixing of pebbles may not always be assumed for certain blanket configurations like a fixed fuel configuration, which presents difficulties in performing accurate and timely calculations. To deal with this, two methods are developed and applied to the depletion problem to reduce computational requirements while maintaining accuracy. Variable time stepping is utilized to automatically adjust the time step size to be a maximum possible while still maintaining the desired accuracy. Automatic mesh refinement is used to adjust the depletion zone size such that regions of high and changing flux are tracked more finely and regions of lower and slower changing flux are tracked more coarsely. To extend the general functionally and reduce the computational requirements of the LNC code, the Adaptive Burnup Library was developed. This standalone C++ library is linked into the LNC code for the burnup calculation. These two methods can result in signification time savings as compared to a fix time step, fixed burnup mesh problem.

Chapter 4

Results and Discussion

God does not care about our mathematical difficulties.

He integrates empirically.

- Albert Einstein -

4.1 LFFH Engine Neutronics Design

As described in Chapter 2, one aspect of this study focused on the development of a design of a DU fueled LFFH engine to fulfill the energy production mission. With that in mind, we are interested in optimizing performance aspects relevant to that mission. These aspects include reaching peak operating power as quickly as possible, achieving maximum theoretical burnup, minimizing the fuel and structural damage rates, maintaining tritium self-sufficiency and maximizing the BOP utilization. These performance metrics are detailed in the following sections of this chapter as part of a parametric study in Section 4.3.3 using a fully mixed fission fuel core. Prior to discussing these results, it should be noted that the results utilize variable time stepping, which enabled those parametric studies to be performed by reducing the computation requirements. The results from this parametric study are used to develop and describe the baseline design in Section 4.3. After developing a system utilizing an average fuel bed composition, we can begin to examine a system utilizing multiple blanket layers, which are depleted independently. To speed these calculations, AMR was developed and incorporated into the code.

4.2 Transport and Depletion Simulation Models

This section describes model fidelity calculations and justifies the models used. The analysis begins with determining the level of geometric detail required for the LFFH transport simulations. That discussion is followed by the description of the depletion models.

4.2.1 MCNP Neutron Transport Model Fidelity

Perhaps the most important phase of the depletion calculation is the neutron and photon transport step. If the models used do not accurately capture the physical neutron flux, all other calculations will be incorrect. This is a well known issue in nuclear reactor design and significant efforts have been made to ensure simulations are as accurate as possible. One advantage of Monte Carlo method, as previously discussed, is the fact that the simulation model can exactly reflect the true geometry and physics of the system. One needs only to include the necessary geometric detail and perform the simulation with accurate statistics.

4.2.1.1 The Question of Accuracy vs. Computational Speed

MCNP simulation models of the LFFH engine can be highly detailed, down to TRISO kernel level or even smaller. One could even conceive of a MCNP model that discretely modeled separate layers of each kernel to allow for differential burnup within a TRISO particle. However, this model fidelity comes at a huge computational expense. In simulating the LFFH engine, we must ask the question of what level of geometric and physics fidelity is required in the transport models to ensure accurate results. As the fidelity increases, we must utilize more computational resources to perform the calculation.

The transport model fidelity can be broken down into two general areas that affect the results: geometric details and statistics. The geometric details can be broken into three separate areas as well: fuel fidelity, structural fidelity and Be pebble layer fidelity. Structural fidelity specifically addresses whether discrete laser beam ports must be modeled individually, or if they can be ignored or lumped into two discrete ports. Details regarding the structural ribbing and coolant piping are not included because of the infancy of the mechanical design. Doing so simplifies the transport calculation, but may adversely impact the neutron leakage rates in the system.

Fuel fidelity refers to the level of detail utilized to model the fission fuel. We are specifically interested spatial self-shielding effects in the fuel [45]. The LFFH fuel blanket consists of a double heterogeneous fuel (TRISO particles, fuel pebbles) surrounded by a strongly absorbing coolant. In the case of a nuclear reactor, there would be no question that the TRISO particles have to be modeled at the fuel kernel level because of the strong effect of self-shielding on the system criticality. To test this assertion for the LFFH, we perform simulations using varying levels of fidelity and compare the neutron spectra in the fuel and reaction rates of interest.

Similar to the fuel pebble resolution, is the question of whether the beryllium pebbles can be simply homogenized with the coolant or must be modeled heterogeneously. The primary physics phenomena in this case is not neutron self-shielding, but neutron streaming effects. In other words, the discrete pebbles could present streaming paths for neutrons to escape from the blanket without interacting with the Be. The decrease in interactions with Be atoms would cause a corresponding decrease in the (n,2n) reactions and decrease the net neutron economy of the system. Homogenizing the Be pebbles with the coolant could

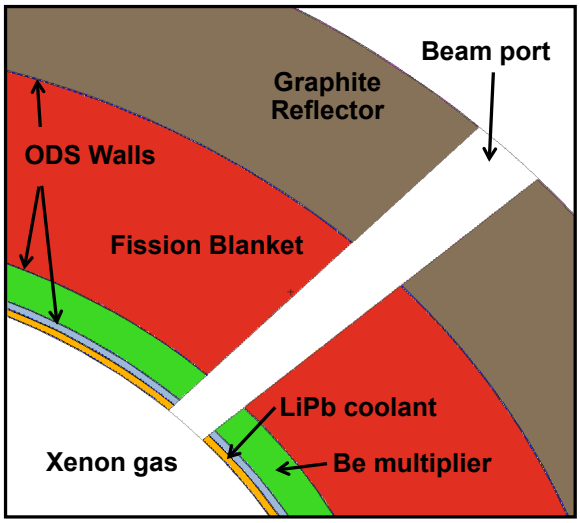

Figure 4.1: Slice of system model using fully homogenized pebble beds showing a discrete beam port and individual walls

save computer time, but the homogenized material would not maintain potential streaming paths for the neutrons to leak out from the blanket.

These two phenomena, spatial self-shielding and neutron streaming, are not unique to a fusion-fission hybrid, but have important implications for the LFFH engine. Spatial self-shielding complicates the transport and depletion simulations because extremely detailed geometry is required to accurately model the system. Likewise, neutron streaming is a potential loss mechanism that is exacerbated by the fact that the source is at the center of the engine. To quantify these two effects, we can take a bottom-up approach starting with fully homogenized fuel and Be pebble layers and further refine the geometry in a systematic manner to determine the appropriate level of fidelity for this analysis.

4.2.1.2 Homogenized Fuel and Multiplier Pebble Beds

One of the first assumptions made in analyzing and designing the LFFH engine was that the system neutronics model could be represented by a volume homogenized material composition for the various pebble blankets. This assumption is known to be very inaccurate for nuclear reactors and warrants checking it for our LFFH depletion calculations. This geometry can be seen in Figure 4.1.

4.2.1.3 Detailed Be Pebbles in Lattice geometry

It is important to capture the details of the Be pebbles because of the neutron multiplication occurring in the layer. To measure this effect, a baseline fully homogenized system model is modified to include discrete Be pebbles and measure the changes in the neutron spectrum,

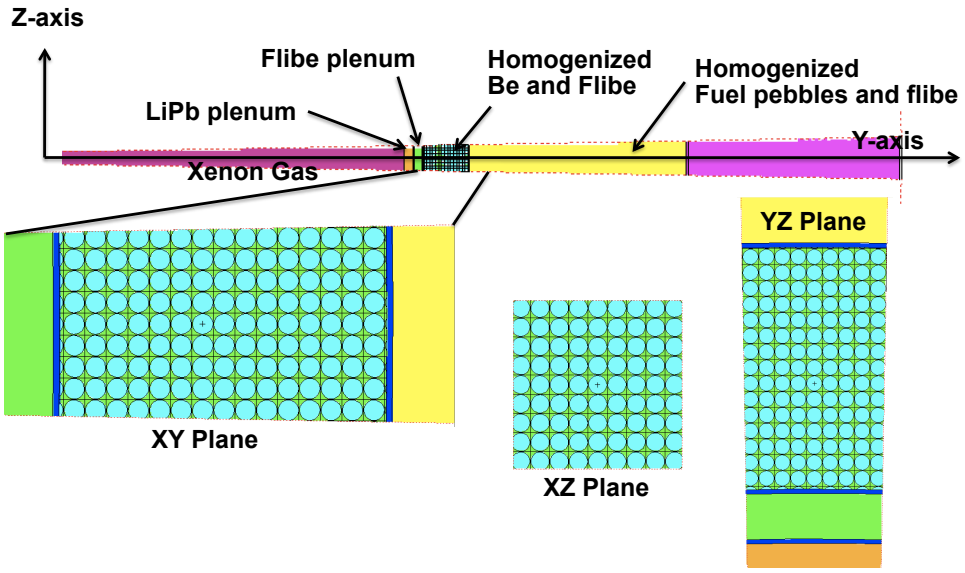

Figure 4.2: Wedge cutout of system model using lattice geometry for Be pebble bed

multiplication and leakage rates. To do so, the Be pebbles are modeled in a lattice geometry supported by MCNP. A cutaway of the model is shown in Figure 4.2. The only change between a fully homogenized model and the detailed Be pebbles is the inclusion of the discrete Be pebbles in the model. The total Be mass is conserved to ensure an accurate comparison. The comparison of the neutron leakage spectra from the Be pebble layer is shown in Figure 4.3 and summarized in Table 4.1.

We can see from the spectral plot that there is a slight increase in the number of neutrons around the 1.7×10^{-7} MeV energy range. This can be explained by the fact that there is a slight increase in the neutron spectrum for discrete geometry because of a 0.75% reduction in the number of Be(n,2n)α reactions. At first, this seems counter intuitive because one would expect more thermalization with an increase in Be(n,2n)α reactions. However, if we examine the total number of ^{6}Li absorptions in the Be layer coolant more closely, there are more ^{6}Li absorptions in a homogeneous model than the heterogeneous one. This occurs because the increase in Be(n,2n)α neutrons also leads to an increase in the number of neutrons at thermal energies which are more likely captured by the ^{6}Li. Hence, the increased probably of a neutron to interact with a ^{6}Li atom reduces the flux in the thermal regime.

Based on these results, we can conclude that modeling the Be pebbles discretely can be neglected unless relative error of ~1.0% is unacceptable.

Although an approximate 0.74% error is introduced when homogenizing the Be pebbles with the flibe coolant, this only addresses part of the issue. In reality, the Be pebbles will be oriented randomly and not in a regular lattice. By utilizing a special function in MCNP we can randomly orient the pebbles within the lattice as shown in Figure 4.4. In this figure, the Be pebbles appear different sizes, but are actually located at different random posi-

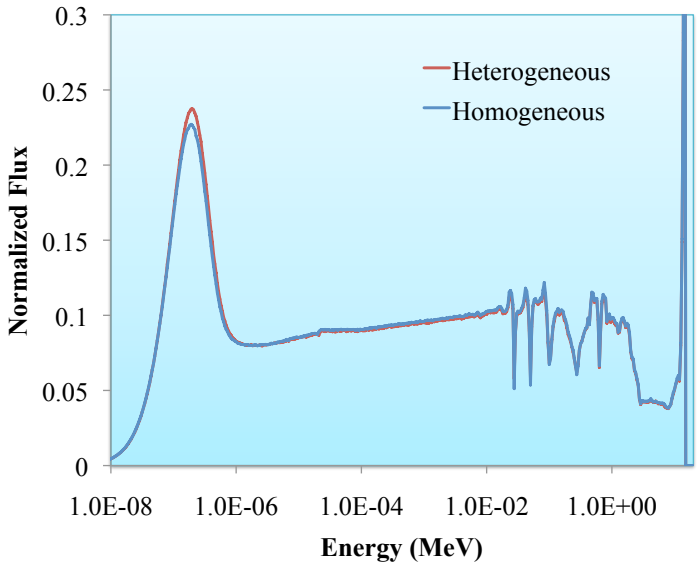

Figure 4.3: Neutron leakage spectra out of the Be region to the fuel bed using homogenized and discrete Be pebble geometry

tions relative to the cutting plane.However, as shown in Table 4.1, the effects of the use of stochastic geometry vs lattice geometry for this problem are negligible. Therefore, for the purposes of this work, the models utilize homogeneous Be pebbles to reduce computation time relative to a truly stochastic orientation of the pebbles in the flibe coolant.

4.2.1.4 Detailed Fuel Kernels and Pebbles in Lattice geometry

Similar to the discrete Be pebbles, we must understand the importance of resolving the fuel pebbles inside the coolant and the TRISO particles down to the kernel inside each pebble.

Be Pebble Geometry	$Be(n,2n)\alpha$ Reactions (reactions/sec)	System Total (n,xn) (reactions/sourced neutron/sec)
Homogeneous	2.093×10^{19}	1.476
Heterogeneous	7.985×10^{19}	1.475
Stochastic Heterogeneous	7.986×10^{19}	1.475

Table 4.1: Summary of differences between fully homogeneous and discrete Be pebble geometry

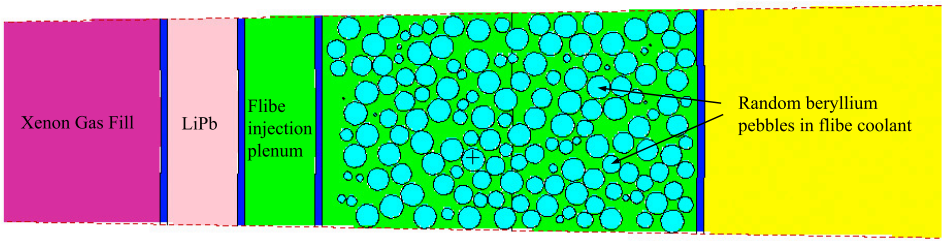

Figure 4.4: Random discrete Be pebble geometry.

To understand how homogenization introduces errors by neglecting spatial self-shielding of the fuel, we again utilize a lattice configuration of the fuel particles inside each pebble and of the pebbles in the blanket. Without this lattice capability, resolving the problem geometry would require resolving approximately 1.5×10^{11} separate cells and transporting a sufficient number of neutrons (roughly 100-1000 particles/cell) through those cells to ensure statistical accuracy if the flux spectrum varies drastically across the fuel bed. This is a calculation that is too large for even the worlds largest supercomputers. As an alternative, we can utilize the lattice geometry capability in MCNP. Many reactor studies have already utilized this feature to perform very large simulations on pebble bed reactors [94, 95, 96, 97, 98, 99]. These studies have shown that for a reactor, the fuel particles can be modeled in a lattice with negligible impact as compared to a truly stochastic orientation. In other words, Brown et al. found that for a critical HTGR reactor, stochastic geometry vs a regular lattice was a negligible effect so it will be negligible for our subcritical system with weak feedback as well. For the LFFH simulations, we employ this same methodology. This model geometry is illustrated in Figure 4.5 where the physical pebble and TRISO particles are represented by a lattice geometry in the MCNP transport model[1]. The TRISO coatings are homogenized with the pebble graphite.

It should be noted that for certain reactor designs, Brown et al. concluded that *clipping* the fuel kernels could result in significant errors because mass is not conserved. They suggest using a finite lattice instead, where the vertical pitch of the lattice is adjusted to preserve the total mass and packing fraction. For LFFH simulations, however, we choose to allow *clipping* and adjusted the mass by varying the blanket volume so that it is conserved relative to a homogenized case. This eliminates the need to manually adjust the lattice pitch in all three directions to achieve mass and packing fraction conservation. This was also the conclusion for fuel particles in multiple reactor studies [98, 100, 94, 96, 101].

Given these characteristics of the heterogeneous model, we can compare the neutron spectra and ^{239}Pu production rate between the homogeneous and heterogeneous models. ^{239}Pu production is of interest because it is the primary isotope that is produced from ^{238}U capture. This capture reaction is increased or decreased depending on the amount of spatial

[1]Courtesy Jeffrey Powers, University of California, Berkeley

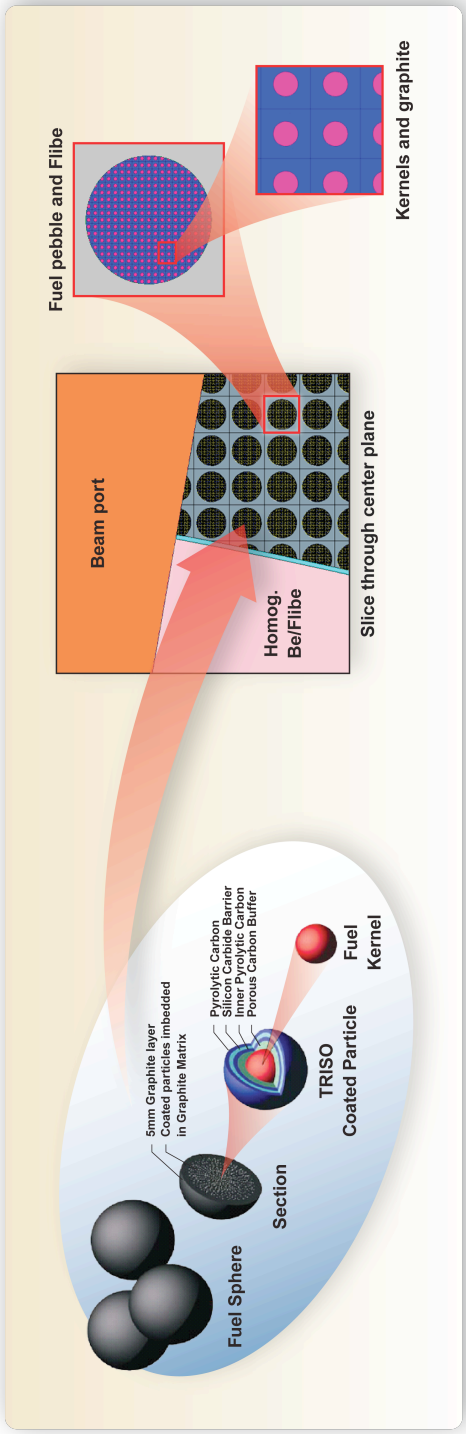

Figure 4.5: The physical and modeled fuel kernels and pebbles

Fuel Model	Conversion Ratio	Peak Pu (MT)	^{238}U Capture (barn)
Homogeneous	13.2	1.46	3.34
Heterogeneous	10.9	1.83	2.56

Table 4.2: Summary differences when using a homogeneous or heterogeneous fuel model

self-shielding. If we completely neglected self-shielding, as in the case of a homogeneous model, we would expect the ^{239}Pu production rate to be much greater than in the reality. This is because neutrons traveling through the homogenized material have an increased probability of ^{238}U capture relative to a heterogeneous model. This can be seen in Figure 4.6a . The heterogeneous model accurately captures the spatial self-shielding, which will reduce the neutron flux in the inner fuel region, reduce the ^{238}U capture, and result in more thermal neutrons available for fission or other reactions. The ^{239}Pu inventory, shown in Figure 4.6b, is in error by as much as $\sim$23% and is an unacceptable error. Additional differences in the conversion ratio and effective capture cross section are given in Table 4.2. To eliminate this effect, all analyses in this dissertation utilize a fully heterogeneous model of the fuel kernels and pebbles with volumes adjusted to conserve mass. Like previous studies, use of truly stochastic geometry does not warrant the added computational expense.

4.2.2 Nuclide Depletion and Activation Models

The depletion models used in this analysis can be grouped into three distinct types: a single depletion zone with full mixing, multiple depletion zones with intrazone mixing, and multiple fixed zone depletion with batch reload. In all cases, the neutron transport is carried out using fully heterogeneous geometry. The different depletion methods simply use different tallied neutron fluxes from the detailed transport calculations. In other words, the depletion methodologies average the neutron flux across a depletion zone, when in reality the flux changes at every point in space. This is done for two reasons. First, the simplifications must be made to make the problem tenable on today's computers. Second, in many areas of the fission blanket, the neutron flux varies slowly as one moves radially outward. This slow change is what allows us to utilize detailed transport models to solve for the flux, but then use simplified depletion models to solve for the nuclide evolution.

4.2.2.1 Single mixed Zone Depletion

Using Monteburns, MCNP and ORIGEN2, the LFFH system can be simulated using multiple models for fuel movement throughout the core. The simplest method depletes the whole core using a uniform flux, termed fully mixed zone depletion. All pebbles begin with the same material composition and continue the burnup process with exactly the same compositions after each depletion step. For this method, two main assumptions are made. First, the pebbles move through the core at a high enough rate that they are well mixed

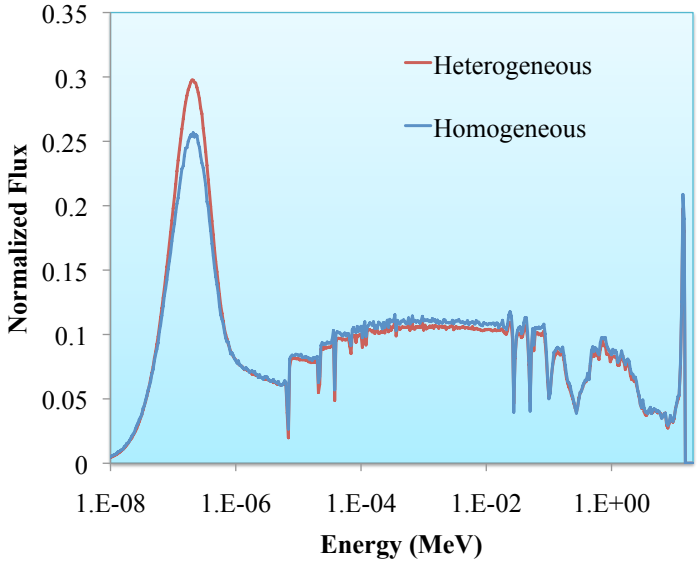

(a) Neutron spectrum in fuel region showing significant differences in thermal flux

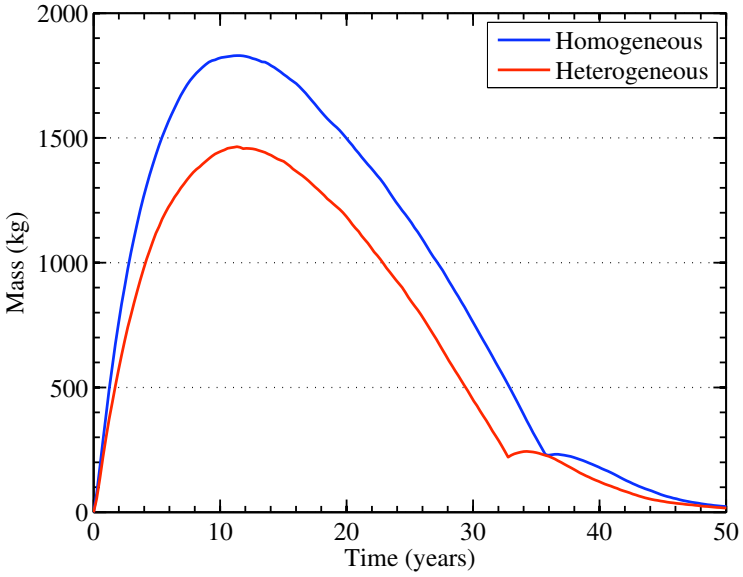

(b) ^{239}Pu inventory shows ∼21% error in peak mass

Figure 4.6: Heterogeneous vs homogeneous fuel geometry results show large differences in both the flux spectrum and the fissile ^{239}Pu inventory

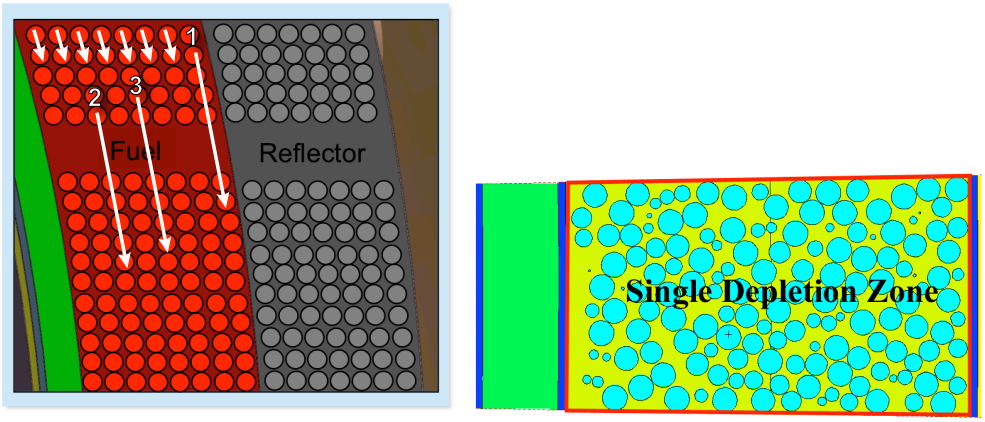

(a) Fully mixed fission blanket with random insertion points

(b) Depletion model with single zone

Figure 4.7: Example of random insertion of fuel pebbles through fission blanket and how they are depleted (pebbles not to scale)

and spend an equal amount of time in the front of the blanket as in the back of the blanket, thus being subjected to each flux regime for the same amount of time. The assumption of random position in the blanket requires periodic removal and reinsertion of pebbles from the LFFH core. An example of this assumption is shown in Figure 4.7a. The arrows at the top indicate the general direction of pebble flow in a downward motion. This is also indicative of the fact that pebbles are reinserted randomly and could be inserted at the back of the blanket in one cycle and in the front of the blanket in the next.

The second assumption is that each pebble, on average, sees a flux throughout the burnup with variations in the flux primarily due to changes in system power. I.E. the LFFH engine never operates in equilibrium, but the average flux the pebbles are exposed to is constant across the fuel bed. This allows for the depletion calculation to be performed on a single depletion zone, reducing memory and CPU requirements. Since a single zone is depleted, a single material composition is evolved. This method is typically used for scaling and optimization studies to determine key system parameters. This assumption presents difficulty in a real system because the flow rates of the pebbles through the blanket would be fast enough to cause severe wear damage from friction. Even so, for the purposes of this study, the fully mixed model is considered a baseline. An example of this model can be seen in Figure 4.7b.

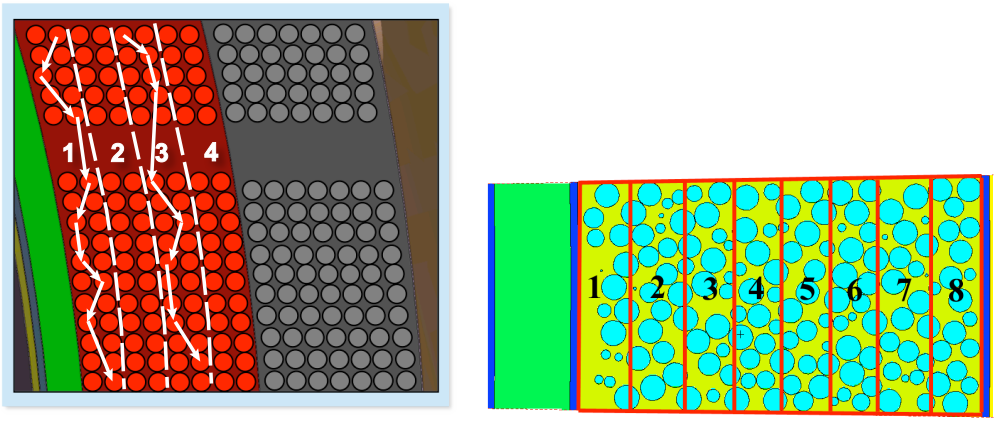

(a) Partially mixed layers with constant insertion points

(b) Depletion model with multiple zones

Figure 4.8: Example of how pebbles move through stratified layers and how they are modeled (pebbles not to scale)

4.2.2.2 Multizone mixing depletion

In reality, the flux in the LFFH engine decreases as one move radially outward through the fission blanket. This results in a continuously decreasing burnup moving radially outward. In order to offset this effect, recirculation rates of the blanket would need to be high [102]. To better capture this effect, we can employ multiple zone depletion with mixing within zones. This method depletes multiple independent burnup zones of finite size larger than a single pebble. Since the depletion zone size is larger than a single pebble, adequate mixing is still assumed, but the assumption of perfect radial mixing is no longer required. Pebbles need not be mixed randomly in the radial direction. Figure 4.8a illustrates this concept using 4 radial zones. Each zone is essentially stratified minimizing inter-zone mixing over a depletion step. Pebbles within each layer can intermix, but not outside of the layer. Since the pebbles are still flowing through the system, this method instead assumes that the pebbles remain stratified in a radial layer and are reinserted in the same radial layer after removal. Also, across this radial layer, the flux is assumed constant. Advantages of this method include reducing the requirements on mixing and pebble flow, and accurate burnup details in a spatially varying sourced system. Multiple layers in the fuel bed are depleted and tracked independently. The main disadvantage of this method is the computational requirements. Each additional depletion zone requires X additional tallies and the memory requirements can become too large for many computer systems.

Multiple mixed zone depletion is an enhancement to the single mixed zone method

in the sense that fuel pebbles are no longer assumed to be fully mixed throughout the blanket, but only within a stratified layer, shown in Figure 4.8b. In this case, the fission blanket is subdivided into multiple zones (<50 due to Monteburns code limitations). Each zonal neutron flux is tallied and evolved independently of the others along with the nuclide inventories. The only assumptions are that pebbles spend an equal amount of time at each point in the stratified layer and the layers stay separated. This again is difficult in practice because there will be some inter-zone mixing of pebbles that is not accounted for in the model. Likewise, the use of lattice geometry results in cutting of pebbles and TRISO particles in a depletion zone because a Cartesian lattice does not fit exactly into a spherical shell. This cutting of zones results in part of a pebble or TRISO particle existing in one depletion zone while the rest of the particle or pebble exists in an adjacent zone. Since, the neutron transport problem is modeled continuously, the depletion zone boundaries do not affect the neutron flux calculation. The nuclide field will, however, evolve differently from zone to zone and potentially result in different isotopic concentrations within a cut TRISO particle. This cannot be avoided unless the TRISO particles and fuel pebbles are manually arranged to prevent cutting of zones. One can even envision depleting each TRISO particle independently if the codes and computers could support such a calculation.

4.2.3 Material Compositions

The materials utilized for all analyses in this dissertation are maintained constant with the exception being the enrichment ratios of ^{6}Li/^{7}Li in the coolants and the fuel kernel due to depletion. All structural and fuel materials are summarized in Table 4.3. The fuel kernel is chosen to be UCO in anticipation of reducing TRISO particle failure probability [55]. The fuel enrichment is actually depleted below natural to 0.253% enrichment. The TRISO particle graphite and SiC coatings are similar compositions and densities to those commonly used in other reactor designs.

The main and secondary coolants, flibe and $Li_{17}Pb_{83}$, were chosen for their superior volumetric heat capacity, tritium breeding and neutron multiplication and moderation properties. The densities of both coolants are treated as constant with respect to temperature for the neutron transport and depletion calculations. The temperature chosen for the coolants is based on external thermal hydraulics calculations performed by Abbott et. al. [44].

Structural materials are composed of an Oxide Dispersed ferritic Steel (ODS) as described in section 2.3.9 of this dissertation. No effort is made to model the material internal structure of the ODS (nanoparticles, etc.). It is simply treated as homogenized with the appropriate atomic fractions of the constituent species included in the material definition. Geometric details including the radial wall thickness and beam ports are included.

Details as to the isotopic compositions and atom fraction of each isotope in the material are given in the example input deck in Appendix B.

Component	Material	Density $\left(g/cm^3\right)$	Temperature $(^\circ C)$
Fuel Kernel	UCO	10.50	900
Carbon Buffer	Carbon	1.10	900
Inner PyC	Pyrolytic Carbon	1.95	900
SiC	SiC	3.20	900
Outer PyC	Pyrolytic Carbon	1.95	900
Matrix	Graphite	1.70	900
Pebble Shell	SiC	3.20	900
Be Pebbles	Be	1.85	600
Main Coolant	Flibe	2.00	600
Secondary Coolant	$Li_{17}Pb_{83}$	9.50	600
Structure	ODS	8.00	900
Reflector	Graphite	1.70	900

Table 4.3: Summary of materials and properties used in LFFH simulation models

4.2.4 Nuclear Data

Early work was performed using the ENDF/B-VI nuclear data cross sections [103]. However, the ENDF/B-VI cross section set was found to be inadequate for modeling a fusion-fission hybrid to high burnup. Challenges arise when isotopes are produced by ORIGEN2 that do not exist in the MCNP transport library. Namely, if a daughter product is produced and transport cross sections do not exist, MCNP cannot perform a transport simulation. To handle this, Monteburns discards the mass of the isotope in question. For low burnup systems, this is acceptable because the discarded mass in question is a very small fraction of the total mass being burned and can be ignored. However, for high burnup systems seeking to achieve greater than 90% FIMA burnup, these errors can become as large as 50% and are unacceptable [38]. One immediate way to improve this situation is to generate cross section data for the missing isotopes in question. This could mean developing cross section data for the entire table of the isotopes. However, the majority of those isotopes are extremely short lived relative to a depletion time step and can be treated as equilibrium daughter products. Alternatively, we can extend our cross section set to include more isotopes of interest by using the ENDF/B-VII cross section set. This data set contains transport cross sections for 393 separate isotopes as compared to 80 in ENDF/B-VI and encompasses most of the isotopes of interest for our problem. Each cross section is broadened to the appropriate temperature of each material to properly treat the Doppler effect [45]. Similarly, thermal scattering kernels are employed for molecularly bound species including graphite, beryllium, and iron in all materials in the system.

4.2.5 Summary of Models

Using Monte Carlo analysis of homogeneous and heterogeneous geometry, we found that the expected neutron streaming effect is negligible in the Be pebble layer and the Be pebbles can be homogenized with the flibe coolant at the expense of 0.75% accuracy in the simulation. Similarly, we found that the spatial self-shielding of fuel kernels has a profound effect on the ^{239}Pu inventory and hence the system criticality. Given this result, the fuel kernels must be modeled discretely in discrete pebbles creating a doubly heterogeneous problem. Truly stochastic modeling of the kernels and pebbles, however, is not needed and the simulations can be performed using a lattice geometry instead. This is provided the mass and volume of the fuel is conserved from simulation to simulation. The transport models include all material details required to accurately capture structural and streaming effects in the system. Likewise, damage rates are tallied in the system for all materials utilizing a macroscopic damage model. The nuclear data utilized in the transport and depletion models is considered the most accurate of the evaluated data sets available and care has been taken to account for bound thermal scattering and Doppler broadening effects. The depletion models rely on assumptions about the flow of pebbles through the pebble bed, but techniques have been developed to deal with fully mixed and partially mixed beds.

4.3 Neutronics Features of LFFH

Throughout this study, the development of the LFFH neutronics simulations begin with the use of a 3D model utilizing a fully mixed fission core. This assumption is utilized for the parametric and general scoping studies throughout this chapter, with the exception of results obtained utilizing multiple zone burnup and AMR. When utilizing multiple zone depletion, pebble mixing with each zone is assumed instead. In general, the LFFH engine neutronics characteristics are described below.

4.3.1 Burnup Characteristics

As discussed in Chapter 2, the LFFH engine thermal power curve, shown in Figure 4.9, is controlled to maximize the time at peak power. Utilizing the design parameters outlined in Table 2.4, the operational power of 2GWth was chosen as a good balance between BOP utilization and power produced. The two red dashed lines illustrate the 50 MWth range that the LNC code maintains the thermal power within. The system takes approximately 1 year to reach full power. This is the result of very little fissile mass existing in the fission blanket at start up because of the DU fuel. There are no enriched seed pebbles to start the system. However, as fusion neutrons are produced and interact with neutron moderating and multiplying layers to the fission blanket, some neutrons are captured by the ^{238}U to produce ^{239}Pu. During this period, the conversion ratio is over 10.0. Fissile isotope production continues past the point of full power, but is controlled via ^{6}Li coolant enrichment to remain at

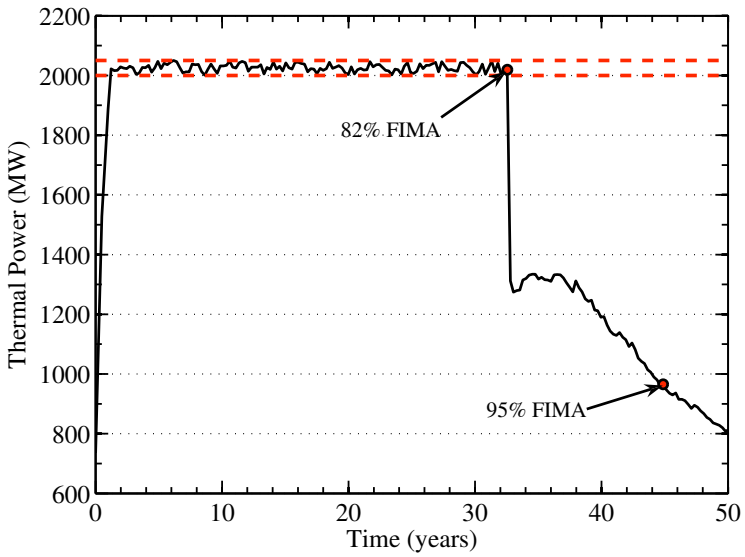

Figure 4.9: Typical LFFH engine thermal power curve

2,000 MWth for over 30 years with no fuel enrichment or reloading. The length of time that the system remains at full power can be adjusted by increasing or decreasing the amount of fuel in the blanket. This particular case illustrates a 20 MT DU fuel load.

Fissile mass in the system primarily consists of ^{235}U, ^{239}Pu and ^{241}Pu, although other fissile isotopes do exist in smaller quantities. Even the ^{235}U mass is small compared to the plutonium inventories as can be seen in Figure 4.10. The ^{239}Pu inventory peaks at about 1.5 MT approximately 11 years into the burn. Although this quantity may seem large, it is distributed across $\sim$13 million pebbles giving less that 0.12 g of ^{239}Pu per pebble. At the point of peak Pu, the system naturally transitions from a conversion ratio above 1.0 to below 1.0 and continues to consume the built up Pu inventory. The ^{241}Pu peaks at a later time, but is lower in total mass by a factor of 3. Most other actinides are also present (shown in Appendix A), but not nearly in the quantities of the Pu isotopes. The inflection points in the curves around 32 years illustrate the transition from operating at constant power to maintaining the TBR above 1.0. This inflection can be seen in the TBR and tritium inventories at this time as well.

The TBR and corresponding tritium inventory are controlled by the LNC code to remain above 1.0 and 0 kg respectively. Figure 4.11 shows how the TBR is adjusted over time and the tritium inventory is maintained. This drop in power is simply due to the fact that the tritium inventory was exhausted.

One alternative that has been suggested as a more efficient means of operation would be to operate at near equilibrium with tritium being fed externally to prevent losses due to tritium decay. In other words, the power could be extended even further (approximately 5-10 years) by supplying the fusion fuel from an external plant. This operating scenario is

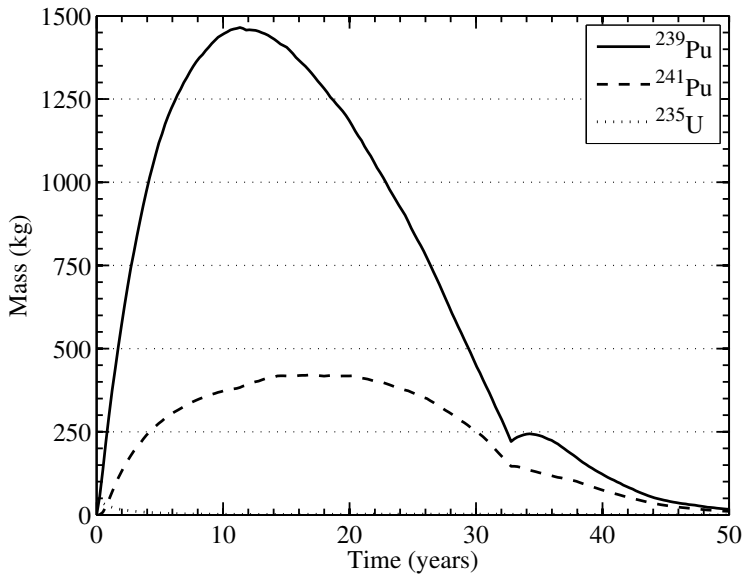

Figure 4.10: Fissile mass of important isotopes as a function of time

under investigation, but beyond the scope of this current work.

The TBR and power are continuously maintained by adjusting the ^{6}Li/^{7}Li ratios in the coolants. The ^{6}Li is initially at 0.1% in flibe and 7.5% in the $Li_{17}Pb_{83}$ and reaches a peak enrichment of 0.7% and 52%, respectively. These enrichment levels are adjusted continuously and automatically starting from the original values. In this case, the flibe is always depleted. However, the $Li_{17}Pb_{83}$ requires enrichment beyond natural. If enrichment to this level is not desirable, alternative coolant enrichment ratios could be explored.

One key feature of the LFFH engine is the significant variation in the neutron spectrum as the system operates. In Figure 4.12, the normalized neutron spectrum in the fission blanket is shown at startup, at time of peak plutonium inventory, at the time of tritium exhaustion and at 99% FIMA. The fuel blanket spectrum shows the 14 MeV fusion source peak, along with a large flux depression where ^{6}Li(n,α)T reactions occur, and other uranium and plutonium resonances. The spectrum starts out very thermalized with a large peak around 0.25 eV. However, as Pu is built up, the spectrum hardens such that the strongest part of the spectrum is from about 10 keV to 1 MeV. The strong resonances seen around 0.2, 0.5 and 0.1 MeV are due to ^{19}F, while the strong resonance at $\sim$0.3 MeV is due to Li constituents. The flux depression above 3 MeV is partially due to ^{9}Be(n,2n) and ^{7}Li(n,d)T reactions, but primarily due to the superposition of the fission and fusion source spectrums. Similarly, the strong ^{238}U capture resonance can be seen at $\sim$7 eV, ^{240}Pu capture at 1 eV, and ^{239}Pu fission around 0.3 eV, 20 eV and 38 eV. As the Pu burns down, the spectrum thermalizes again, but not to the extent as at startup until the fuel is fully burned. This constantly adjusting fuel-to-moderator ratio makes it challenging to tailor the spectrum at any given time to increase Pu production rates. Typical metrics are challenging to apply to

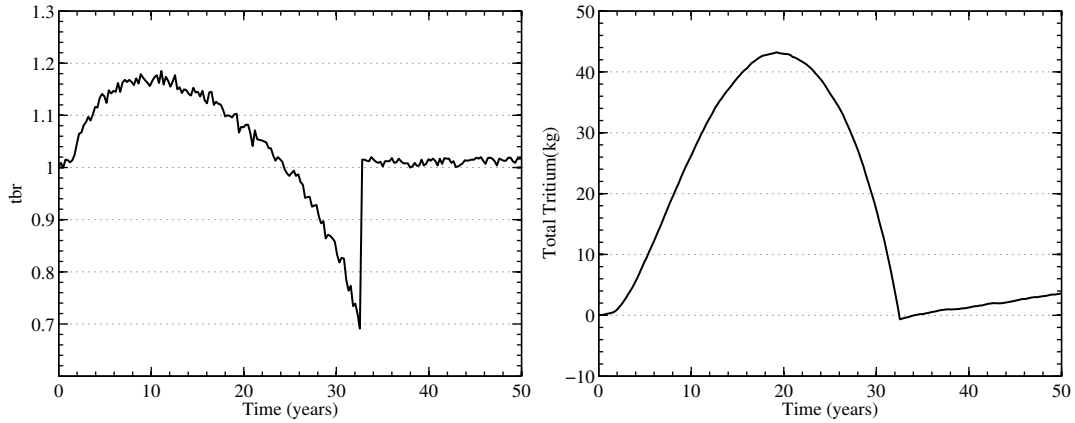

(a) TBR as a function of time for 20 MT baseline system

(b) Tritium inventory as a function of time for 20 MT baseline system

Figure 4.11: TBR and tritium operational characteristics

this time evolving system, but a few system level metrics have been defined. These include the balance of plant utilization and maximum burnup while at full power.

4.3.1.1 BOP Utilization

One key metric used in the parameter study detailed in Section 4.3.3 is the concept of balance of plant utilization (BOP). This metric is important when considering different engine design variables because the primary focus is to provide energy. BOP is a measure of how long the plant operates at it's desired thermal power. Since the LFFH power curve contains breed up and burn down transients, it is important to account for the amount of time that the system is not operating at full power if the system is operated through an incineration phase. Of course, a theoretical optimum would have a power curve shaped like a step function. When the system is turned on, it reaches full power immediately. When finished burning the fuel to the desired burnup, it is shutdown immediately as well. In this case, the BOP is 100%, assuming no down time for maintenance. The BOP for a LFFH thermal power curve can be calculated as

$$\frac{\int_0^t P_{th}(t)dt}{\int_0^t P_{max}dt} \times 100\%, \tag{4.1}$$

where $P_{th}(t)$ is the time dependent system thermal power integrated over time divided by the maximum or operating system power, P_{max}. For the LFFH engine described, the BOP utilization is approximately 78%. This value could be improved by using more advanced fuel and tritium management schemes that reduce the time ramping up to power and incinerating the remaining fuel actinides. For instance, if the system was simply shutdown when

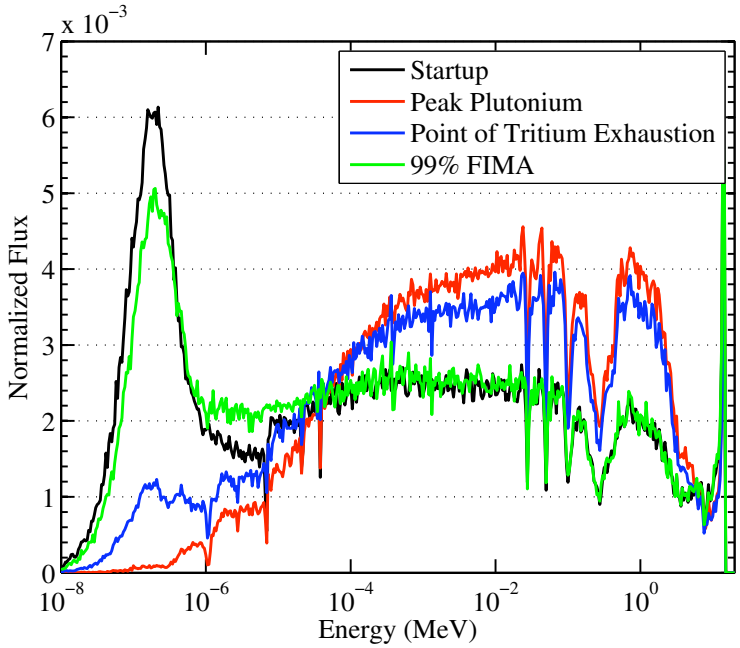

Figure 4.12: Neutron spectrum in DU LFFH engine averaged over the fission blanket at time of startup, peak Pu, tritium exhaustion and shutdown

the tritium inventory was exhausted, the BOP jumps to nearly 98%. This could generally be the case if the fuel were discarded to waste with an average burnup of 82% FIMA. Theoretical burnup in this system does not account for practically attainable burnup as a result of structural or fuel material damage.

4.3.1.2 Structural and Fuel Material Damage

Given the encouraging theoretical results of the LFFH engine performance, it is prudent to discuss the issues of fuel and structural wall survivability. When neutrons irradiate the structural materials and fuel, they cause transmutations in the material, which can alter the material properties in a negative way. In addition, even if those same neutrons do not cause transmutations, they can displace atoms out of the lattice structure. This has historically been an important metric in determining the amount of damage done to a material by neutrons in fusion systems. The displacements per atom (DPA) is a measure of the number of times each atom has moved in the material lattice.

Achieving such high burnup of the nuclear fuel is inhibited by the DPA as well as gas pressure buildup. It is believed that the fuel can be designed to withstand the gas pressure build up, but how the fuel survives under high DPA is unknown. As shown in Figure 4.13 the DPA rates on the first wall and Be layers exceed 10 DPA/year, which means the components will most likely require replacement prior to a full system burn. The first wall

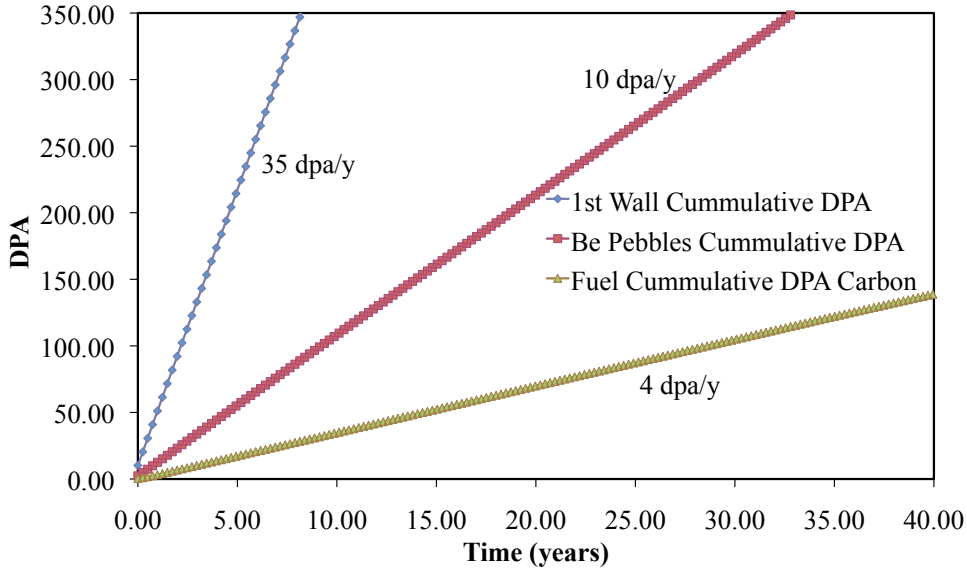

Figure 4.13: DPA as a function of time in the first wall, fuel and Be layers

could potentially last 3-5 years, based on current estimates of ODS ferritic steel strength [104]. The Be pebbles would likely require replacement or processing every 6-12 months because of neutron induced swelling [105]. Even so, both the Be pebbles and structural materials can be designed to be replaced. The fuel, however, is more challenging. It must survive to the level of burnup desired. If we desire 99% FIMA and assume a constant 4 DPA/yr damage rate, the fuel will sustain $\sim$230 DPA to reach this burnup. Although the fusion community routinely discusses high damage rates (100-200 DPA) in structural materials, there is no data in the literature to suggest the fuel could survive this level of damage. Instead, fuel materials damage has been discussed in the 10's of DPA [106]. In the 1980's, the Germans irradiated 50,000 LEU UCO TRISO fuel particles (with 300 μm kernel diameters) and no failures were observed after 18-22% FIMA burnups with a fluence of $1.4 - 2.5 \times 10^{25}$ n/m^2 [107]. Even so, issues regarding material properties of SiC and this high level of burnup remain [108, 109]. It is unlikely that today's fuel materials will survive this high irradiation damage and requires furthers research. If instead, we only desire reaching 50% FIMA, the fuel damage becomes $\sim$80 DPA. With that said, it is not within the scope of this work to address the details of fuel failure and its mechanisms. Instead, we note the damage rates as part of the theoretical performance limitations but present the LFFH engine neutronics design without damage considerations as the limiting factor.

4.3.1.3 Subcritical Design

Early on, it is noted that one of the primary design constraints for the LFFH engine is to remain subcritical at all times. Tritium production for LFFH is analogous to control rod insertion and removal for a nuclear reactor with two key differences. First, the ^{6}Li control mechanism provides a useful reaction product (tritium) as opposed to simply acting as a parasitic neutron absorber. Second, the control system is expected to be completely independent of the safety system. More specifically, since the system is externally driven by a fusion source, that fusion source can be shutdown extremely quickly. In the event of off normal operation, the lasers can be abruptly shut off thereby providing an extremely fast (< .08 sec) way to shut down the LFFH engine. The effect is similar to a reactor SCRAM where emergency control rods are inserted to shut down the reactor. However, the LFFH is slightly different because it is envisioned that the safety systems would first verify safe operation before injecting a target and firing the laser instead of actively attempting to quench a critical chain reaction. Regardless, the fission blanket is maintained subcritical at all times during operation. Even without controlling the system power, the LFFH engine cannot become critical under normal operation or uncontrolled scenarios. Although detailed safety analysis is beyond the scope of this work, we can examine what the LFFH engine criticality would be under a uncontrolled scenario since the flibe is such a strong neutron absorber[2]. For subcritical externally sourced system (with the source operating), we can define the multiplication factor as

$$k_{eff} = \frac{f_{mult} - 1}{f_{mult} - 1/\nu}, \tag{4.2}$$

where f_{mult} is the net multiplication of the system, and ν is the average number of neutrons produced per fission event. Using this definition, Figure 4.14 shows the system k_{eff} over time for a 20MT, DU system for both normal and uncontrolled operation. Even without control, the LFFH engine k_{eff} remains below 0.7 when the peak ^{239}Pu inventory exists in the blanket.

More detailed analysis is required, but initial estimates of the k_{eff} suggest that a LFFH engine can be designed to stay subcritical at all points during normal and off normal operation.

4.3.1.4 Temperature and Void Reactivity Feedback

Two potential concerns for any nuclear design are positive feedback due to temperature excursions or coolant voiding. If these reactivity parameters are positive, a runaway chain reaction could result. For instance, if a system has a positive temperature coefficient, an increase in temperature will cause an increase in system reactivity, which will cause an

[2]For safety calculations standard definitions of k_{eff} apply and MCNP kcode is used when studying detailed accident scenarios or reactivity coefficients assuming the fusion source is no longer active.

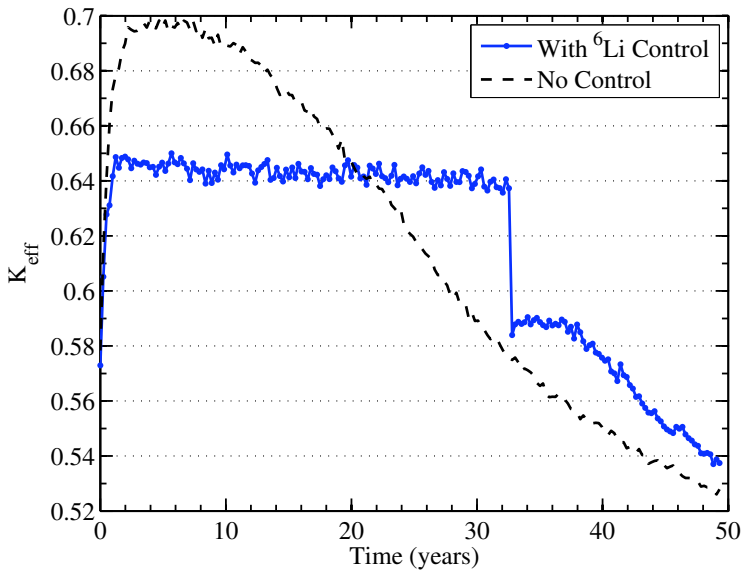

Figure 4.14: LFFH 2000 MW$_{th}$ DU LFFH engine criticality over time

corresponding increase in temperature and so on. The result is a runaway process that could cause catastrophic damage to the fuel from melting, etc. A positive void coefficient is similar with the driver being voids in the coolant or a loss of coolant for some reason.

The LFFH engine temperature response has been studied in some detail and it maintains a negative temperature coefficient[3] (for temperature response only) as shown in Table 4.4 [110]. The temperature coefficient for the coolants and fuel is negative for this system because of the large amount of ^{238}U in the fuel. As the temperature increases, Doppler broadening causes resonances in the various isotopes to broaden and increase the effective reaction rate. ^{238}U has a strong capture resonance that dominates fission resonances in the fuel and causes the reactivity to decrease as temperature increases. This is true at all times throughout the burn because the ^{238}U content is always greater than the fissile fuel content.

	Startup	Time of Peak Pu
k$_{eff}$	0.05435 ± 0.00008	0.45646 ± 0.00038
Temperature $(\Delta\rho_{th})$ (pcm/°K)	-173.5	-0.6
Void $(\Delta\rho_v)$	$\sim$10.3	$\sim$0.16

Table 4.4: Temperature and void coefficients of the LFFH engine

The void coefficient, however, does not stay negative and is actually strongly positive. This is from the strongly absorbing ^{6}Li used in the coolant to control the system power.

[3]Using MCNP kcode and assuming the fusion source is turned off.

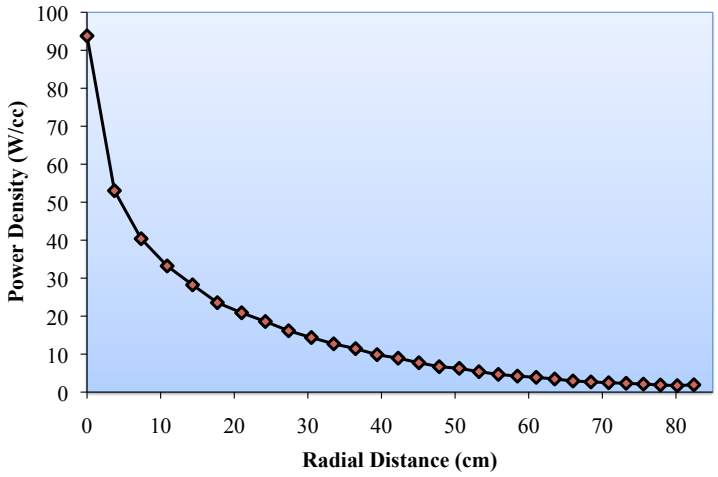

Figure 4.15: LFFH 2000 MW_{th} DU LFFH engine shows a power peaking factor of 6.

If the LFFH engine were a critical system, this would likely be unacceptable for safety reasons. A loss of coolant could cause a runaway criticality excursion. However, the LFFH engine operates with a very low k_{eff} of about 0.45646 ± 0.00038 and even though the void coefficient is positive, a total loss of coolant would only result in a peak k_{eff} of 0.49154 ± 0.00074.

4.3.1.5 Power Density and Peaking

The thermal power in the LFFH engine is generated directly from fusion, fission and other reactions. The utilization of a central fusion neutron source causes the flux in the fission blanket to be peaked toward the inner radius of the blanket. The actual power peaking factor is a function of the neutron flux and the fission rate occurring in the different regions of the blanket. Figure 4.15 shows that a power peaking factor of approximately 6 exists in the fission blanket at beginning of life with a maximum power density of 95 W/cm^2. Efforts to reduce this peaking factor are underway, but remain as future work. Insertion of control elements or other alterations to the core composition and geometry could reduce this power peaking and flatten the fission power across the bed. The shape of this power density shows that most of the fission occurs in the front of the blanket. Likewise, the neutron flux is almost $10\times$ larger in the front than the back of the blanket. This warrants the use of multiple depletion zones across the blanket to capture the differential burnup in the pebbles on a finer scale if the pebbles are not flowing through the system fast enough to assume an equilibrium core composition. Similarly, the relatively low flux region in the 2nd half of the blanket can utilize larger zones because the average changes in the flux are minimal. This is further discussed in Section 4.4.

4.3.2 Summary of Design

The LFFH engine is designed to operate at a continuous power of 2,000 MWth for up to 3 decades. During this time, the system produces its own tritium and is self-sufficient. It remains subcritical at all times and is safe from reactivity excursions driven by temperature effects or coolant voiding. As with all fusion systems, the material damage rates are very high. This issue is exacerbated by the fact that the fuel must survive to the desired burnup. A 35 DPA/yr damage rate on the first wall will require its replacement every 5-7 years. The Be pebbles will require replacement or heat treating every year. The survival of the fuel to high burnup is questionable and LFFH will most likely require a new fuel form to be qualified to these high burnups. The focus of this study remains to provide theoretical insight into the LFFH hybrid system performance.

4.3.3 Parametric Studies

As part of this study, various parameters were investigated to achieve the previously described design. Prior to embarking on this work (as part of the overall LLNL effort), the LFFH concept did not exist and many details needed to be considered to achieve the results. For instance, questions like what fuel loading is required? What TRISO particle packing fraction should be used? What should the chamber radius, fission blanket gain and fusion input power be? These and other questions were investigated as part of this study and results are detailed below.

4.3.3.1 Fuel loading

The LFFH engine can operate with virtually any amount of DU fuel. The effect of increasing the fuel load results in a longer time at full power. However, as Figure 4.16a shows, the time to burn down or incinerate the remaining actinides after tritium inventory exhaustion also increases[4]. This is illustrated by the increased shoulder to the right of each burn curve with 50 MT maintaining the longest full power burn, but also requiring the longest amount of time incinerate remaining actinides. Similarly, the time to reach full power is increased with an increasing fuel load (shown in Figure 4.16b). The end result is a lower BOP utilization for larger fuel loads. Likewise, running the power plant for 100-150 years becomes quite impractical because of the aforementioned fuel damage rates, etc. Based on this fact, a fuel load of 20 MT of DU fuel, identified by the solid green curve, is chosen as a baseline. Alternatively, Figure 4.16c shows the same thermal power curves vs. burnup. Notice, that as a function of burnup, the thermal power for almost all fuel loads is no longer sustainable within a range of 80%-90% FIMA. A fuel load of 20-25 MT maximizes the time and burnup at full power.

[4]Blanket thicknesses are 22.18 cm, 41.46 cm, 58.62 cm, 74.18 cm, 88.45 cm, 101.67 cm, 114.03 cm, 125.64 cm, 136.61 cm and 147.03 cm, respectively

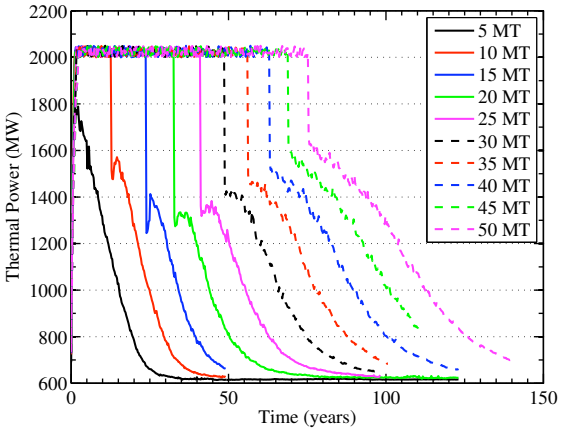

(a) Thermal powers vs time

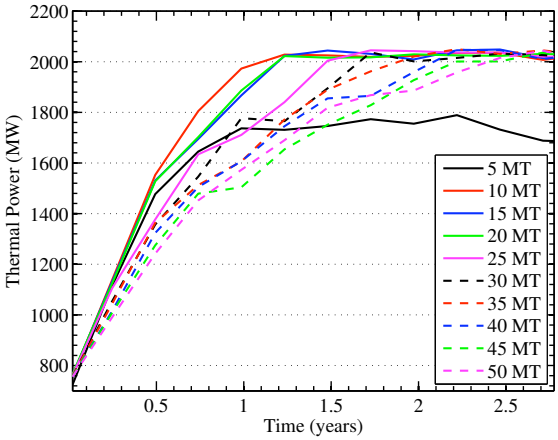

(b) Thermal power vs time zoomed into ramp up period only

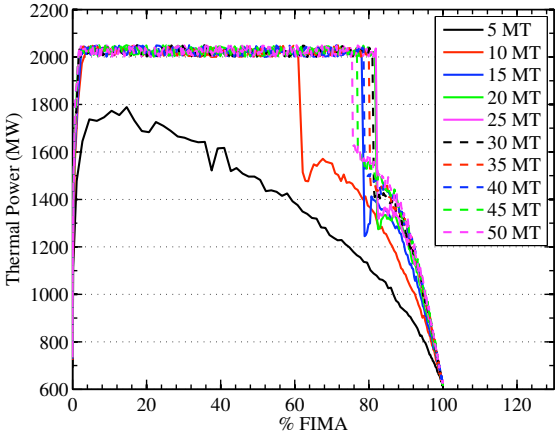

(c) Thermal powers vs burnup

Figure 4.16: Thermal power as a function of time and burnup for different fuel loads

As discussed earlier, the drop from full power is the result of the control algorithm in the LNC code. Either the tritium inventory is exhausted, or the fission blanket simply doesn't generate enough power to sustain the desired blanket gain. In the case of 5 MT fuel loading, we see from Figure 4.17a that although the tritium inventory is above 5 kg for the entire burn, the fission blanket simply can't generate enough thermal power to operate the system at 2GW. The TBR in this case is held at 1.0, shown in Figure 4.17b.This is in contrast to the other fuel loadings that fall from full power due to tritium inventory exhaustion. Hence, the optimum fuel loading balances the total fission occurring in the blanket with the necessary tritium inventory to sustain that fission rate. A 20 MT fuel loading accomplishes just this.

4.3.3.2 Fuel Kernel Size

Varying the fuel kernel size for a given TRISO packing fraction and heavy metal loading allows tailoring of the Carbon-to-Heavy Metal (C/HM) ratio in the fission blanket. If we hold the overall maximum diameter of the TRISO particle constant and adjust the kernel size, we effectively increase or decrease the C/HM ratio. An example of this can be seen in Figure 4.18. Figure 4.19 shows the effect of varying the fuel kernel size. The optimum kernel size is 300 μm diameter for this system. Two effects occur when changing the fuel kernel size. First, the C/HM ratio changes the level of moderation of the neutrons in the fuel. Second, larger fuel kernels self-shield the inner fuel regions from neutrons at epithermal and thermal energies. The result is less ^{238}U capture and production of ^{239}Pu. Smaller kernels reduce the self-shielding effect and result in a faster more energetic neutron spectrum. These combined effects can be seen in Figure 4.20. The smaller diameter kernels result in a reduced spectrum at the ^{238}U capture resonance and less ^{239}Pu is produced. The spatial self-shielding effect is effectively reduced. Alternatively, larger diameter kernels reduce the overall C/HM ratio, result in a harder spectrum and increase the self-shielding effect. For this study, a good balance is achieved using a 300 μm radius kernel giving a maximum achievable full power burn of $\sim$36 years.

4.3.3.3 TRISO Packing Fraction

An additional way to change the C/HM ratio in the LFFH engine is by adjusting the TRISO packing fraction within each fuel pebble. Alternative methods to adjust the C/HM ratio include inserting pure carbon pebbles into the blanket, but this method results in unattractively large blanket thicknesses. The TRISO packing fraction is one of the more important parameters in determining how well the LFFH engine burns it fuel. This is because the TRISO packing fraction significantly impacts the neutron flux spectrum as shown in Figure 4.21 . By adjusting the TRISO packing fraction from 5% to 50%, we see that the maximum achievable burnup while maintaining full power can be reached using a 20% packing fraction, shown in Figure 4.22 . A 20% packing fraction is the optimal for a 300 μm radius kernel because the fast flux is required to produce ^{239}Pu at a high enough rate

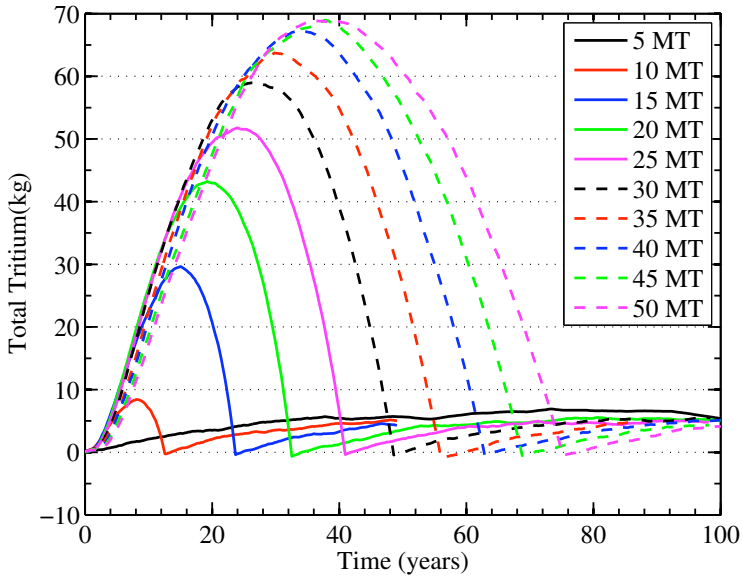

(a) Tritium inventory over time

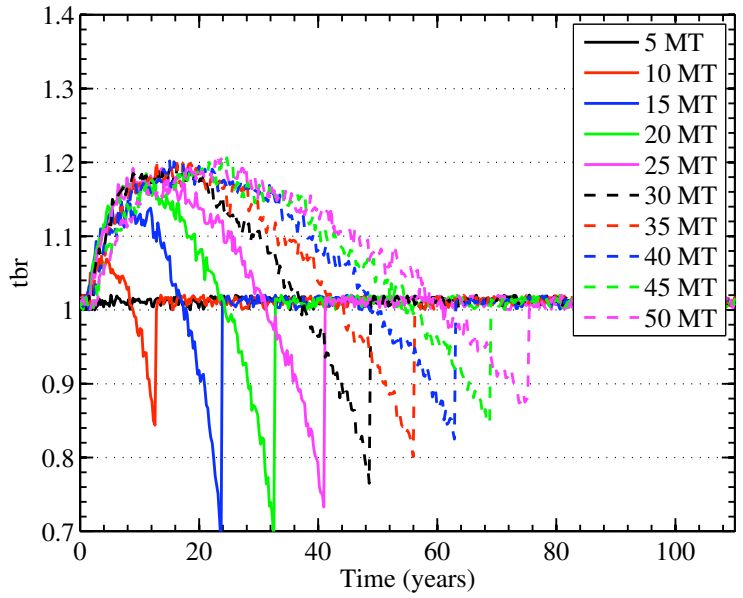

(b) TBR over time

Figure 4.17: Tritium inventory and TBR over time for different fuel loads

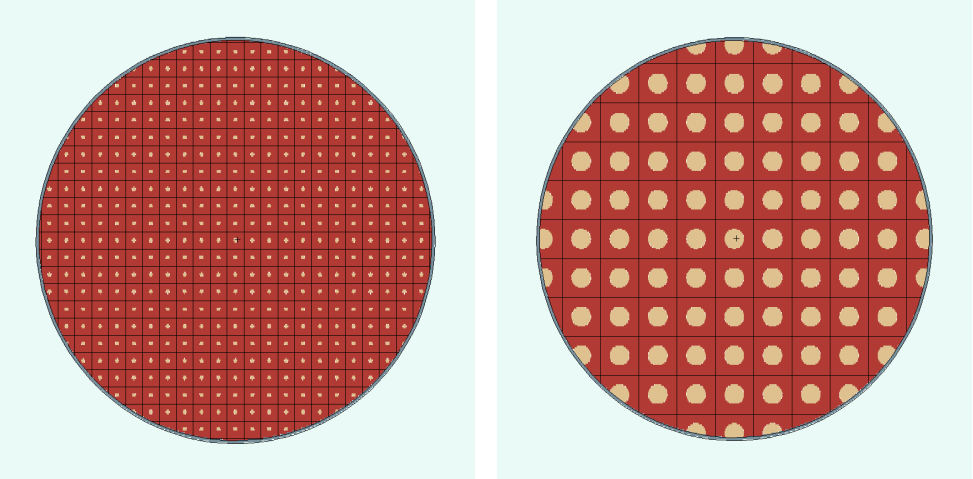

(a) Pebble with 100 μm kernels (b) Pebble with 500 μm kernels

Figure 4.18: Two different sized fuel kernels in TRISO particle and modeled lattice

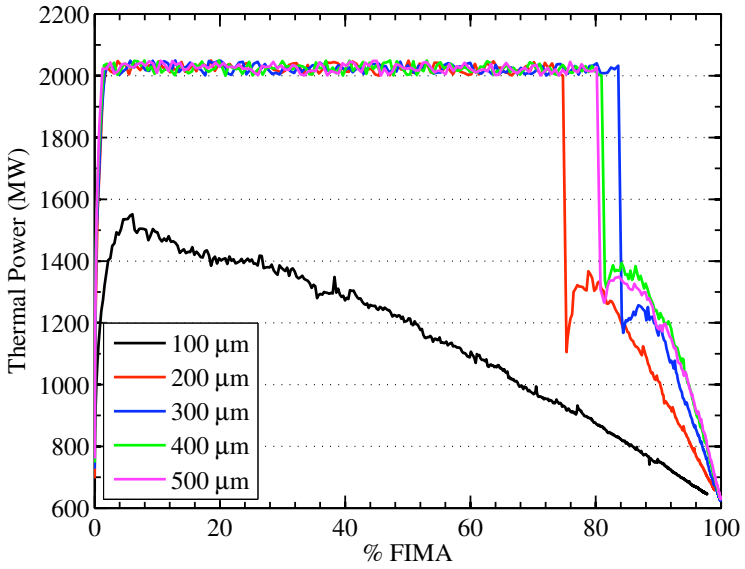

Figure 4.19: Fuel kernel size thermal power vs maximum attainable burnup

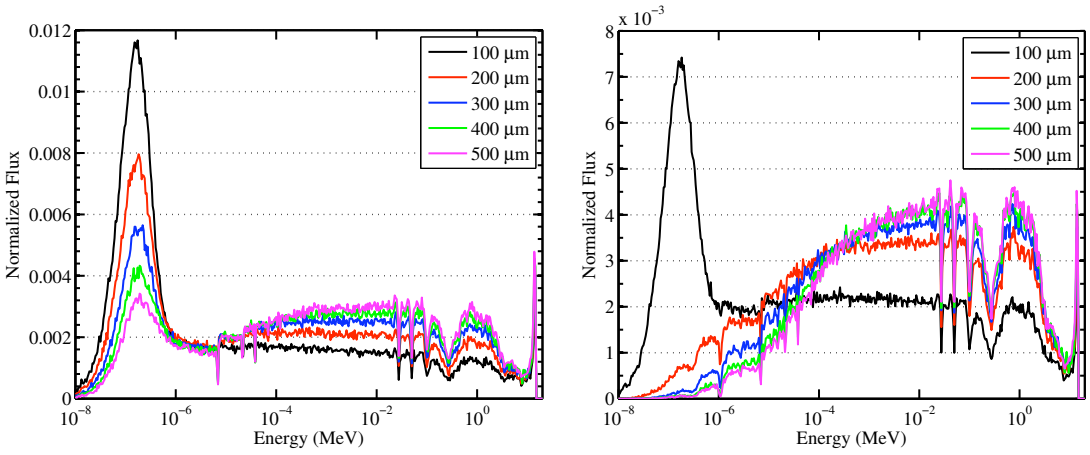

(a) At startup

(b) At time of peak plutonium

Figure 4.20: Neutron flux at startup and peak plutonium for different fuel kernel sizes

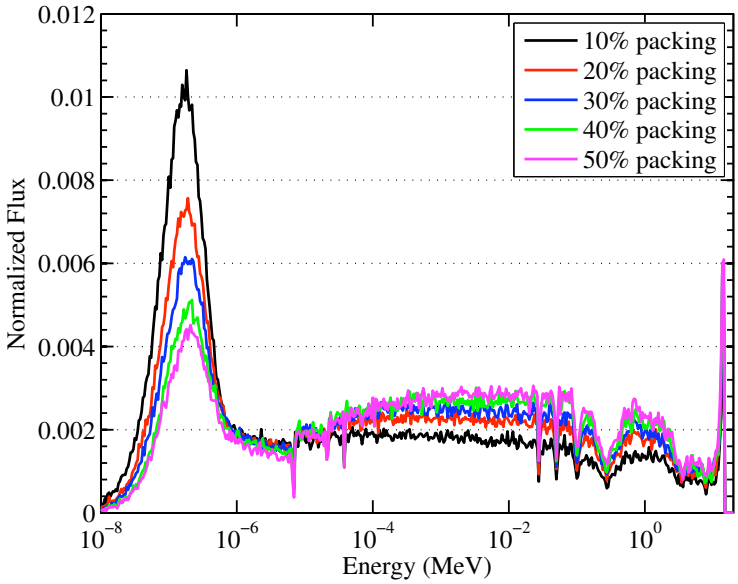

Figure 4.21: Neutron flux at startup for different TRISO packing fractions using a 300 μm kernel with a 20 MT fuel load

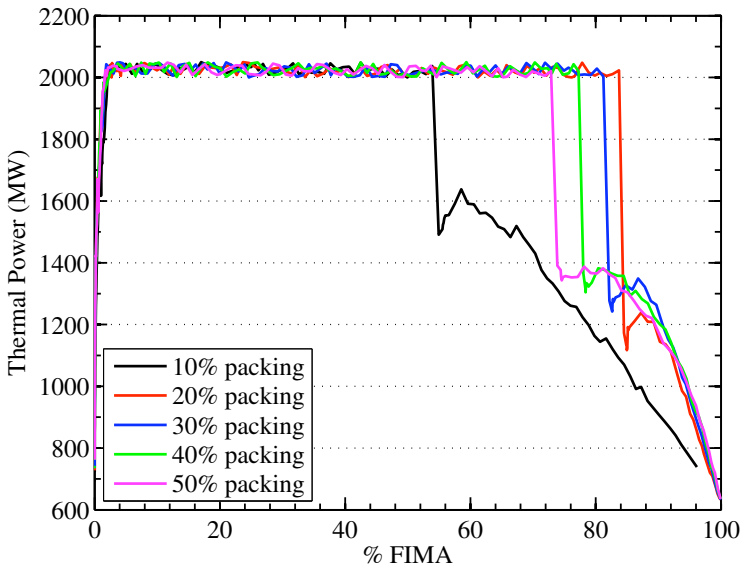

Figure 4.22: Maximum achievable burnup as a function of TRISO packing

to sustain the burn. Hence, the balance between conversion ratio, tritium production and fission power is optimized with a 20% packing fraction.

4.3.3.4 Chamber Radius and Fusion Neutron Flux

The fusion chamber radius plays an important role in determining the first wall lifetime and the peak flux on the innermost regions of the fission fuel blanket. Namely as the radius is reduced for a given fusion power, the neutron flux on the first wall and in the fission blanket increases primarily due to geometric, R^2 effects. At the same time, the radiation damage rate increases. Figure 4.23 shows how the thermal power curve improves with decreasing radius. However, the first wall damage rate increases as well. A choice must be made to operate with an acceptable damage rate causing more frequent replacement of the first wall and the improved burnup performance. This compromise lead to the choice of a 2.5m radius fusion chamber. The first wall damage rate at this radius is about 30 DPA/year. At that rate and assuming ODS ferritic steel can withstand 150-200 DPA before structural properties begin significantly degrading, the first wall would require replacement approximately every 5-7 years. True estimates of the plant down time to replace the first wall have not yet been performed. However, the operations required are expected to be similar to that of a nuclear reactor fuel assembly removal, which can take many days to finish.

The input fusion power for a fixed first wall radius has the effect similar to changing the chamber radius. The neutron flux going through the first wall is increased and the fission blanket performance increases from the higher flux throughout the blanket. One advantage

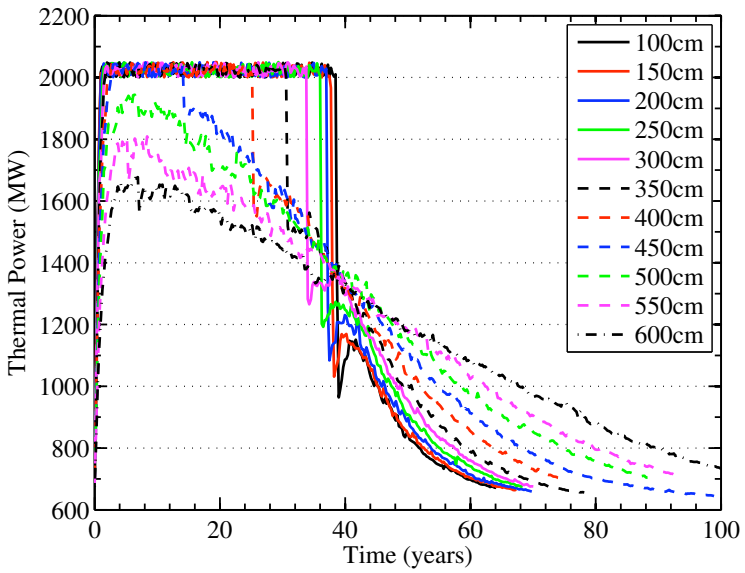

Figure 4.23: Thermal power as a function of first wall radius using a 20 MT loading, 300 μm kernel and 20% TRISO packing fraction

to adjusting the fusion power is relevant to the laser system. If fusion targets and the laser can not be scaled to lower yields economically, the higher yield targets could be taken advantage of by increasing the first wall radius. The net effect is an attempt to balance the flux in the fission blanket to be similar to the baseline design of 500 MW fusion with a 2.5 m radius chamber.

4.3.3.5 Blanket Gain

Key to the energy production mission is the overall system gain relative to the fusion input power. If we examine the hybrid LFFH engine in the context of fission blanket gain, we can define the blanket gain as a multiplier of the fusion power. For instance, a gain 2 system using 500 MW of fusion power would generate a total 1,000 MWth. The fission blanket gain also determines how large the relative fission contribution to total thermal power must be. Higher gain systems typically require larger fuel loadings to maintain these powers effectively with all other variables being constant. However, utilizing earlier results, we can examine the performance of the LFFH design for various blanket gains using a 20 MT fuel loading with 20% TRISO packing and a 300 μm kernel diameter. Figure 4.24a shows that as the blanket gain increases, the thermal power cannot be maintained for as long. In other words, the achievable burnup while maintaining that thermal power is lower and the BOP utilization falls as well. If it were not economically valuable to provide as much power as possible, a blanket gain of 2.5 would yield the highest BOP utilization to incinerate the fuel to 99% FIMA, shown in Figure 4.24b. In this case, blanket gain is varied

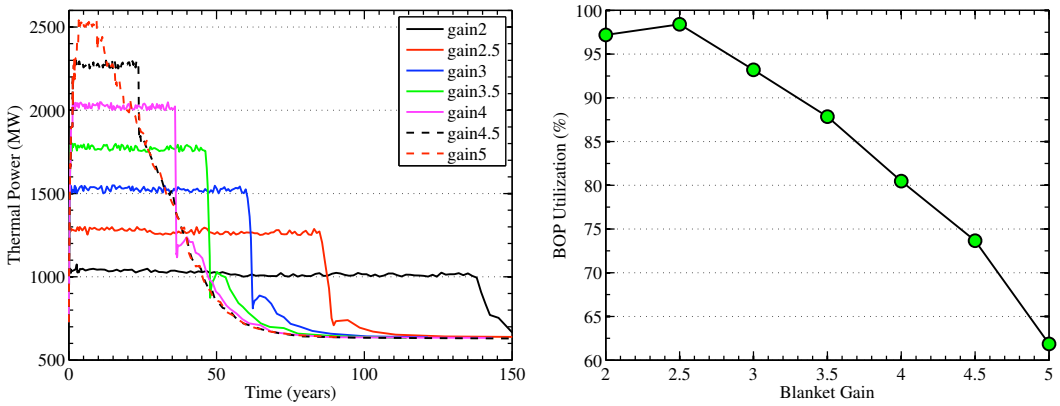

(a) Thermal power for different blanket gains

(b) BOP Utilization

Figure 4.24: Thermal power and BOP utilization for different fission blanket gains

by adjusting ^{6}Li concentration, thereby producing more or less tritium. However, since it is economically valuable to provide power, a sacrifice in BOP utilization must be made to achieve higher thermal output. This is a consequence of the fact that increased blanket gain requires a nominally higher fission power production for a given fuel loading. However, sustaining this power is primarily achieved at the expense of tritium production. A choice is made to use blanket gain of 4 with the desire to produce at least 2 GWth (primarily for economics reasons) at the expense of BOP utilization.

4.3.3.6 Be Blanket Thickness

As discussed in Chapter 2, the Be blanket thickness is a key parameter in optimizing the engine design. The Be blanket serves to moderate the 14 MeV fusion neutrons down to epithermal and thermal energies and to multiply those same neutrons primarily via ^{9}Be(n,2n) reactions. The difference between using a Be blanket and not is quite apparent in the neutron spectrum and is shown at both startup and time of peak Pu in Figure 4.25. The neutron spectra in the fission blanket is highly peaked at 14 MeV in the case of no Be blanket. Carbon is not as effective a moderator as Be and the resulting neutrons escape from the fission blanket relatively easily due to their high energy. Alternatively, adding the Be blanket significantly thermalizes the fusion neutrons to the point that at startup, the spectrum is dominant in the thermal region. As fissile isotopes are built up in the blanket, though, the spectrum gets harder with a larger portion of the neutrons in the fission blanket being born from fission.

Efforts were unsuccessful in achieving a design without a Be blanket. Alternative materials like $Li_{17}Pb_{83}$ and molten salts were studied, but with poor results. The optimum Be layer thickness turns out to be ~16 cm thick. Too thin of a blanket results in less neutron multiplication and poorer performance. Too thick of a blanket can actually cause too

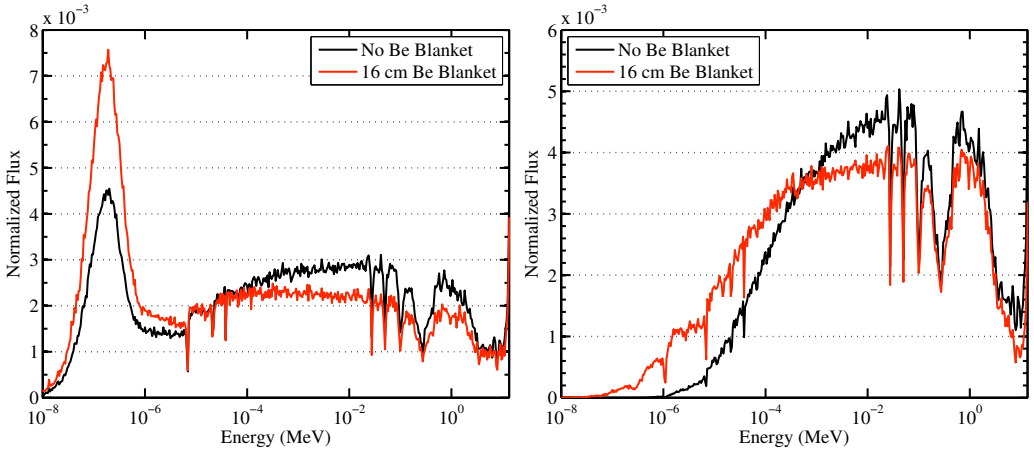

(a) At startup (b) At time of peak Pu

Figure 4.25: Neutron flux spectra in fuel blanket with and without a Be pebble blanket

much thermalization of the fusion neutrons and the production rate of ^{239}Pu suffers. We can see this result in Figure 4.26. A Be layer thickness of ∼16 cm provides the maximum achievable burnup while at full power.

Similarly, the Be layer thickness also impacts the fuel DPA by softening the spectrum. This effect can be seen in Figure 4.27. As we increase the Be layer thickness, the fuel DPA rate decreases, which is reflected in the slope of each curve as a function of burnup. A slight reduction in the damage rate is seen by increasing the layer thickness from 12 cm to 16 cm with little loss to attainable burnup in Figure 4.26. Thus, a Be layer thickness of 16 cm is chosen as a baseline for the design.

4.3.3.7 Summary of Resulting Design

After studying the parameters previously described, we can choose a design point that offers the optimum burnup for the energy production mission. These results were previously eluded to in Table 2.4 and are presented again for completeness in Table 4.5 with some additional parameters of interest. We see from the previous study that a LFFH engine loaded with 20 MT of DU fuel, loaded into 300 μm radius kernels with a 20% packing fraction of TRISO particles in pebbles achieves the highest attainable burnup, ∼906 GWday/MT$_{HM}$ while at full power. Similarly, operating the system with a higher fusion input power or smaller radius can result in a more rapid burnup of the fuel, but also significantly increases the first wall and fuel damage rates. For these reasons, a 2.5 m chamber radius with a 500 MW fusion driver is chosen. Likewise, the system can operate at a higher blanket gain than 4, but the resulting decrease in BOP utilization motivates operating at a lower gain.

As part of this study, we are interested in also exploring the use of a fixed fuel blanket instead of assuming the fuel pebbles continuously flow through the system fast enough to

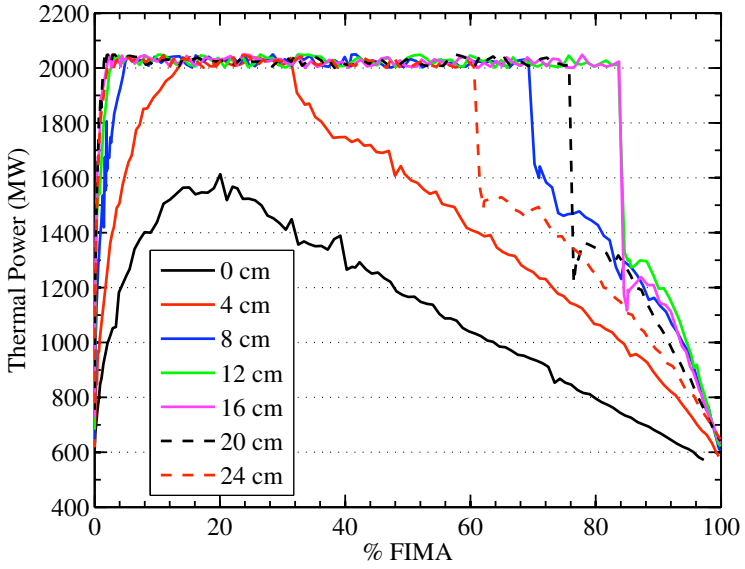

Figure 4.26: Power vs burnup for different Be pebble layer thicknesses using a 300 μm kernel size, 30% TRISO packing and 20MT fuel loading

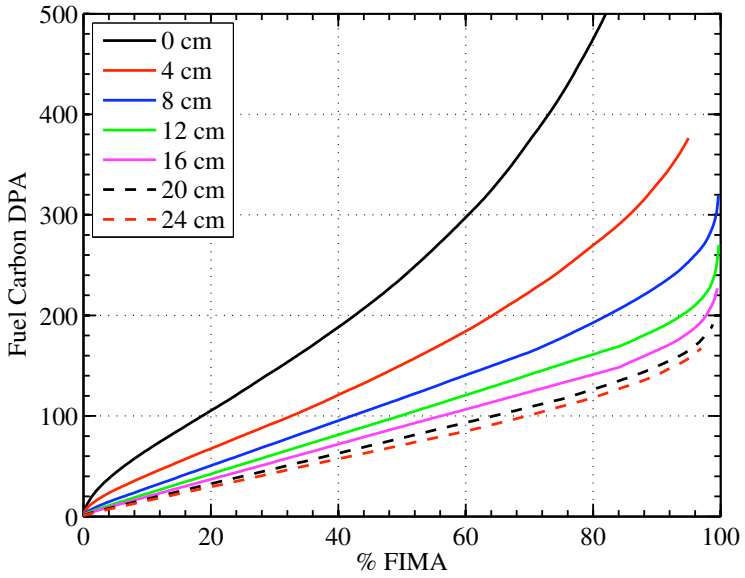

Figure 4.27: DPA in fuel carbon layers as a function of Be layer thickness showing a thicker Be layer results in lower fuel damage

Design Parameter	Value
Thermal Power (MWth)	2000
Fusion Yield (MWth)	500
Corresponding Fission Blanket Gain	4
Fission Blanket Heavy Metal Mass (MT)	20
Fuel kernel radius (μm)	300
First Wall Coolant	$Li_{17}Pb_{83}$
Primary Coolant	2LiF + BeF_2
First Wall Inner Radius (m)	2.5
TRISO packing fraction (%)	20
Fuel Pebble packing fraction (%)	60
Be multiplier thickness (cm)	16
Be pebble packing fraction (%)	60
Fission blanket thickness (cm)	74
Graphite reflector thickness (cm)	75
Graphite pebble packing (%)	60
Number of fuel pebbles	$\sim 13 \times 10^6$

Table 4.5: Optimized design parameters for LFFH engine design

ensure good mixing. To model a fixed, or slowly moving system, we must examine multiple separate depletion zones.

4.4 Multiple Zone Depletion Modeling

As discussed in Chapter 3, a fully mixed fission blanket is one possible design option. However, the blanket design does not exclude alternative fuel handling like more advanced shuffling or reload schemes. One such scheme is that of central promotion. This concept involves irradiating the fuel for a fixed period of time, then discarding the innermost blanket layers and replacing the outer layers with fresh fuel. Unfortunately, this refuel method using modeling discrete fuel pebble layers in order to capture the flux variations across the blanket can be quite computationally taxing. Although fuel shuffling and optimized reload schemes are left as future work, the groundwork for these simulations using both fixed zone depletion and AMR is examined.

4.4.1 Fixed Zone depletion

When the fuel is treated as fixed over the course of a series of depletion steps, care must be taken to discritize the depletion problem appropriately. Too large of depletion zones

can result in the incorrect average neutron flux being used to deplete the fuel in that zone. Similarly, if the depletion zones are sized too small, significantly more computational effort is required to calculate the solution. Figure 4.28 shows four different possible depletion zoning schemes for a fixed zone problem. They are shown with 5, 10, 15 and 20 depletable regions. The challenge arises in first determining which scheme is appropriate for the problem in question. Each time the problem is changed enough to vary the flux throughout the blanket, this decision must be revisited. For a time dependent problem, the desired zoning scheme could change over time. Namely, we may want a finely zoned problem in the inner most region and course zones in the outer most region at startup, but something different later in the burn. Consequently, the only way to accurately deal with this is to utilize a finely zoned burnup mesh throughout the whole fission blanket at the expense to computational time.

Using even 20 separate uniform depletion zones, however, does not accurately capture the fluxes and reaction rates in the inner regions of the LFFH fuel blanket. This is illustrated in Figure 4.29. The flux variations from surface to surface across each depletion zone in the 20 zone depletion case are large for the first 5 adjacent zones, greater than 10%, and much lower as we move further out in the blanket. The resulting reaction rates of capture and fission are affected by a similar amount. This illustrates that even in a more detailed problem like this, we are not capturing the true flux in the inner regions of the blanket. Similarly, we are too finely zoned in the outer regions of the blanket. This causes additional memory overhead because of the requirement to separately track the isotopic evolution in each burnable region. An increase in overall processor overhead is also seen because additional particle histories must be followed to ensure acceptable statistics in the outer blanket zones. If we linearly extrapolate the difference in the 1-group flux, it would require ~40 equal volume depletion zones to keep the variations below 10% for this problem.

The system thermal power and burnup is affected by using a fixed fuel configuration. Figure 4.30a shows that the thermal power falls at a point roughly half that of the fully mixed system. This is to be expected because the fuel is now subjected to the flux profile shown in Figure 4.29 as opposed to a single average value. Thus, the fuel in the front of the blanket depletes more quickly than the fuel in the back of the blanket. In the process, a fission product barrier is created, further reducing the net number of neutrons leaking to the back of the blanket. The overall tritium production in the system is also lower and system performance suffers (Figure 4.30b). Table 4.6 shows that the fuel at the front of the blanket has reached 98% FIMA while the fuel at the back of the blanket reaches only $\sim$16.5 %FIMA. The average burnup across the fuel blanket is 42% FIMA instead of 82% FIMA as in the fully mixed case. One proposed way to deal with this, yet to be fully explored, is to employ fuel shuffling where fully burned fuel is discarded, layers are promoted into higher flux regions, and fresh fuel is inserted in the back [111]. The potential exists to reach an equilibrium operational mode using this approach, but is beyond the current scope of this dissertation.

One question of immediate concern is if the fuel is kept fixed in the core and continu-

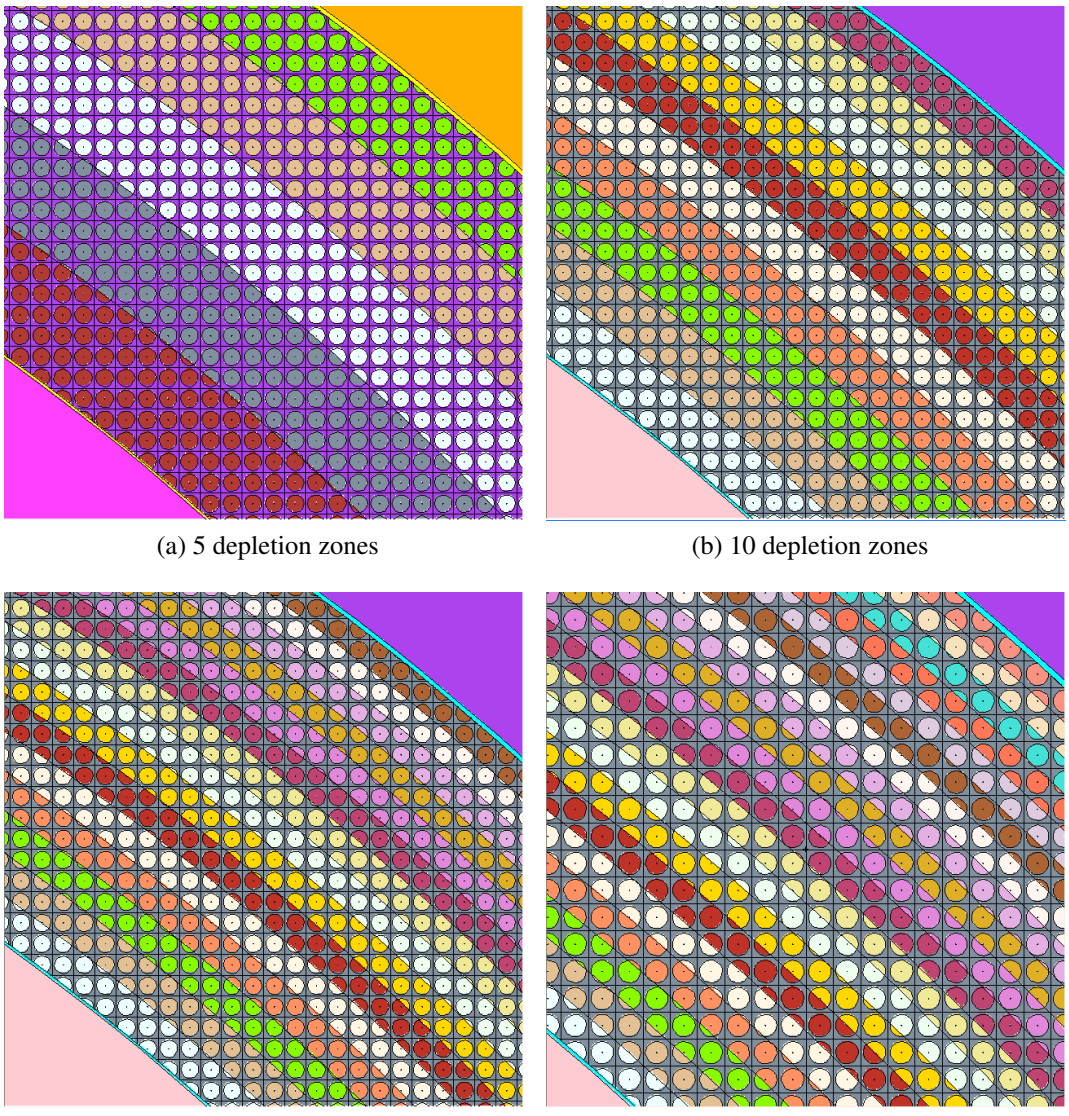

(a) 5 depletion zones

(b) 10 depletion zones

(c) 15 depletion zones

(d) 20 depletion zones

Figure 4.28: Different Monteburns depletion models utilizing 5, 10, 15 and 20 separate depletable regions

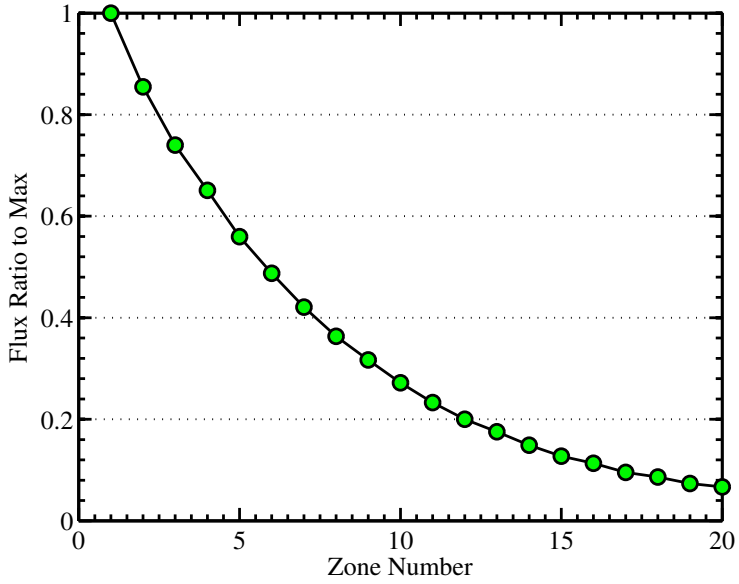

Figure 4.29: Ratio of 1 group total flux to max for 20 depletion zone mesh at BOL

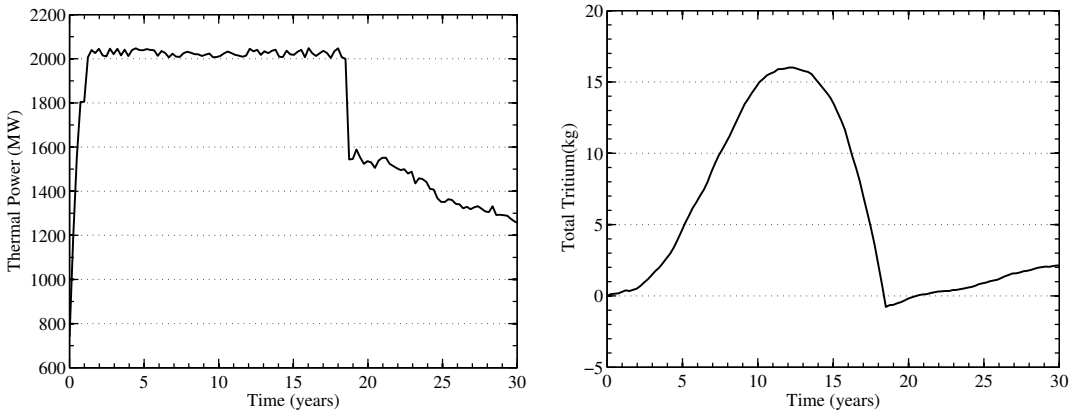

(a) Power over time

(b) Tritium inventory over time

Figure 4.30: Thermal power and tritium inventory for 20 zone fixed fuel irradiation problem

Radial Zone	Burnup (%FIMA)
1	98.15
2	92.7
3	85.24
4	76.76
5	68.02
6	58.15
7	49.8
8	43.84
9	38.54
10	34.14
11	30.52
12	26.93
13	24.1
14	21.65
15	19.41
16	17.51
17	15.89
18	15.07
19	14.87
20	16.52

Table 4.6: Average radial zone burnup in the fuel blanket at time of tritium exhaustion

ously irradiated, how do we best perform that depletion problem. It does not make much sense to maintain a finely zoned problem in a region where the fuel has been completely consumed. One possible solution is to manually adjust the depletion mesh to tailor it to the problem of interest. However, this process resembles an informed trial-and-error approach, where transport calculations determine the appropriate depletion zone size at the current time step. The process would have to be periodically performed again and again as the fuel breeds up and burns down fissile material. One other alternative is to use AMR.

4.4.2 Adaptive Mesh Depletion

Simulating a fixed fuel system can be performed by employing AMR on the burnup mesh. Two issues that must be addressed first are whether AMR improve accuracy and whether it speeds up the calculation. The goal of this work is to accomplish both at the same time. By setting the allowable flux variations, as well as, absorption and fission fractions to be below an allowed threshold, we can ensure the depletion results will be accurate to within that threshold. The AMR routines are developed as part of the ABL library offer an automated way to ensure the depletion fluxes are with a specified range for the zones in question.

If we begin a depletion calculation with a single depletion zone and allow AMR to operate on it, we see that the burnup mesh will evolve similar to that shown in Figure 4.31. In this example, after the first pass, the single zone is split into 2 depletion zones of equal thickness. After the splitting, the AMR routine recalculates the fluxes across each zone and the relative zone importance fraction to total absorption and fission. The remaining passes result in more and more zones, but the finer zones are located towards the inner region of the fission blanket as opposed to evenly space throughout. This effect is anticipated because the flux is about an order of magnitude higher in the front than the back, as shown in Figure 4.29. In this particular case, the maximum 1 group flux variation across a cell as well as the maximum fractional absorption and fission are set to 10%. This implies that if a burnup zone has more than a 10% flux variation or contributes to more than 10% of total system absorption or fission, it will be split. Likewise, if the flux variation across two adjacent cells, or the sum of the absorption or fission fraction is below 10%, the two zones are combined. In the case of AMR, this maximum value can be dictated for each individual simulation. If higher accuracy is desired, a lower threshold can be input by the user. The same is not true of fixed zone depletion. It is up to the user to determine the depletion mesh throughout the burnup calculation.

The ratio of peak flux to the flux in each zone can now be seen to be below 10% from zone to zone, shown in Figure 4.32. The slight inflection points in the curve illustrate where the mesh zoning becomes courser. We see that utilizing AMR and requiring a 10% maximum change in the relative fluxes and reaction rates across each zone yields 14 depletable zones. This zoning scheme, shown in Figure 4.31f, results in fewer depletion zones and a relatively higher accuracy of the average flux used to deplete each zone. For this example, a 10% threshold was chosen, but this choice can be varied as needed.

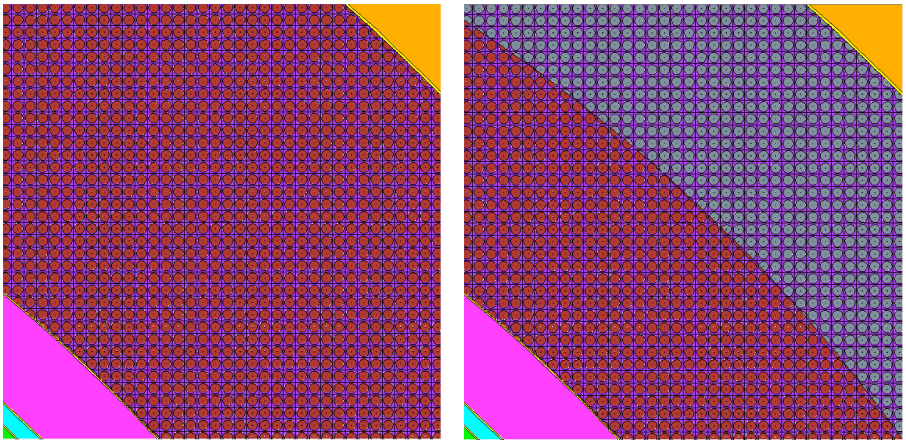

(a) Burnup mesh before AMR

(b) Burnup mesh after 1st pass

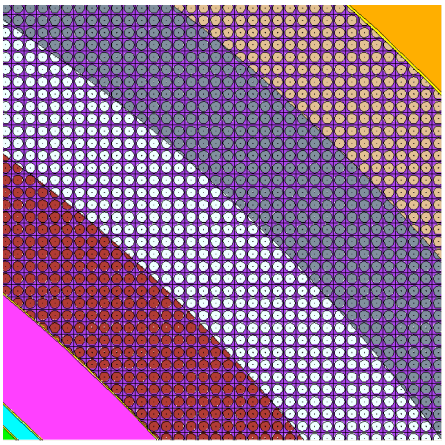

(c) Burnup mesh after 2nd pass

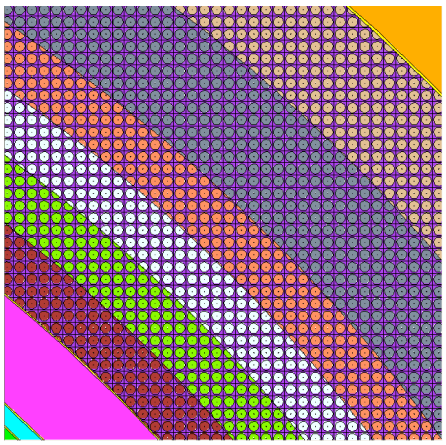

(d) Burnup mesh after 3rd pass

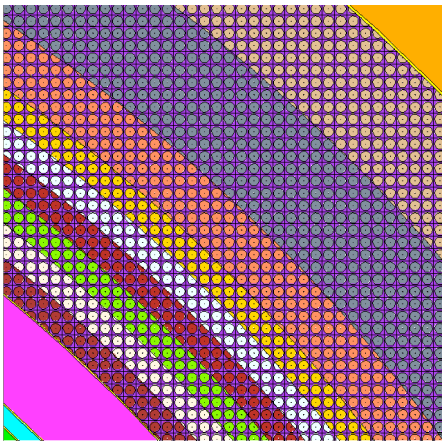

(e) Burnup mesh after 4th pass

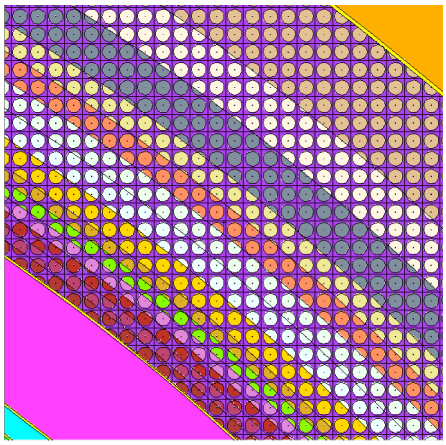

(f) Burnup mesh after 5th pass

Figure 4.31: AMR burnup zones after multiple rounds of zone splitting and combination

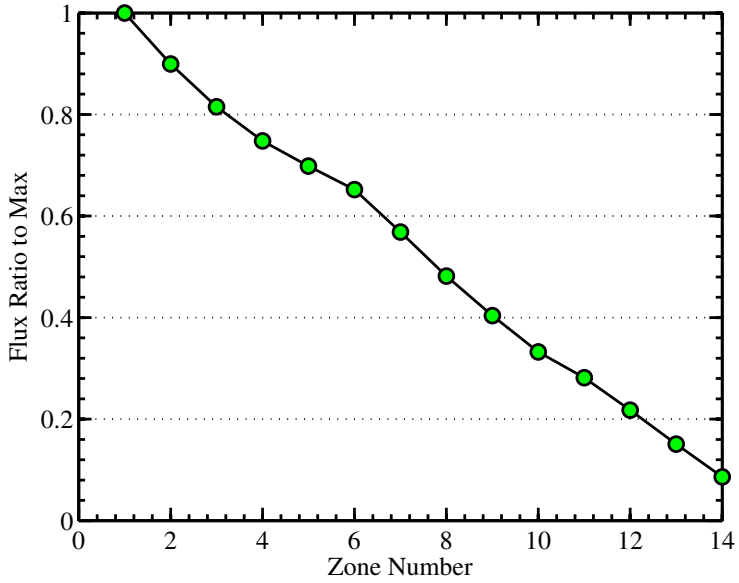

Figure 4.32: Ratio of 1 group total flux to max for AMR zone mesh

4.4.3 Fixed Zones vs AMR Comparisons

Direct comparisons between the fixed zone and AMR problems are difficult to make due to the constantly changing AMR burnup mesh. However, we can examine a few key metrics like the system thermal power and tritium inventory. If we compare the system thermal power between a 20 zone fixed depletion and AMR problem, shown in Figure 4.33a, we see that the thermal powers on average are similar to using a fixed zone depletion method. The AMR calculation reaches full power in 270 days as opposed to the 20 zone calculation, which takes 450 days. The AMR calculation has less averaging of the true flux across the front fuel pebbles and they are thus irradiated with a higher average flux. This causes a faster breeding rate of fissile mass and increased tritium production early in time. However, since the number of neutrons available for tritium production is lower, the AMR case reaches a lower peak tritium inventory in the burnup, shown in Figure 4.33b.

If we examine the burnup in each different depletion zone, we see the two problems track quite closely. Figure 4.34 shows the burnup in each depletion zone when the average blanket burnup is at 42.4% FIMA, the point at which the system power drops. At this point, the AMR mesh has expanded to utilize 18 total depletion zones instead of the original 14. The mesh should evolve with the burnup. We can see that the AMR case has a finer zoning in the front of the blanket as shown by the bars in blue. The zoning then increases in size as the radius increases. The 20 zone fixed case, has more overall zones, but fewer in the front of the blanket relative to AMR. This results in more coarsely averaged burnup in the front of the blanket, but less averaging in the outer regions, as compared to AMR. Since the majority of fission, capture and power generation is occurring in the front of the blanket, it

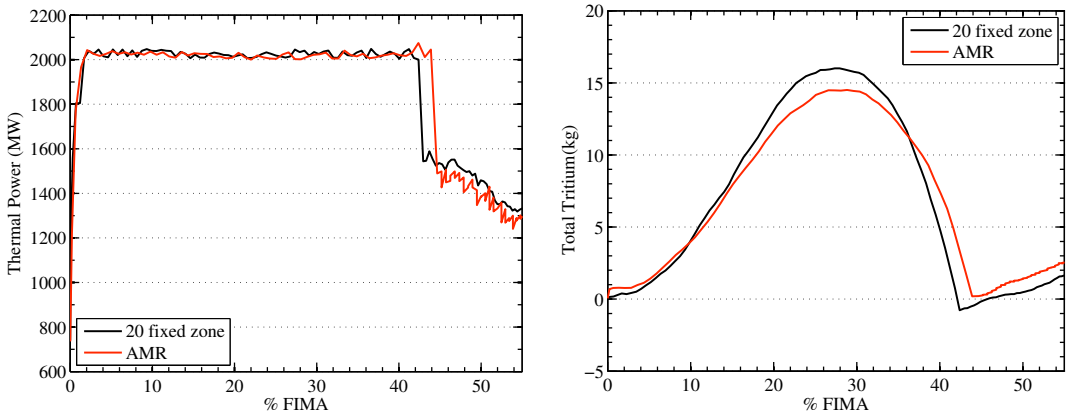

(a) Power vs %FIMA for 20 fixed zone and AMR calculations

(b) Tritium inventory versus burnup for 20 fixed zone and AMR calculations

Figure 4.33: Thermal power and tritium inventory for Adaptively Meshed fixed fuel irradiation problem

is more important to finely resolve this region than the back. That being said, the maximum relative difference between the two calculations is $\sim$10% in the outer blanket region, shown in Figure 4.34. We also see that the largest relative differences occur in the outer region of the blanket from the larger zones in AMR. Of course, these errors occur in the low flux regions where the burnups are small. These differences can again be adjusted by changing the maximum threshold to split a zone.

4.4.4 Computational Savings

AMR improves the use of computational resources by reducing the requirements to perform the simulation to a desired accuracy. The number of depletable zones is reduced in the problem, reducing the average number of histories to maintain good statistics. Accuracy can be maintained, and generally enhanced, by requiring that the stochastically tallied fluxes across a zone and key reaction rates within that zone not vary by more than a user defined amount. Table 4.7 shows how these two problems differed in wall clock time and CPU-hrs to reach an average blanket burnup of 50% FIMA. When compared to a 20 zone fixed mesh calculation, the ARM simulation offers about a 1.25$\times$ improvement in speed. As noted earlier, using 20 fixed size depletion zones does not capture the neutron fluxes and reaction rates to better than 15% in the inner region of the blanket. To reduce this, finer zoning is required.

The speedup by using AMR is modest because of the chosen operator splitting for the problem. In other words, the AMR operation is performed every depletion step. Since AMR requires at least two additional transport calculations (one for the volume and one

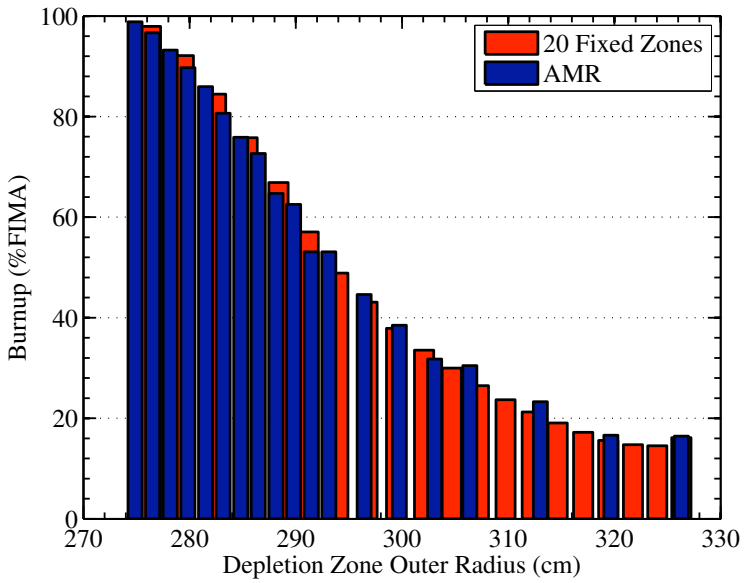

Figure 4.34: Burnup of each depletion zone as a function of radius

for the flux and reaction rate tallies), additional transport work is being added to the solution at each depletion step. One alternative, to be explored as future work, involves only performing AMR when the flux or reaction rates in each zone have changed by a specified amount relative to a previous depletion step. This could offer a further improvement in computational savings by only performing AMR at times it is required. To implement this requires additional rework of the LNC code and remains as future work.

	20 Zone Fixed	AMR
Wall Clock Time	91 (hr.)	73 (hr.)
CPU-hrs	3,640	2,920
Speedup	-	1.25×

Table 4.7: Computational speedup from AMR

4.5 Summary

A neutronics-based assessment of the LFFH engine design has been presented. The design is complicated by the fact that we wish to keep the engine tritium self-sufficient and subcritical while maintaining the maximum BOP utilization possible. The system thermal power is controlled by adjusting coolant ^{6}Li enrichment. The tritium self-sufficiency requirement implies the tritium inventory cannot fall below 0 kg and thermal power and BOP utilization are sacrificed at the expense of tritium production.

A baseline design utilizing a fully mixed fuel pebble bed was developed using multiple parametric studies. The fuel loading, TRISO packing fraction, kernel size, Be blanket layer thickness, fission blanket gain and chamber radius were all varied parametrically. The resulting design utilizes a 20 MT DU fission blanket with the fuel contained in TRISO particles with 300 μm diameter kernels. The TRISO particles are randomly packed within 2 cm fuel pebbles at a 20% packing fraction. Those pebbles are naturally packed at ~60% packing fraction in the bed. The Be pebble layer thickness is 16 cm with the overall fusion chamber being 2.5 m radius. Although higher blanket gains are possible, a gain of 4 is chosen as a balance between BOP utilization and economic factors.

In order to extend this analysis, two additional methods were developed: variable time stepping and AMR. Variable time stepping enables a large number of calculations to be performed with fewer computational resources. AMR enables the simulation of an approximately fixed fuel system, while ensuring that the fluxes used to deplete zone are controlled to a user specified accuracy.

Chapter 5

Nonproliferation Aspects

The issues and challenges surrounding nuclear non-proliferation are continuously evolving. They've changed dramatically at several junctures in recent memory.

- Spencer Abraham -

5.1 Proliferation Resistance of LFFH Design

Nuclear nonproliferation refers to the limitation of the production or spread of nuclear weapons and knowledge required to produce those weapons. Nonproliferation is a paramount concern for all nuclear systems today. In fact, as part of the Generation IV Nuclear Systems Initiative, nonproliferation is a key aspect in development of those new reactor concepts [112, 113, 114, 115, 116]. This proliferation resistance and physical protection (PR&PP) methodology identifies a basic framework within which one can analyze a nuclear energy system (NES). This framework includes the identification of challenges or threats, development of a system response and an assessment of the outcome. Although it is not the goal of this work to analyze in its entirety the LFFH plant and fuel cycle proliferation resistance, an effort is made to employ the PR&PP methodology in studying some basic aspects of the system.

LFFH plant threats can be considered to be performed by either a state or non-state (terrorist) actor. These NES state-based threats can include concealed diversion of declared materials, concealed misuse of declare facilities, overt misuse of facilities and materials and development of clandestine dedicated facilities. Nonstate threats include radiological sabotage and material or information theft. These threats could be applicable to a large variety of components, including the nuclear fuel. Primary threats of interest by a state include clandestine facilities and misuse of known facilities or materials, while that of a non-state actor is radiological sabotage. For the purposes of this work, focus on efforts by both types of actors specifically address the issues in terms attractiveness of the fuel for

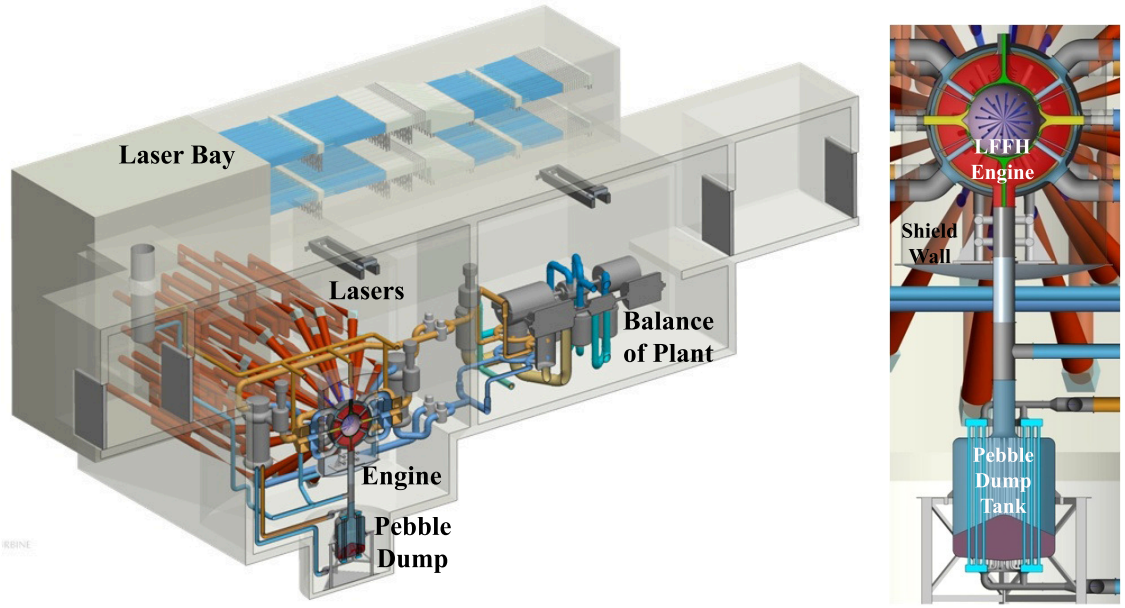

(a) LFFH plant layout

(b) Engine dump tank

Figure 5.1: Proposed LFFH plant layout showing engine with pebble dump tank

LFFH concept.

To aid in discussing the proliferation issues with the LFFH concept, a proposed plant layout is shown in Figure 5.1a[1] . The central chamber is shown with associated lasers (shown in red), coolant piping (shown in orange and blue) and the pebble dump tank, which is used for pebble removal from the LFFH engine. To the right of the LFFH engine is the balance of plant and behind it is the laser bay. If we examine the engine and dump tank more closely, shown in Figure 5.1b, we see that the proposed design does include the ability to circulate fuel outside of the main engine. The design currently allows for pebbles to be extracted from the engine to the dump tank and then to be reinserted from the top of the engine. It also includes a defueling system to allow periodic inspection and reinsertion of the pebbles. It is at the times that the pebbles are outside the fission blanket that drives the proliferation risks.

To study the impacts of material theft, a definition of the quantity of material is required. We can utilize the IAEA definition of a significant quantity (SQ) of plutonium (8 kg) defined as the approximate quantity of nuclear material in respect of which, taking into account any conversion process involved, the possibility of manufacturing a nuclear explosive device cannot be excluded [117]. This means that if 8 kg of plutonium exist, the potential to manufacture a nuclear explosive device exists. This definition does not include any details about the dilution of that plutonium within other materials, but analysis of the

[1]Courtesy Ryan Abbott and Kevin Morris of LLNL

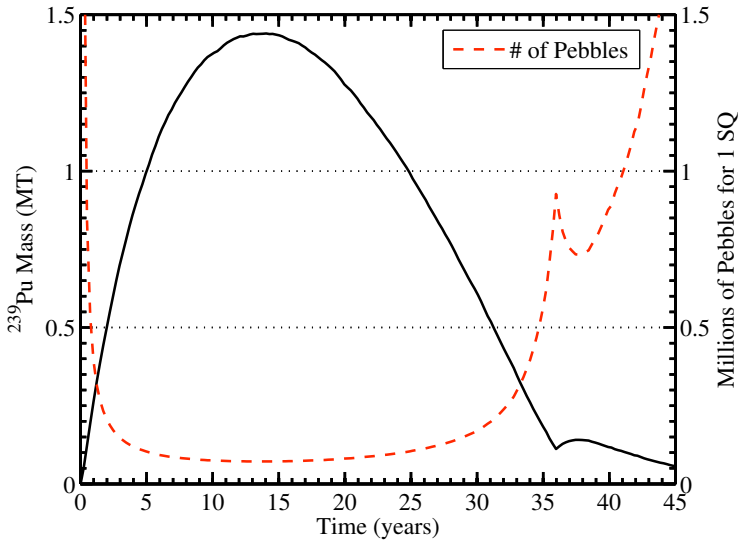

Figure 5.2: Number of pebbles required to obtain 1 SQ of Pu

theft risk should attempt to assess it. Namely, if it requires theft of the whole fission blanket to obtain 1 SQ, the likelihood of this being achieved without detection is extremely low. To that point, Figure 5.2 shows the net ^{239}Pu inventory in a LFFH fission blanket as a function of time. That material is spread across roughly ∼13 million fuel pebbles in the blanket. Shown in the same figure is the number of pebbles required to obtain 1 SQ of material. We see that although the fissile inventory system wide increases to 1.43 MT or ∼179 SQs, that inventory is diluted across all the pebbles. As expected, a minimum number of fuel pebbles is required at the time of peak plutonium inventory. This seemingly large amount of plutonium actually requires ∼72,000 pebbles to obtain 1 SQ at the minimum. Given the fact that each pebble is 2 cm in diameter, and assuming a 60% packing fraction of pebbles in a container, this number of pebbles would occupy a 0.5 m^3 volume. As we will see, obtaining this quantity of pebbles could be detected by radiation detectors, infrared cameras and portal monitors.

5.1.1 Radiation Dose

One hindrance to theft of fuel pebbles is the radiation dose accompanied by the pebbles in this form. As the fissile fuel is produced inside the LFFH fuel pebble, fission products are also produced at a rate equivalent to that of fission. If we examine radiation dose from 1 SQ of fuel pebbles at 14 years, time of peak ^{239}Pu inventory, we can begin to see how attractive the fuel pebbles might be to a actor interested in stealing them for weapons use. Figure 5.3 shows that the fuel pebbles are above 1,000 Rad/hr. for over 50 years if removed at the point of peak Pu inventory and slightly lower if removed 5 years into the burnup. This dose exceeds the IAEA defined limit for a nuclear material to be self-protecting of 100 rad/hr. In

other words, dose from handling the fuel pebbles required for 1 SQ will result in radiation sickness within hours of exposure. Another way to say this is that 1 SQ of fuel pebbles at the point of peak plutonium content (~6.5% by mass) is self-protecting. This is not to say that individual pebbles are self-protecting. Quite the contrary, the dose for a single pebble is much lower (~1-2 rad/hr). We see from Figure 5.3 that the longer the fuel is out of LFFH engine, the less radiologically active it becomes as isotopes decay away.

A conclusion can be drawn that any non-suicidal actor intent on theft of the fuel pebbles would most likely do so in small increments (<1 SQ of pebbles at a time) to reduce overall dose and potential detection. This poses logistical issues in that a small enough quantity must be taken as to limit the dose and detection, but enough to assemble the 1 SQ in a reasonable number of thefts. Likewise, to limit the dose, a cooling period must be allowed. If we assume the 72,000 pebbles are taken in batches that limit the dose to 100 rad/hr, a simple calculation suggests that 1,000 separate thefts of ~75 pebbles would be required. This calculation can be adjusted according to different assumptions, but the conclusion to be drawn from this example is that the actor must either be exposed to a dose exceeding the self-protecting limit during a theft, or a numerous number of thefts must occur. An outside actor acting alone would most likely have to take all the material at once. Alternatively, an inside actor would likely take small batches of material in many separate instances to avoid detection. The likelihood of either being successful without detection and response is very low. The dose from 1 SQ of pebbles is too high to handle safely and the fuel pebbles are active enough alone to enable detection through radiation portal monitors if an inside actor chose to steal 1 pebble at a time. This is not including the fact that the pebbles must be somehow removed from the operating fission blanket. Lastly, the fissile material in each pebble is contaminated with multiple fission products and other actinides again requiring mechanical and chemical separation to get at the fissile materials. For these reasons, it is deemed unlikely that a non-state actor could obtain and utilize LFFH DU pebbles for weapons material. Even so, it is prudent to examine the material attractiveness, which is a function of the dose and decay heat, to determine if the material is actually worth stealing by either inside or outside actors.

5.1.2 Decay Heat

LFFH fuel pebbles are not only radiologically hot from fission product decay, but they are also thermally hot. Keep in mind the designed operating temperature is 1100 °C so the initial temperature of each pebble will prohibitive to handle. However, if for some reason pebbles are removed and allowed to cool, their decay heat will still be high. Figure 5.4 shows that a SQ of pebbles removed from the LFFH fission blanket at time of peak ^{239}Pu and at 5 years into the burnup and immediately after it's removed generates about 30 kW of thermal power spread over the 72,000 pebbles. As a whole, the heat generation is difficult to cool. However, an individual pebble will only generate about ∼0.42 watts. This is hardly enough to be a deterrent. Individual pebble theft concerns warrant the use of portal

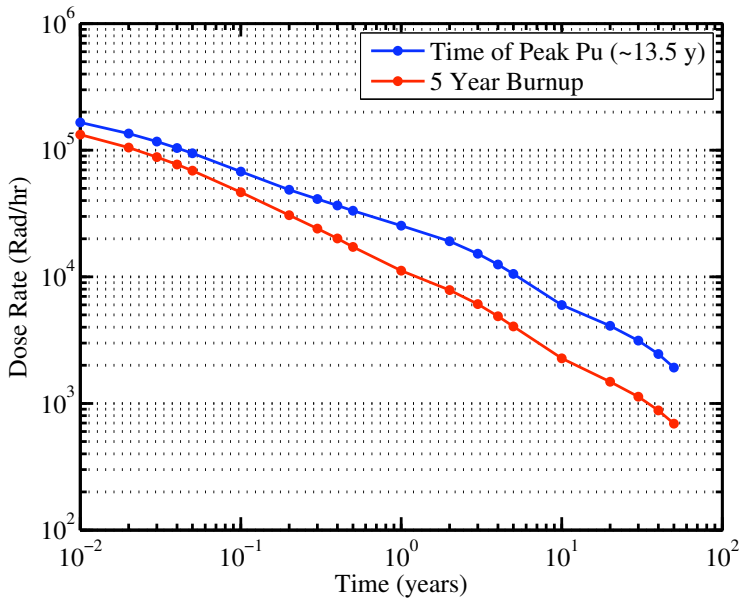

Figure 5.3: Baseline system design radiation dose of 1 SQ

monitoring, remote cameras and material inventory safeguards for the LFFH plant.

5.1.3 Material Attractiveness

Given the potentially low dose and decay heat associated with each individual pebble, we now examine the usefulness or attractiveness of the LFFH fuel pebbles. Using the previously described inventory, radiation dose and decay heat, we can determine how attractive this material might be for weapons use. Originally proposed by Bathke, et al., a metric used for evaluating the attractiveness of special nuclear material (SNM) is described as a figure of merit (FOM) [118, 119]. They define the FOM as

$$FOM = 1 - log_{10}\left(M\left[\frac{1}{800}+\frac{h}{4500}\right]+\frac{M}{50}\left[\frac{D}{500}\right]^{\frac{1}{log_{10}(2)}}\right), \tag{5.1}$$

where M is bare critical mass of the metal in kg, h is the heat content in W/kg, and D is the dose rate of a $0.2M$ sphere evaluated at 1 m from the surface in rad/hr. This metric has been proposed to the DOE as part of a measure of attractiveness of nuclear materials in Department of Energy (DOE) nuclear facilities [119, 120]. The authors also define a mapping of the FOM into utility for use in weapons [119]. This mapping is shown in Table 5.1. As a NES systems designer, we desire to design the system such that the FOM is low or off scale to ensure that the material has a low potential proliferation risk. With this in mind, we can apply this FOM to measure how attractive LFFH DU fuel might be using

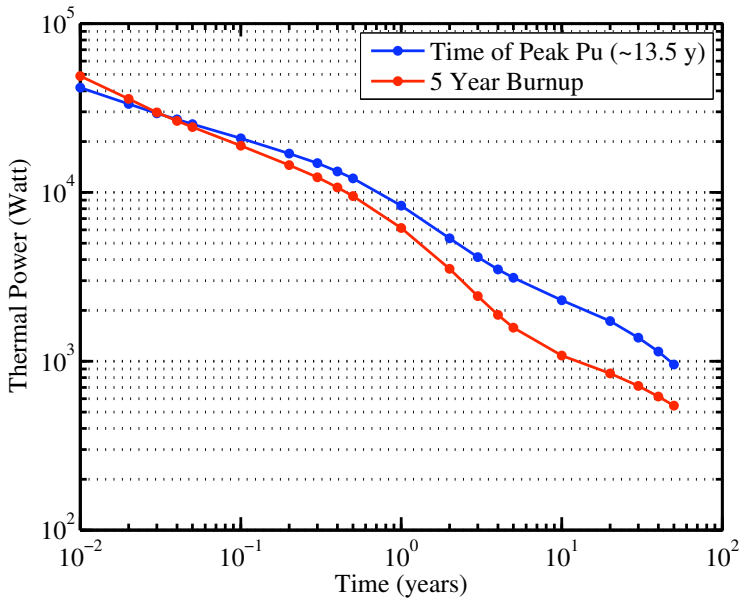

Figure 5.4: Decay heat from 1 SQ of fuel pebbles as a function of time

the previously calculated heat content and dose from 1 SQ of pebbles. The resulting FOM over time is shown in Figure 5.5. The FOM, in this case, is calculated for Pu, actinides and fission products at the time that the material contains the maximum amount of ^{239}Pu and plotted as a function of time out of the fission blanket. This point in the burnup requires the fewest number of fuel pebbles to obtain 1 SQ (also shown is 5 years into the burnup). We can see that the FOM begins low because of the high dose and decay heat. As time goes on, the FOM rises to a peak after 50 years as the fission products decay away to stable isotopes. Even at this point, the FOM is considered off scale meaning that the material is unattractive. Given this result, the likelihood of obtaining weapons usable material via alternative means can be considered to be much higher. It is not expected that the LFFH DU fuel, unless reprocessed, will be very attractive to either state or non-state actor.

It should be noted, that this FOM does not account for the dilution of material across fuel elements. It only accounts for dose and internal heat generation from that material as

FOM for Metals	Utility
> 2	High
1-2	Moderate
0-1	Low
< 0	Off Scale

Table 5.1: Mapping of FOM into utility for use in weapons

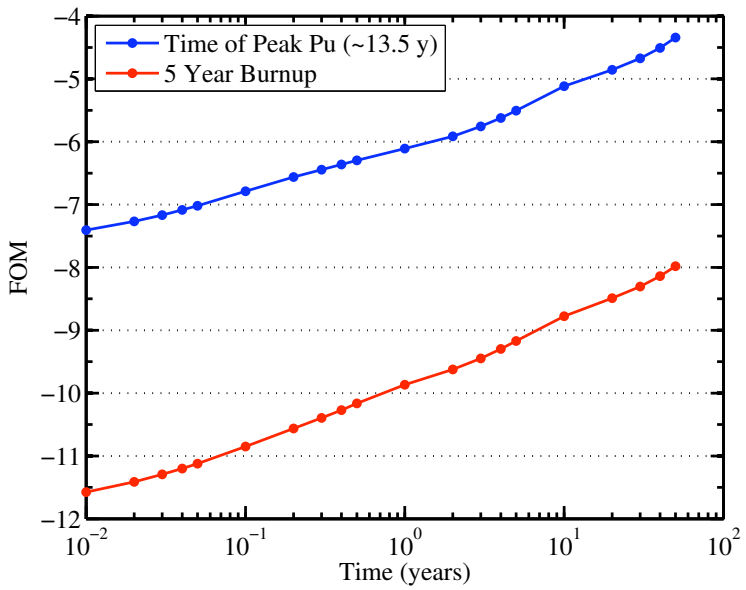

Figure 5.5: FOM for LFFH DU fuel over time

a whole. Namely, if the same quantity of ^{239}Pu is contained in one fuel element vs 50 and the dose and decay heat are the same, the FOM will not capture this effect. For this reason, care should be taken keep in mind that the FOM is simply a measure of the material and not its fuel form.

If we now assume that a state possesses chemical reprocessing technology and is interested in using the LFFH fuel to produce Pu, we can examine the FOM assuming a breakout or concealed production scenario. In this case, the fuel isotopic composition and TRISO particle layers act as the primary technical barriers to obtaining the pure Pu metal. Of course, the makeup of that Pu metal contributes to the overall FOM. Figure 5.6 shows the primary isotopic composition for three different times; startup, time of peak ^{239}Pu and the time that full power can no longer be maintained (~84 %FIMA). Startup contains the most ^{239}Pu relative to other isotopes, but $\sim$1/5 of the whole fission blanket would be required to obtain 1 SQ, assuming 100% reprocessing efficiency. Based on this, we can examine the 1 SQ of Pu metal extracted from the fission blanket at time of peak plutonium assuming 100% reprocessing efficiency. The total dose rate and thermal power from 1 SQ of the Pu metal is shown in 5.7a . The resulting figure of merit is shown in 5.7b. We can see that the decay heat and dose rate terms are much lower in the case of reprocessed material. Consequently, the FOM is above 2.0 for over 50 years and can be considered to have high utility. This is expected as Bathke, et al. found various reprocessed plutonium streams to have high FOM as well. This suggests that states possessing both LFFH and reprocessing technologies pose a potential proliferation risk that must be addressed through the use of additional IAEA safeguards, inspections and treaties.

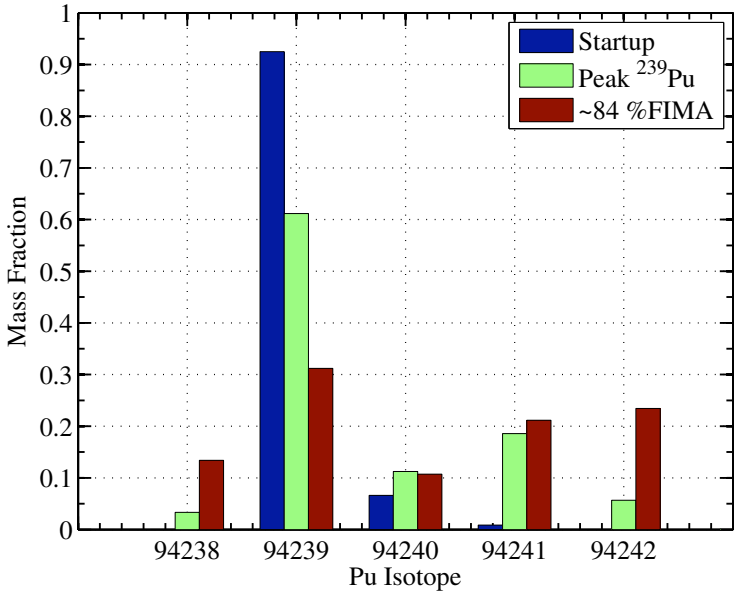

Figure 5.6: Primary Pu isotopes shown by mass fraction

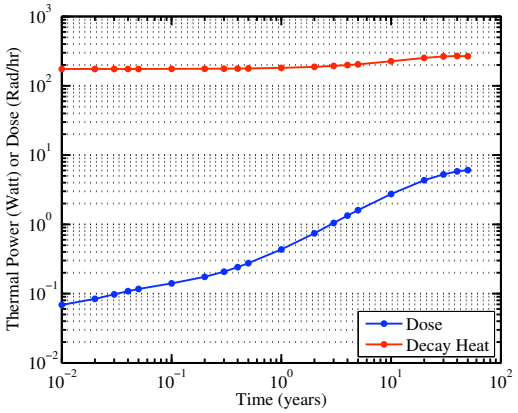

(a) Dose rate and Decay heat vs decay time

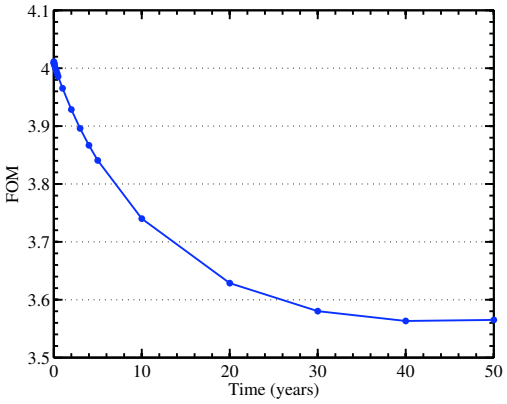

(b) Figure of merit vs time after being reprocessed at time of peak ^{239}Pu

Figure 5.7: Radiation dose, decay heat and FOM associated with Pu metal

5.1.4 FOM Applied to Reprocessing Schemes

Bathke, et. al. originally proposed the FOM at the request of the U.S. DOE to assess the attractiveness of special nuclear materials, from a safeguards and physical protection perspective. They specifically addressed reprocessing and dilution schemes and advanced fuel cycles proposed as part of the Gen. IV road map. They found that advanced reprocessing approaches for LWR spent fuel where plutonium is separated with one or more minor actinides does not make it unattractive for developing weapons material. Instead, only when co-extracting Cm and Am produces an unattractive material. They also found that dilution of plutonium by $\sim$80% is required to render material unattractive [119]. In the case of LFFH fuel, at the time of peak ^{239}Pu inventory, the ^{238}U content is approximately 50% by mass. At earlier times, this percentage is higher. This fact, coupled with the high fission product content, yields a very low FOM for 1 SQ of unprocessed LFFH fuel when compared to other Gen IV based reprocessing schemes.

5.2 Proliferation Resistance to State Actors

In the context of proliferation resistance, we can assume the state actor will have physical control over the LFFH facility and all materials associated with it. This presents interesting and difficult challenges. On the one hand, if a state were given, sold or licensed the technology to build LFFH plants, there would not be a reasonable need to produce uranium enrichment plants and potentially reprocessing facilities, other than to produce weapons usable material (assuming it did not maintain a nuclear reactor fleet in parallel). LFFH plants could provide power in place of nuclear reactors and not require enriched fuel. Given this scenario, the state would have neither the technical knowledge or nuclear capabilities to develop enrichment or reprocessing facilities on its own. This makes the likelihood of a LFFH plant increasing a state actor's capability to directly produce weapons usable material low. However, misuse of this technology could potentially act as an alternative to an enrichment plant, albeit a much more costly and technologically challenging one. A LFFH engine functions by utilizing an external fusion neutron source to breed and consume otherwise unusable nuclear fuel. These same neutrons could potentially be diverted for use in production of undeclared materials. Likewise, once a country possesses the technology to build a LFFH plant, economic and political factors would be the primary hindrance to building clandestine facilities for alternative use. Additional factors that could hinder the building of a clandestine facility include detection of materials and components by export control, human intelligence, national technical means, IAEA-based satellite imagery and environmental monitoring.

If the state possessed a declared reprocessing facility, the signatures generated by a parallel clandestine program could be disguised, but one of the goals in this work includes eliminating the legitimate need for reprocessing or enrichment technology. This is a fundamental premise of the LFFH concept. If legitimate reprocessing and enrichment are

allowed, additional safeguards similar to that of a pebble bed reactor would be required.

The LFFH concept is potentially susceptible to concealed diversion of fissile materials, concealed production of fissile materials, and the development of clandestine facilities. These proliferation risks are discussed below.

5.2.1 Concealed Diversion of Fissile Materials

As stated earlier, the LFFH fission blanket is initially composed of DU and of little use for anything outside of a LFFH power plant. However, after operation for a matter of days, fissile inventories build up within the fuel pebbles. The challenge is to detect (via safeguards) and deter a state actor from periodically extracting fuel pebbles and replacing them with fresh fuel. This could give the perception that the engine was operating normally, but in reality, the fuel was being extracted after a prolonged exposure to the high neutron flux. The consequences of successful diversion of fissile material implies the state is able to collect a sufficient number of fuel pebbles, without detection, to obtain an IAEA 1 SQ of fissile material.

Detection measures for pebble bed reactors (PBR) have been suggested including material inventory schemes like bar coding individual pebbles or chemically tagging each pebble [121]. In practice, applying a serial number to each individual pebble when potentially billions of pebbles could be manufactured is very challenging. Application of a serial number to separate lots of fuel pebbles could be easier. Then one would be able to check to see if an entire lot was still present, and if the burn up and other characteristics of each lot are reasonable. This serial numbering of each lot, coupled with chemical or radiological tagging of each pebble could act as sufficient deterrence from concealed diversion. One type of tag suggested includes use of microspheres placed inside the pebble graphite matrix composed of specific mixtures of rare earth elements [122]. These tags could aid in tracking and preventing illicit shipments. The difficulty with this approach is that it may require destructive examination of the pebbles and requires more development. Similarly, since the LFFH potentially only requires refueling on the order of decades, it is implied that there should be no storage of SNF. Lack of SNF storage eliminates this possible diversion mechanism where SNF pebbles are replaced with substitute pebbles. In theory, fresh pebbles are loaded in the LFFH and fully burned pebbles are discarded after irradiation.

However, even if a state actor extracted fuel pebbles after they've built up a sizable fissile inventory, they would need to divert a large number of pebbles, tens of thousands, before a sizable amount of plutonium could be extracted and be considered a safeguards challenge. As we have seen, those same pebbles also contain large quantities of fission products. The neutron irradiation produces fission products and higher actinides as well as attractive materials. To extract the fissile material would, in essence, require mechanical and chemical separation. These separation efforts would also have to be undetectable via IAEA safeguards, inspections and other detection methods.

Concealed diversion requires undetected removal of thousands of fuel pebbles, devel-

opment of reprocessing facilities and circumvention of all IAEA safeguards while doing so. A detailed safeguards approach will be required and remains to be developed. Ultimately, it is unlikely that a state would take this path towards weapons material production. This path to obtain material requires more effort and resources than other pathways and contains an inherent lower probability of success. A more likely scenario would be an attempt to produce additional material that was not part of the original inventory.

5.2.2 Concealed Production of Fissile Materials

Production of fissile material in a LFFH engine occurs as part of its normal operation. However, one could imagine placing specific breeder materials in or near the fission blanket to undergo irradiation. For these reasons, the initial and final material quantities would have to be inventoried and regularly inspected. Likewise, the LFFH engine would as part of the design be a remotely handled system to prevent insertion of extra materials into it. In fact, the neutron radiation levels are high enough immediately outside of the reflector region that a completely sealed and monitored shield building will be required, with safeguards similar to those proposed for PBR's. Additional cameras and radiation detection portals at entry points could capture any radioactive material flow in and out of the shield wall. This would deter a state actor from placing a "black box" of material near the LFFH engine after inspectors had left.

The use of an external driver to operate the system presents these challenges as well as some opportunities to implement system wide interlocks. One possible solution to preventing operation outside of allowed scenarios could be a system wide electronic interlock that prevents the fusion system from firing its lasers or injecting targets if triggered. This system could go so far as to intentionally damage necessary components like laser optics that are not easily replaced. It could be remotely controlled by a governing body, like the IAEA to prevent a state from removing inspectors, withdrawing from associated non-proliferation treaties and operating the LFFH engine on it's own as a nuclear material production facility. Although this might deter concealed misuse, it does not necessarily prevent a break out. Since the state has control over the facility, a break out scenario would require a much more elaborate system to prevent misuse.

Consequences of successful production of material include a state developing the ability to produce weapons usable material without enrichment and the ability for that state to stockpile that material. If proper safeguards and inspections are not put in place prior to operation, this pathway has a higher probability of success than concealed diversion. Similarly, this justifies a system design where the fission fuel pebbles are not directly accessible until decommissioning. As it is expected that periodic defueling will be required to replace the first wall, safeguards and material inventory schemes for the pebbles will likely mimic those of PBR's. The pebble dump, handling, and inspection systems must be designed with remote operation in mind as part of the pebble circulation loop.

5.2.3 Development of Clandestine Facilities

As with any NES, once a state possesses full knowledge and ability to produce one facility, it can produce more. This can often be done more cheaply and faster than the previous. Preventing clandestine LFFH facilities is difficult if all of the technology is freely given away or sold. A better alternative is to maintain control over key technologies and components. Two additional barriers to preventing clandestine facilities include inspections and economics. In general, a clandestine graphite moderated, natural uranium reactor, or a clandestine centrifuge enrichment facility would be much easier for a weapons production program than a clandestine LFFH system. It is also unlikely that most states would possess all of the technologies needed to construct LFFH plants on their own. For this reason, export controls should be helpful in detecting attempts to acquire dual-use technologies for use in clandestine facilities. Again, successfully building a clandestine facility would require avoiding detection by export controls, human intelligence, satellite imagery and environmental monitoring. In this case, protection of the knowledge (and economic barriers) to produce the components are hindrances to preventing a host country from duplicating that technology in a clandestine manner.

5.3 Physical Protection from Non-State Actors

To analyze the plant protection of the LFFH engine, we must consider the fuel form and the ability to remove it from a facility for use in nuclear explosives. We must also consider elements required to physically protect the plant from these threats. Specifically, at what points would the fuel contain enough fissile inventory to be of interest and what quantity must be obtained? Since the fuel contains no fissile material at startup, it will only be of interest after it has been irradiated for some time. In fact, for enough fissile material to be built up without removing a large fraction of the fission blanket (<1/5), the system would have to be operated for 3-5 years before the fuel pebbles become attractive. It would be extremely challenging for terrorists to steal pebbles, since they have high radiation levels and are fully remotely handled to transport them and inspect them.

The challenge would be to successfully remove enough fuel pebbles to obtain 1 SQ of ^{239}Pu without detection. Potential actors include outside terrorists, outsiders colluding with insiders or insiders alone. To know the appropriate time to attempt a theft involves knowing operational schedules and details of when the plant went online, as well as details into the inventories, operating power, etc. This knowledge could possibly be obtained by direct outsiders, but is more likely to be obtained via collusion with a worker knowledgeable of these details. Of course, a concealed theft would likely be detectable (assuming the state is not part of the threat) because 1/5 of the fission blanket could not be removed all at once because a sudden drop in operating power would be apparent. At the same time, the likelihood of a prolonged theft is low. Barriers to a forced theft include high radiation levels inside of the primary shield wall, high radioactivity and decay heat of fuel pebbles, as well

as a low FOM for the material in its raw form.

5.3.1 Radiological Sabotage

The primary credible threat from a non-state actor is radiological sabotage. This includes sabotage to the LFFH engine to cause a catastrophic failure, or use of fuel pebbles in creating a dirty bomb. Several possibilities exist as a means to sabotage the LFFH plant. These include intentionally causing a fission product release, tritium release or simply damaging the facility. Tritium release could potentially be caused by damaging containment systems. However, only if the independent safety and control systems were damaged could an attempt at fission product release occur. Damage to the pebble dump system could potentially lead to an overheat of the structural material, but not a fuel failure. The TRISO particles are designed to withstand temperatures exceeding 1600°C and the fuel temperature is not expected to reach this even under LOCA. Nevertheless, safety systems should be designed to initiate if a detected intrusion occurs outside the primary shield wall.

Construction of a dirty bomb implies the fuel pebbles have been successfully removed from the facility. It is assumed that the fuel pebbles would be utilized in their operational form because the likelihood of a sub-national group having access to mechanical and chemical reprocessing technology after a theft is low. Even so, the fuel form itself is the final barrier to use in this manner. TRISO particles are robust and are difficult to exploit in a dirty bomb [123]. If most of the TRISO particles remain intact during an explosion the particles would only be dispersed 10's of meters and fission products could potentially be contained. To adequately determine this threat, further study of TRISO particle structural integrity under these conditions is required.

5.4 Summary

By starting to replace conventional nuclear reactors throughout the world with LFFH engines, we could address the growing world energy needs and potentially reduce proliferation risks associated with nuclear power. At the beginning of this study, a goal was set to enable the LFFH design without enrichment or reprocessing of the fuel to aid with the nonproliferation aspects and to close the fuel cycle. This goal, from a neutronics and nonproliferation perspective, can be achieved. However, care must be taken to protect the technology from proliferation. The LFFH technology offers a unique path to potentially reducing nuclear proliferation by eliminating the justified use of uranium enrichment and reprocessing plants, while minimizing the weapons utility of the nuclear material used to produce energy. If a non-nuclear weapons state is utilizing LFFH plants to produce its nuclear energy, there is not justifiable reason for either enrichment or reprocessing. This also implies that if reprocessing were eliminated worldwide, damaged fuel pebbles would have to be discarded. Fuel failure rates, fabrication and disposal issues obviously play a

deciding role.

The unprocessed LFFH fuel at all points in its lifetime is undesirable for weapons material because there are easier and less costly ways to develop that same material. Radiological dose and decay heat from 1 SQ of material are prohibitive for anything but remote handling under controlled conditions. Depending on whether collusion with an inside actor is possible, either one large theft or up to 1,000 separate thefts of material would be required to obtain 1 SQ of ^{239}Pu.

The principal concern for proliferation resistance will be to detect misuse or diversion of material by a state actor. This could include producing fissile material near a LFFH engine by utilizing leakage neutrons or development of a clandestine facility devoted for that purpose. The fusion based source of neutrons could potentially be misused. Under this scenario the primary detection methods include IAEA safeguards, satellite imagery, human intelligence and export controls. That being said, the proposed LFFH fuel cycle can be considered closed if fuel is burned to high burnup and not reprocessed. Likewise, diversion or theft of fissile material during enrichment and transport is not likely because the fuel is primarily ^{238}U upon delivery to the LFFH and consists of mainly fission products upon its ultimate removal. Using the FOM methodology, the LFFH fuel material is unattractive unless it can be reprocessed.

Chapter 6

Synthesis

6.1 Conclusions

This study investigated the neutronic characteristics of the DU fueled fusion-fission hybrid LFFH engine. The goals of this study were specifically to model the neutronics aspects of this hybrid fusion-fission system based on laser ICF for an energy production mission using a depleted uranium fuel. The concept requires in-situ breeding of the fission fuel as the fusion driver breeds the necessary fissile material, while fissioning the fuel to the maximum burnup possible. Reprocessing is potentially also eliminated if the decision is made to directly dispose of partially irradiated damaged fuel pebbles. The system is designed to remain subcritial at all times and is tritium self-sufficient. For an energy production mission, the goal was to accomplish all this while maximizing the BOP utilization and minimizing proliferation aspects. This study addresses many of the neutronics modeling and code development issues requiring resolution prior to development of a self-contained design.

To study the LFFH concept and ultimately arrive at the design, a new software code was developed. The LNC code serves to incorporate neutron transport results from MCNP with nuclide depletion results provided by Monteburns 2.0. It also acts as a controller code to continuously adjust the operating parameters of the LFFH engine such that a fully time-dependent simulation of this fusion-fission hybrid, controlled via coolant ^{6}Li enrichment, could be performed. In addition, an external library was developed, named the adaptive burnup library, and incorporated into the LNC code to improve the computational modeling efficiency. The ABL library included adaptive time stepping and adaptive mesh refinement. It was found that a factor of $\sim 7\times$ speedup was possible by utilizing variable time stepping. Similarly, AMR resulted in a $\sim 1.25\times$ speedup while improving accuracy in the simulation for a fixed core model.

After development of the LNC code and its associated ABL library, multiple simulations of neutron transport and nuclear burnup as a function of time were performed. A parametric study was performed to arrive at the baseline design. The main fusion chamber

is surrounded by a first wall, $Li_{17}Pb_{83}$ first wall coolant, flibe cooled beryllium multiplier, DU fission and carbon reflector pebble blanket layers. The LFFH engine is designed to operate using DU as the fissionable fuel. The DU fuel is contained in TRISO particles packed into larger fuel pebbles. Parametric studies showed that a 300 μm kernel diameter with a 20% TRISO packing for a 20 MT DU fuel load resulted in optimal burnup performance. Similarly, Be blanket was found to optimize at 12 cm with a 60% packing fraction. The graphite reflector optimized at 75 cm thick. Both $Li_{17}Pb_{83}$ and flibe are enriched to control the fission blanket gain to be 4, yielding a net system thermal power of 2000 MW_{th} utilizing a 2.5 m chamber radius.

The LFFH concept, if implemented, offers a novel means of closing the fuel cycle for energy production missions. Although radiation damage is likely to limite the maximum attainable burnup, o fuel enrichment or reprocessing is necessary or can be justified, thus reducing proliferation concerns for weapons material development. Similarly, the LFFH fuel at the point of peak plutonium concentration is unattractive due to the presence of large amounts of fission product poisons and minor actinides. 1 SQ of fuel pebbles are self-protecting for over 50 years. The associated material attractiveness FOM is negative for up to 40 years after removal from the fission blanket. This implies that the fuel is unattractive and the LFFH concept can remove some proliferation concerns regarding theft, but clandestine development of facilities and material produced at those facilities remains an issue.

6.2 Future Work

Every effort was made to make this study as comprehensive and self-contained as possible. However, there are many areas related to the LFFH engine design, non-proliferation aspects and code development that require further study. These areas include the fuel and structural materials development and enterprise level proliferation assessments.

The codes utilized to analyze this system were in most cases the current state of the art. However, the fact that the different software programs shared information via file interchange limits the computational flexibility. Specifically, the parallelism is significantly impacted after approximately 40-48 cpu's such that no further performance gains are achieved. To improve this, the codes should be incorporated into a single software package that transfers data in memory and supports highly parallel systems. This will reduce the time to perform a simulation and encourage widespread adoption of Monte Carlo depletion. Along these same lines, an effort to better model the fuel geometry and burnup could improve the results. Similarly, additional work to optimize the operator splitting of the AMR method within the depletion time step is necessary. Namely, how frequently does AMR need to be performed to obtain similar results.

The LFFH engine design has been optimized to fulfill an energy mission while burning DU fuel. Alternative fuels could include HEU, WgPu or thorium and the resulting designs

will most likely vary because of different neutronic or proliferation concerns associated with each particular fuel. In theory, the LFFH concept is equally applicable to these different fuels and their respective missions, but these systems must be analyzed in depth. In addition, a practical system for controlling the ^{6}Li enrichment in the coolants must be devised. Similarly, detailed development of the safety and shutdown systems for the DU design are required. This study touched on a few of the issues related to safety analysis like criticality and reactivity excursions, but is by no means a detailed investigation into the subject. Fuel reload and shuffling schemes are also enabled by mutliple zone depletion. Future efforts will include better fuel shuffling and blanket optimization strategies. Coupling a fuel shuffling scheme with AMR is problematic because of volume and mass conservation issues. The LNC code is currently not designed to allow for automated fuel shuffling and much more work is required to do so. Additional work is also required in addressing thermal hydraulic constraints. This includes reducing the power peaking designing the blanket for the maximum managable power density. Further effort is required to identify and work within radiation damage constraints to the first wall, structural materials and fuel materials. Lastly, practical considerations including the modularity, human factors, industrial scalability and operational constraints of the design need to be examined.

Some proliferation aspects of the LFFH concept were examined in this work. Focus on physical security was also addressed in the context of quantifying how attractive the fuel pebbles would be to a terrorist group interested in developing weapons. State actors utilizing the technology will ultimately be the primary focus on how proliferation resistant the LFFH design is. This must be analyzed further within the PR&PP framework at an enterprise level. Once developed, the LFFH plants could be examined as part of an overall non-proliferation effort verifiable by inspections and enforceable by international treaties.

Bibliography

[1] Rembrandt H.E.M. Koppelaar. World production and peaking outlook, September 2006. 1.1

[2] Werner Zittel and Jorg Schindler. Crude oil: The supply outlook, October 2007. 1.1

[3] Peak oil - wikipedia, the free encyclopedia. http://en.wikipedia.org/wiki/Peak_oil#cite_note-mkinghubbert1956-0. 1.1

[4] Marion King Hubbert. Nuclear energy and the fossil fuels 'Drilling and production practice'. In *Spring Meeting of the Southern District. Division of Production*, pages 22–27, San Antonio, Texas, June 1956. Shell Development Company. 1.1

[5] Adam R. Brandt. Testing hubbert. *Energy Policy*, 35(5):3074–3088, May 2007. 1.1

[6] Nick A. Owen, Oliver R. Inderwildi, and David A. King. The status of conventional world oil reserves–Hype or cause for concern? *Energy Policy*, In Press, Corrected Proof. 1.1

[7] David JC MacKay. *Sustainable Energy - Without The Hot Air*. UIT, Cambridge, England, 2009. 1.1, 1.1.2.2

[8] Office of Integraged Analysis Energy Information Administration and U.S. Department of Energy Forecasting. EIA - international energy outlook 2009 with projections to 2030, 2007. 1.1.1, 1.1.2, 1.1.2.1

[9] E.H. SIMS, R.N. Schock, A. Adegbululgbe, J. Fenhann, I. Konstantinaviciute, W. Moomaw, H.B. Nimir, B. Schlamadinger, J. Torres-Martinez, C. Turner, Y. Uchiyama, S.J.V. Vuori, N. Wamukonya, and X. Zhang. Energy supply. in climate change 2007: Mitigation. contribution of the working group III of the forth assessment report of the intergovernmental panel on climate change. Cambridge University Press, 2007. 1.1.1, 1.1.2

[10] Office of Energy Statistics from the U.S. Government Energy I. How much coal is left - energy explained, your guide to understanding energy. http://tonto.eia.doe.gov/energyexplained/index.cfm?page=coal_reserves. 1.1.2.1

[11] Coal - wikipedia, the free encyclopedia. http://en.wikipedia.org/wiki/Coal#cite_note-52. 1.1.2.1

[12] Technology Committee on Coal Research and Resource Assessments to Inform Energy Policy. *Coal Research and Development*. The National Academies Press, Washington, D.C., 2007. 1.1.2.1

[13] International Energy Agency. Key world energy statistics, 2006. 1.1.3

[14] U.S. Nuclear Regulatory Commission. NRC: nuclear fuel pool capacity. http://www.nrc.gov/waste/spent-fuel-storage/nuc-fuel-pool.html. 1.1.3.1

[15] U.S. Nuclear Regulatory Commission. NRC: spent fuel storage regulations, guidance, and communications. http://www.nrc.gov/waste/spent-fuel-storage/regs-guides-comm.html. 1.1.3.1

[16] Thomas James Dolan. *Fusion Research*, volume I - Principles. Pergamon Press, New York, 1982. 1.1.3.2

[17] Jeffery F. Latkowski. *Inertial Fusion Energy: A Clearer View of the Environmental and Safety Perspectives*. Ph.D thesis, University of California, Berkeley, November 1996. 1.1.3.2, 2.1

[18] ITER - the way to new energy. http://www.iter.org/default.aspx. 1.1.3.2

[19] Laboratory for Laser Energetics. A unique national resource - visitor's guide. 1.1.3.2

[20] U.S. Department of Energy. Inertial fusion fact sheet, September 1988. 1.1.3.2

[21] J.P. Holdren, D.H. Berwald, R.J. Budnitz, J.G. Crocker, J.G. Delene, R.D. Endicott, M.S. Kazimi, R.A.Krakowski, B.G. Logan, and K.R. Schultz. Report of the senior committee on environmental, safety, and economic aspects of magnetic fusion energy, September 1989. 1.1.3.2

[22] J.H. Nuckolls, L. Wood, A. Thiessen, and G.B. Zimmerman. Laser compression of mater to Super-High densities: Thermonuclear (CTR) applications. *Nature*, 239(139), 1972. 1.1.3.2

[23] J.T. Hunt, K.R. Manes, J.R. Murray, P.A. Renard, R.W. Sawicki, J.B. Trenholme, and W. Williams. Laser design basis for the national ignition facility. New Orleans, LA, June 1994. See NTIS DE94016700. 1.1.3.2

[24] J.D. Lindl. *Inertial Confinement Fusion*. Springer-Verlag, 1998. 1.1.3.2, 2.3.2

[25] J.D. Lindl. The physics basis for ignition using indirect-drive targets on the national ignition facility. *Physics of Plasmas*, 11(2):339, 2004. 1.1.3.2, 2.3.2

[26] Office of Chief Financial Officer. FY 2010 congressional budget request, May 2009. 1.1.3.3

[27] A. Sakharov. *Memoirs*. New York, 1990. 1.1.3.3

[28] H. A. Bethe. The fusion hybrid. *Physics Today*, pages 44–51, 1979. 1.1.3.3

[29] E. Greenspan, A. Schneider, D. Gilai, and P. Levin. Natural-Uranium Light-Water breeding hybrid reactors. In *Proc. 2nd Topical Meeting on the Technology of Controlled Nuclear Fusion*, CONF-760975-P3, pages 1061–1072, 1976. 1.1.3.3

[30] E. Greenspan, A. Schneider, D. Gilai, and A. Misolovin. Constant power hybrid reactor blankets and lithium control. *Trans. American Nuclear Society*, 30:55–56, 1978. 1.1.3.3

[31] E. Greenspan. Fusion-Fission hybrid reactors. In *Advances in Nuclear Science and Technology*, volume 16, pages 289–515. Plenum Publishing Co., 1984. 1.1.3.3

[32] E. Greenspan. Fusion reactors blanket nucleonics. In *Progress in Nuclear Energy*, 17. Pergamon Press, 1986. 1.1.3.3

[33] M. Kotschenreuther et al. Fusion-Fission transmutation Scheme–Efficient destruction of nuclear waste. *Fusion Engineering Design*, 84:83–88, 2009. 1.1.3.3

[34] J.A. Maniscalco and L.F. Hansen. Status of laser driven fusion-fission energy systems, 1978. 1.1.3.3

[35] L.W. Gray, T. Kan, W.G. Sutcliffe, J.M. McKibben, and W. Danker. Disposition of surplus fissile materials via immobilization. Palm Desert, CA, July 1995. 2.1.3

[36] National Academy of Sciences. Management and disposition of excess weapons pu, 1994. 2.1.3

[37] E.I. Moses, T. Diaz de la Rubia, J.F. Latkowski, J.C. Farmer, R.P. Abbott, K.J. Kramer, P.F. Peterson, H.F. Shaw, and R.F. Lehman II. A sustainable nuclear fuel cycle based on laser inertial fusion energy (LIFE). *Fusion Science and Technology*, 56(2):566–572, August 2009. 2.2, 2.2, 2.3.3

[38] K.J. Kramer, J.F. Latkowski, R.P. Abbott, J.K. Boyd, J.J. Powers, and J.E. Seifried. Neutron transport and nuclear burnup analysis for the laser inertial confinement Fusion-Fission energy (LIFE) engine. *Fusion Science and Technology*, 56(2):625–631, August 2009. 2.2, 4.2.4

[39] K.J. Kramer, W.R. Meier, J.F. Latkowski, and R.P. Abbott. Parameter study of the LIFE engine nuclear design. *Energy Convers Manage*, article in press, 2010. 2.2

[40] W.R. Meier. Two-Dimensional neutronics calculation for the HYLIFE converter. Technical Report UCRL-83595, Lawrence Livermore National Laboratory, Livermore, CA, November 1979. 2.3.3

[41] R.W. Moir and et al. HYLIFE-II progress report. Technical Report UCID-21816, Lawrence Livermore National Laboratory, Livermore, CA, December 1991. 2.3.3

[42] Rene. A Raffray. An introduction to our proposed solutions to address the ion threat to the chamber wall, October 2008. 2.3.3

[43] S.C. Wilks, B.I. Cohen, J.F. Latkowski, and E.A. Williams. Evaluation of several issues concerning laser beam propagation through the LIFE target chamber. *Fusion Science and Technology*, 56:652–657, August 2009. 2.3.3

[44] R.P. Abbott, M.A. Gerhard, K.J. Kramer, J.F. Latkowski, K.L. Morris, P.F. Peterson, and J.E. Seifried. Thermal and mechanical design aspects of the LIFE engine. *Fusion Science and Technology*, 56(2):618–624, August 2009. 2.3.4, 2.3.6, 2.3.9, 4.2.3

[45] James J. Duderstadt and Louis J. Hamilton. *Nuclear Reactor Analysis*. John Wiley & Sons, Ann Arbor, Michigan, 1976. 2.3.6, 3.1.2, 4.2.1.1, 4.2.4

[46] W. J. Kovacs, K. Bongartz, and D. Goodin. TRISO-Coated HTGR fuel Pressure-Vessel performance models, October 1983. 2.3.8.1

[47] T.B. Lindemer and R.L. Pearson. Kernel migration for HTGR fuels from the system Th-U-Pu-C-O-N. 60(1-2):5–14, 1976. 2.3.8.1

[48] R. Benz and A. Naoumidis. Stability of unirradiated TRISO-coated UC2-UO2 particles with different UC2 contents at elevated temperatures. *Jou*, 97:15–24, 1981. 2.3.8.1

[49] R.E. Bullock. Fission-Product release during postirradiation annealing of several types of fuel particles. *Journal of Nuclear Materials*, 125:304–319, 1984. 2.3.8.1

[50] R.C. Martin. Compilation of fuel performance and fission product transport models and database for MHTGR design, 1993. 2.3.8.1

[51] Final Report Under the International Nuclear Energy Research Initiative (I-NERI). Development of improved models and designs for Coated-Particle gas reactor fuels. Technical Report INEEL/EXT-05-02615, Idaho National Engineering and Environmental Laboratory, Idaho Falls, Idaho, December 2004. 2.3.8.1

[52] G.K. Miller, J.T. Maki, D.L. Knudson, and D.A. Petti. Current capabilities of the fuel performance modeling code parfume, September 2004. 2.3.8.1

[53] Kazuhiro Sawa and Shohei Ueta. Research and development of HTGR fuel in the HTTR project. *Nuclear Engineering and Design*, 233:163–172, 2004. 2.3.8.1

[54] Gregory K. Miller, David A. Petti, John T. Maki, and Darrell L. Knudson. Updated solution for stresses and displacements in TRISO-coated fuel particles. *Journal of Nuclear Materials*, 374:129–137, 2008. 2.3.8.1

[55] Caro Magdalena, J. Marian, P. DeMange, and A. Caro. Design of fuels for LIFE engines. Technical Report LLNL-TR-416654, Lawrence Livermore National Laboratory, Livermore, CA, September 2009. 2.3.8.1, 4.2.3

[56] B.A. Pint and I.G. Wright. Long-term high temperature oxidation behavior of ODS ferritics. *Journal of Nuclear Materials*, 307-311:763–768, 2002. 2.3.9

[57] Shigeharu Ukai and Masayuki Fujiwara. Perspective of ODS alloys application in nuclear environments. *Journal of Nuclear Materials*, 307-311:749–757, 2002. 2.3.9

[58] S. Ukai, M. Harada, H. Okada, M. Inoue, S. Nomura, S. Shikakura, K. Asabe, T. Nishida, and M. Fujiwara. Alloying design of oxide dispersion strengthened ferritic steel for long life FBR's core materials. *Journal of Nuclear Materials*, 204:65–73, 1993. 2.3.9

[59] G. Yu, N. Nita, and N. Baluc. Thermal creep behaviour of the EUROFER 97 RAFM steel and two european ODS EUROFER 97 steels. *Fusion Engineering and Design*, 75-79:1037–1041, 2005. 2.3.9

[60] Steven J. Zinkle. Advanced materials for fusion technology. *Fusion*, 74:31–40, 2005. 2.3.9

[61] Steven J. Zinkle and N.M. Ghoniem. Operating temperature windows for fusion reactor structural materials. *Fusion Engineering and Design*, 51-52:55–71, 2000. 2.3.9

[62] T. Arisawa, Y. Maruyama, Y. Suzuki, and K. Shiba. Lithium isotope separation by laser. *Applied Physics B Photophysics and Laser Chemistry*, 28(1):73–76, 1982. 2.4.1

[63] M. Saleem, S. Hussain, M.A. Zia, and M.A. Baig. An efficient pathway for li6 isotope enrichment. *Applied Physics B*, 87(4):723–726, 2007. 2.4.1

[64] Jeffery F. Latkowski. Internal communication, 2009. 2.4.1

[65] Los Alamos National Laboratory. MCNP - a general monte carlo N-Particle transport code. *LA-UR-03-1987*, 2003. 3.1.3, 3.1.3.3

[66] R.J. Procassini and M.S. McKinley. The mercury monte carlo web site, http://nuclear.llnl.gov/mercury, 2005. 3.1.3, 3.6.3

[67] J. Cetnar, W. Gudowski, and J. Wallenius. MCB: a continuous energy monte carlo burnup simulation code. Technical Report EUR 18898 EN, OECD/NEA, 1999. 3.1.3

[68] Oak Ridge Nationa Laboratory. SCALE: a modular code system for performing standardized computer analyses for licensing evaluations. Technical Report ORNL/TM-2005/39, Version 5.1, Vols I-III, Radiation Safety Information Computational Center, November 2006. 3.1.3

[69] T.D. Newton and J.L. Hutton. The next generation WIMS lattice code: WIMS9. In *Proc. from PHYSOR 2002*, Seoul, South Korea, October 2002. 3.1.3

[70] J. von Neumann. Statistical methods in neutron diffusion, 1947. 3.1.3

[71] A.A. Markov. Issledovanie zamechatelnogo sluchaya zavisimyh ispytanij. *Izvestiya Akademii Nauk*, 1(3):61–80, 1907. 3.1.3

[72] F.B. Brown. Theory & practice of criticality calculations with MCNP5. Technical Report LA-UR-08-0849, Los Alamos National Laboratory, Los Alamos, NM, 2009. 3.1.3.1

[73] E.D. Cashwell and C.J. Everett. *A Practical Manual on the Monte Carlo Method for Random Walk Problems*. Pergamon Press, Los Angeles, CA, 1959. 3.1.3.3

[74] E.E. Lewis and W.F., Jr. Miller. *Computational Methods of Neutron Transport*. American Nuclear Society, La Grange Park, IL, 1993. 3.1.3.3

[75] F.B. Brown. Fundamentals of monte carlo particle transport. Technical Report LA-UR-05-4983, Los Alamos National Laboratory, Los Alamos, NM, 2005. 3.1.3.3

[76] F.B. Brown, A.C. Kahler, G.W. McKinney, R.D. Mosteller, and M.G. White. MCNP5+Data+MCNPX workshop. In *Workshop presentation at the 2007 ANS Mathematics & Computation Division Topical Meeting (M&C+SNA-2007)*, Monterey, CA, April 2007. 3.1.3.3

[77] A.G. Croff. ORIGEN2: a versatile computer code for calculating the nuclide compositions and characteristics of nuclear materials. *Nuclear Technology*, 62:335–352, September 1983. 3.2.1

[78] D.L. Poston and H.R. Trellue. Users manual, version 2.0 for MONTEBURNS version 1.0, 1999. 3.2.1, 3.5

[79] M. J. Bell. ORIGEN - the ORNL isotope generation and depletion code, May 1973. 3.2.2, 3.2.2, 3.2.2

[80] A.G. Croff, R. L. Haese, and N.B. Gove. Updated decay and photon libraries for the ORIGEN code, February 1979. 3.2.2

[81] H. Bateman. Solution of a system of differential equations occurring in the theory of radioactive transformations. *Proc. Cambridge Philos. Soc.*, 15:423–427, 1910. 3.2.2

[82] K. Furuta, Y. Oka, and S. Kondo. BISON 1.5 a one-dimensional transport and burnup calculation code., 1987. 3.2.2

[83] W.B. Wilson, T.R. England, and K.A. Van Riper. Status of CINDER90 codes and data. In *Proceedings of the IV SARE Workshop*, page 69, Knoxville, TN, September 1998. 3.2.2

[84] Jerzy Cetnar. A method of transmutation trajectories analysis in accelerator driven system. In *Proceedings of the IAEA Technical Commitee Meeting on Feasibility and Motivation for Hybrid Concepts for Nuclear Energy Generation and Transmutation*, volume TC-903.3, pages 419–428, Madrid, September 1997. IAEA. 3.2.2, 3.6.2

[85] Jerzy Cetnar. General solution of bateman equations. *Annals of Nuclear Energy*, 33:640–645, 2006. 3.2.2, 3.6.2

[86] International Atomic Energy Agency. Recommendations of the IAEA working group on reactor radiation measurements. *Nuclear Engineering Design*, 33(92), 1975. 3.3

[87] L.R. Greenwood and R.K. Smither. SPECTER: neutron damage calculations for materials irradiations. Technical Report ANL/FPP/TM-197, Argonne National Laboratory, Argonne, Illinois, 1985. 3.3

[88] A. Hogenbirk. An easy way to perform a radiation damage calculation in a complicated geometry. *Fusion Energineering and Design*, 83:1828–1831, 2008. 3.3

[89] R.E. MacFarlane and D.W. Muir. The NJOY nuclear data processing system, version 91, October 1994. 3.3

[90] J. Sanz, J.M. Perlado, D. Guerra, and A.S. Perez. ACAB: activation code for fusion applications, user's manual v1.0. Technical Report DENIM-284, Instituto de Fusion Nuclear/Universidad Politecnica de Madrid, 1992. 3.4.1

[91] J. Sanz. ACAB, activation code for fusion applications: User's manual v5.0. Technical Report UCRLMA-143238, Lawrence Livermore National Laboratory, Livermore, CA, February 2000. 3.4.1

[92] O. Cabellos, J. Sanz, N. Garcia-Herranz, S. Diaz, S. Reyes, and S. Piedloup. Transmutation analysis of realistic low-activation steels for magnetic fusion reactors and IFMIF. *Journal of Nuclear Materials*, 367-370 Part 2:1562–1567, August 2007. 3.4.1

[93] J. Sanz, O. Cabellos, and N. Garcia-Herranz. ACAB inventory code for nuclear applications: User's manual v6.0. Technical report, December 2008. 3.4.1

[94] Z. Karriem, C. Stoker, and F. Reitsma. MCNP modeling of HTGR Pebble-Type fuel. In *Proc. Monte Carlo 2000 Conference*, pages 841–846, Lisbon, Spain, 2000. 4.2.1.4, 4.2.1.4

[95] R. Plukiene and D. Ridikas. Modelling of HTRs with monte carlo: from a homogeneous to an exact heterogeneous core with microparticles. *Annals of Nuclear Energy*, 30:1573–1585, 2003. 4.2.1.4

[96] F.B. Brown, W.R. Martin, W. Ji, J.L. Conlin, and J.C. Lee. Stochastic geometry and HTGR modeling for MCNP5. Chattanooga, TN, April 2005. American Nuclear Society. 4.2.1.4, 4.2.1.4

[97] W. Ji, J.L. Conlin, W.R. Martin, J.C. Lee, and F.B. Brown. Explicit modeling of particle fuel for the Very-High temperature Gas-Cooled reactor. In *Trans. Am. Nucl. Soc.*, volume 92. American Nuclear Society, June 2005. 4.2.1.4

[98] W. Ji. *Neutronic Analysis of Stochastic Distribution of Fuel Particles in Very High Temperature Gas-Cooled Reactors*. Ph.D thesis, University of Michigan, 2008. 4.2.1.4, 4.2.1.4

[99] Massimiliano Fratoni. *Development and applications of methodologies for the neutronic design of the Pebble Bed Advanced High Temperature Reactor (PB-AHTR)*. Ph.D thesis, University of California, Berkeley, 2009. 4.2.1.4

[100] M. Armishaw, N. Smith, and E. Shuttlesworth. Particle packing considerations for pebble bed fuel systems. In *Proc. ICNC 2003 Conference*, Tokai-mura, Japan, 2003. 4.2.1.4

[101] F.C. Difilippo. Monte carlo calculations of pebble bed benchmark configurations of the PROTEUS facility. *Nucl. Sci. Eng.*, 143:240–253, 2003. 4.2.1.4

[102] R. Abbott. Internal communication, 2009. 4.2.2.2

[103] Cross Sections Evaluation Working Group. The ENDF-6 format manual: Data formats and procedures for the evaluated nuclear data file ENDF/B-VI and ENDF/B-VII. Technical Report BNL-90365-2009, Brookhaven National Laboratory, Upton, NY, June 2009. 4.2.4

[104] J.C. Farmer. Opportunities in materials science and engineering driven by ICF hybrids -Materials for LIFE. Gaithersburg, MD, October 2009. 4.3.1.2

[105] Paul DeMange, Jaime Marian, Magdalena Serrano de Caro, and Alfredo Caro. Thermo-mechanical and neutron lifetime modeling and design of be pebbles in the neutron multiplier for the LIFE engine. Technical Report LLNL-JRNL-412221, Lawrence Livermore National Laboratory, Livermore, CA, April 2009. 4.3.1.2

[106] Nuclear Energy Research Advisory Committee and the Generation IV International Forum. Generation IV roadmap - crosscutting fuels and materials R&D scope report. Technical Report GIF-010-00, December 2002. 4.3.1.2

[107] J.T. Maki, D.A. Petti, D.L. Knudson, and G.K. Miller. The challenges associated with high burnup, high temperature and accelerated irradiation for TRISO-coated particle fuel. *Journal of Nuclear Materials*, 371:270–280, 2007. 4.3.1.2

[108] L. Sandell. A review of radionuclide release from HTGR cores during normal operation. Final Report 1009382, EPRI, February 2004. 4.3.1.2

[109] Lance L. Snead, Takashi Nozawa, Yutai Katoh, Thak-Sang Byun, Sosuke Kondo, and David A. Petti. Handbook of SiC properties for fuel performance modeling. *Journal of Nuclear Materials*, 271:329–377, 2007. 4.3.1.2

[110] Jeffrey E. Seifried. Thermal modeling and feedback requirements for LIFE neutronics simulations. Technical Report LLNL-TR-416167, Lawrence Livermore National Laboratory, Livermore, CA, August 2009. 4.3.1.4

[111] Massimiliano Fratoni, Kevin J. Kramer, Jeffrey F. Latkowski, Ryan P. Abbott, Jeffrey E. Seifried, and Jeffrey J. Powers. Attainable burnup in a LIFE engine loaded with depleted uranium. In *Proc. PHYSOR 2010*, Pittsburg, PA, May 2010. American Nuclear Society. 4.4.1

[112] The Proliferation Resistance and Physical Protection Evaluation Methodology Expert Group of the Generation IV International Forum. Evaluation methodology for proliferation resistance and physical protection of generation IV nuclear energy systems. Technical Report GIF/PRPPWG/2006/005, Generation IV International Forum, November 2006. 5.1

[113] Peterson Per. Elements of the proliferation resistance and physical protection (PR&PP) evaluation methodology. In *Proc. of the Global 2009 International Conference on the Nuclear Fuel Cycle*, Paris, France, September 2009. 5.1

[114] Bary Robert A. Proliferation resistance and physical protection (PR&PP) evaluation methodology: Objectives, accomplishments, and future directions. In *Proc. of the*

Global 2009 International Conference on the Nuclear Fuel Cycle, Paris, France, September 2009. 5.1

[115] G.G.M. Cojazzi, J. Hassberger, and G. Renda. Applying the PR&PP methodology for a qualitative assessment of a misuse scenario in a notional generation IV example sodium fast reactor. assessing design variations. In *Proceedings of Global 2009*, Paris, France, September 2009. 5.1

[116] T. Bjornard, R. Bean, S. DeMuth, P. Durst, M. Ehinger, M. Golay, D. Hebditch, J. Hockert, and J. Morgan. Safeguards-by-Design: early integration of physical protection and safeguardability into design of nuclear facilities. In *Proc. of the Global 2009 International Conference on the Nuclear Fuel Cycle*, Paris, France, September 2009. 5.1

[117] International Atomic Energy Agency. IAEA safeguards glossary 2001 edition. Technical Report ISSN 1020-6205; no.3, International Atomic Energy Agency, Vienna, Austria, 2001. 5.1

[118] G. Bathke Charles and et. al. An assessment of the proliferation resistance of materials in advanced nuclear fuel cycles. Portland, Oregon, April 2008. 5.1.3

[119] G. Bathke Charles, Jarvinen Gordon D., Wallace Richard K., Ireland John R., Johnson M. W., Sleaford Brad W., Ebbinghaus Bartley B., Bradley Keith S., Collins Brian A., Smith Brian W., and Prichard Andrew W. Further assessments of the attractiveness of materials in advanced nuclear fuel cycles from a safeguards perspective. In *Proc. of the Global 2009 International Conference on the Nuclear Fuel Cycle*, Paris, France, September 2009. 5.1.3, 5.1.3, 5.1.4

[120] U.S. Department of Energy. Nuclear material control and accountability. Technical Report DOE M 470.4-6 Chg 1, U.S. Department of Energy, August 2006. 5.1.3

[121] C.W. Forsberg and D.L. Moses. Safeguards challenges for Pebble-Bed reactors designed by people's republic of china. Technical Report ORNL/TM-2008/229, Oak Ridge National Laboratory, Oak Ridge, TN, November 2009. 5.2.1

[122] M. J. Haire and C.W. Forsberg. Tags to track illicit uranium and plutonium. In *Proc. Global 2007: Advanced Nuclear Fuel Cycles and Systems*, La Grange Park, IL, September 2007. American Nuclear Society. 5.2.1

[123] Marvin Baker and Ike Chang. Mobile nuclear power for future land combat. *NDU Press*, (52):49–55, 2009. 5.3.1

Appendix A

Additional Neutronics Modeling Details

A.1 Masses of Additional Isotopes Tracked

The following figures illustrate the evolution of most of the isotopes that are tracked in a typical simulation. Isotopes are identified by a zzzaaa number representing the six digit identifier for each isotope. The blanket tracked uses 300 μm kernels, a 20% TRISO packing fraction, a 20 MT fuel load, 16 cm thick Be blanket and $\sim$60% pebble packing fraction in the coolant. These results reflect the design illustrated in Table 4.5. The Monteburns threshold utilized is 1×10^{-10} for typical case.

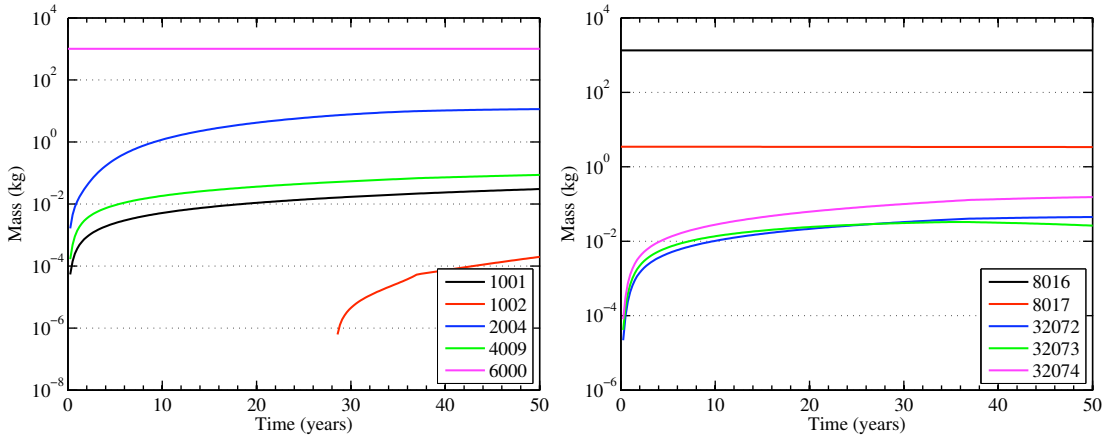

(a) (b)

Figure A.1: Masses of some key isotopes with zzzaaa numbers of 1001 to 32074

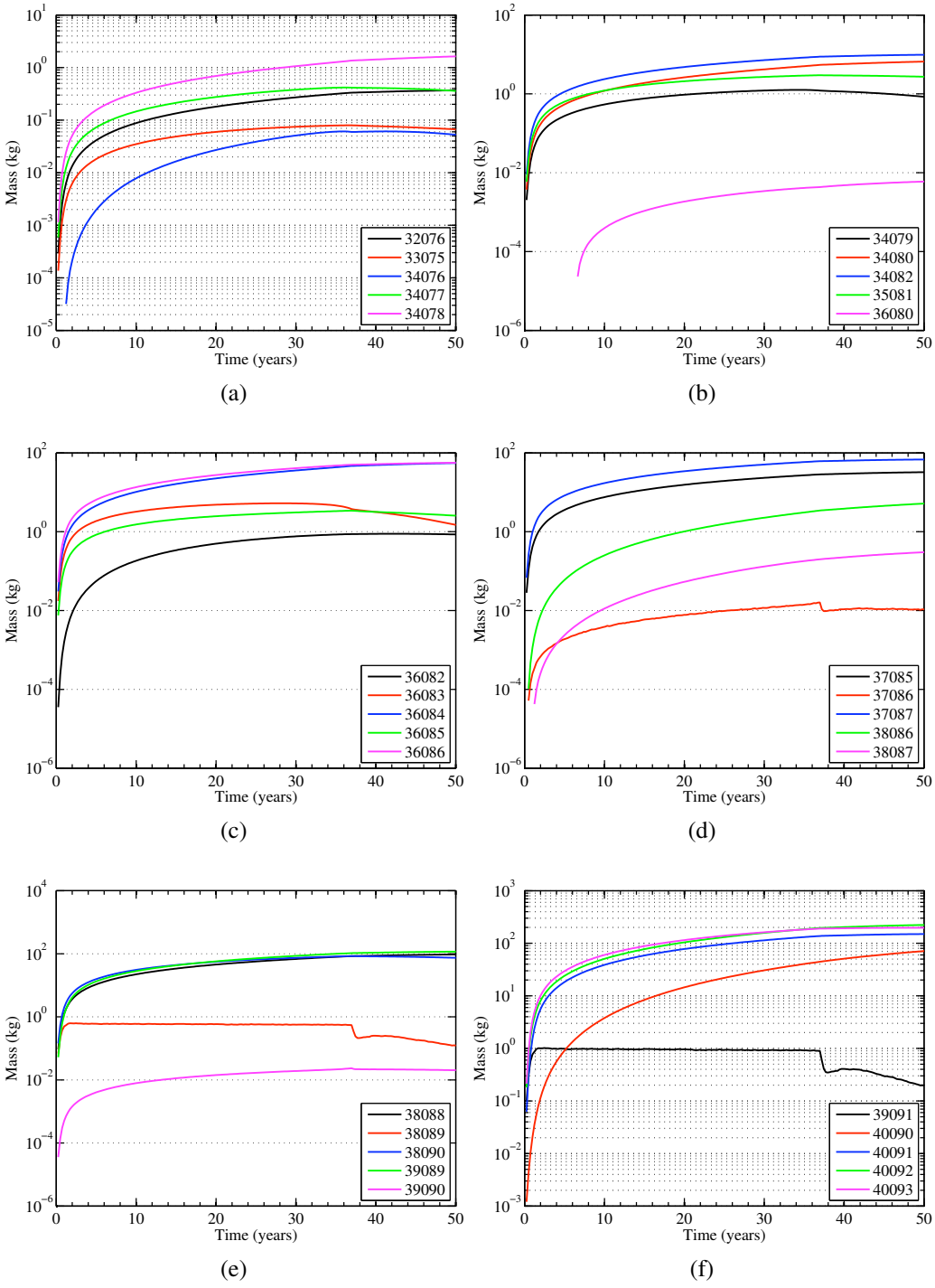

Figure A.2: Masses of some key isotopes with zzzaaa numbers of 32076 to 40093

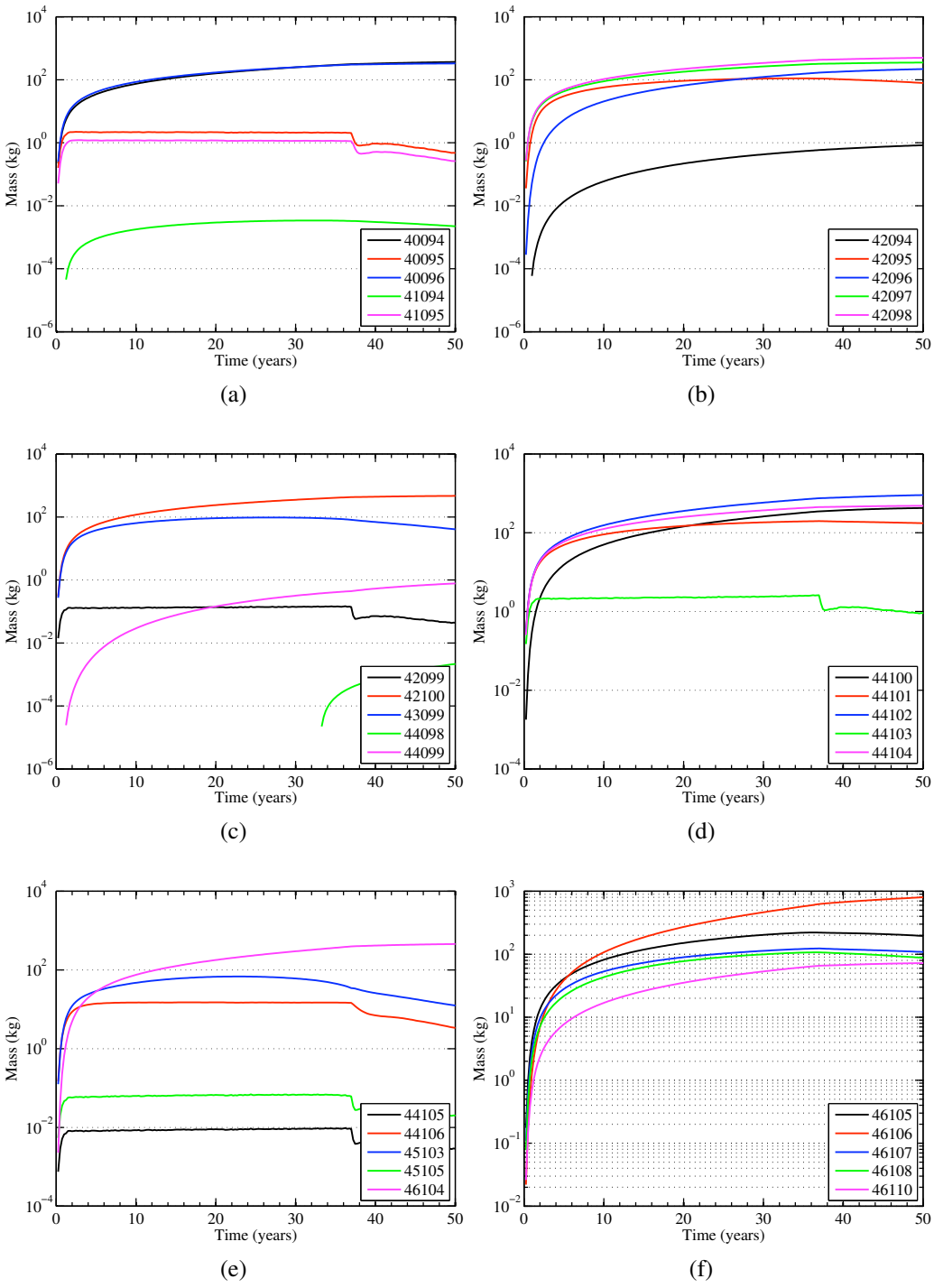

Figure A.3: Masses of some key isotopes with zzzaaa numbers of 40094 to 46110

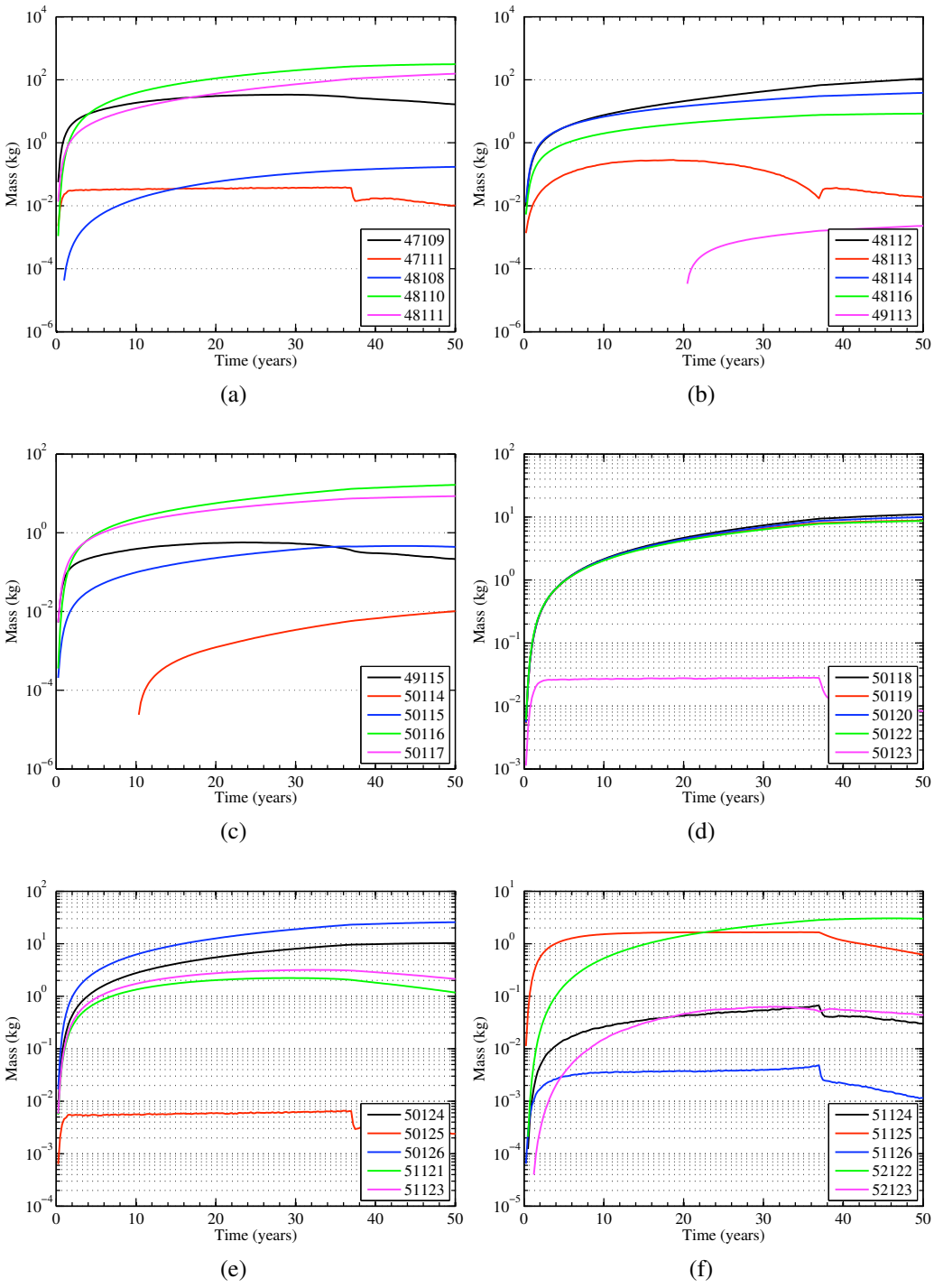

Figure A.4: Masses of some key isotopes with zzzaaa numbers of 47109 to 52123

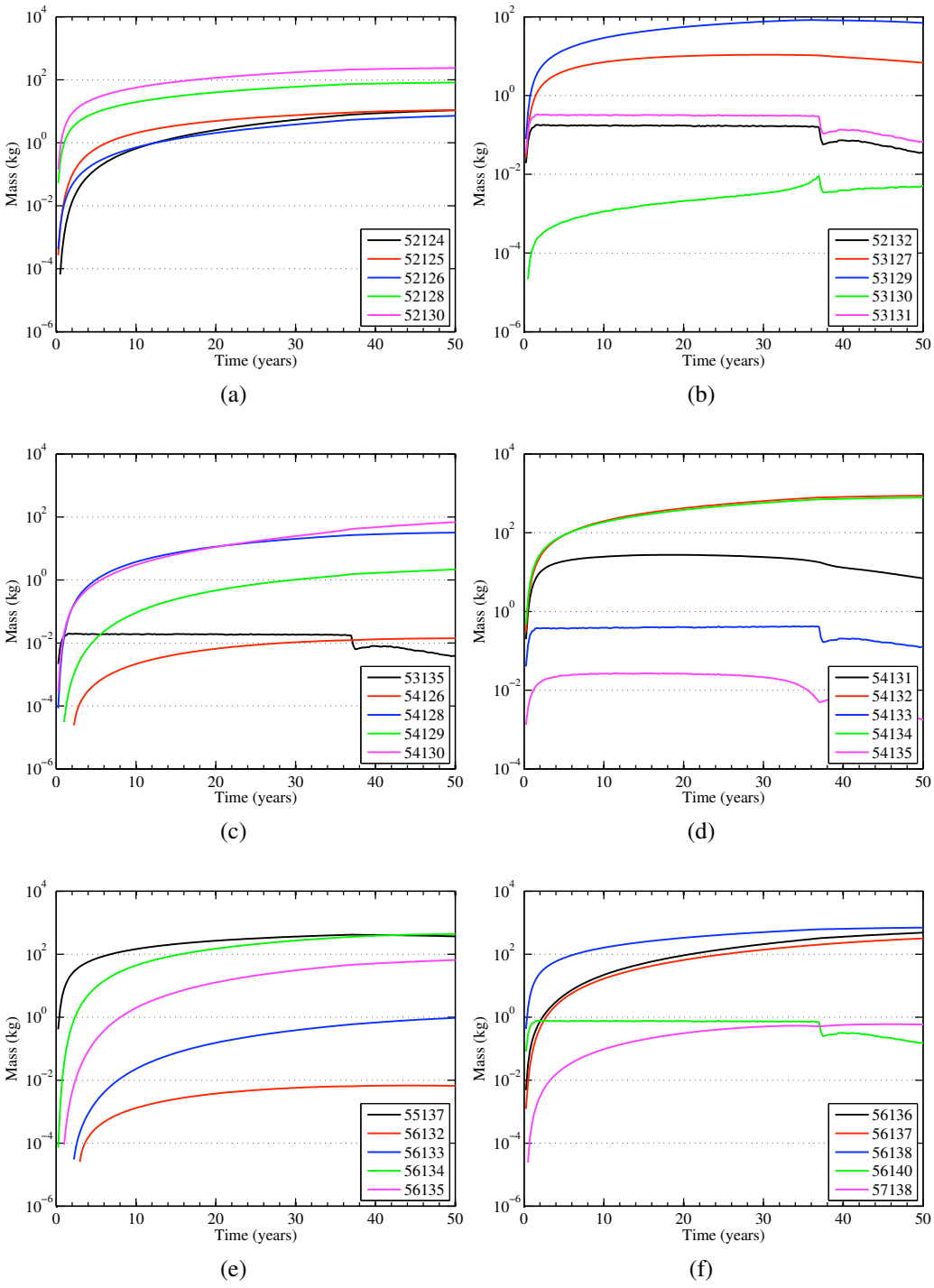

Figure A.5: Masses of some key isotopes with zzzaaa numbers of 52124 to 57138

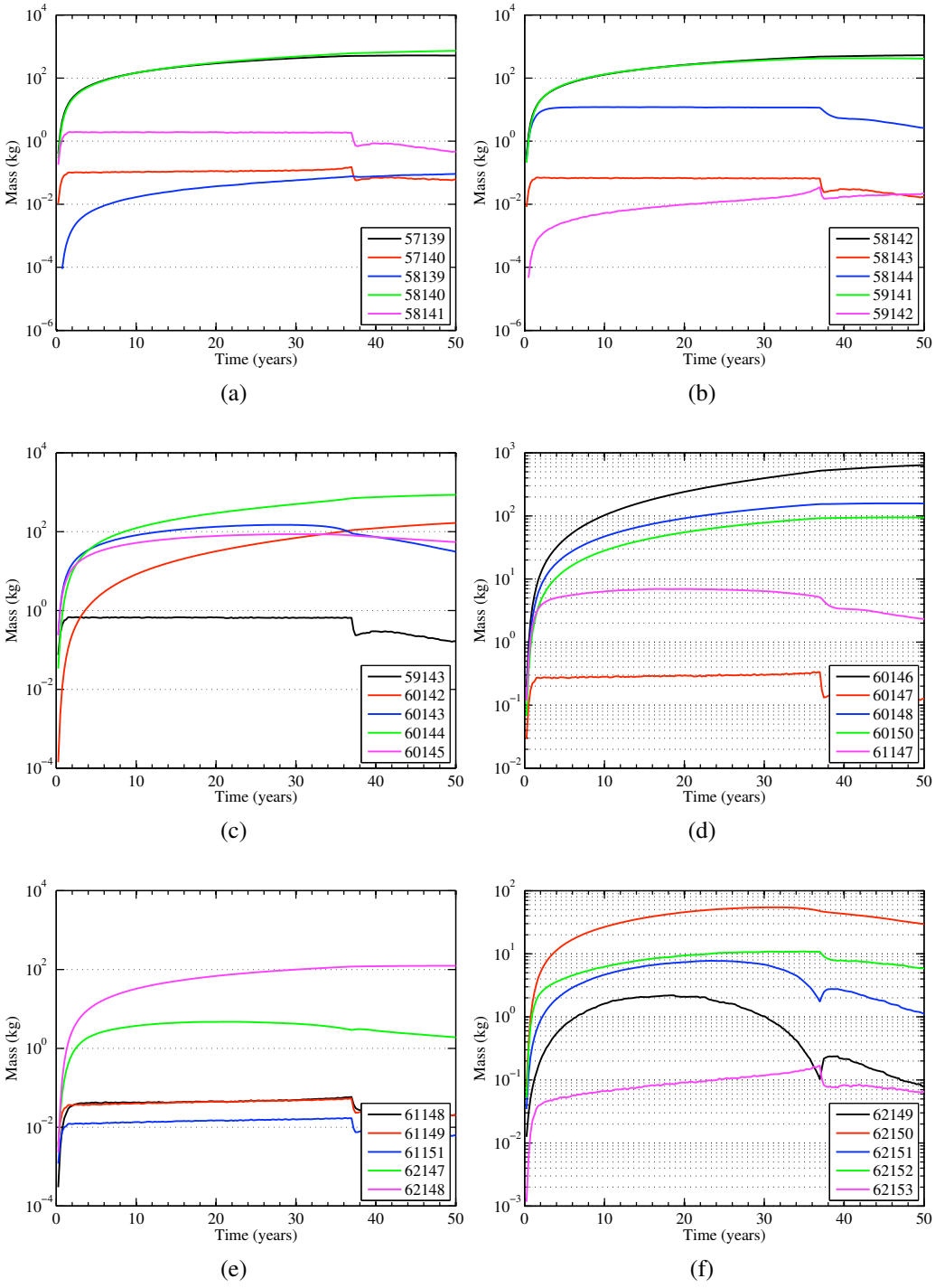

Figure A.6: Masses of some key isotopes with zzzaaa numbers of 57139 to 62153

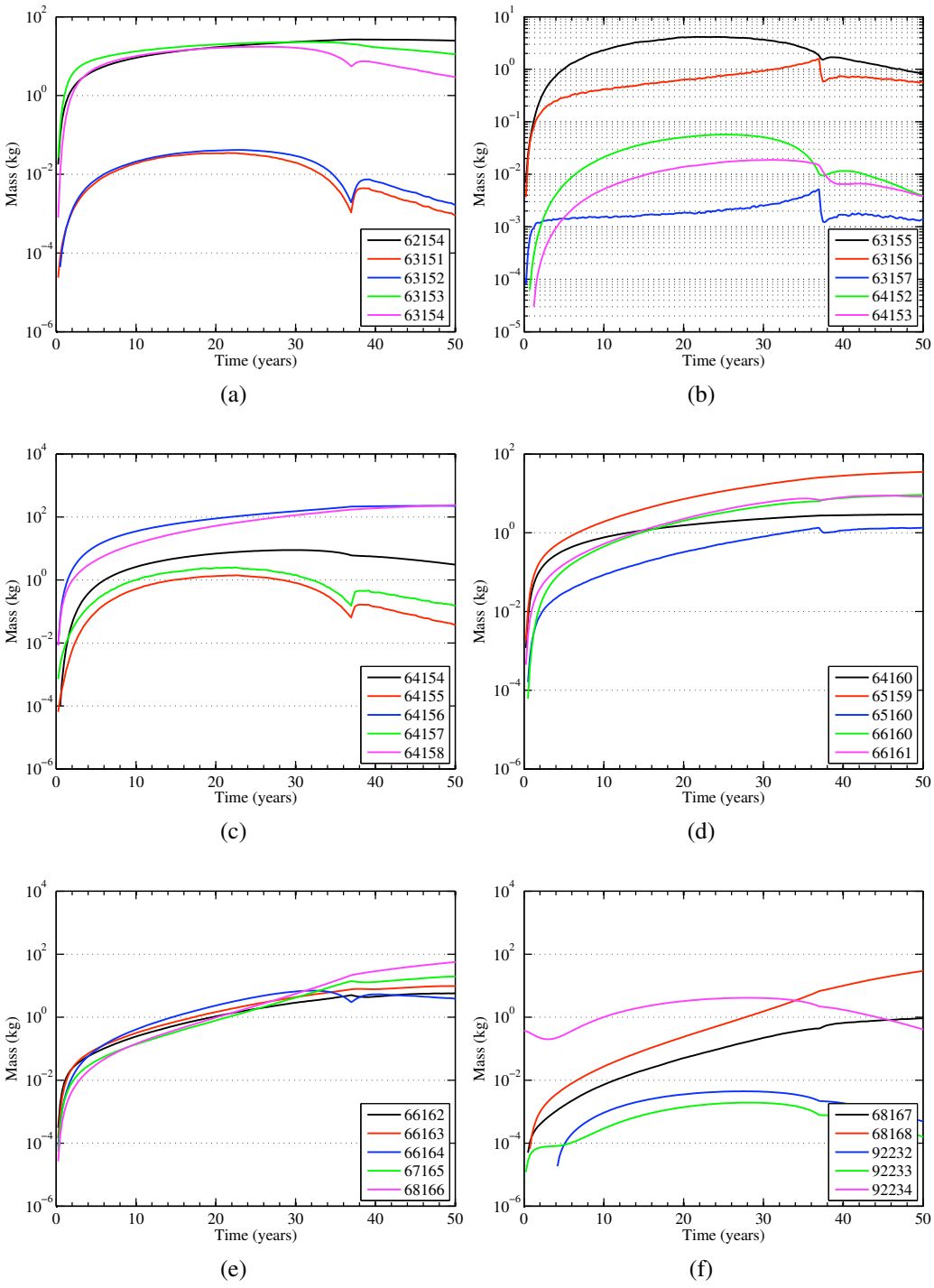

Figure A.7: Masses of some key isotopes with zzzaaa numbers of 62154 to 92234

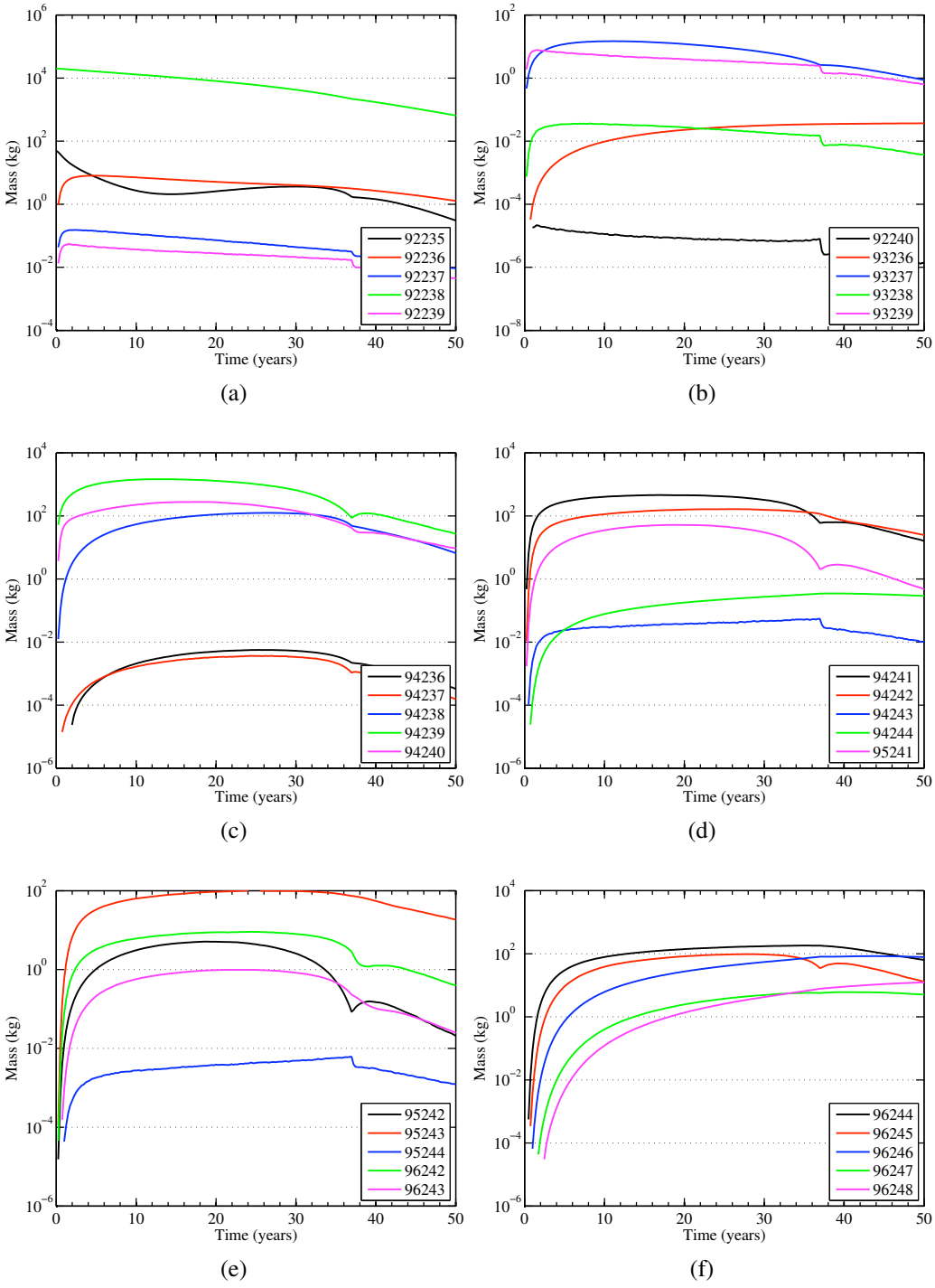

Figure A.8: Masses of some key isotopes with zzzaaa numbers of 92235 to 96248

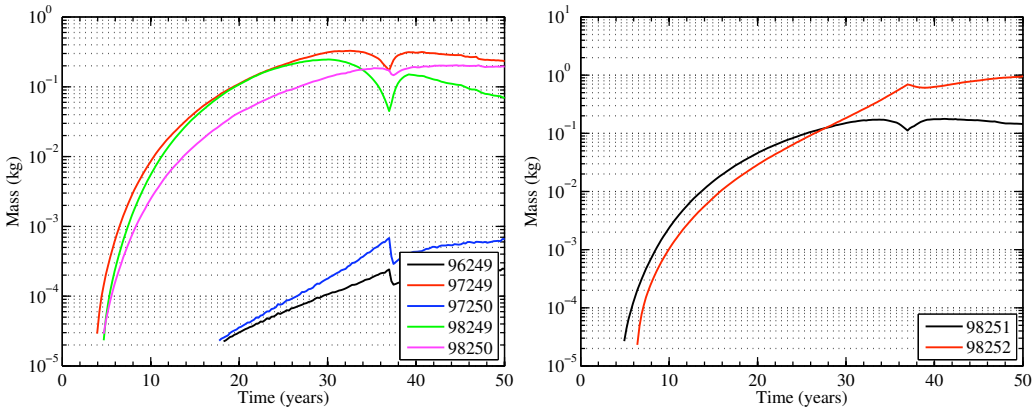

(a) (b)

Figure A.9: Masses of some key isotopes with zzzaaa numbers of 96249 to 98252

Appendix B

Example Input

B.1 Example LNC Input Deck

```
// This is a test life.inp file
// Comment lines are prefaced with '//' and ignored
// Blank lines are ignored
// Commands must contain the known command (all lower case) followed by a ':'

power steps: 300

mb steps: 2

base name: ba2

//restart step: 1

// This is either "PC" or "UNIX"
system type: UNIX

// Operating modes are "Power" and "TBR"
run mode: Power

// Only used when in Power mode
power range: 2000 2050

// Normalization values, but are not used currently
num sourced neutrons: 355100000000000000.0
fusion energy: 37.5
repetition rate: 13.333

// Fusion power in MW is now required
fusion power: 500

// Range to maintain tbr when in TBR mode
tbr range: 0.3 3.0 0.0 3.02 0.0 3.02

// Multiplier and Divisor used when iterating to within Power or TBR range
iteration multiplier: 1.04
iteration divisor: 1.06

// A factor that is applied to the multiplier and divisor to come back into range factor via
// the formula (multiplier - 1.0)*factor + 1.0 after switching from power to tbr mode
```

```
iteration factor: 5.0

// Minium tritium inventory allowed (kg) is the minimum allowed in the calculation
minimum tritium: 0.0

// Li-6 maximum enrichment (fraction)---default 1
// Li-6 maximum enrichment: 0.90

// List of cells with fixed Li-6 enrichment
// fixed Li-6 enrichment cells: 5 7 13 319

// Command to archive MONTEBURNS files (options: Archive_All, Remove_All)
// keep files: Archive_All

// Command to execute mcnp on this specific system
mcnp command: srun -N $NNODES mcnp5mpi tasks $NTASKS balance

// Number of simulation particles to use in mcnp runs
mcnp nps: 100000

// Maximum number of iterations before switching from Power mode to TBR mode,
// or exiting with an error in TBR mode
max num iterations: 10

// List of Monteburns burnup materials
mb burnup materials: 51

// Enable variable time stepping
variable timesteps: 25 50 0.1 1.0

// Enable AMR with 4 passes each burn step and a threshold of 10%
AMR num passes: 4
AMR threshold: 0.10

// List of isotopes to remove from the problem
remove iso percent atom: 1003 100.0

// List of isotopes to reset at each power step
reset isotopes: 9019 4009

// List of isotopes to include in the calculation of % burnup using method #2
include burnup isos: 92233 92235 93237 94235 94236 94237 94238 94239 94240 94241
94242 94243 94244 94245 94246 94247 95240 95241 95242 95243 95244 95245 95246 95247

// List of isotopes to remove from calculation of % burnup using method #2
// because they are part of the coolant
coolant isos: 9019 4009 3006 3007

// time step size of the outer burn steps using in monteburns
mb delta_t: 1

// Don't take credit for decay heat
take credit for decay heat: yes
```

B.2 Example MCNP Input Deck

```
LFFH - TRISO fuel
1    1    -6.5E-06        -1
                          tmp=7.95478E-08  vol=6.5450E+07  imp:n,p 1
c
c  Tungsten coating on first wall
3    3    -19.3            1 -2
                         21 22 23 24 25 26 27 28 29 30 31 32
                         33 34 35 36 37 38 39 40 41 42 43 44
                            tmp=7.95478E-08  vol=1.9205E+04  imp:n,p 1
c
c  First wall -- ODS-FS (full density)
4    4    -8.0             2 -3
                         21 22 23 24 25 26 27 28 29 30 31 32
                         33 34 35 36 37 38 39 40 41 42 43 44
                            tmp=7.95478E-08  vol=2.1151E+05  imp:n,p 1
c
c  Dedicated LiPb cooling
5    5    -9.40            3 -4
                         21 22 23 24 25 26 27 28 29 30 31 32
                         33 34 35 36 37 38 39 40 41 42 43 44
                            tmp=5.36968E-08  vol=2.3377E+06  imp:n,p 1
c
c  Second wall -- ODS-FS (full density)
6    4    -8.0             4 -5
                         21 22 23 24 25 26 27 28 29 30 31 32
                         33 34 35 36 37 38 39 40 41 42 43 44
                            tmp=6.48989E-08  vol=2.3684E+05  imp:n,p 1
c
c  Flibe cooling injection plenum
7    7    -1.9820          5 -6
                         21 22 23 24 25 26 27 28 29 30 31 32
                         33 34 35 36 37 38 39 40 41 42 43 44
                            tmp=7.61010E-08  vol=2.3994E+06  imp:n,p 1
c
c  Third wall -- ODS-FS (porous)
8    4    -6.0             6 -7
                         21 22 23 24 25 26 27 28 29 30 31 32
                         33 34 35 36 37 38 39 40 41 42 43 44
                            tmp=7.61829E-08  vol=2.4305E+05  imp:n,p 1
c
c  Beryllium w/ flibe cooling (60/40 vol)
9    9    -1.9409          7 -8
                         21 22 23 24 25 26 27 28 29 30 31 32
                         33 34 35 36 37 38 39 40 41 42 43 44
                            tmp=7.62639E-08  vol=1.3803E+07  imp:n,p 1
c
c  Fourth wall -- ODS-FS (porous)
10   4    -6.0             8 -9
                         21 22 23 24 25 26 27 28 29 30 31 32
                         33 34 35 36 37 38 39 40 41 42 43 44
                            tmp=7.72480E-08  vol=2.7489E+05  imp:n,p 1
c
c  Fuel zone -- mix of pebbles and flibe coolant (60/40 vol)
51   0                    9 -10
                         21 22 23 24 25 26 27 28 29 30 31 32
                         33 34 35 36 37 38 39 40 41 42 43 44 imp:n,p 1
          fill=101
c
c  Back wall to fuel region
```

```
12  4   -6.0          10 -11
                      21 22 23 24 25 26 27 28 29 30 31 32
                      33 34 35 36 37 38 39 40 41 42 43 44
                         tmp=7.86861E-08  vol=7.4259E+05 imp:n,p 1
c
c  Graphite reflector
13  13  -1.8069       11 -12
                      21 22 23 24 25 26 27 28 29 30 31 32
                      33 34 35 36 37 38 39 40 41 42 43 44
                         tmp=7.87215E-08  vol=1.3733E+08  imp:n,p 1
c
c  Final wall
14  4   -6.0          12 -13
                      21 22 23 24 25 26 27 28 29 30 31 32
                      33 34 35 36 37 38 39 40 41 42 43 44
                         tmp=7.86861E-08  vol=1.1002E+06  imp:n,p 1
c
c ---------------------Pebble and TRISO lattice ----------------------
c
101  51  -10.5 -51 tmp=9.24733E-08  vol=2.1289E+06  imp:n,p 1 u=401
102  16  -1.7662 51 tmp=8.81648E-08  vol=5.0784E+07  imp:n,p 1 u=401
201  0                -53 54 -55 56 -57 58
          lat=1 fill=401                                  imp:n,p 1 u=301
c
c  Pebble unit cell---BCC
301  0                  -61
          fill=301                                        imp:n,p 1 u=201
302  17  -1.70          61 -62  tmp=7.95694E-08 vol=1  imp:n,p 1 u=201
303  0                  -63
          fill=301                                        imp:n,p 1 u=201
304  17  -1.70          63 -64  tmp=7.95694E-08 vol=1  imp:n,p 1 u=201
305  0                  -65
          fill=301                                        imp:n,p 1 u=201
306  17  -1.70          65 -66  tmp=7.95694E-08 vol=1  imp:n,p 1 u=201
307  0                  -67
          fill=301                                        imp:n,p 1 u=201
308  17  -1.70          67 -68  tmp=7.95694E-08 vol=1  imp:n,p 1 u=201
309  0                  -69
          fill=301                                        imp:n,p 1 u=201
310  17  -1.70          69 -70  tmp=7.95694E-08 vol=1  imp:n,p 1 u=201
311  0                  -71
          fill=301                                        imp:n,p 1 u=201
312  17  -1.70          71 -72  tmp=7.95694E-08 vol=1  imp:n,p 1 u=201
313  0                  -73
          fill=301                                        imp:n,p 1 u=201
314  17  -1.70          73 -74  tmp=7.95694E-08 vol=1  imp:n,p 1 u=201
315  0                  -75
          fill=301                                        imp:n,p 1 u=201
316  17  -1.70          75 -76  tmp=7.95694E-08 vol=1  imp:n,p 1 u=201
317  0                  -77
          fill=301                                        imp:n,p 1 u=201
318  17  -1.70          77 -78  tmp=7.95694E-08 vol=1  imp:n,p 1 u=201
c
319  18  -1.9700        62 64
                       66 68 70 72 74 76 78
                         tmp=7.82320E-08  vol=3.5275E+07 imp:n,p 1 u=201
901  0                 -81 82 -83 84 -85 86
          lat=1 fill=201                                  imp:n,p 1 u=101
c
c ---------------------------------------------------------------------
c ---------------------------------------------------------------------
c  Leakage zone
```

```
15   0                    13                                    imp:n,p 0
c
c   Beamports
21   1     -6.5E-06       1 -13 -21          tmp=7.95478E-08 imp:n,p 1
22   1     -6.5E-06       1 -13 -22          tmp=7.95478E-08 imp:n,p 1
23   1     -6.5E-06       1 -13 -23          tmp=7.95478E-08 imp:n,p 1
24   1     -6.5E-06       1 -13 -24          tmp=7.95478E-08 imp:n,p 1
25   1     -6.5E-06       1 -13 -25          tmp=7.95478E-08 imp:n,p 1
26   1     -6.5E-06       1 -13 -26          tmp=7.95478E-08 imp:n,p 1
27   1     -6.5E-06       1 -13 -27          tmp=7.95478E-08 imp:n,p 1
28   1     -6.5E-06       1 -13 -28          tmp=7.95478E-08 imp:n,p 1
29   1     -6.5E-06       1 -13 -29          tmp=7.95478E-08 imp:n,p 1
30   1     -6.5E-06       1 -13 -30          tmp=7.95478E-08 imp:n,p 1
31   1     -6.5E-06       1 -13 -31          tmp=7.95478E-08 imp:n,p 1
32   1     -6.5E-06       1 -13 -32          tmp=7.95478E-08 imp:n,p 1
33   1     -6.5E-06       1 -13 -33          tmp=7.95478E-08 imp:n,p 1
34   1     -6.5E-06       1 -13 -34          tmp=7.95478E-08 imp:n,p 1
35   1     -6.5E-06       1 -13 -35          tmp=7.95478E-08 imp:n,p 1
36   1     -6.5E-06       1 -13 -36          tmp=7.95478E-08 imp:n,p 1
37   1     -6.5E-06       1 -13 -37          tmp=7.95478E-08 imp:n,p 1
38   1     -6.5E-06       1 -13 -38          tmp=7.95478E-08 imp:n,p 1
39   1     -6.5E-06       1 -13 -39          tmp=7.95478E-08 imp:n,p 1
40   1     -6.5E-06       1 -13 -40          tmp=7.95478E-08 imp:n,p 1
41   1     -6.5E-06       1 -13 -41          tmp=7.95478E-08 imp:n,p 1
42   1     -6.5E-06       1 -13 -42          tmp=7.95478E-08 imp:n,p 1
43   1     -6.5E-06       1 -13 -43          tmp=7.95478E-08 imp:n,p 1
44   1     -6.5E-06       1 -13 -44          tmp=7.95478E-08 imp:n,p 1

c Surface cards
1 so 250.00000000
2 so 250.02500000
3 so 250.30000000
4 so 253.30000000
5 so 253.60000000
6 so 256.60000000
7 so 256.90000000
8 so 272.90000000
9 so 273.20000000
10 so 347.37556555
11 so 347.87556555
12 so 422.87556555
13 so 423.37556555
c
21 1 kz 0 0.00183397
22 2 kz 0 0.00183397
23 3 kz 0 0.00183397
24 4 kz 0 0.00183397
25 5 kz 0 0.00183397
26 6 kz 0 0.00183397
27 7 kz 0 0.00183397
28 8 kz 0 0.00183397
29 9 kz 0 0.00183397
30 10 kz 0 0.00183397
31 11 kz 0 0.00183397
32 12 kz 0 0.00183397
33 13 kz 0 0.00183397
34 14 kz 0 0.00183397
35 15 kz 0 0.00183397
36 16 kz 0 0.00183397
37 17 kz 0 0.00183397
38 18 kz 0 0.00183397
39 19 kz 0 0.00183397
```

```
40 20 kz 0 0.00183397
41 21 kz 0 0.00183397
42 22 kz 0 0.00183397
43 23 kz 0 0.00183397
44 24 kz 0 0.00183397
c
51 so  0.03000000
53 px  0.07056557
54 px -0.07056557
55 py  0.07056557
56 py -0.07056557
57 pz  0.07056557
58 pz -0.07056557
c
61 so  1.00000000
62 so  1.01500000
63 s   1.22205804  1.22205804  1.22205804  1.00000000
64 s   1.22205804  1.22205804  1.22205804  1.01500000
65 s   1.22205804  1.22205804 -1.22205804  1.00000000
66 s   1.22205804  1.22205804 -1.22205804  1.01500000
67 s   1.22205804 -1.22205804 -1.22205804  1.00000000
68 s   1.22205804 -1.22205804 -1.22205804  1.01500000
69 s   1.22205804 -1.22205804  1.22205804  1.00000000
70 s   1.22205804 -1.22205804  1.22205804  1.01500000
71 s  -1.22205804  1.22205804  1.22205804  1.00000000
72 s  -1.22205804  1.22205804  1.22205804  1.01500000
73 s  -1.22205804  1.22205804 -1.22205804  1.00000000
74 s  -1.22205804  1.22205804 -1.22205804  1.01500000
75 s  -1.22205804 -1.22205804 -1.22205804  1.00000000
76 s  -1.22205804 -1.22205804 -1.22205804  1.01500000
77 s  -1.22205804 -1.22205804  1.22205804  1.00000000
78 s  -1.22205804 -1.22205804  1.22205804  1.01500000
81 px  1.22205804
82 px -1.22205804
83 py  1.22205804
84 py -1.22205804
85 pz  1.22205804
86 pz -1.22205804
c

c ******************** RUN DATA ********************
c
c  Source definition
sdef par=1 erg=14.1 x=0 y=0 z=0
nps 50000
c kcode 10 1 10 50
c ksrc  300.01  0. 0. -300 0. 0.
mode n p
c prdmp 10000 10000 0 1 10000
totnu
c
c ******************** TALLIES ********************
c
F6:n     3 4 5 6 7 8 9 10 12 13 14
         101 102 319
F16:p    3 4 5 6 7 8 9 10 12 13 14
         101 102 319
f204:n   3 4 5 6 7 8 9 10 12 13 14
         101 102 319
e204 1.00E-11 1.05E-11 1.10E-11 1.15E-11 1.20E-11 1.26E-11
     1.32E-11 1.38E-11 1.45E-11 1.51E-11 1.58E-11 1.66E-11
     1.74E-11 1.82E-11 1.91E-11 2.00E-11 2.09E-11 2.19E-11
```

2.29E−11 2.40E−11 2.51E−11 2.63E−11 2.75E−11 2.88E−11
3.02E−11 3.16E−11 3.31E−11 3.47E−11 3.63E−11 3.80E−11
3.98E−11 4.17E−11 4.37E−11 4.57E−11 4.79E−11 5.01E−11
5.25E−11 5.50E−11 5.75E−11 6.03E−11 6.31E−11 6.61E−11
6.92E−11 7.24E−11 7.59E−11 7.94E−11 8.32E−11 8.71E−11
9.12E−11 9.55E−11 1.00E−10 1.05E−10 1.10E−10 1.15E−10
1.20E−10 1.26E−10 1.32E−10 1.38E−10 1.45E−10 1.51E−10
1.58E−10 1.66E−10 1.74E−10 1.82E−10 1.91E−10 2.00E−10
2.09E−10 2.19E−10 2.29E−10 2.40E−10 2.51E−10 2.63E−10
2.75E−10 2.88E−10 3.02E−10 3.16E−10 3.31E−10 3.47E−10
3.63E−10 3.80E−10 3.98E−10 4.17E−10 4.37E−10 4.57E−10
4.79E−10 5.01E−10 5.25E−10 5.50E−10 5.75E−10 6.03E−10
6.31E−10 6.61E−10 6.92E−10 7.24E−10 7.59E−10 7.94E−10
8.32E−10 8.71E−10 9.12E−10 9.55E−10 1.00E−09 1.05E−09
1.10E−09 1.15E−09 1.20E−09 1.26E−09 1.32E−09 1.38E−09
1.45E−09 1.51E−09 1.58E−09 1.66E−09 1.74E−09 1.82E−09
1.91E−09 2.00E−09 2.09E−09 2.19E−09 2.29E−09 2.40E−09
2.51E−09 2.63E−09 2.75E−09 2.88E−09 3.02E−09 3.16E−09
3.31E−09 3.47E−09 3.63E−09 3.80E−09 3.98E−09 4.17E−09
4.37E−09 4.57E−09 4.79E−09 5.01E−09 5.25E−09 5.50E−09
5.75E−09 6.03E−09 6.31E−09 6.61E−09 6.92E−09 7.24E−09
7.59E−09 7.94E−09 8.32E−09 8.71E−09 9.12E−09 9.55E−09
1.00E−08 1.05E−08 1.10E−08 1.15E−08 1.20E−08 1.26E−08
1.32E−08 1.38E−08 1.45E−08 1.51E−08 1.58E−08 1.66E−08
1.74E−08 1.82E−08 1.91E−08 2.00E−08 2.09E−08 2.19E−08
2.29E−08 2.40E−08 2.51E−08 2.63E−08 2.75E−08 2.88E−08
3.02E−08 3.16E−08 3.31E−08 3.47E−08 3.63E−08 3.80E−08
3.98E−08 4.17E−08 4.37E−08 4.57E−08 4.79E−08 5.01E−08
5.25E−08 5.50E−08 5.75E−08 6.03E−08 6.31E−08 6.61E−08
6.92E−08 7.24E−08 7.59E−08 7.94E−08 8.32E−08 8.71E−08
9.12E−08 9.55E−08 1.00E−07 1.05E−07 1.10E−07 1.15E−07
1.20E−07 1.26E−07 1.32E−07 1.38E−07 1.45E−07 1.51E−07
1.58E−07 1.66E−07 1.74E−07 1.82E−07 1.91E−07 2.00E−07
2.09E−07 2.19E−07 2.29E−07 2.40E−07 2.51E−07 2.63E−07
2.75E−07 2.88E−07 3.02E−07 3.16E−07 3.31E−07 3.47E−07
3.63E−07 3.80E−07 3.98E−07 4.17E−07 4.37E−07 4.57E−07
4.79E−07 5.01E−07 5.25E−07 5.50E−07 5.75E−07 6.03E−07
6.31E−07 6.61E−07 6.92E−07 7.24E−07 7.59E−07 7.94E−07
8.32E−07 8.71E−07 9.12E−07 9.55E−07 1.00E−06 1.05E−06
1.10E−06 1.15E−06 1.20E−06 1.26E−06 1.32E−06 1.38E−06
1.45E−06 1.51E−06 1.58E−06 1.66E−06 1.74E−06 1.82E−06
1.91E−06 2.00E−06 2.09E−06 2.19E−06 2.29E−06 2.40E−06
2.51E−06 2.63E−06 2.75E−06 2.88E−06 3.02E−06 3.16E−06
3.31E−06 3.47E−06 3.63E−06 3.80E−06 3.98E−06 4.17E−06
4.37E−06 4.57E−06 4.79E−06 5.01E−06 5.25E−06 5.50E−06
5.75E−06 6.03E−06 6.31E−06 6.61E−06 6.92E−06 7.24E−06
7.59E−06 7.94E−06 8.32E−06 8.71E−06 9.12E−06 9.55E−06
1.00E−05 1.05E−05 1.10E−05 1.15E−05 1.20E−05 1.26E−05
1.32E−05 1.38E−05 1.45E−05 1.51E−05 1.58E−05 1.66E−05
1.74E−05 1.82E−05 1.91E−05 2.00E−05 2.09E−05 2.19E−05
2.29E−05 2.40E−05 2.51E−05 2.63E−05 2.75E−05 2.88E−05
3.02E−05 3.16E−05 3.31E−05 3.47E−05 3.63E−05 3.80E−05
3.98E−05 4.17E−05 4.37E−05 4.57E−05 4.79E−05 5.01E−05
5.25E−05 5.50E−05 5.75E−05 6.03E−05 6.31E−05 6.61E−05
6.92E−05 7.24E−05 7.59E−05 7.94E−05 8.32E−05 8.71E−05
9.12E−05 9.55E−05 1.00E−04 1.05E−04 1.10E−04 1.15E−04
1.20E−04 1.26E−04 1.32E−04 1.38E−04 1.45E−04 1.51E−04
1.58E−04 1.66E−04 1.74E−04 1.82E−04 1.91E−04 2.00E−04
2.09E−04 2.19E−04 2.29E−04 2.40E−04 2.51E−04 2.63E−04
2.75E−04 2.88E−04 3.02E−04 3.16E−04 3.31E−04 3.47E−04
3.63E−04 3.80E−04 3.98E−04 4.17E−04 4.37E−04 4.57E−04
4.79E−04 5.01E−04 5.25E−04 5.50E−04 5.75E−04 6.03E−04

```
      6.31E-04 6.61E-04 6.92E-04 7.24E-04 7.59E-04 7.94E-04
      8.32E-04 8.71E-04 9.12E-04 9.55E-04 1.00E-03 1.05E-03
      1.10E-03 1.15E-03 1.20E-03 1.26E-03 1.32E-03 1.38E-03
      1.45E-03 1.51E-03 1.58E-03 1.66E-03 1.74E-03 1.82E-03
      1.91E-03 2.00E-03 2.09E-03 2.19E-03 2.29E-03 2.40E-03
      2.51E-03 2.63E-03 2.75E-03 2.88E-03 3.02E-03 3.16E-03
      3.31E-03 3.47E-03 3.63E-03 3.80E-03 3.98E-03 4.17E-03
      4.37E-03 4.57E-03 4.79E-03 5.01E-03 5.25E-03 5.50E-03
      5.75E-03 6.03E-03 6.31E-03 6.61E-03 6.92E-03 7.24E-03
      7.59E-03 7.94E-03 8.32E-03 8.71E-03 9.12E-03 9.55E-03
      1.00E-02 1.05E-02 1.10E-02 1.15E-02 1.20E-02 1.26E-02
      1.32E-02 1.38E-02 1.45E-02 1.51E-02 1.58E-02 1.66E-02
      1.74E-02 1.82E-02 1.91E-02 2.00E-02 2.09E-02 2.19E-02
      2.29E-02 2.40E-02 2.51E-02 2.63E-02 2.75E-02 2.88E-02
      3.02E-02 3.16E-02 3.31E-02 3.47E-02 3.63E-02 3.80E-02
      3.98E-02 4.17E-02 4.37E-02 4.57E-02 4.79E-02 5.01E-02
      5.25E-02 5.50E-02 5.75E-02 6.03E-02 6.31E-02 6.61E-02
      6.92E-02 7.24E-02 7.59E-02 7.94E-02 8.32E-02 8.71E-02
      9.12E-02 9.55E-02 1.00E-01 1.05E-01 1.10E-01 1.15E-01
      1.20E-01 1.26E-01 1.32E-01 1.38E-01 1.45E-01 1.51E-01
      1.58E-01 1.66E-01 1.74E-01 1.82E-01 1.91E-01 2.00E-01
      2.09E-01 2.19E-01 2.29E-01 2.40E-01 2.51E-01 2.63E-01
      2.75E-01 2.88E-01 3.02E-01 3.16E-01 3.31E-01 3.47E-01
      3.63E-01 3.80E-01 3.98E-01 4.17E-01 4.37E-01 4.57E-01
      4.79E-01 5.01E-01 5.25E-01 5.50E-01 5.75E-01 6.03E-01
      6.31E-01 6.61E-01 6.92E-01 7.24E-01 7.59E-01 7.94E-01
      8.32E-01 8.71E-01 9.12E-01 9.55E-01 1.00E+00 1.05E+00
      1.10E+00 1.15E+00 1.20E+00 1.26E+00 1.32E+00 1.38E+00
      1.45E+00 1.51E+00 1.58E+00 1.66E+00 1.74E+00 1.82E+00
      1.91E+00 2.00E+00 2.09E+00 2.19E+00 2.29E+00 2.40E+00
      2.51E+00 2.63E+00 2.75E+00 2.88E+00 3.02E+00 3.16E+00
      3.31E+00 3.47E+00 3.63E+00 3.80E+00 3.98E+00 4.17E+00
      4.37E+00 4.57E+00 4.79E+00 5.01E+00 5.25E+00 5.50E+00
      5.75E+00 6.03E+00 6.31E+00 6.61E+00 6.92E+00 7.24E+00
      7.59E+00 7.94E+00 8.32E+00 8.71E+00 9.12E+00 9.55E+00
      1.00E+01 1.05E+01 1.10E+01 1.15E+01 1.20E+01 1.26E+01
      1.32E+01 1.38E+01 1.45E+01 1.51E+01 1.58E+01 1.66E+01
      1.74E+01 1.82E+01 1.91E+01 2.00E+01
c
fc207  Fission energy deposition tally
f207:n     101
c
c  iron DPA w/ Ed=40eV to 1stwall
f244:n 4
fm244 (1 4 444)
c e244 0.625e-6 20
c   beryllium DPA w/ Ed=40eV to Be/flibe region
f344:n 9
fm344 (1 9 444)
c e344 0.625e-6 20
c  carbon DPA w/ Ed=20eV to 1st fuel zone
f444:n  102
fm444 (2 16 444)
c e444 0.625e-6 20
c
M20 4009.71c 1.0
M22  6000         1.0
c
c
c  Rotation matrixes for the 48 beamports
*tr1    0 0 0   79.7   25.9 66.5 168.8  78.8 90   94.5 113.   23.5
*tr2    0 0 0  154.1   79.7 66.5 101.3 168.8 90   67.    94.5 23.5
```

```
*tr3    0 0 0   100.3  154.1  66.5   11.3  101.3  90   85.5   67.   23.5
*tr4    0 0 0    25.9  100.3  66.5   78.8   11.3  90  113.    85.5  23.5
*tr5    0 0 0    44.7   61.   59.4  124.3   34.3  90  114.8  106.7  30.6
*tr6    0 0 0   118.8   43.9  60.   146.3  123.8  90   73.9  114.6  30.
*tr7    0 0 0   135.3  119.   59.4   55.7  145.7  90   65.2   73.3  30.6
*tr8    0 0 0    61.2  136.1  60.    33.8   56.3  90  106.1   65.4  30.
*tr9    0 0 0    46.8   78.5  45.5  106.3   16.3  90  132.3  101.3  44.5
*tr10   0 0 0    70.7   50.8  45.5  152.5   62.5  90  108.9  128.4  44.5
*tr11   0 0 0   101.5   46.8  45.5  163.7  106.3  90   78.7  132.3  44.5
*tr12   0 0 0   129.2   70.7  45.5  117.5  152.5  90   51.6  108.9  44.5
*tr13   0 0 0   133.2  101.5  45.5   73.7  163.7  90   47.7   78.7  44.5
*tr14   0 0 0   109.3  129.2  45.5   27.5  117.5  90   71.1   51.6  44.5
*tr15   0 0 0    78.5  133.2  45.5   16.3   73.7  90  101.3   47.7  44.5
*tr16   0 0 0    50.8  109.3  45.5   62.5   27.5  90  128.4   71.1  44.5
*tr17   0 0 0    60.3   65.8  40.   129.7   39.7  90  126.1  119.3  50.
*tr18   0 0 0    86.4   50.2  40.   174.4   84.4  90   94.3  139.7  50.
*tr19   0 0 0   114.1   60.2  40.   140.6  129.4  90   60.9  126.3  50.
*tr20   0 0 0   129.8   86.4  40.    95.6  174.4  90   40.3   94.3  50.
*tr21   0 0 0   119.7  114.2  40.    50.3  140.3  90   53.9   60.7  50.
*tr22   0 0 0    93.6  129.8  40.     5.6   95.6  90   85.7   40.3  50.
*tr23   0 0 0    65.9  119.8  40.    39.4   50.6  90  119.1   53.7  50.
*tr24   0 0 0    50.2   93.6  40.    84.4    5.6  90  139.7   85.7  50.
c
c Extra Tallies
c
c ********************************************************************
c Reaction Rate tallies - output is [rxn/(source neut - atom)]; to get
c actual RR: FMn*nparticls*N*Vol or FMn*nparticles*(# atoms)*(10^-24)
c
c Output:
c bin1: U238 (n,gamma)
c bin2: U238 (n,fission)
c bin3: Pu239 (n,fission)
c bin4: Be9 (n,2n)
c bin5: Be9 (n,3n)
c bin6: Li6 (n, total T) [MT=205 cross section,sums MT=105 + other]
c bin7: Li7 (n, total T) [MT=205 cross section,sums MT=105 + other]
c bin8: Th232 (n,gamma) [approximates U233 breeding rate]
c
c For TBR calc: sum (bin5*n(Li6) + bin6*n(Li7)) for each cell
c
c         (1 5405 (17) (105))           $    Be9:n,3n,T prod
c Materials used for reaction rate tallies
c Tallies will be summed for all reactions even if the material
c is not in the cell!!!!! MCNP just does a xsec lookup.
M5401 92238.72c 1.0
M5402 92235.72c 1.0
M5404 94239.72c 1.0
M5405 4009.72c  1.0
M5406 3006.72c  1.0
M5407 3007.72c  1.0
M5408 94240.72c 1.0
M5409 94241.72c 1.0
f304:n 5 7 91 51 13 $ Flux-weighted Microscopic XS
c set the zone volume to 1.0 cc so whole cell is used
c sd54 1.0 5r
fm304    (1 5402 (-2) (-6))           $    U235:capture,fission
         (1 5401 (-2) (-6))           $    U238:capture,fission
         (1 5404 (-2) (-6))           $    Pu239:capture,fission
         (1 5408 (-2) (-6))           $    Pu240:capture,fission
         (1 5409 (-2) (-6))           $    Pu241:capture,fission
         (1 5405 (16) (105))          $    Be9:n,2n,T prod
```

```
        (1 5406 (105))                  $     Li6:total T prod
        (1 5407 (205))                  $     Li7:total T prod (missing from LANL)
e304  1.00E-11 1.05E-11 1.10E-11 1.15E-11 1.20E-11 1.26E-11
      1.32E-11 1.38E-11 1.45E-11 1.51E-11 1.58E-11 1.66E-11
      1.74E-11 1.82E-11 1.91E-11 2.00E-11 2.09E-11 2.19E-11
      2.29E-11 2.40E-11 2.51E-11 2.63E-11 2.75E-11 2.88E-11
      3.02E-11 3.16E-11 3.31E-11 3.47E-11 3.63E-11 3.80E-11
      3.98E-11 4.17E-11 4.37E-11 4.57E-11 4.79E-11 5.01E-11
      5.25E-11 5.50E-11 5.75E-11 6.03E-11 6.31E-11 6.61E-11
      6.92E-11 7.24E-11 7.59E-11 7.94E-11 8.32E-11 8.71E-11
      9.12E-11 9.55E-11 1.00E-10 1.05E-10 1.10E-10 1.15E-10
      1.20E-10 1.26E-10 1.32E-10 1.38E-10 1.45E-10 1.51E-10
      1.58E-10 1.66E-10 1.74E-10 1.82E-10 1.91E-10 2.00E-10
      2.09E-10 2.19E-10 2.29E-10 2.40E-10 2.51E-10 2.63E-10
      2.75E-10 2.88E-10 3.02E-10 3.16E-10 3.31E-10 3.47E-10
      3.63E-10 3.80E-10 3.98E-10 4.17E-10 4.37E-10 4.57E-10
      4.79E-10 5.01E-10 5.25E-10 5.50E-10 5.75E-10 6.03E-10
      6.31E-10 6.61E-10 6.92E-10 7.24E-10 7.59E-10 7.94E-10
      8.32E-10 8.71E-10 9.12E-10 9.55E-10 1.00E-09 1.05E-09
      1.10E-09 1.15E-09 1.20E-09 1.26E-09 1.32E-09 1.38E-09
      1.45E-09 1.51E-09 1.58E-09 1.66E-09 1.74E-09 1.82E-09
      1.91E-09 2.00E-09 2.09E-09 2.19E-09 2.29E-09 2.40E-09
      2.51E-09 2.63E-09 2.75E-09 2.88E-09 3.02E-09 3.16E-09
      3.31E-09 3.47E-09 3.63E-09 3.80E-09 3.98E-09 4.17E-09
      4.37E-09 4.57E-09 4.79E-09 5.01E-09 5.25E-09 5.50E-09
      5.75E-09 6.03E-09 6.31E-09 6.61E-09 6.92E-09 7.24E-09
      7.59E-09 7.94E-09 8.32E-09 8.71E-09 9.12E-09 9.55E-09
      1.00E-08 1.05E-08 1.10E-08 1.15E-08 1.20E-08 1.26E-08
      1.32E-08 1.38E-08 1.45E-08 1.51E-08 1.58E-08 1.66E-08
      1.74E-08 1.82E-08 1.91E-08 2.00E-08 2.09E-08 2.19E-08
      2.29E-08 2.40E-08 2.51E-08 2.63E-08 2.75E-08 2.88E-08
      3.02E-08 3.16E-08 3.31E-08 3.47E-08 3.63E-08 3.80E-08
      3.98E-08 4.17E-08 4.37E-08 4.57E-08 4.79E-08 5.01E-08
      5.25E-08 5.50E-08 5.75E-08 6.03E-08 6.31E-08 6.61E-08
      6.92E-08 7.24E-08 7.59E-08 7.94E-08 8.32E-08 8.71E-08
      9.12E-08 9.55E-08 1.00E-07 1.05E-07 1.10E-07 1.15E-07
      1.20E-07 1.26E-07 1.32E-07 1.38E-07 1.45E-07 1.51E-07
      1.58E-07 1.66E-07 1.74E-07 1.82E-07 1.91E-07 2.00E-07
      2.09E-07 2.19E-07 2.29E-07 2.40E-07 2.51E-07 2.63E-07
      2.75E-07 2.88E-07 3.02E-07 3.16E-07 3.31E-07 3.47E-07
      3.63E-07 3.80E-07 3.98E-07 4.17E-07 4.37E-07 4.57E-07
      4.79E-07 5.01E-07 5.25E-07 5.50E-07 5.75E-07 6.03E-07
      6.31E-07 6.61E-07 6.92E-07 7.24E-07 7.59E-07 7.94E-07
      8.32E-07 8.71E-07 9.12E-07 9.55E-07 1.00E-06 1.05E-06
      1.10E-06 1.15E-06 1.20E-06 1.26E-06 1.32E-06 1.38E-06
      1.45E-06 1.51E-06 1.58E-06 1.66E-06 1.74E-06 1.82E-06
      1.91E-06 2.00E-06 2.09E-06 2.19E-06 2.29E-06 2.40E-06
      2.51E-06 2.63E-06 2.75E-06 2.88E-06 3.02E-06 3.16E-06
      3.31E-06 3.47E-06 3.63E-06 3.80E-06 3.98E-06 4.17E-06
      4.37E-06 4.57E-06 4.79E-06 5.01E-06 5.25E-06 5.50E-06
      5.75E-06 6.03E-06 6.31E-06 6.61E-06 6.92E-06 7.24E-06
      7.59E-06 7.94E-06 8.32E-06 8.71E-06 9.12E-06 9.55E-06
      1.00E-05 1.05E-05 1.10E-05 1.15E-05 1.20E-05 1.26E-05
      1.32E-05 1.38E-05 1.45E-05 1.51E-05 1.58E-05 1.66E-05
      1.74E-05 1.82E-05 1.91E-05 2.00E-05 2.09E-05 2.19E-05
      2.29E-05 2.40E-05 2.51E-05 2.63E-05 2.75E-05 2.88E-05
      3.02E-05 3.16E-05 3.31E-05 3.47E-05 3.63E-05 3.80E-05
      3.98E-05 4.17E-05 4.37E-05 4.57E-05 4.79E-05 5.01E-05
      5.25E-05 5.50E-05 5.75E-05 6.03E-05 6.31E-05 6.61E-05
      6.92E-05 7.24E-05 7.59E-05 7.94E-05 8.32E-05 8.71E-05
      9.12E-05 9.55E-05 1.00E-04 1.05E-04 1.10E-04 1.15E-04
      1.20E-04 1.26E-04 1.32E-04 1.38E-04 1.45E-04 1.51E-04
```

```
      1.58E-04 1.66E-04 1.74E-04 1.82E-04 1.91E-04 2.00E-04
      2.09E-04 2.19E-04 2.29E-04 2.40E-04 2.51E-04 2.63E-04
      2.75E-04 2.88E-04 3.02E-04 3.16E-04 3.31E-04 3.47E-04
      3.63E-04 3.80E-04 3.98E-04 4.17E-04 4.37E-04 4.57E-04
      4.79E-04 5.01E-04 5.25E-04 5.50E-04 5.75E-04 6.03E-04
      6.31E-04 6.61E-04 6.92E-04 7.24E-04 7.59E-04 7.94E-04
      8.32E-04 8.71E-04 9.12E-04 9.55E-04 1.00E-03 1.05E-03
      1.10E-03 1.15E-03 1.20E-03 1.26E-03 1.32E-03 1.38E-03
      1.45E-03 1.51E-03 1.58E-03 1.66E-03 1.74E-03 1.82E-03
      1.91E-03 2.00E-03 2.09E-03 2.19E-03 2.29E-03 2.40E-03
      2.51E-03 2.63E-03 2.75E-03 2.88E-03 3.02E-03 3.16E-03
      3.31E-03 3.47E-03 3.63E-03 3.80E-03 3.98E-03 4.17E-03
      4.37E-03 4.57E-03 4.79E-03 5.01E-03 5.25E-03 5.50E-03
      5.75E-03 6.03E-03 6.31E-03 6.61E-03 6.92E-03 7.24E-03
      7.59E-03 7.94E-03 8.32E-03 8.71E-03 9.12E-03 9.55E-03
      1.00E-02 1.05E-02 1.10E-02 1.15E-02 1.20E-02 1.26E-02
      1.32E-02 1.38E-02 1.45E-02 1.51E-02 1.58E-02 1.66E-02
      1.74E-02 1.82E-02 1.91E-02 2.00E-02 2.09E-02 2.19E-02
      2.29E-02 2.40E-02 2.51E-02 2.63E-02 2.75E-02 2.88E-02
      3.02E-02 3.16E-02 3.31E-02 3.47E-02 3.63E-02 3.80E-02
      3.98E-02 4.17E-02 4.37E-02 4.57E-02 4.79E-02 5.01E-02
      5.25E-02 5.50E-02 5.75E-02 6.03E-02 6.31E-02 6.61E-02
      6.92E-02 7.24E-02 7.59E-02 7.94E-02 8.32E-02 8.71E-02
      9.12E-02 9.55E-02 1.00E-01 1.05E-01 1.10E-01 1.15E-01
      1.20E-01 1.26E-01 1.32E-01 1.38E-01 1.45E-01 1.51E-01
      1.58E-01 1.66E-01 1.74E-01 1.82E-01 1.91E-01 2.00E-01
      2.09E-01 2.19E-01 2.29E-01 2.40E-01 2.51E-01 2.63E-01
      2.75E-01 2.88E-01 3.02E-01 3.16E-01 3.31E-01 3.47E-01
      3.63E-01 3.80E-01 3.98E-01 4.17E-01 4.37E-01 4.57E-01
      4.79E-01 5.01E-01 5.25E-01 5.50E-01 5.75E-01 6.03E-01
      6.31E-01 6.61E-01 6.92E-01 7.24E-01 7.59E-01 7.94E-01
      8.32E-01 8.71E-01 9.12E-01 9.55E-01 1.00E+00 1.05E+00
      1.10E+00 1.15E+00 1.20E+00 1.26E+00 1.32E+00 1.38E+00
      1.45E+00 1.51E+00 1.58E+00 1.66E+00 1.74E+00 1.82E+00
      1.91E+00 2.00E+00 2.09E+00 2.19E+00 2.29E+00 2.40E+00
      2.51E+00 2.63E+00 2.75E+00 2.88E+00 3.02E+00 3.16E+00
      3.31E+00 3.47E+00 3.63E+00 3.80E+00 3.98E+00 4.17E+00
      4.37E+00 4.57E+00 4.79E+00 5.01E+00 5.25E+00 5.50E+00
      5.75E+00 6.03E+00 6.31E+00 6.61E+00 6.92E+00 7.24E+00
      7.59E+00 7.94E+00 8.32E+00 8.71E+00 9.12E+00 9.55E+00
      1.00E+01 1.05E+01 1.10E+01 1.15E+01 1.20E+01 1.26E+01
      1.32E+01 1.38E+01 1.45E+01 1.51E+01 1.58E+01 1.66E+01
      1.74E+01 1.82E+01 1.91E+01 2.00E+01
c
c ************************END TALLIES ************************
c
c
c ******************** MATERIALS ********************
c
c Scattering kernels
mt4    fe56.15t
mt9    fe56.15t be.15t
mt16   grph.15t
mt17   grph.15t
mt13   grph.15t
c
m1     7014 7.81387E-01
           8016 2.10549E-01
           18040 4.64703E-03
m3     74182.72c  2.66200E-01
       74183.72c  1.43100E-01
       74184.72c  3.06400E-01
```

```
      74186.72c   2.84300E-01
m4    26054.72c   4.96578E-02
      26056.72c   7.79522E-01
      26057.72c   1.80026E-02
      26058.72c   2.39581E-03
      24050.72c   5.80127E-03
      24052.72c   1.11872E-01
      24053.72c   1.26854E-02
      24054.72c   3.15765E-03
      74182.72c   2.45170E-03
      74183.72c   1.31795E-03
      74184.72c   2.82194E-03
      74186.72c   2.61840E-03
      22046.72c   3.79418E-04
      22047.72c   3.42166E-04
      22048.72c   3.39038E-03
      22049.72c   2.48806E-04
      22050.72c   2.38228E-04
      39089.72c   1.23900E-03
       8016.72c   1.85349E-03
       8017.72c   4.51494E-06
m5     3006.71c   1.19000E-02
       3007.71c   1.58100E-01
      82204.71c   1.16200E-02
      82206.71c   2.00030E-01
      82207.71c   1.83430E-01
      82208.71c   4.34920E-01
m7     3006.72c   2.85714E-04
       3007.72c   2.85429E-01
       4009.72c   1.42857E-01
       9019.72c   5.71429E-01
m9     3006.72c   8.96059E-05
       3007.72c   8.95163E-02
       4009.72c   7.26225E-01
       9019.72c   1.79212E-01
      26054.72c   2.46180E-04
      26056.72c   3.86450E-03
      26057.72c   8.92481E-05
      26058.72c   1.18773E-05
      24050.72c   2.87599E-05
      24052.72c   5.54607E-04
      24053.72c   6.28879E-05
      24054.72c   1.56541E-05
      74182.72c   1.21544E-05
      74183.72c   6.53377E-06
      74184.72c   1.39899E-05
      74186.72c   1.29808E-05
      22046.72c   1.88097E-06
      22047.72c   1.69629E-06
      22048.72c   1.68079E-05
      22049.72c   1.23346E-06
      22050.72c   1.18102E-06
      39089.72c   6.14237E-06
       8016.72c   9.18869E-06
       8017.72c   2.23829E-08
m13    3006.72c   1.13172E-04
       3007.72c   1.13059E-01
       4009.72c   5.65862E-02
       9019.72c   2.26345E-01
       6000.72c   6.03897E-01
m16    6000.72c   9.66110E-01
      14028.72c   3.12563E-02
```

```
      14029.72c   1.58712E-03
      14030.72c   1.04624E-03
m17    6000.72c   1.0
m18    3006.72c   2.85714E-04
       3007.72c   2.85429E-01
       4009.72c   1.42857E-01
       9019.72c   5.71429E-01
m51    6000.72c   3.33333E-01
       8016.72c   3.32523E-01
       8017.72c   8.10000E-04
      92234.72c   6.36574E-06
      92235.72c   8.33333E-04
      92238.72c   3.32494E-01
```

B.3 Example AMR MCNP Input Deck

A Depleted Uranium fertile burner LNC input deck:

```
LFFH - TRISO fuel
1 1 -6.5e-006  -1 vol=6.545e+007 tmp=7.95478e-008 imp:n,p 1
c
c  Tungsten coating on first wall
3 3 -19.3   1 -2 21 22 23 24 25 26 27 28
                   29 30 31 32 33 34 35 36 37 38
                   39 40 41 42 43 44
                   vol=19205 tmp=7.95478e-008 imp:n,p 1
c
c  First wall -- ODS-FS (full density)
4 4 -8   2 -3 21 22 23 24 25 26 27 28
                   29 30 31 32 33 34 35 36 37 38
                   39 40 41 42 43 44
                   vol=211510 tmp=7.95478e-008 imp:n,p 1
c
c  Dedicated LiPb cooling
5 5 -9.4   3 -4 21 22 23 24 25 26 27 28
                   29 30 31 32 33 34 35 36 37 38
                   39 40 41 42 43 44
                   vol=2.3377e+006 tmp=5.36968e-008 imp:n,p 1
c
c  Second wall -- ODS-FS (full density)
6 4 -8   4 -5 21 22 23 24 25 26 27 28
                   29 30 31 32 33 34 35 36 37 38
                   39 40 41 42 43 44
                   vol=236840 tmp=6.48989e-008 imp:n,p 1
c
c  Flibe cooling injection plenum
7 7 -1.982   5 -6 21 22 23 24 25 26 27 28
                   29 30 31 32 33 34 35 36 37 38
                   39 40 41 42 43 44
                   vol=2.3994e+006 tmp=7.6101e-008 imp:n,p 1
c
c  Third wall -- ODS-FS (porous)
8 4 -6   6 -7 21 22 23 24 25 26 27 28
                   29 30 31 32 33 34 35 36 37 38
                   39 40 41 42 43 44
                   vol=243050 tmp=7.61829e-008 imp:n,p 1
c
c  Beryllium w/ flibe cooling (60/40 vol)
9 9 -1.9409   7 -8 21 22 23 24 25 26 27 28
                   29 30 31 32 33 34 35 36 37 38
                   39 40 41 42 43 44
                   vol=1.3803e+007 tmp=7.62639e-008 imp:n,p 1
c
c  Fourth wall -- ODS-FS (porous)
10 4 -6   8 -9 21 22 23 24 25 26 27 28
                   29 30 31 32 33 34 35 36 37 38
                   39 40 41 42 43 44
                   vol=274890 tmp=7.7248e-008 imp:n,p 1
c
c  Fuel zones -- mix of pebbles and flibe coolant (60/40 vol)
51 0   9 -105 21 22 23 24 25 26 27 28
                   29 30 31 32 33 34 35 36 37 38
                   39 40 41 42 43 44
                   fill=101 imp:n,p 1
4051 0   105 -103 21 22 23 24 25 26 27 28
                   29 30 31 32 33 34 35 36 37 38
```

```
                    39 40 41 42 43 44
                    fill=4101 imp:n,p 1
2051 0  103 -106 21 22 23 24 25 26 27 28
                    29 30 31 32 33 34 35 36 37 38
                    39 40 41 42 43 44
                    fill=2101 imp:n,p 1
5051 0  106 -102 21 22 23 24 25 26 27 28
                    29 30 31 32 33 34 35 36 37 38
                    39 40 41 42 43 44
                    fill=5101 imp:n,p 1
1051 0  102 -107 21 22 23 24 25 26 27 28
                    29 30 31 32 33 34 35 36 37 38
                    39 40 41 42 43 44
                    fill=1101 imp:n,p 1
6051 0  107 -104 21 22 23 24 25 26 27 28
                    29 30 31 32 33 34 35 36 37 38
                    39 40 41 42 43 44
                    fill=6101 imp:n,p 1
3051 0  104 -101 21 22 23 24 25 26 27 28
                    29 30 31 32 33 34 35 36 37 38
                    39 40 41 42 43 44
                    fill=3101 imp:n,p 1
52 0  101 -10 21 22 23 24 25 26 27 28
                    29 30 31 32 33 34 35 36 37 38
                    39 40 41 42 43 44
                    fill=102 imp:n,p 1
c
c  End of Fuel zones
c
c  Back wall to fuel region
12 4 -6  10 -11 21 22 23 24 25 26 27 28
                    29 30 31 32 33 34 35 36 37 38
                    39 40 41 42 43 44
                    vol=795120 tmp=7.86861e-008 imp:n,p 1
c
c  Graphite reflector
13 13 -1.8069  11 -12 21 22 23 24 25 26 27 28
                    29 30 31 32 33 34 35 36 37 38
                    39 40 41 42 43 44
                    vol=1.4605e+008 tmp=7.87215e-008 imp:n,p 1
c
c  Final wall
14 4 -6  12 -13 21 22 23 24 25 26 27 28
                    29 30 31 32 33 34 35 36 37 38
                    39 40 41 42 43 44
                    vol=1.1639e+006 tmp=7.86861e-008 imp:n,p 1
c
c Start of fuel kernel and pebble lattice definitions
c
101 51 -10.5  -51 vol=1.9325e+006 tmp=9.24733e-008 u=401 imp:n,p 1
102 16 -1.8014  51 vol=3.009e+007 tmp=8.81648e-008 u=401 imp:n,p 1
201 0  -53 54 -55 56 -57 58
                    fill=401 lat=1 u=301 imp:n,p 1
301 0  -61 fill=301 u=201 imp:n,p 1
303 0  -63 fill=301 u=201 imp:n,p 1
305 0  -65 fill=301 u=201 imp:n,p 1
307 0  -67 fill=301 u=201 imp:n,p 1
309 0  -69 fill=301 u=201 imp:n,p 1
311 0  -71 fill=301 u=201 imp:n,p 1
313 0  -73 fill=301 u=201 imp:n,p 1
315 0  -75 fill=301 u=201 imp:n,p 1
317 0  -77 fill=301 u=201 imp:n,p 1
```

```
319 18 -1.97  61 63 65 67 69 71 73 75 77
                    vol=2.1348e+007 tmp=7.8232e-008 u=201 imp:n,p 1
901 0  -81 82 -83 84 -85 86
                    fill=201 lat=1 u=101 imp:n,p 1
4102 16 -1.8014  51 vol=3.009e+007 tmp=8.81648e-008 u=4401 imp:n,p 1
4101 56 -10.5  -51 vol=1.9325e+006 tmp=9.24733e-008 u=4401 imp:n,p 1
4201 0  -53 54 -55 56 -57 58
                    fill=4401 lat=1 u=4301 imp:n,p 1
4319 18 -1.97  61 63 65 67 69 71 73 75 77
                    vol=2.1348e+007 tmp=7.8232e-008 u=4201 imp:n,p 1
4317 0  -77 fill=4301 u=4201 imp:n,p 1
4315 0  -75 fill=4301 u=4201 imp:n,p 1
4313 0  -73 fill=4301 u=4201 imp:n,p 1
4311 0  -71 fill=4301 u=4201 imp:n,p 1
4309 0  -69 fill=4301 u=4201 imp:n,p 1
4307 0  -67 fill=4301 u=4201 imp:n,p 1
4305 0  -65 fill=4301 u=4201 imp:n,p 1
4303 0  -63 fill=4301 u=4201 imp:n,p 1
4301 0  -61 fill=4301 u=4201 imp:n,p 1
4901 0  -81 82 -83 84 -85 86
                    fill=4201 lat=1 u=4101 imp:n,p 1
2102 16 -1.8014  51 vol=3.009e+007 tmp=8.81648e-008 u=2401 imp:n,p 1
2101 54 -10.5  -51 vol=1.9325e+006 tmp=9.24733e-008 u=2401 imp:n,p 1
2201 0  -53 54 -55 56 -57 58
                    fill=2401 lat=1 u=2301 imp:n,p 1
2319 18 -1.97  61 63 65 67 69 71 73 75 77
                    vol=2.1348e+007 tmp=7.8232e-008 u=2201 imp:n,p 1
2317 0  -77 fill=2301 u=2201 imp:n,p 1
2315 0  -75 fill=2301 u=2201 imp:n,p 1
2313 0  -73 fill=2301 u=2201 imp:n,p 1
2311 0  -71 fill=2301 u=2201 imp:n,p 1
2309 0  -69 fill=2301 u=2201 imp:n,p 1
2307 0  -67 fill=2301 u=2201 imp:n,p 1
2305 0  -65 fill=2301 u=2201 imp:n,p 1
2303 0  -63 fill=2301 u=2201 imp:n,p 1
2301 0  -61 fill=2301 u=2201 imp:n,p 1
2901 0  -81 82 -83 84 -85 86
                    fill=2201 lat=1 u=2101 imp:n,p 1
5101 57 -10.5  -51 vol=1.9325e+006 tmp=9.24733e-008 u=5401 imp:n,p 1
5102 16 -1.8014  51 vol=3.009e+007 tmp=8.81648e-008 u=5401 imp:n,p 1
5201 0  -53 54 -55 56 -57 58
                    fill=5401 lat=1 u=5301 imp:n,p 1
5301 0  -61 fill=5301 u=5201 imp:n,p 1
5303 0  -63 fill=5301 u=5201 imp:n,p 1
5305 0  -65 fill=5301 u=5201 imp:n,p 1
5307 0  -67 fill=5301 u=5201 imp:n,p 1
5309 0  -69 fill=5301 u=5201 imp:n,p 1
5311 0  -71 fill=5301 u=5201 imp:n,p 1
5313 0  -73 fill=5301 u=5201 imp:n,p 1
5315 0  -75 fill=5301 u=5201 imp:n,p 1
5317 0  -77 fill=5301 u=5201 imp:n,p 1
5319 18 -1.97  61 63 65 67 69 71 73 75 77
                    vol=2.1348e+007 tmp=7.8232e-008 u=5201 imp:n,p 1
5901 0  -81 82 -83 84 -85 86
                    fill=5201 lat=1 u=5101 imp:n,p 1
1102 16 -1.8014  51 vol=3.009e+007 tmp=8.81648e-008 u=1401 imp:n,p 1
1101 53 -10.5  -51 vol=1.9325e+006 tmp=9.24733e-008 u=1401 imp:n,p 1
1201 0  -53 54 -55 56 -57 58
                    fill=1401 lat=1 u=1301 imp:n,p 1
1319 18 -1.97  61 63 65 67 69 71 73 75 77
                    vol=2.1348e+007 tmp=7.8232e-008 u=1201 imp:n,p 1
1317 0  -77 fill=1301 u=1201 imp:n,p 1
```

```
1315 0   -75 fill=1301 u=1201 imp:n,p 1
1313 0   -73 fill=1301 u=1201 imp:n,p 1
1311 0   -71 fill=1301 u=1201 imp:n,p 1
1309 0   -69 fill=1301 u=1201 imp:n,p 1
1307 0   -67 fill=1301 u=1201 imp:n,p 1
1305 0   -65 fill=1301 u=1201 imp:n,p 1
1303 0   -63 fill=1301 u=1201 imp:n,p 1
1301 0   -61 fill=1301 u=1201 imp:n,p 1
1901 0   -81 82 -83 84 -85 86
                    fill=1201 lat=1 u=1101 imp:n,p 1
6101 58 -10.5   -51 vol=1.9325e+006 tmp=9.24733e-008 u=6401 imp:n,p 1
6102 16 -1.8014   51 vol=3.009e+007 tmp=8.81648e-008 u=6401 imp:n,p 1
6201 0   -53 54 -55 56 -57 58
                    fill=6401 lat=1 u=6301 imp:n,p 1
6301 0   -61 fill=6301 u=6201 imp:n,p 1
6303 0   -63 fill=6301 u=6201 imp:n,p 1
6305 0   -65 fill=6301 u=6201 imp:n,p 1
6307 0   -67 fill=6301 u=6201 imp:n,p 1
6309 0   -69 fill=6301 u=6201 imp:n,p 1
6311 0   -71 fill=6301 u=6201 imp:n,p 1
6313 0   -73 fill=6301 u=6201 imp:n,p 1
6315 0   -75 fill=6301 u=6201 imp:n,p 1
6317 0   -77 fill=6301 u=6201 imp:n,p 1
6319 18 -1.97   61 63 65 67 69 71 73 75 77
                    vol=2.1348e+007 tmp=7.8232e-008 u=6201 imp:n,p 1
6901 0   -81 82 -83 84 -85 86
                    fill=6201 lat=1 u=6101 imp:n,p 1
3101 55 -10.5   -51 vol=1.9325e+006 tmp=9.24733e-008 u=3401 imp:n,p 1
3102 16 -1.8014   51 vol=3.009e+007 tmp=8.81648e-008 u=3401 imp:n,p 1
3201 0   -53 54 -55 56 -57 58
                    fill=3401 lat=1 u=3301 imp:n,p 1
3301 0   -61 fill=3301 u=3201 imp:n,p 1
3303 0   -63 fill=3301 u=3201 imp:n,p 1
3305 0   -65 fill=3301 u=3201 imp:n,p 1
3307 0   -67 fill=3301 u=3201 imp:n,p 1
3309 0   -69 fill=3301 u=3201 imp:n,p 1
3311 0   -71 fill=3301 u=3201 imp:n,p 1
3313 0   -73 fill=3301 u=3201 imp:n,p 1
3315 0   -75 fill=3301 u=3201 imp:n,p 1
3317 0   -77 fill=3301 u=3201 imp:n,p 1
3319 18 -1.97   61 63 65 67 69 71 73 75 77
                    vol=2.1348e+007 tmp=7.8232e-008 u=3201 imp:n,p 1
3901 0   -81 82 -83 84 -85 86
                    fill=3201 lat=1 u=3101 imp:n,p 1
103 52 -10.5   -51 vol=1.9325e+006 tmp=9.24733e-008 u=402 imp:n,p 1
104 16 -1.8014   51 vol=3.009e+007 tmp=8.81648e-008 u=402 imp:n,p 1
202 0   -53 54 -55 56 -57 58
                    fill=402 lat=1 u=302 imp:n,p 1
321 0   -61 fill=302 u=202 imp:n,p 1
323 0   -63 fill=302 u=202 imp:n,p 1
325 0   -65 fill=302 u=202 imp:n,p 1
327 0   -67 fill=302 u=202 imp:n,p 1
329 0   -69 fill=302 u=202 imp:n,p 1
331 0   -71 fill=302 u=202 imp:n,p 1
333 0   -73 fill=302 u=202 imp:n,p 1
335 0   -75 fill=302 u=202 imp:n,p 1
337 0   -77 fill=302 u=202 imp:n,p 1
339 18 -1.97   61 63 65 67 69 71 73 75 77
                    vol=2.1348e+007 tmp=7.8232e-008 u=202 imp:n,p 1
902 0   -81 82 -83 84 -85 86
                    fill=202 lat=1 u=102 imp:n,p 1
c
```

```
c Leakage zone
15 0  13 imp:n,p 0
c
c Beamports
21 1 -6.5e-006  1 -13 -21 tmp=7.95478e-008 imp:n,p 1
22 1 -6.5e-006  1 -13 -22 tmp=7.95478e-008 imp:n,p 1
23 1 -6.5e-006  1 -13 -23 tmp=7.95478e-008 imp:n,p 1
24 1 -6.5e-006  1 -13 -24 tmp=7.95478e-008 imp:n,p 1
25 1 -6.5e-006  1 -13 -25 tmp=7.95478e-008 imp:n,p 1
26 1 -6.5e-006  1 -13 -26 tmp=7.95478e-008 imp:n,p 1
27 1 -6.5e-006  1 -13 -27 tmp=7.95478e-008 imp:n,p 1
28 1 -6.5e-006  1 -13 -28 tmp=7.95478e-008 imp:n,p 1
29 1 -6.5e-006  1 -13 -29 tmp=7.95478e-008 imp:n,p 1
30 1 -6.5e-006  1 -13 -30 tmp=7.95478e-008 imp:n,p 1
31 1 -6.5e-006  1 -13 -31 tmp=7.95478e-008 imp:n,p 1
32 1 -6.5e-006  1 -13 -32 tmp=7.95478e-008 imp:n,p 1
33 1 -6.5e-006  1 -13 -33 tmp=7.95478e-008 imp:n,p 1
34 1 -6.5e-006  1 -13 -34 tmp=7.95478e-008 imp:n,p 1
35 1 -6.5e-006  1 -13 -35 tmp=7.95478e-008 imp:n,p 1
36 1 -6.5e-006  1 -13 -36 tmp=7.95478e-008 imp:n,p 1
37 1 -6.5e-006  1 -13 -37 tmp=7.95478e-008 imp:n,p 1
38 1 -6.5e-006  1 -13 -38 tmp=7.95478e-008 imp:n,p 1
39 1 -6.5e-006  1 -13 -39 tmp=7.95478e-008 imp:n,p 1
40 1 -6.5e-006  1 -13 -40 tmp=7.95478e-008 imp:n,p 1
41 1 -6.5e-006  1 -13 -41 tmp=7.95478e-008 imp:n,p 1
42 1 -6.5e-006  1 -13 -42 tmp=7.95478e-008 imp:n,p 1
43 1 -6.5e-006  1 -13 -43 tmp=7.95478e-008 imp:n,p 1
44 1 -6.5e-006  1 -13 -44 tmp=7.95478e-008 imp:n,p 1

c Surface cards
1 so 250
2 so 250.025
3 so 250.3
4 so 253.3
5 so 253.6
6 so 256.6
7 so 256.9
8 so 272.9
9 so 273.2
105 so 279.313
103 so 285.426
106 so 291.539
102 so 297.652
107 so 303.765
104 so 309.878
101 so 322.105
10 so 359.46
11 so 359.96
12 so 434.96
13 so 435.46
51 so 0.03
61 so 1
62 so 1
c
21 1 kz 0 0.00183397
22 2 kz 0 0.00183397
23 3 kz 0 0.00183397
24 4 kz 0 0.00183397
25 5 kz 0 0.00183397
26 6 kz 0 0.00183397
27 7 kz 0 0.00183397
28 8 kz 0 0.00183397
```

```
29 9 kz 0 0.00183397
30 10 kz 0 0.00183397
31 11 kz 0 0.00183397
32 12 kz 0 0.00183397
33 13 kz 0 0.00183397
34 14 kz 0 0.00183397
35 15 kz 0 0.00183397
36 16 kz 0 0.00183397
37 17 kz 0 0.00183397
38 18 kz 0 0.00183397
39 19 kz 0 0.00183397
40 20 kz 0 0.00183397
41 21 kz 0 0.00183397
42 22 kz 0 0.00183397
43 23 kz 0 0.00183397
44 24 kz 0 0.00183397
c
53 px  0.06164470
54 px -0.06164470
55 py  0.06164470
56 py -0.06164470
57 pz  0.06164470
58 pz -0.06164470
c
63 s   1.20399807  1.20399807  1.20399807  1.00000000
64 s   1.20399807  1.20399807  1.20399807  1.00000000
65 s   1.20399807  1.20399807 -1.20399807  1.00000000
66 s   1.20399807  1.20399807 -1.20399807  1.00000000
67 s   1.20399807 -1.20399807 -1.20399807  1.00000000
68 s   1.20399807 -1.20399807 -1.20399807  1.00000000
69 s   1.20399807 -1.20399807  1.20399807  1.00000000
70 s   1.20399807 -1.20399807  1.20399807  1.00000000
71 s  -1.20399807  1.20399807  1.20399807  1.00000000
72 s  -1.20399807  1.20399807  1.20399807  1.00000000
73 s  -1.20399807  1.20399807 -1.20399807  1.00000000
74 s  -1.20399807  1.20399807 -1.20399807  1.00000000
75 s  -1.20399807 -1.20399807 -1.20399807  1.00000000
76 s  -1.20399807 -1.20399807 -1.20399807  1.00000000
77 s  -1.20399807 -1.20399807  1.20399807  1.00000000
78 s  -1.20399807 -1.20399807  1.20399807  1.00000000
81 px  1.20399807
82 px -1.20399807
83 py  1.20399807
84 py -1.20399807
85 pz  1.20399807
86 pz -1.20399807
c

c ******************** RUN DATA ********************
c
c  Source definition
sdef par=1 erg=14.1 x=0 y=0 z=0
c kcode 10 1 10 50
c ksrc  300.01  0. 0. -300 0. 0.
mode n p
prdmp 10000 10000 0 1 10000
nps 5e4
totnu
c
c ******************** TALLIES ********************
c
c
```

```
c  Special Tallies required for ABL AMR calcultion
fc994  Adaptive Burnup Library AMR Cell Flux Tally
f994:n 101 4101 2101 5101 1101 6101 3101 103
c
fc614  Adaptive Burnup Library AMR Absorption/Fission Rate Tally
f614:n 101
fm614 -1.0 51  (-2) (-6)
c
fc624  Adaptive Burnup Library AMR Absorption/Fission Rate Tally
f624:n 4101
fm624 -1.0 56  (-2) (-6)
c
fc634  Adaptive Burnup Library AMR Absorption/Fission Rate Tally
f634:n 2101
fm634 -1.0 54  (-2) (-6)
c
fc644  Adaptive Burnup Library AMR Absorption/Fission Rate Tally
f644:n 5101
fm644 -1.0 57  (-2) (-6)
c
fc654  Adaptive Burnup Library AMR Absorption/Fission Rate Tally
f654:n 1101
fm654 -1.0 53  (-2) (-6)
c
fc664  Adaptive Burnup Library AMR Absorption/Fission Rate Tally
f664:n 6101
fm664 -1.0 58  (-2) (-6)
c
fc674  Adaptive Burnup Library AMR Absorption/Fission Rate Tally
f674:n 3101
fm674 -1.0 55  (-2) (-6)
c
fc684  Adaptive Burnup Library AMR Absorption/Fission Rate Tally
f684:n 103
fm684 -1.0 52  (-2) (-6)
c
fc992  Adaptive Burnup Library AMR Surface Flux Tally
f992:n 9 105 103 106 102 107 104 101 10
sd992 937932 980375 1.02376e+006 1.06808e+006 1.11334e+006 1.15954e+006
          1.20668e+006 1.30378e+006 1.62372e+006
c
c  Rotation matrixes for the 48 beamports
c
*tr1   0 0 0   79.7  25.9 66.5 168.8  78.8 90  94.5 113.  23.5
*tr2   0 0 0  154.1  79.7 66.5 101.3 168.8 90  67.   94.5 23.5
*tr3   0 0 0  100.3 154.1 66.5  11.3 101.3 90  85.5  67.  23.5
*tr4   0 0 0   25.9 100.3 66.5  78.8  11.3 90 113.   85.5 23.5
*tr5   0 0 0   44.7  61.  59.4 124.3  34.3 90 114.8 106.7 30.6
*tr6   0 0 0  118.8  43.9 60.  146.3 123.8 90  73.9 114.6 30.
*tr7   0 0 0  135.3 119.  59.4  55.7 145.7 90  65.2  73.3 30.6
*tr8   0 0 0   61.2 136.1 60.   33.8  56.3 90 106.1  65.4 30.
*tr9   0 0 0   46.8  78.5 45.5 106.3  16.3 90 132.3 101.3 44.5
*tr10  0 0 0   70.7  50.8 45.5 152.5  62.5 90 108.9 128.4 44.5
*tr11  0 0 0  101.5  46.8 45.5 163.7 106.3 90  78.7 132.3 44.5
*tr12  0 0 0  129.2  70.7 45.5 117.5 152.5 90  51.6 108.9 44.5
*tr13  0 0 0  133.2 101.5 45.5  73.7 163.7 90  47.7  78.7 44.5
*tr14  0 0 0  109.3 129.2 45.5  27.5 117.5 90  71.1  51.6 44.5
*tr15  0 0 0   78.5 133.2 45.5  16.3  73.7 90 101.3  47.7 44.5
*tr16  0 0 0   50.8 109.3 45.5  62.5  27.5 90 128.4  71.1 44.5
*tr17  0 0 0   60.3  65.8 40.  129.7  39.7 90 126.1 119.3 50.
*tr18  0 0 0   86.4  50.2 40.  174.4  84.4 90  94.3 139.7 50.
*tr19  0 0 0  114.1  60.2 40.  140.6 129.4 90  60.9 126.3 50.
```

```
*tr20   0 0 0   129.8   86.4  40.    95.6 174.4  90   40.3   94.3  50.
*tr21   0 0 0   119.7  114.2  40.    50.3 140.3  90   53.9   60.7  50.
*tr22   0 0 0    93.6  129.8  40.     5.6  95.6  90   85.7   40.3  50.
*tr23   0 0 0    65.9  119.8  40.    39.4  50.6  90  119.1   53.7  50.
*tr24   0 0 0    50.2   93.6  40.    84.4   5.6  90  139.7   85.7  50.
c
c ******************** MATERIALS ********************
c
m1    7014   0.781387
       8016   0.210549
       18040   0.00464703
m3    74182.71c   0.2662
       74183.71c   0.1431
       74184.71c   0.3064
       74186.71c   0.2843
m4    26054.71c   0.0496578
       26056.71c   0.779522
       26057.71c   0.0180026
       26058.71c   0.00239581
       24050.71c   0.00580127
       24052.71c   0.111872
       24053.71c   0.0126854
       24054.71c   0.00315765
       74182.71c   0.0024517
       74183.71c   0.00131795
       74184.71c   0.00282194
       74186.71c   0.0026184
       22046.71c   0.000379418
       22047.71c   0.000342166
       22048.71c   0.00339038
       22049.71c   0.000248806
       22050.71c   0.000238228
       39089.71c   0.001239
       8016.71c   0.00185349
       8017.71c   4.51494e-006
m5    3006.71c   0.0119
       3007.71c   0.1581
       82204.71c   0.01162
       82206.71c   0.20003
       82207.71c   0.18343
       82208.71c   0.43492
m7    3006.71c   0.000285714
       3007.71c   0.285429
       4009.71c   0.142857
       9019.71c   0.571429
m9    3006.71c   8.96059e-005
       3007.71c   0.0895163
       4009.71c   0.726225
       9019.71c   0.179212
       26054.71c   0.00024618
       26056.71c   0.0038645
       26057.71c   8.92481e-005
       26058.71c   1.18773e-005
       24050.71c   2.87599e-005
       24052.71c   0.000554607
       24053.71c   6.28879e-005
       24054.71c   1.56541e-005
       74182.71c   1.21544e-005
       74183.71c   6.53377e-006
       74184.71c   1.39899e-005
       74186.71c   1.29808e-005
       22046.71c   1.88097e-006
```

```
        22047.71c   1.69629e-006
        22048.71c   1.68079e-005
        22049.71c   1.23346e-006
        22050.71c   1.18102e-006
        39089.71c   6.14237e-006
        8016.71c    9.18869e-006
        8017.71c    2.23829e-008
m13     3006.71c    0.000113172
        3007.71c    0.113059
        4009.71c    0.0565862
        9019.71c    0.226345
        6000.71c    0.603897
m16     6000.71c    0.947906
        14028.71c    0.0480463
        14029.71c    0.00243967
        14030.71c    0.00160825
m18     3006.71c    0.000285714
        3007.71c    0.285429
        4009.71c    0.142857
        9019.71c    0.571429
m51     6000.71c    0.333333
        8016.71c    0.332523
        8017.71c    0.00081
        92234.71c    6.36574e-006
        92235.71c    0.000833333
        92238.71c    0.332494
m52     6000.71c    0.333333
        8016.71c    0.332523
        8017.71c    0.00081
        92234.71c    6.36574e-006
        92235.71c    0.000833333
        92238.71c    0.332494
m53     6000.71c    0.333333
        8016.71c    0.332523
        8017.71c    0.00081
        92234.71c    6.36574e-006
        92235.71c    0.000833333
        92238.71c    0.332494
m54     6000.71c    0.333333
        8016.71c    0.332523
        8017.71c    0.00081
        92234.71c    6.36574e-006
        92235.71c    0.000833333
        92238.71c    0.332494
m55     6000.71c    0.333333
        8016.71c    0.332523
        8017.71c    0.00081
        92234.71c    6.36574e-006
        92235.71c    0.000833333
        92238.71c    0.332494
m56     6000.71c    0.333333
        8016.71c    0.332523
        8017.71c    0.00081
        92234.71c    6.36574e-006
        92235.71c    0.000833333
        92238.71c    0.332494
m57     6000.71c    0.333333
        8016.71c    0.332523
        8017.71c    0.00081
        92234.71c    6.36574e-006
        92235.71c    0.000833333
        92238.71c    0.332494
```

```
m58     6000.71c   0.333333
        8016.71c   0.332523
        8017.71c   0.00081
        92234.71c   6.36574e-006
        92235.71c   0.000833333
        92238.71c   0.332494
```